Alma Mater Studiorum – Università di Bologna

DOTTORATO DI RICERCA IN

Chimica

Ciclo XXX

Settore Concorsuale: 03/B1

Settore Scientifico Disciplinare: CHIM/03

A JOURNEY AROUND IRON COMPLEXES: LIGANDS DESIGN, SUSTAINABILITY, CATALYTIC AND BIO-INORGANIC APPLICATIONS

Presentata da: Andrea Cingolani

Coordinatore Dottorato

Prof. Aldo Roda

Supervisore

Dr. Rita Mazzoni

Co-supervisore

Prof. Valerio Zanotti

Esame finale anno 2018

Abstract.

The work described in this thesis has been devoted to the synthesis and study of novel carbonyl iron(0) complexes bearing two type of ligands: cyclopentadienone (CpO) and N-heterocyclic carbene (NHC). Different substituted CpO and NHC have been employed in order to better understand the reactivity of this class of iron compounds. The CpO, supported by the NHC, acts as non-innocent ligand, allowing the oxidation of iron centre from 0 to +2 *via* an intramolecular redox reaction, generating a new species featuring new properties.

The CpO-NHC-iron system has been employed in catalytic reactions such as transfer hydrogenation with poor results and dehydrocoupling of ammonia-borane with interesting results. Electrochemical insights revealed activity as good water oxidation catalyst under basic conditions, which are due to the presence of NHC ligand. Furthermore, the NHC has been exploited as linker to a polymeric thin film coated over an electrode in order to design new chemically modified electrodes (CMEs). A CME has been synthesised and evaluated as glucose sensor.

Compounds bearing an amino group on the lateral chain of the NHC ligand have been evaluated as anticancer drugs against pancreatic cancer cells, with an IC_{50} comparable to Carboplatin. This result is remarkable given the robustness of pancreatic cancer cells.

Finally, the reactivity in the hydrogen evolution reaction of a different class of iron compounds (iron dinuclear complexes) has been examined in depth both by DFT calculation and by electrochemical and spectroscopic analysis.

Abstract.

Il lavoro descritto in questa tesi si occupa della stintesi e studio di nuovi complessi carbonilici di ferro(0) coordinati a due tipi di leganti: ciclopentadienone (CpO) e carbene-N-eterociclico (NHC). In questo studio sono stati impiegati CpO e NHC con diversi gruppi funzionali in modo tale da comprendere approfonditamente la reattività di questa classe di composti. Il CpO, supportato dal NHC, agisce da legante non innocente, permettendo l'ossidazione del ferro centrale da 0 a +2 attraverso una reazione redox intramolecolare, e generando una nuova specie con le sue proprie caratteristiche e proprietà.

Il sistema CpO-NHC è stato impiegato in reazione catalitiche di trasferimento d'idrogeno con risultati poco accattivanti e deidroaccoppiamento di ammonia-borani con risultati interessanti. Studi di elettrochimica hanno rivelato una buona attività come catalizzatore per l'ossidazione di acqua e sviluppo di ossigeno in condizioni basiche, dovuta alla presenza del legante NHC. Inoltre, il NHC è stato sfruttato come connettore ad un film sottile polimerico depositato su elettrodo, in modo tale da progettare un nuovo elettrodo chimicamente modificato (ECM). Un ECM è stato sintetizzato e valutato come sensore per il glucosio.

Complessi di ferro aventi un gruppo amminico in catena laterale al legante NHC sono stati esaminati come antitumorali contro cellule cancerose del pancreas ed hanno esibito un IC_{50} comparabile al Carboplatino. Questo risultato è notevole considerando la resistenza delle cellule tumorali del pancreas.

Infine, la reattività nella reazione di sviluppo di idrogeno di una diversa classe di complessi di ferro (complessi dinucleari di ferro) è stata analizzata dettagliatamente sia attraverso calcoli DFT sia per via elettrochimica e analisi spettroscopica.

Table of contents.

Chapter I

Synthesis and reactivity of N-Heterocyclic Carbene Iron complexes

Chapter II

Reactivity study of NHC cyclopentadienone iron complexes in transfer hydrogenation and alcohol oxidation

Chapter III

NHC-Knölker type iron complexes as ammonia-borane dehydrocoupling catalysts

Chapter IV

Cyclopentadienone-NHC iron(0) system as water oxidation catalyst

Chapter V

Beyond dithiolate paradigm in [FeFe] hydrogenase models: diiron complexes bearing hydrocarbyl ligands and mechanistic insight into the electrocatalytic H_2 production by $[Fe_2(CN)\{\mu\text{-}CN(Me)_2\}(\mu\text{-}CO)(CO)(Cp)_2]$.

Chapter VI

NHC-iron(0) complexes as redox mediators: immobilisation and glucose amperometric detection.

Chapter VII

Cyclopentadienone-NHC iron(0) complexes as anticancer drugs

List of abbreviations.

AA: amino acids

AB: ammonia-borane

APT: atom proton transfer

BCTB: B-(cyclotriborazanyl)aminoborane

BZ: borazine

C.E.: catalytic efficiency

CME: chemically modified electrode

CpO: cyclopentadienone

CTB: cyclotriborazane

DA: dopamine

DSP: disodium phosphate

Glu: glucose

GOx: glucose oxidase

HER: hydrogen evolution reaction

HOMO: highest occupied molecular orbital

ITO: indium tin oxide

LUMO: lowest unoccupied molecular orbital

NHC: N-heterocyclic carbene

PCET: proton-coupled electron transfer

PEDOT: poly(3,4-ethylenedioxythiophene)

PEM: proton exchange membrane

PSS: poly(styrene-4-sulfonate)

QM: quinone methides

ROS: reactive oxygen species

TMS: trimethylsilyl-

TOF: turnover frequency

TS: transition state

VMPP: modified glass PEDOT:PSS

Introduction

In last decades, sustainability has emerged as a new paradigm in scientific research as response to the major economic, environmental and social challenges facing our society. Indeed, meeting future energy demands, reducing pollution, minimizing waste releases, reducing the use of essential raw materials or finding substitutes etc., can only be solved through a sustainability based approach. Many concepts, ideas and theories have developed about the central role that chemistry can play in order to address the above mentioned challenges. In particular, two terms have been extensively used: "Green Chemistry" and "Sustainable Chemistry". Anastas and Warner first defined Green Chemistry as "a set of 12 principles that applied in the design of chemical products and processes, enables to reduce the quantities of chemicals having a negative impact on human health and the environment". [1] Sustainable Chemistry is defined as "the part of chemistry which is essential to a sustainable society with a view to product design, manufacturing, consumption of resources, health and safety at work, economic success and technical innovation not only in industrialized nations but in emerging and developing countries".

Thus Green and Sustainable Chemistry are receiving ever increasing attention and are developing rapidly into almost all the areas related to chemical science and technology. One of the emerging sustainability concepts emphasize the use of environmentally benign, earth abundant and inexpensive first row transition metals such as iron instead of the traditional second and third row transition metals. This has a major impact in the area of transition metal homogeneous catalysis, in that the most relevant advances were obtained (so far) using noble transition metals such as palladium, rhodium, platinum, iridium, which are toxic, rare and cannot sustain large scale applications. Replacing these noble metals with iron, whilst maintaining excellently catalytic properties, is very challenging and implies a new approach to the metal –ligand design. For example, many efforts in the research of catalytic iron based substitutes are inspired by naturally occurring enzymes. Indeed, nature widely uses non precious metals to perform specific and highly efficient catalysed reactions with the help of powerful ligands. Cooperation between ligands and metal centre is the key prerogative in order to exploit earth abundant metals. Recently, the use of non innocent ligands gave access to high reactivity in interesting catalytic reactions such as artificial photosynthesis (i.e. water oxidation and hydrogen reduction), asymmetric hydrogenation and

dehydrogenation. In the bio-inorganic field, bio-mimetic compounds have been developed to be employed as drugs in treating the most dangerous diseases.
Inspiration from natural well-known molecules and design of redox-active metal-ligand combinations are undergoing a rebirth in science and they are likely to inspire new applications. In the following introduction, the first part will be focused on an overview of non-innocent ligands, which inspired the design of a new class of iron compounds described in this thesis. The second section will be focused on a series of application fields where these new iron complexes have been used. These will include transfer hydrogenation, ammonia-borane dehydrocoupling, water oxidation, bioinorganic applications (e.g. dehydrogenase models and biomedical) and electrochemistry based on chemically modified electrodes.

Non innocent ligands.

Non innocent ligands (NILs) are redox-active molecules, which can be used to easily tune the electronic properties of a metal complex. The term non innocent ligands was first defined by C. K. Jørgensen in 1966,who was trying to better understand the oxidation states of metal centres: "Ligands are innocent when they allow oxidation states of the central atoms to be defined. The simplest case of suspect ligand is NO."[2] Nitric oxide(NO) has indeed more than one energetically accessible level and, consequently, the possibility to bind to a metal either as NO^+, with a linear geometry, or as NO^-, with a bent geometry, due to its radical character.
An easy case study is the $[Fe(NO)(H_2O)_5]^{2+}$, known as "the brown ring test" to detect nitrate in solution. The ion might be described as $Fe^{(I)}/NO^+$, $Fe^{(II)}/NO\bullet$ or $Fe^{(III)}/NO^-$; later, a set of spectroscopic data (IR, Mössbauer, EPR and Uv-Vis) showed that the nitrosyl iron complex is best described as $Fe^{(III)}/NO^-$.[3]

NILs behaviours.

In nature, NILs are extensively exploited to perform multi-electron reactions with Earth-abundant base metals (e.g. Fe, Cu), which involve a single electron event. On the contrary, in homogeneous catalysis precious noble metals (e.g. Ru, Rh, Ir) are utilized, since they undergo a $2e^-$ oxidation state changes, thus they are able to easily perform two-electron processes. In this point of view, NIL is a useful tool to imitate a noble metal, but exploiting more Earth-abundant and cheaper first row base metals.[4]

Non innocent activity can be divided in two main behaviours.[5]

A. Spectator ligand, which influences the metal atom, that is the reactive site, either accepting or releasing electron from and to the metal atom.
B. Actor ligand, which interacts directly with the substrate by forming or breaking bonds.

On this basis, four main approaches may be employed to take advantage of NILs:

1. Reduction/oxidation of the ligand to modify the Lewis acidity of the metal;
2. "Electron reservoir", accepting and donating electron density from the ligand to the metal in order to avoid uncommon and high-energy oxidation state of the metal;
3. Radical generation on the ligand to actively participate in breaking/forming new bonds;
4. Radical generation on the ligand and transfer to the substrate to activate it and modify its reactivity.

Approaches 1 and 2 are typical of type A ligands, whilst 3 and 4 of type B ones.

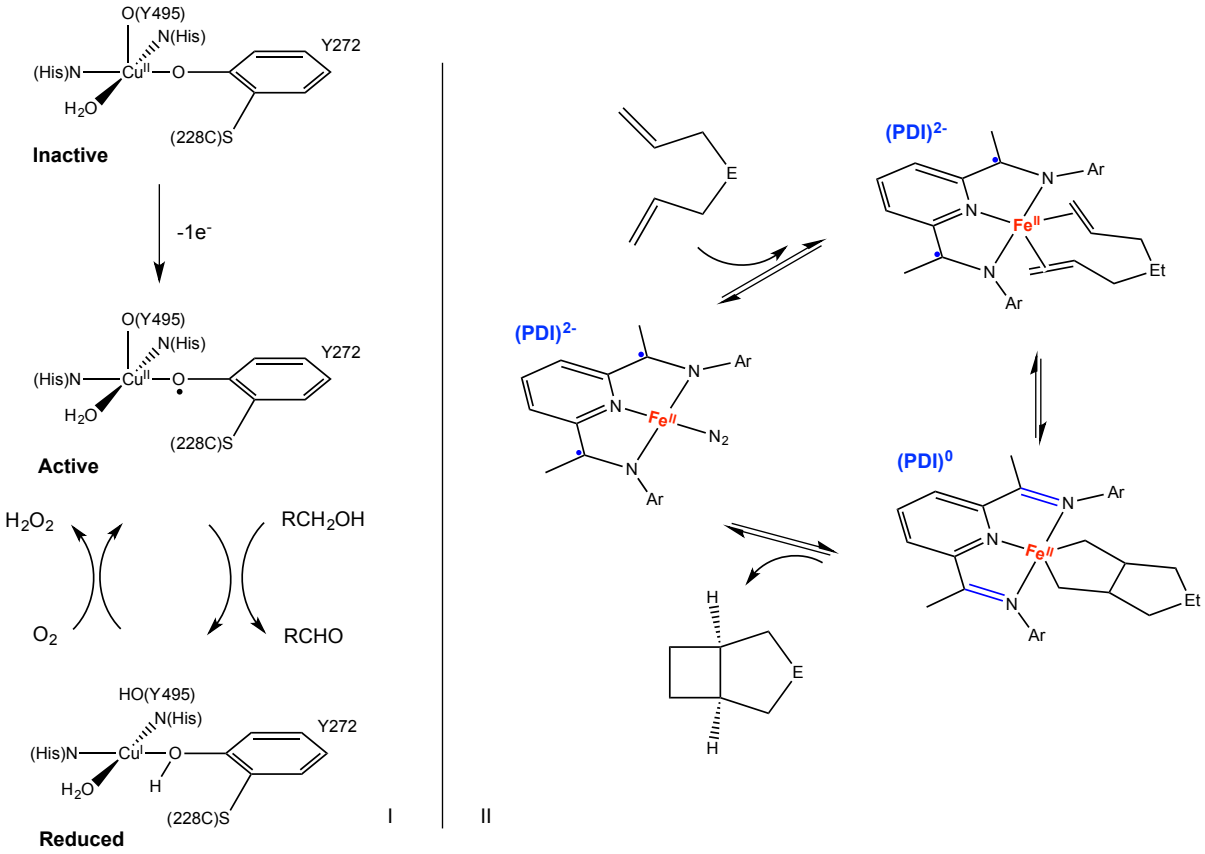

Scheme 1. On the left the Cu centre of galactose oxidase in the active (Cu^{II}/Y272•) and reduced (Cu^{I}/Y272) form. On the right the PDI-iron complex with different oxidation levels of the non-innocent ligand. E=O, NH, CH_2.

The use of NILs in metal complexes draws inspiration from enzymes in nature. One example is the galactose oxidase (GOase), a $Cu^{(II)}$ centre which is able to perform a two electron oxidation of alcohols to aldehydes.[56] The active site is made up of a Cu active site coordinated to two histidine and two tyrosine residues (Scheme 1, I).[7] Activation occurs through addition of one electron to a tyrosine to form a tyrosyl radical. The reduced form is made of a $Cu^{(I)}$ site and a tyrosinate residue, which is then oxidized by an oxygen molecule back to the active form. Notably, the one-electron couples $Cu^{(I)}/Cu^{(II)}$-Y272/Y272• are able to perform a two-electron overall oxidation; this is an example of a redox-active ligand of type B, where the ligand is directly involved in breaking bonds.

An example of type A NIL is the synthetic bis(imino)pyridine-type ligand (PDI), where four different oxidation levels are permitted: neutral, mono-, di- and tri-anions. The well-defined (PDI)-$Fe^{(II)}$ complex developed by Brookhart et al. and Gibson et al. is able to polymerize olefins[8] as well as to perform other catalytic reactions such as hydrogenation and hydrosilylation. Notably, in the example reported in Scheme 1-II,[9] a cyclization of diynes, electrons are shuttled from and to the PDI ligand without changing the oxidation state of the iron centre.

Iron Cyclopentadienone complexes

One of the most famous and employed catalyst bearing a non-innocent ligand is the Shvo's ruthenium catalyst,[10] discovered in middle 1980s and known for its robustness and versatile activity in hydrogenation of polar double bonds. Its mechanism implicates a simultaneous transfer of separated hydrogen atoms from the metal centre and the ligand, which is known as ligand-metal bifunctional catalysis. Also, the Knölker's iron analogue[11] is of highly attractive considering the use of less expensive and toxic iron. The two possible species of iron complex, due to the ambiguity of the oxidation state of the iron centre, confirm the non-innocent nature of the ligand, which might be classified as an "electron reservoir" (Scheme 2).

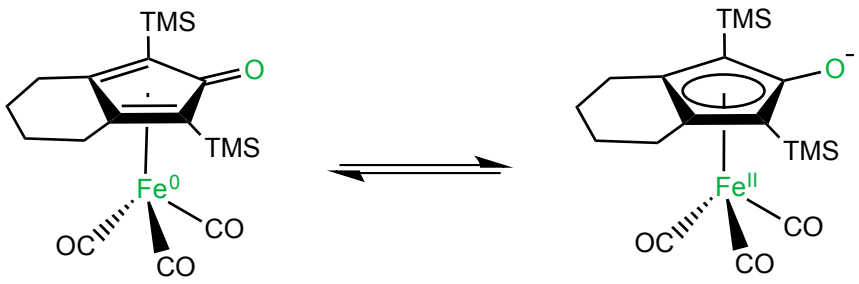

Scheme 2. The possibility of representing the Knölker's iron complex as Fe^0 or as Fe^{II} corroborates the non-innocent nature of cyclopentadienone ligand.

This class of iron complexes was first discovered in 1953, when Reppe and Vetter studied the reactivity of iron carbonyls with acetylenes, but were not able to identify this new species. Only six years later, Schrauzer[12] found the structure of an iron(0) triscarbonyl complex bearing a cyclopentadienone ligand, coordinated by two π-interactions. Moreover, the electronic and steric properties of cyclopentadienone can be easily designed providing appropriate substituents (e.g. electron withdrawing or donating group on the alkynes).

In 1990s the complexes were employed to access the high value free cyclopentadienone ligands, until Knölker discovered the first Fe-hydride species.[13] Treating iron triscarbonyl precursor with aqueous NaOH, followed by acidification with H_3PO_4, which is a Hieber-type reaction, yielded an iron hydride hydroxycyclopentadienyl complex.

In 2007 the new Knölker complexes were exploited by Casey et al.[14,15] as catalysts in the efficient hydrogenation of polar double bonds (e.g. ketones, aldehydes and imines) either by dihydrogen molecule or 2-propanol.

Since Casey's discovery, the Knölker complex has been used extensively[16] in several hydrogenations, oxidations as well as challenging dual catalysis. Another challenge is the functionalization of the iron complex in order to modify its reactivity and electronic properties: so far, this has been achieved either by changing substituents on cyclopentadienone or upon replacement of a carbonyl with another ligand.

For instance, Renaud's group focused on various cyclopentadienones[17,18] and synthesized a bench-stable catalyst by displacement of carbonyl with a more labile acetonitrile.[19] Berkessel et al. introduced a chiral phosphoramidite, obtaining the highest enantiomeric excess of 31%ee in the hydrogenation of acetophenone.[20]

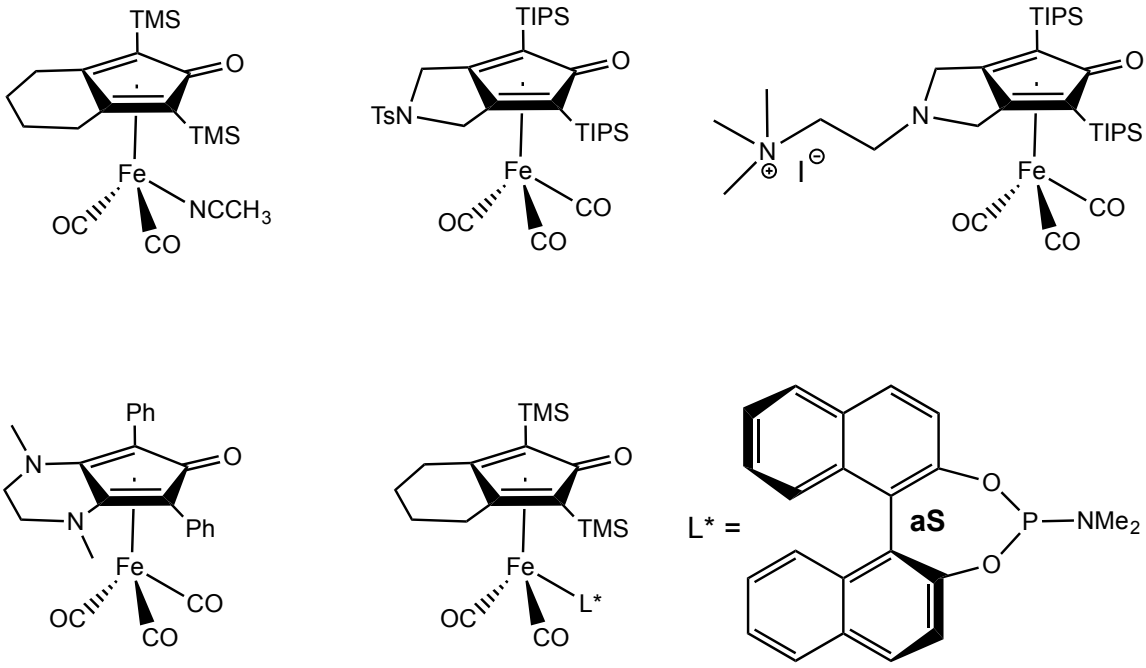

Figure 1. Structures of some modified iron compounds inspired by Knölker's iron complex. TMS, trimethylsilane; TIPS, triisopropylsylane, Ts, tosylate.

Concerning this topic, good candidates in substitution of a carbonyl are N-Heterocyclic Carbenes, well-known universal ligands in organometallic chemistry.

N-Heterocyclic Carbenes

Carbenes are 6-electron divalent carbon compounds, which have two non-bonding electrons on the carbene carbon.[21,22]

Their isolation, as free compounds, was actively pursued since the mid 1900s. In 1964 Fischer[23] isolated the first stable carbene complex characterized by an electrophilic carbon; a few years later in 1974, Schrock[24] isolated another type of carbene complex, but with a nucleophilic carbon. Both these complexes are now well-known as Fischer- and Schrock-type carbenes.

In between these two paramount discoveries, Wanzlick[25] and Öfele[26] reported autonomously the first N-Heterocyclic Carbene (NHC) complexes in 1968. The explosion of the NHC as ligand in Organometallic chemistry started with the isolation of the first

stable and "bottleable" carbene reported by Arduengo et al. in 1991. [27] The unexpected stability of NHC was thoroughly studied by several groups in order to shed some light on this species.

A carbene is a X_2C centre that might be linear or bent: the linear form is described as a triplet, whilst the bent can be either singlet or a triplet state (Figure 2).[28] The electronic configuration of these systems are strongly influenced by the α-substituents.

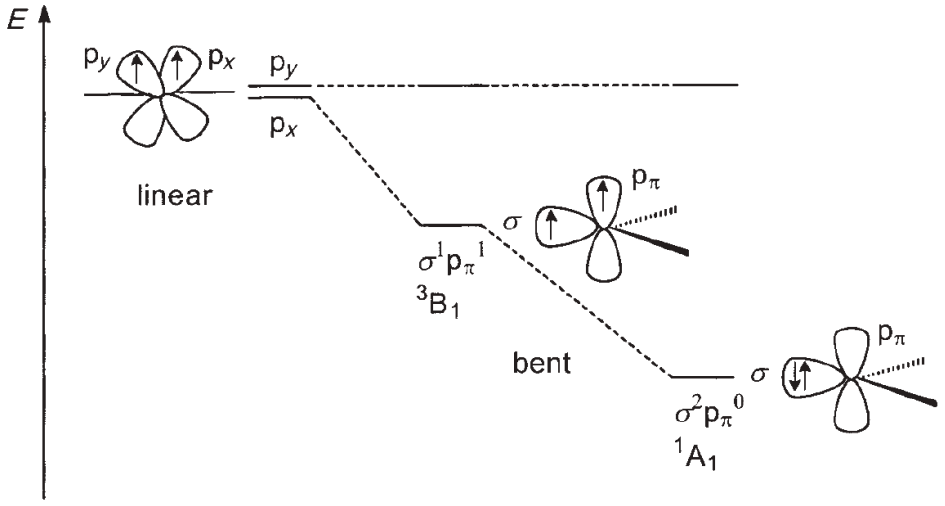

Figure 2. Diagram with energy of a linear carbene in a triplet state, and a bent carbene in a triplet $^3B_1$ or singlet $^1A_1$. Calculations have shown that an energy gap of 2eV is required to stabilze the singlet A.

NHC is a X_2C bent centre, where the carbon adopts a sp^2-hybridised form in a singlet ground state configuration. The singlet state is well-described as a highest occupied molecular orbital (HOMO) sp^2-hybridised lone pair, and a lowest occupied molecular orbital (LOMO) p-orbital on the C atom (Figure 3).[29] The electronic stabilization of the singlet is provided by the α-nitrogen atoms due to a double role: inductively, the sigma withdrawing effect stabilizes the non-bonding lone pair lowering the energy of the σ-orbital (HOMO); mesomerically, the donation of the π-amino lone pair into the vacant pπ-orbital, increases the energy of the empty p-orbital. Furthermore, the incorporation of the X_2C centre into a five-membered ring forces the bent sp^2-arrangement. Another source of stability is the partial aromaticity due to the backbone, which has been

calculated to be about 25 kcal mol^{-1}, and this explains why also the simplest di-methyl-substituted NHC (IMe) is persistent in solution.

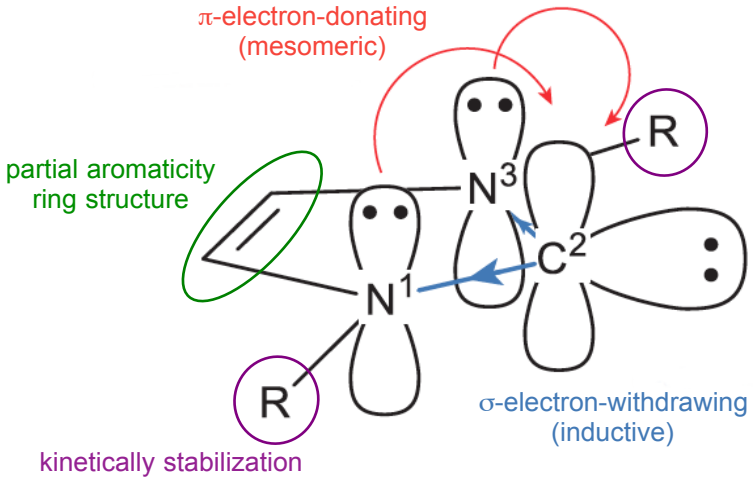

Figure 3. A representative carbene, where R is an alkyl or aryl substituent, N the nitrogen atoms and C the carbene carbon centre. All the features that make the NHC a stable compound are here summarised: the inductive and mesomeric effect of nitrogen atoms; the partial aromaticity due to the backbone; the kinetic stabilization by hindered R groups; the ring size, which forces the carbene centre to a bent form.

Concerning the R substituent on the heteroatoms, bulkier functional groups allow a kinetic-stabilization of the NHC, avoiding the dimerization into the olefin: this phenomenon is known as Wänzlick equilibrium.

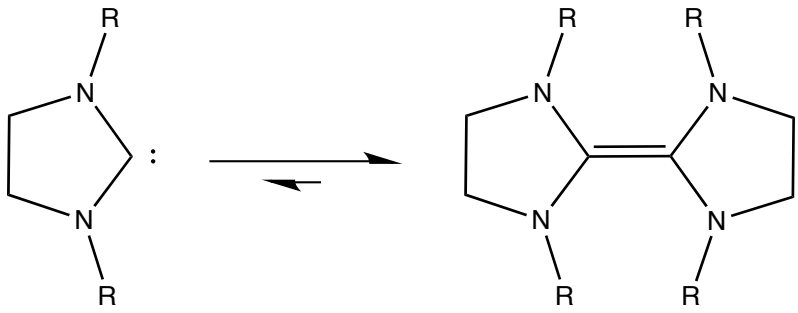

Scheme 3. The Wänzlick equilibrium involves the free carbene (on the left) and its corresponding dimer, an olefin (on the right). The equilibrium is far to the right.

The NHCs are stable to air, but they must be stored under argon atmosphere due to hydrolysis. Water reacts with NHC by cleavage of C-N bond, yielding acyclic products.[30] These properties are general and apply to all NHCs, even though there are little variations due to the specific kind of compound. (Figure 4)

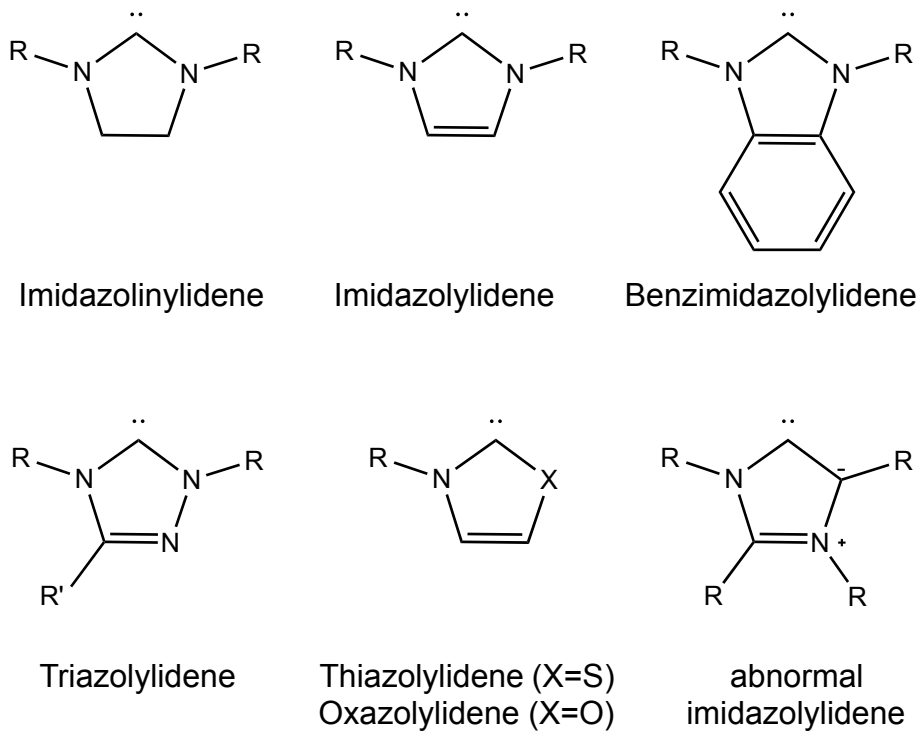

Figure 4. Some of the most common carbenes that have been applied in coordination chemistry and catalysis. R is any alkyl or aryl group.

Electronic and steric properties.

The electronic configuration of NHCs allows us to understand their properties: the lone pair lying on the ring plane makes the NHC a good ligand, which implies strong σ-donor ability. Therefore, NHCs provide a good alternative to the well-known phosphines. Both of them are sterically and electronically tunable, but with strong differences.

In phosphines, the R substituents are directly linked to the donor atom (P), thus a change on the R groups will change both the steric and electronic properties. Conversely, in the NHC, the R groups are far away from the donor central atom (C), having strong effects on the steric properties but a limited influence on the electronic properties. Changes of the electronic properties are usually obtained by modifying the nature of the ring.[31]

As for the phosphines, also with NHCs it is possible to quantify the electronic and steric properties with two parameters:

I. The Tolman electronic parameter (TEP)[32] allows one to quantify the donor ability of the ligand, by measuring the stretching frequencies of carbonyl ligands in some model metal carbonyl complexes. The more electron donating the ligand, the more electron-rich will be the metal centre, then the stronger will be the π-donation to

the carbonyl empty orbitals, weakening the order of the C-O bond. These modifications are measured by infrared spectroscopy. A lot of data have been collected and are available for several NHCs.[33,34] In general, NHCs are stronger σ-donors than phosphines, this reflects the strong and robust NHC-metal bond in organometallic complexes.

II. The buried volume parameter ($\%V_{bur}$)[35] allows to quantify the steric properties and it can be considered as the Tolman's cone angle for phosphines. The $\%V_{bur}$ is the part of the sphere, centred on the metal atom, occupied by the NHC ligand upon coordination. The larger the $\%V_{bur}$, the bigger the steric influence of the ligand on the metal centre. Comparing NHCs to phosphines, phosphine substituents are best described as a cone-shaped spatial arrangement, whilst in NHCs they point towards the metal centre in a fan- or umbrella-shaped arrangement, protecting the metal.

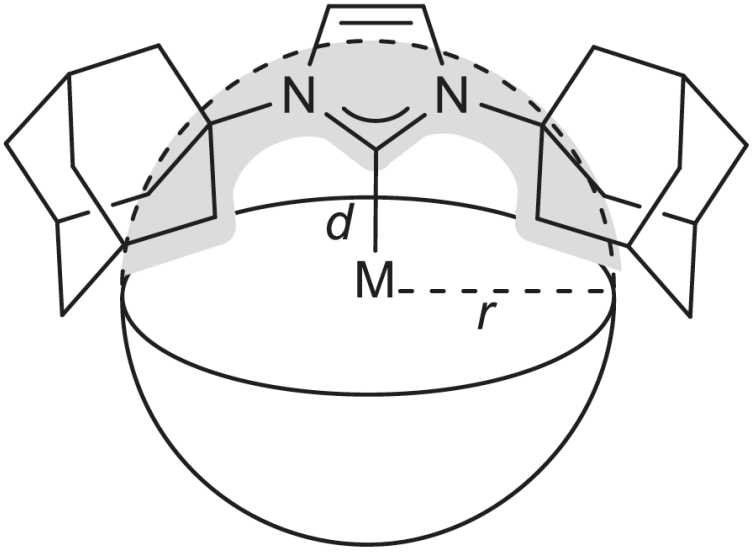

Figure 5. The buried volume of NHC. The M indicates the metal centre, whilst the N the nitrogen atoms. The common parameters are 2Å for the carbene-metal distance d and 3Å for the sphere radius r.

Both electronic and steric features of NHCs make the resulting metal complexes more thermally and oxidative stable compare to the phosphine-metal compounds.[36]

Precursor synthesis.

NHCs are interesting not only for their properties but also for their accessibility starting from imidazole, followed by deprotonation by means of a strong base (eg. Potassium HexaMethylDiSilazide, KHMDS). NHCs are derived from imidazolium salts, which can

be easily synthesized and several routes are shown below (Scheme 4).[37]

- The straightforward one-pot reaction involving glyoxal, primary amine and formaldehyde yields symmetrical imidazolium (R_1, R_1) (eq.1).
- In order to get unsymmetrical imidazolium (R_1, R_2), a variation of the first route involves cyclization of glyoxal, primary amine, aldehyde and ammonium chloride, followed by alkylation of the mono-substituted imidazole by alkyl-/aryl- halide (eq.2).

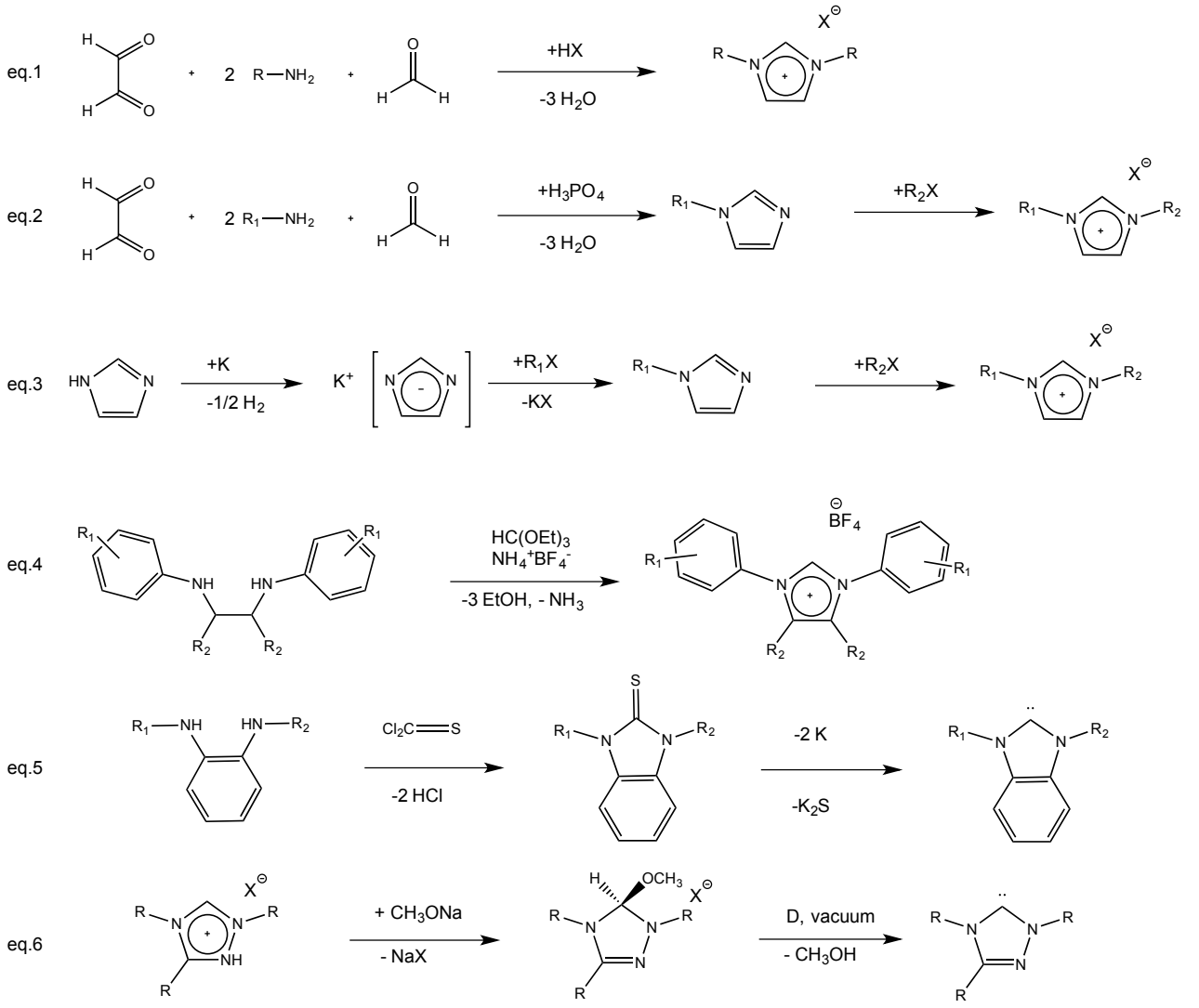

Scheme 4. Various reaction routes to imidazolium salt (eq.1-4) and carbenes (eq.5-6). The R indicates any alkyl or aryl groups, and X is a halogen atom.

- The alkylation of imidazolide anion by different alkyl-/aryl- halides, is another route to get unsymmetrical imidazolium (eq.3).
- The 1,2-diamines, reasonably accessible compounds, can be converted to the corresponding imidazolium salts by treatment with orthoformate (eq.4).

- Desulfurization of thiourea yields the corresponding carbene. The reaction needs harsh conditions, though it works well for some compounds (eq.5).[38]
- Methoxy imidazolium derivatives undergo vacuum pyrolysis and yield the corresponding ylidenes in good yields (eq.6).

The nature of Metal-NHC bond

NHCs act as 2 electron σ-donor neutral ligands and they strongly coordinate to metal leading to relatively stable NHC-metal complexes. The most useful methods to prepare these metal complexes are shown below.

a. Reacting the free stable carbene with metal complexes.
b. Reacting the imidazolium salt precursor with a metal compound bearing ligand acting as a base.
c. Reacting silver oxide (Ag_2O) with the imidazolium salts yields the corresponding silver(I)-carbene complex, which is a special NHC-transfer reagent[39] to other transition metals. This last route can be really useful in case of functionalized imidazolium salt with sensitive substituents.

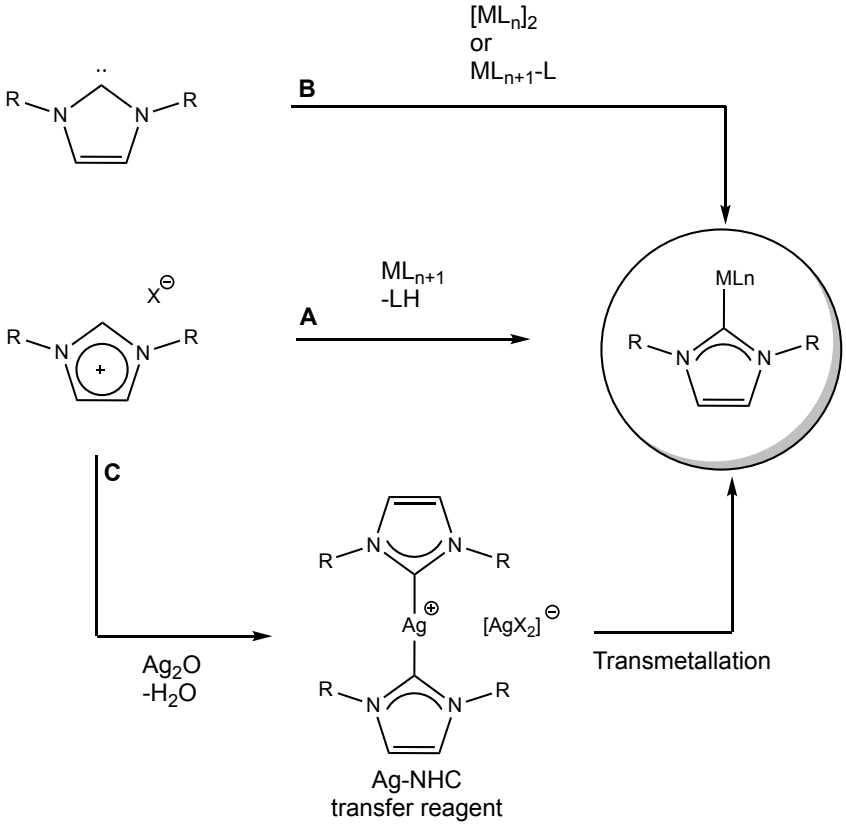

Scheme 5. The most common methods to prepare NHC-metal complexes. Ln, ligand, X, halogen, R any alkyl or aryl groups.

Several X-ray structures of metal carbenes are now available. A big difference between a conventional carbene and an NHC is the M-C^2 bond distance, which is longer (>210 ppm) in the classical ones and lower in NHCs (<200ppm); this is due to the back-bond character of the NHC and reflects the possibility of rotation around the M-C^2 bond axis, depending on the steric environment. Indeed, as shown in Figure 5,[40] the NHC is not a simple σ-donor, but the three orbital contributions in bonding involve also a π-NHC to d-M donation and a d-M to π*-NHC backdonation.

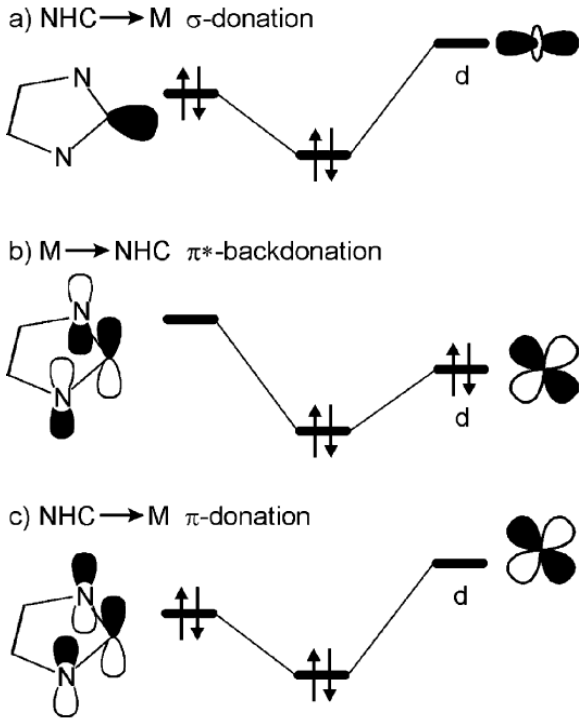

Figure 6. The three different contributions of NHC-M bond. a) sigma donation from carbene to metal centre; b) π-backdonation from d-orbitals of the metal to the π* of the carbene; c) π-donation from π fo carbene to the d-orbitals of the metal.

NHC binds strongly to metal centre. Indeed, it has been demonstrated by DFT[41] that M-CX_2 bond is about 44-45 kcal·mol^{-1}, far more than M-PR_3 bond, which is about 25-37 kcal·mol^{-1}. This bond prevents ligand dissociation in metal catalysts even in harsh conditions (eg. high temperatures, strong pH). In addition, versatility in synthesis of NHC might be a big advantage in many applications (Scheme 6)[38]: chirality, immobilization on solid support, water solubility of hydrophobic starting compounds, functionalization on the alkyl chain and chelate effect on metal centre.

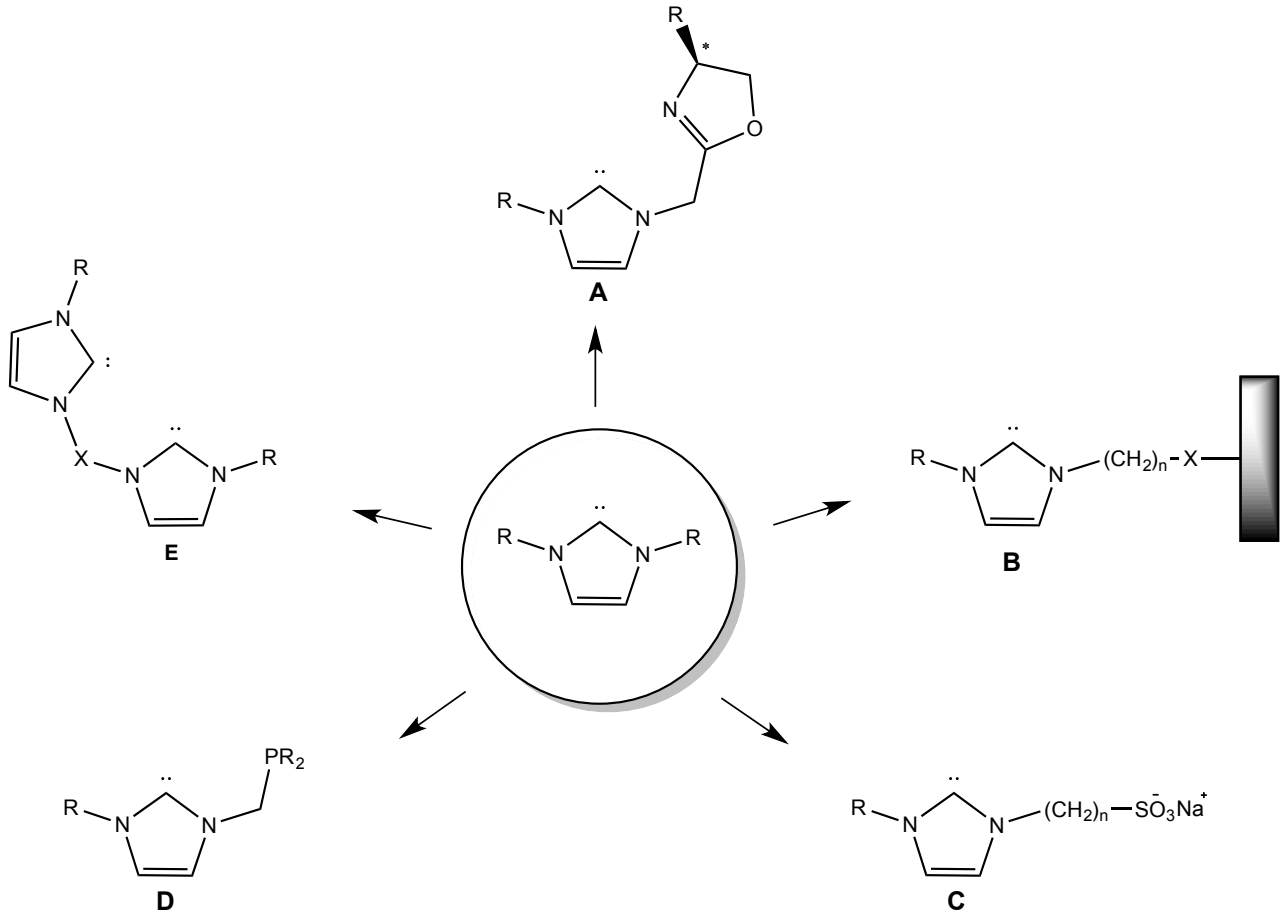

Scheme 6. Attractive features of NHC as ligands for organometallic compounds: a) chirality, b) immobilization, c) water solubility, d) functionalization and e) chelate effect. R, alkyl or aryl groups.

Catalysis.

The organometallic catalysis is a powerful tool, finding increasing application in the industrial production of fine and pharmaceutical chemicals. Transition-metal catalysts play an important role in the development of green chemistry, which involves less energy consumption and lower waste production by means of chemical reactions with high atom efficiency. Most of the processes have been, so far, mediated by catalysts based on noble metals such as: rhodium, iridium, palladium and ruthenium. In last decades, due to their limited availability, toxicity and price, there is a growing interest in replacement with more environmental benign, less toxic, bio-relevant and more available metals. In this respect, iron complexes and salts are among the most interesting.

Since 2004, when Bolm[42] reviewed the iron catalysis and its application in several fields, the development of new catalysts based on iron has undergone a drastic increase.

Herein, are reported applications of iron complexes in selected catalytic reactions, which are of interest for the scope of this thesis.

Transfer hydrogenation.

Hydrogenation is one of the most important catalytic reaction for industrial application, and generally involves the use of high pressure H_2 gas. Another strategy is the transfer hydrogenation (TH), in which hydrogen addition comes from a non-H_2 hydrogen source, as 2-propanol. The TH[43] is an attractive alternative to hydrogenation due to four main reasons:

I. It does not require the use of elaborate experimental setup or high hazardous H_2 pressure;
II. Hydrogen donors are usually easy to handle and not expensive;
III. The side products might be recycled;
IV. The catalyst involved in the catalytic cycle are usually not sensitive and readily available.

The first hydrogen transfer reaction was achieved by Knoevenagel[44] in 1903: the disproportion of dimethyl 1,4-dihydroterephtalate into dimethyl terephatalate and *cis*-hexahydroterephtalate, involving identical donor and acceptor units.

The first TH of carbonyl compounds is the Meerwein-Ponndorf-Verley (MPV)[45,46] reduction described in 1925: a ketone was hydrogenated to the corresponding alcohol in the presence of a secondary alcohol as a hydrogen donor and of aluminium alkoxide. Later, other metals such as zirconium, ytterbium, cerium, lanthanium and samarium have been reported.[47] The MPV mechanism goes through a six-membered ring intermediate (Scheme 7), in which the reducing alcohol and carbonyl compound are coordinated to the same metal atom.

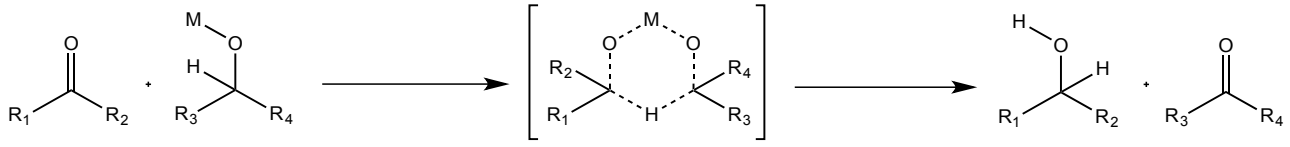

Scheme 7. The MPV six-membered ring intermediate allows the hydrogen transfer from a secondary alcohol to a ketone. R, any alkyl group.

A decisive finding in TH was the use of late transition-metal catalysts involving groups 8 to 11. One of the most famous examples is the asymmetric TH reported by

Noyori,[48,49,50] that is of high value in pharmaceutical and drugs industry. His contributions to the field earned him the Nobel Prize in 2001.[51]

Mechanistic studies on metal-based TH, involving a ketone as model substrate, demonstrated two possible mechanisms: inner-sphere and outer-sphere.

I. In the inner-sphere mechanism, the substrate must coordinate to the metal centre by insertion into a M-H bond. The new metal-alkoxide is then protonated by an external hydrogen source, followed by releasing of the corresponding alcohol product.

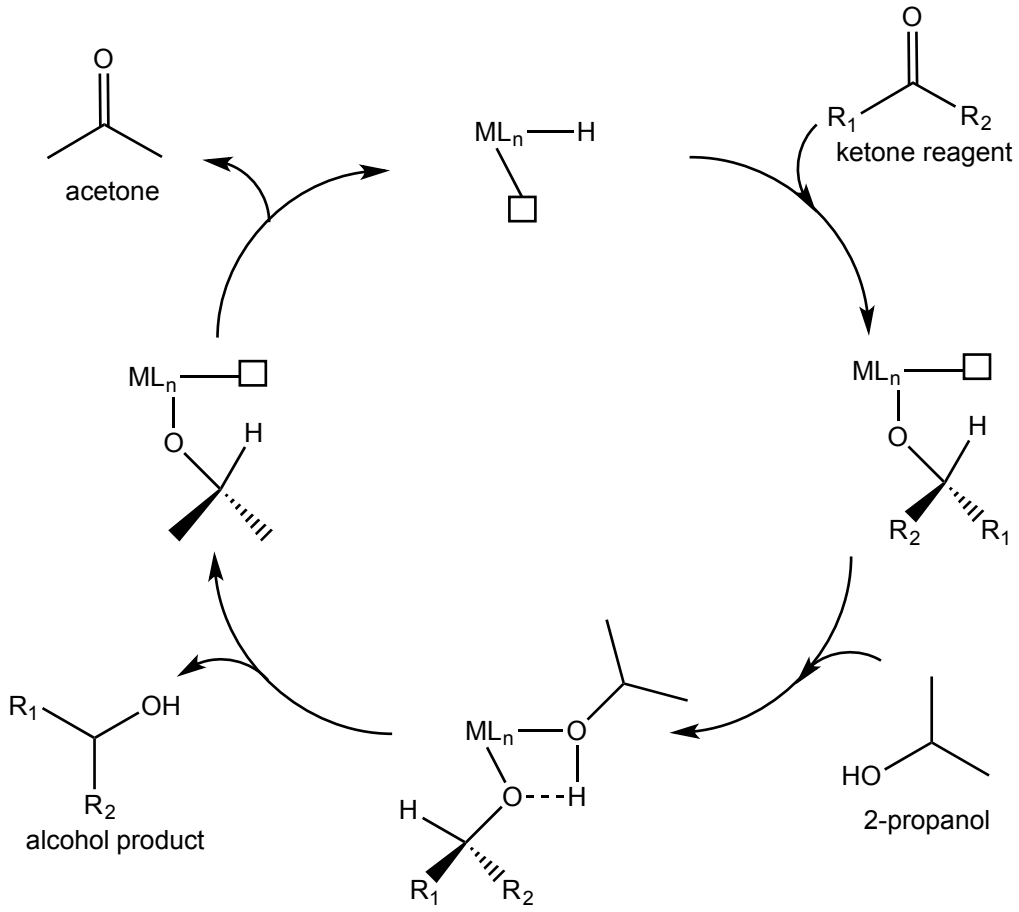

Scheme 8. Inner sphere mechanism with 2-propanol as reducing reagent. The reagent coordinate to the metal in order to perform the transformation. R, alkyl or aryl group; L_n, ligand.

II. In the outer-sphere mechanism, no substrate coordination is involved, and both a basic site, usually a nitrogen in one ligand, and an acidic site, the metal centre, should be present. The basic ligand allows deprotonation of the hydrogen source (eg. a secondary alcohol) with simultaneous hydride transfer to the metal atom. Then, a simultaneous H^+/H^- transfer from the catalyst to the ketone yields the corresponding alcohol product.

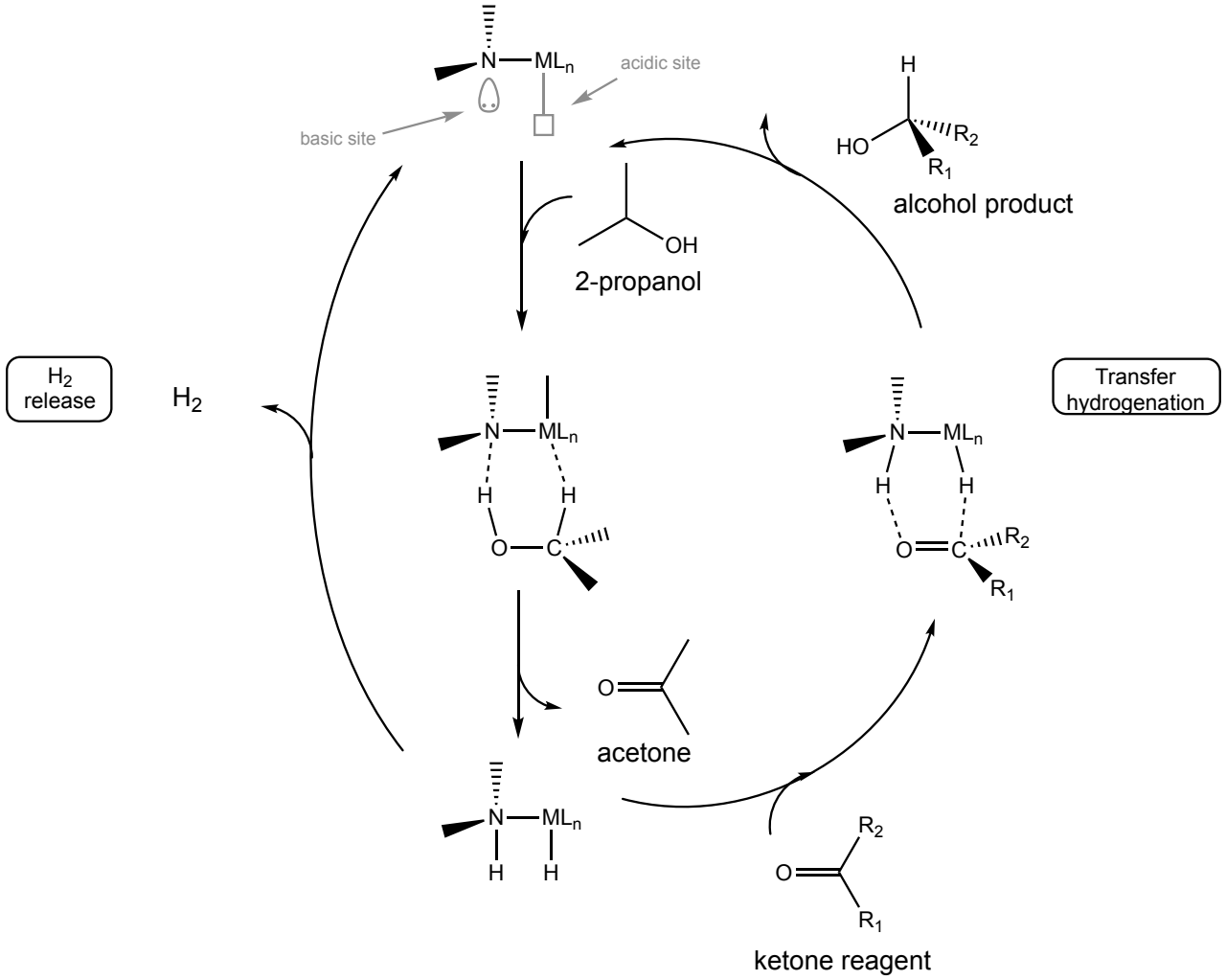

Scheme 9. Outer sphere mechanism with an amido-metal complex and 2-propanol as reducing reagent. R, alkyl or aryl groups; L_n, ligand.

Several hydrogen sources have been employed through the years, but only 2-propanol and formate are now exploited due to their low cost. Up to now, many noble metal-based catalysts have been reported such as ruthenium, rhodium, iridium and palladium; only in last years, iron analogues have been described as greener alternative TH-systems.

Iron-based TH

In the 1990s Bianchini et al.[52] reported an interesting example of chemoselective reduction of α,β-unsaturated ketones. The corresponding alcohols were obtained with good selectivity in the presence of the non-classical trihydride iron complex **Fe1** and a mixture of 2-propanol and dioxane. Noteworthy, no base addition was needed in presence of **Fe1**, but the reaction was affected by the bulkiness of the R substituents.

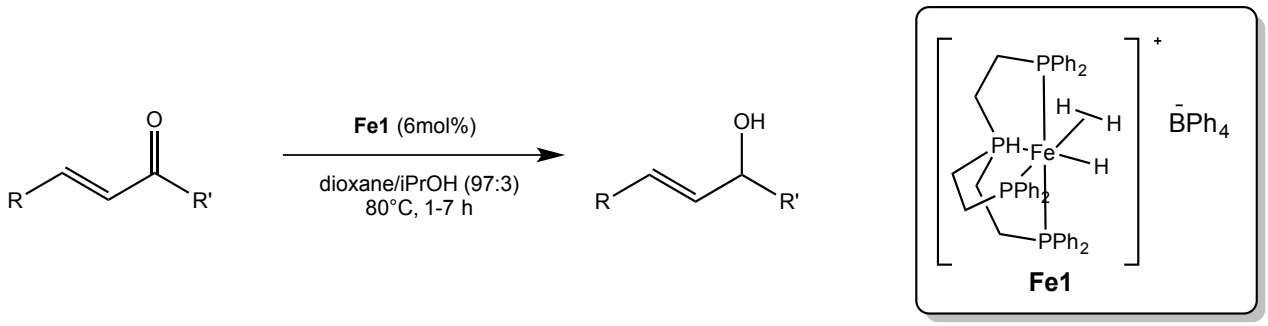

Scheme 10. Transfer hydrogenation of trihydride **Fe1**, described by Bianchini.

In 2006 the group of Beller[53] reported a general TH for aliphatic and aromatic ketones applying the three component catalyst made of $Fe_3(CO)_{12}$, 2,2':6',2"-terpyridine (terpy) and triphenylphosphine (PPh_3). The reaction required a strong base and the best results were obtained with ^{i}PrONa and ^{t}BuONa. Mechanistic and spectroscopic investigations revealed incorporation of deuterium in acetophenone when 2-propanol-*d*$_1$ was employed as reducing agent: this result was in agreement with a monohydride pathway from the donor molecule to the substrate. In parallel, a similar three component catalyst with a bio-mimetic porphyrin system was developed.[54] The porphyrin complex was inert toward oxygen and moisture, less base-dependant and displayed higher activities than the previous iron system.

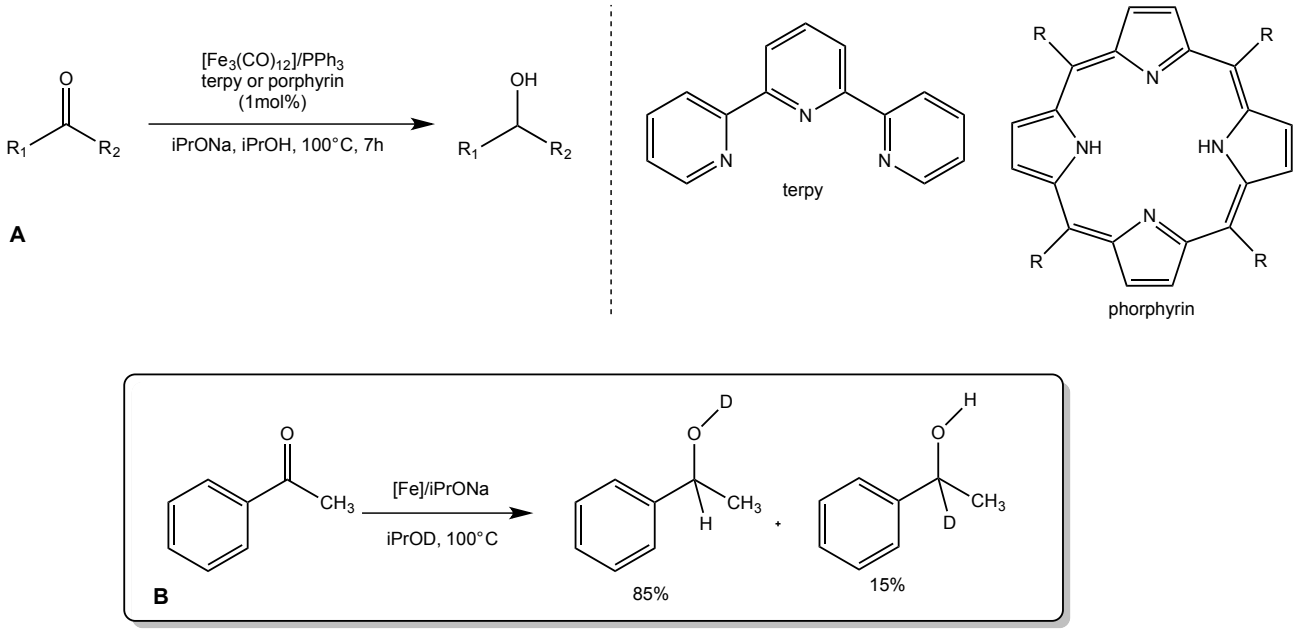

Scheme 11. A) The iron system developed by Beller et al. with a terpy ligand and its bio-mimetic porphyrin evolution. B) Deuterium incorporation in acetophenone model experiment. R, alkyl or aryl.

In 2007, Casey and Guan[55] discovered the catalytic application of the well-defined Knölker complex **Fe2** in hydrogenation of carbonyl derivatives under mild conditions.

They also explored **Fe2** as catalyst in TH of acetophenone. Intramolecular trapping experiments[56] supported a concerted transfer of proton from the hydroxyl group and a hydride from the iron centre to aldehydes. The catalyst displayed good functional group tolerance and chemoselectivity.

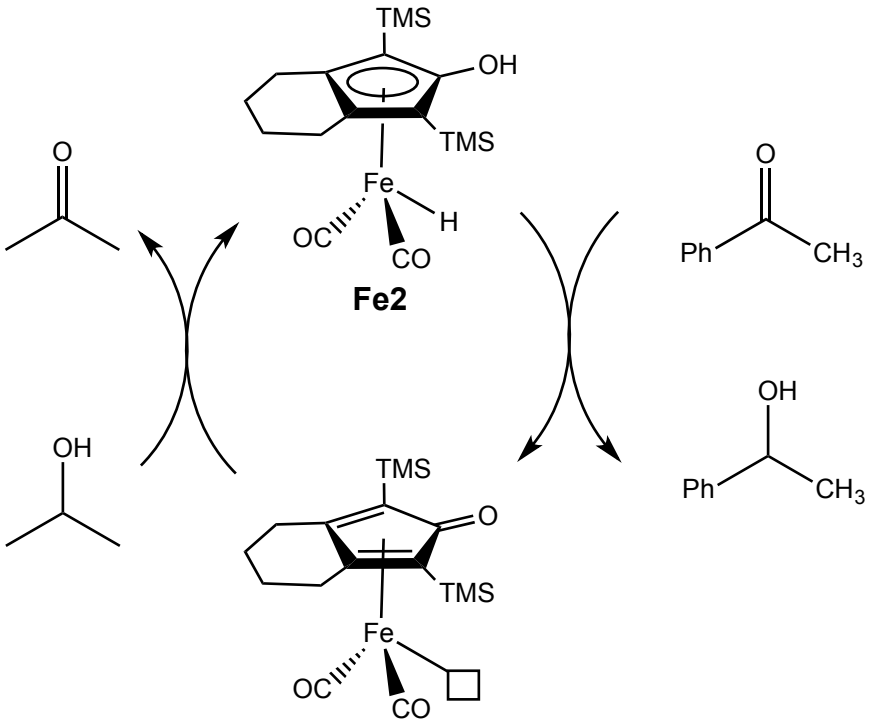

Scheme 12. The Knölker complex performing TH of acetophenone with 2-propanol as donor agent.

In 2010 Morris et al.[57] prepared a series of iron pre-catalysts containing different substituted tetradentate diiminodiphosphine (PNNP) ligands: all of them displayed good activity in TH of acetophenone with KO^{t}Bu and 2-propanol under mild conditions. It was noted that the size of the substituents in the backbone of the ligands influenced the activity of the catalyst, indicating that electronic and steric properties were tunable. The group of Morris reported the five coordinate catalyst **Fe3**, resulting from a double deprotonation of the PNNP ligand.[58] The **Fe3** displayed high activity toward acetophenone with 0.5mol% loading and without any base addition. Afterwards, complexes **Fe4** and **Fe5** were synthesized containing a partial reduced PNNP ligand with both amine and imine functionalities.[59,60] These two iron compounds are two of the most active catalysts known for asymmetric TH of polar double bonds of ketone and imines, without an activation period. Catalyst **Fe5** was capable of reducing ketones to alcohols within 10 seconds and imines to amines in about 3 minutes with high TOFs, TONs and ee.

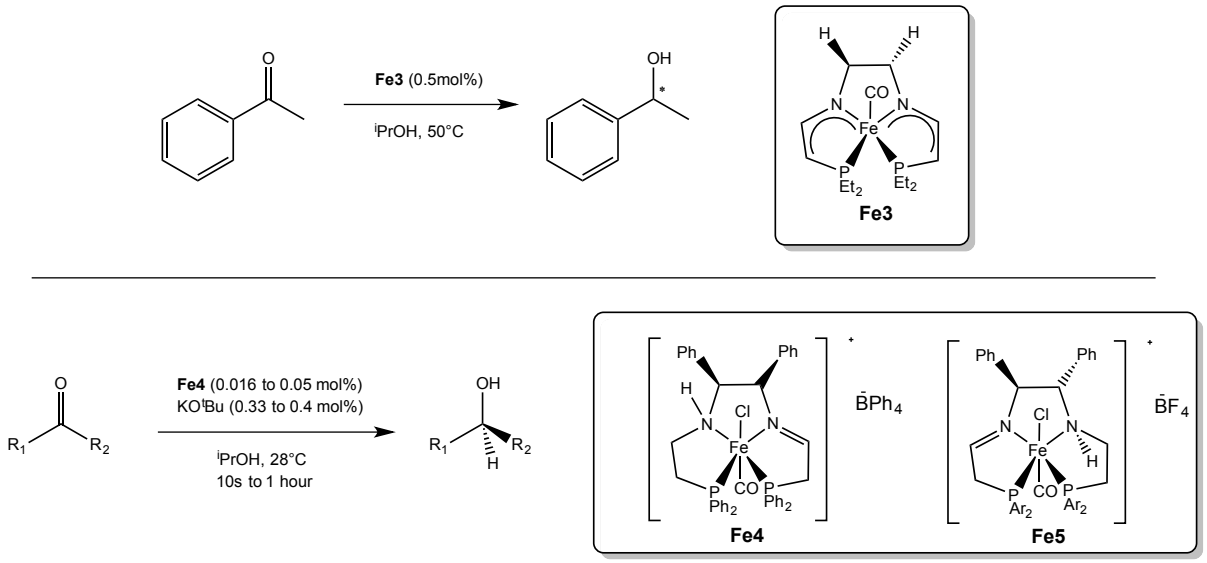

Scheme 13. PNNP iron complexes described by Morris. BPh_4,tetraphenylborate ;BF_4, tetrafluoroborate; Ph, phenyl; Ar, aryl; Et, ethyl.

Concerning PNNP type catalyst, in 2011 Beller et al.[61] first reported the iron mediated asymmetric TH of imine to amine. The catalyst was easily accessible in situ from the precursor $[Et_3NH][HFe_3(CO)_{11}]$ and obtained in high yield and selectivity.

Furthermore, since the discovery of the first stable NHC by Arduengo,[27] a series of NHC-Fe complexes were obtained and employed in TH of carbonyl derivatives. The group of Peris and Royo[62] described cyclopentadienyl-functionalised NHC iron complexes **Fe6** and **Fe7** for TH of aromatic ketones and cyclohexanones. Both complexes displayed good reactivities with 1mol% Fe loading with KOH and 2-propanol; **Fe6** was active also in hydrosilylation reaction. Glorius et al.[63] reported the tetrahedral NHC complex **Fe8** and the square-planar complex **Fe9**, which has been obtained upon replacement of chlorides by methyl groups. Both **Fe8** and **Fe9** were active in TH of 2'-acetonaphthone with only 0.1mol% catalyst loading and lithium isopropoxide.

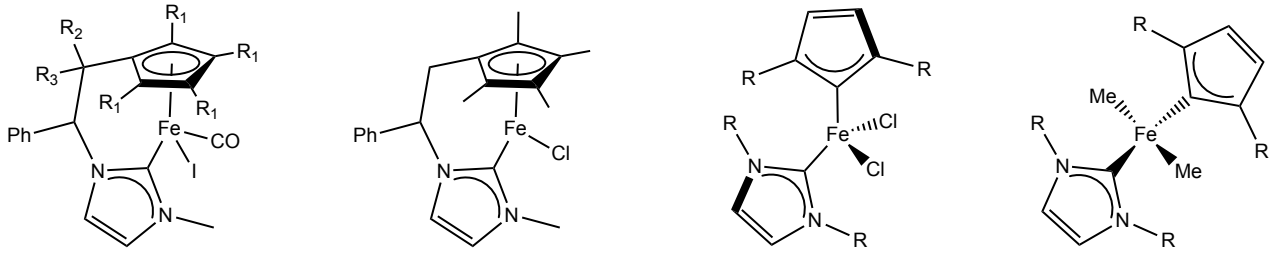

Fe6a, R_1= CH_3; R_2, R_3 = H
Fe6b, R_1= H; R_2, R_3 = Ph
Fe6c, R_1 = CH_2Ph; R_2 = Ph, R_3 = H

Fe7

Fe8a, R = Mes
Fe8b, R = (R)-1'-EtPh

Fe9

Figure 7. NHC-Fe complexes described by Peris, Royo and Glorius. **Fe6**, **Fe8** and **Fe9** were also active in hydrosilylation reaction. Ph, phenyl; R, alkyl or aryl.

Iron complexes not only have been used for TH of polar double bonds, but also of non-polar compounds as alkynes, alkenes and nitroarenes. Beller's group[64,65] described the TH of alkynes and nitroarenes to alkenes and anilines, employing a catalyst generated *in situ* from $[Fe(BF_4)_2 \cdot 6H_2O]$ and tris[(2-diphenyl-phosphino)-ethyl]phosphine (PP_3), using formic acid as reducing agent. The reaction showed excellent yields under mild conditions without any base.

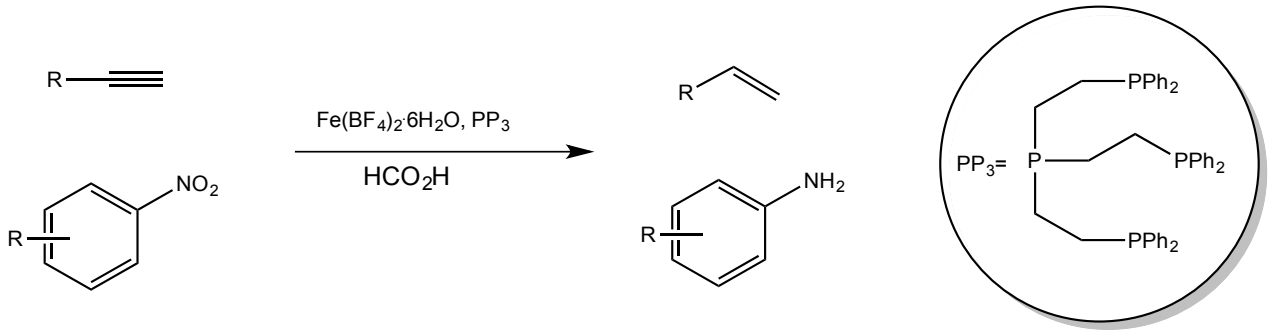

Scheme 14. Beller's transfer hydrogenation of non-polar triple/double bonds.

Ammonia-borane dehydrocoupling.

Hydrogen (H_2) has been proposed as valuable energy vector, alternative to traditional hydrocarbon fuels to sustain the global socioeconomic changes, (so called hydrogen economy). However, two major points have to be addressed: the generation of hydrogen from renewable resources and its storage. Hydrogen is indeed hazardous to handle (due to possible explosions) and to transport, so a possible solution is to store H_2 in chemical compounds easy to handle and that can easily release H_2 on demand. One approach is the use of hydrogen rich B-N species, such as ammonia-borane (BH_3NH_3, AB).[66] AB contains up to 19.5 wt % H_2 and is stable under standard conditions. These species have both protic (N-H) and hydridic (B-H) hydrogens, which can easily form hydrogen bonds due to opposite polarity. This particular bond makes the thermal decomposition of AB with H_2 release happen at low temperatures (< 100°C); in addition, the H_2 released is pure, but traces of borazine byproduct might be present. However, thermal decomposition is unsuitable for practical uses.

Another route to H_2 release is the metal-catalysed dehydrocoupling of AB mediated by metal-based catalysts. These catalysts are able to tune both the rate and extent of H_2 loss and to lower the H_2 release temperature. Commonly employed catalysts are metal

hydride complexes both classical [$ML_n(H)_x$] and non-classical [$MLn(\eta^2\text{-}H_2)_x$]. Indeed, the polarization of metal-hydrogen bond is a good starting point for AB interaction.

Interaction with metal centre and AB might begin with B-H bond, N-H bond or simultaneous N-H/B-H bond activation. A metal complex with an empty coordination or with two active hydrogen atoms with different polarity (that is a proton and a hydride), can undergo the simultaneous B-H and N-H bond activation (Scheme 14, A). A metal complex bearing both acidic M-$H^{\delta+}$ and basic M-$H^{\delta-}$ is known as bifunctional catalyst. Metal complexes with different nature of M-H bond (i.e. acidic or basic hydride) will interact preferentially with BH_3 or NH_3 moiety (Scheme 14, B). After the first interaction depending on the kind of metal-hydride complex, a first equivalent of H_2 is released and boryl- or amido-metal complex is formed, which can undergo a second dehydrogenation to produce another equivalent of H_2 and amino-borane (BH_2=NH_2, known as "inorganic ethylene"). This monomer is highly unstable and reacts in solution to for linear or cyclic products such as cyclotriborazane (CTB) and B-(cyclotriborazanyl)aminoborane (BCTB). When the dehydrogenation extent is higher (two equivalent or more of H_2), these intermediates are then converted into borazine (benzene analogue) and polyborazylenes as final products. Metal complex with an unsaturated coordination (Scheme 14, C), might react with BH_3 in a η^1 or η^2 bond formation, which is followed by loss of NH_3 with borohydride complex formation or by loss of H_2 and amino-borane as byproduct.

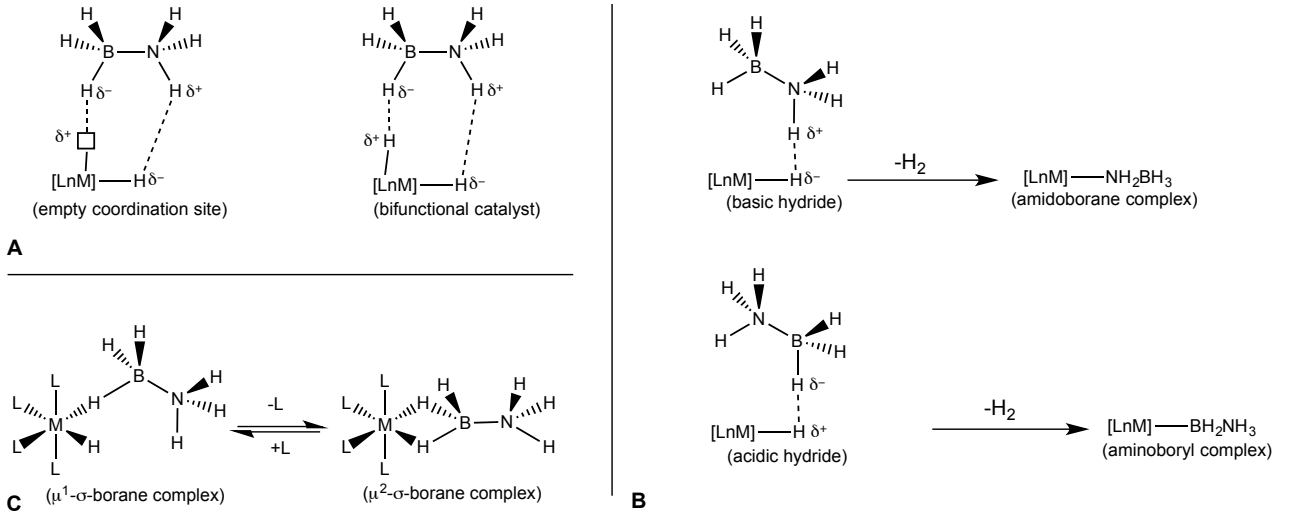

Scheme 15. Metal-ammonia-borane interactions depending on the nature of metal catalyst. A) bifunctional; B) Basic or acidic hydride-metal bonds; C) coordinative saturated metal complex.

The B-N polymer obtained in the dehydrogenation of AB (usually the last products) might be of interest for ceramic and inorganic polymer materials. Their structure and synthesis were studied by the groups of Manners and Baker.[67] In general, if up to one equivalent of H_2 is released, linear polyaminoboranes $B_xN_xH_{4x+2}$ or cyclic products $B_xN_xH_{4x}$ might be formed. If two equivalents of H_2 are produced, borazine $B_3N_3H_6$ is the final byproduct of the reaction. When more than two equivalents of H_2 per AB moiety are released, the condensation of borazine rings lead to cross-linked-borazine or polyborazylene BNH_x (with x>2).

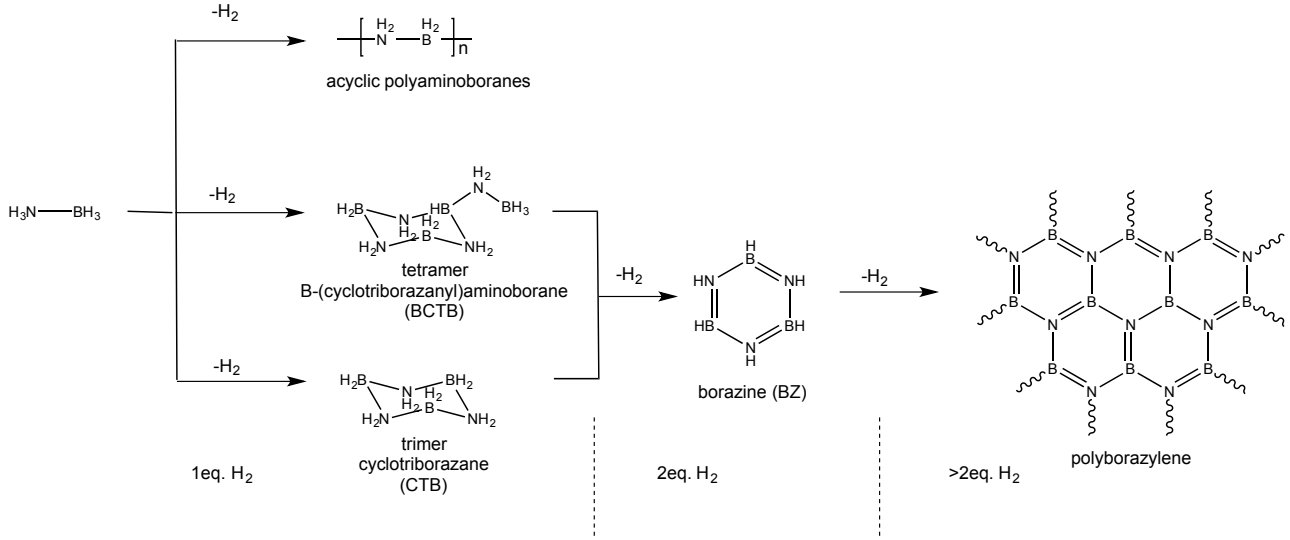

Scheme 16. Major byproducts of AB dehydrogenation. Depending on the extent of hydrogenation, different selectivities can be achieved.

The organometallic catalysts for AB dehydrogenation might be divided into two classes[68] depending on their behaviour and final byproducts:

I. Type I, they release up to one equivalent of H_2 per AB moiety and produce mainly insoluble linear polyaminoboranes;
II. Type II, they release more than one equivalent of H_2 and have borazine or polyborazylenes as products.

The two types of catalyst can be divided on the basis of a chemical trapping experiment proposed by Baker et al.[69]: addition of cyclohexene to reaction mixture that is hydroborated by the free aminoborane monomer (NH_2BH_2). In type I catalyst, the rate and final products of reaction are not affected by addition of cyclohexene, then suggesting that free NH_2BH_2 is not available in solution for trapping but it might be rapidly consumed by the metal complex-based polyaminoborane-chain formation. On the other hand, in type II mechanism, the free NH_2BH_2 released by catalyst is readily

entrapped, leading to only hydroboration products (Cy_2BNH_2). However, whether a metal-based catalyst will behave as type I or II might depend also on experimental conditions such as temperature and solvent.

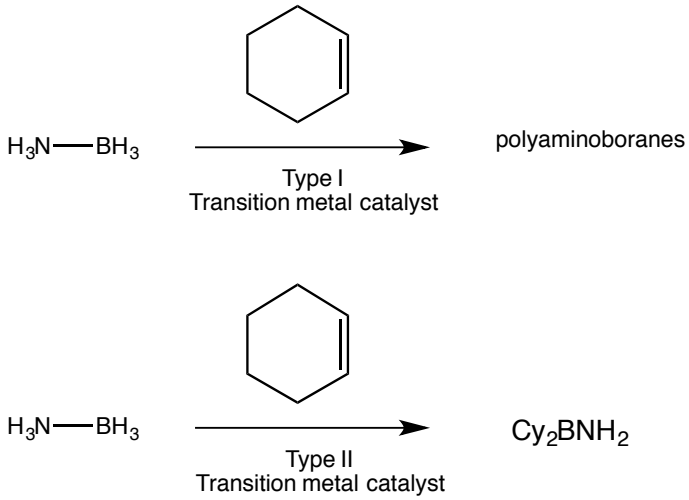

Scheme 17. Discrimination of Type I and II catalyst by trapping experiment proposed by Baker.

Iron-based catalyst.

Only recently, a handful of iron-based complexes have been reported in the dehydrocoupling of ammonia-borane.

In 2012 Baker et al.[70] described four iron complexes bearing a mix of amido and phosphine supporting ligands. **Fe10** and **Fe11** released about 1.7 equivalents of H_2 per AB, but they decomposed and were not recyclable; whilst **Fe12** containing a bidentate P-N ligand was more robust and re-usable for a second-cycle. The symmetric analogue of **Fe12**, **Fe13**, produced only insoluble linear polyaminoboranes $(NH_2BH_2)_n$ at very mild conditions (room temperature in a few minutes). In their work they pointed out that a possible explanation to the different behaviours (increase of rate vs. extent of H_2 release) is reduction from Fe(II) to soluble Fe(0) species, which further dehydrogenate ammonia-borane byproducts.

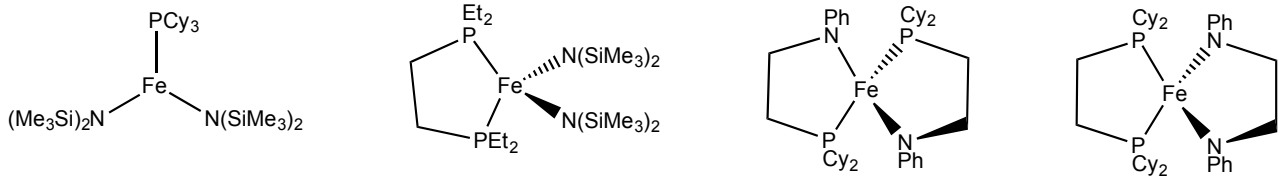

Fe10
1.5-1.7 eq. H_2

Fe11
1.2 eq. H_2

Fe12
1.3-1.5 eq. H_2

Fe13
1 eq. H_2

Figure 8. A series of amido and phosphine iron complexes described by Baker.

In 2014 Manners[71] reported two carbonyl iron compounds **Fe14** and **Fe15**, which were both active in the dehydrogenation of AB under UV irradiation. First experimental studies, performed with Me_2NHBH_3, revealed that **Fe14** proceeded via aminoborane $Me_2N{=}BH_2$ intermediate, which cyclodimerized in solution. Instead, **Fe15** proceeded via a $Me_2NH\text{-}BH_2\text{-}NMe_2\text{-}BH_3$ intermediate, affording then the same cyclic product by means of a metal-mediated step. Mechanistic studies performed by the groups showed two different pathways: **Fe14** gave rise to an heterogeneous catalyst, since iron(0) nanoparticles were found in solution; **Fe15** was an homogeneous catalyst involving the $[CpFe(CO)]^+$ as a key intermediate.

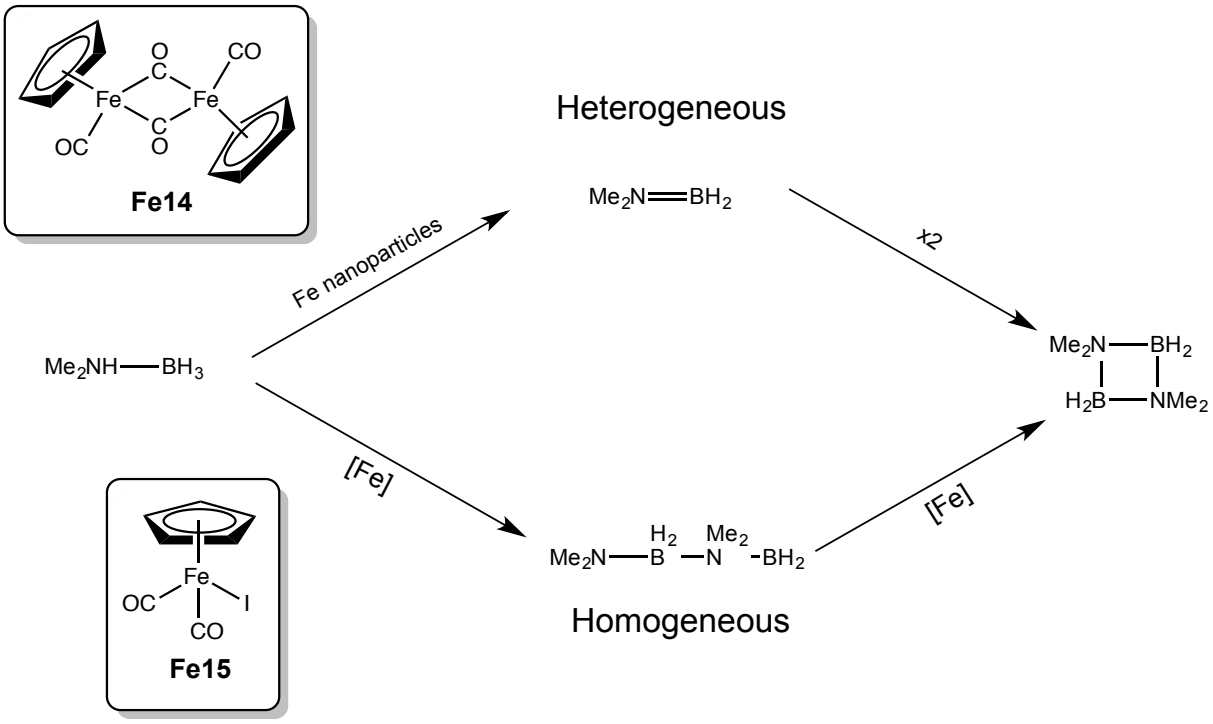

Scheme 18. Manners iron complexes different behaviours under UV irradiation. Homogeneous vs. heterogeneous pathways.

In the same year, Guan and co-workers[72] described a series of well-defined bis(phosphinite) iron (II) POCOP complexes. All complexes were found to be active in the dehydrogenation of AB, among which **Fe16** was the best, and the most active iron system in term of rate and extent of H_2 release. Indeed, **Fe16** released up to 2.7 equivalents of H_2 in 24 hours with borazine and polyborazylenes as byproducts. NMR and KIE experiments suggested an involvement of the "non-innocent" pincer ligand with a bifunctional-type mechanism: a first phosphine dissociation step is followed by a simultaneous transfer of H^+ to the pincer *ipso* carbon and H^- to iron.

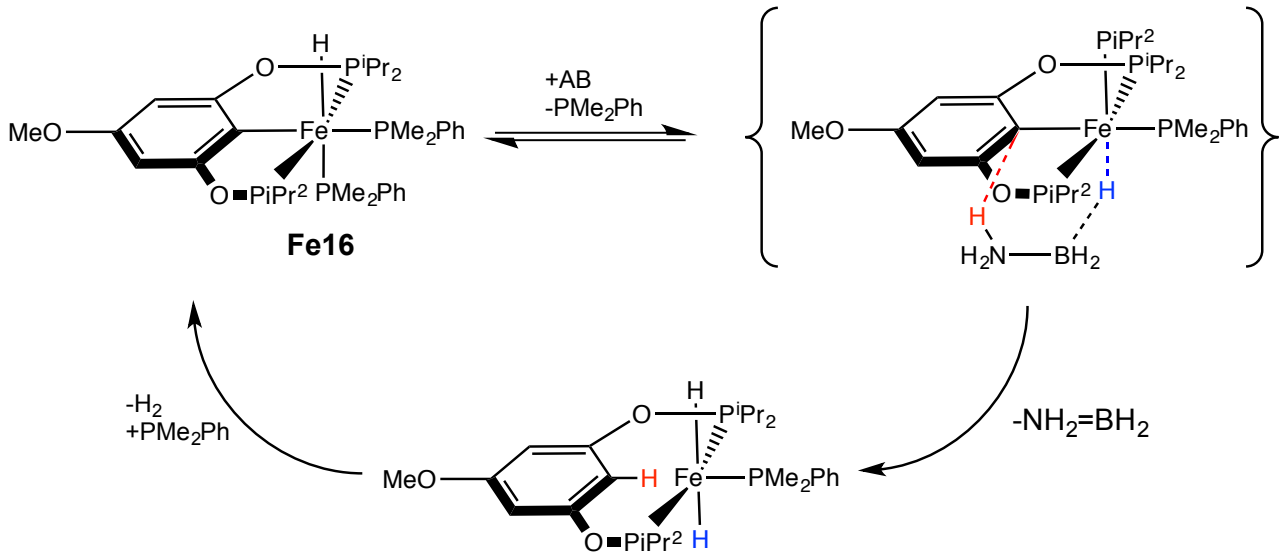

Scheme 19. The iron(II) POCOP complex is able to release up to 2.7 eq. of H_2. In the proposed mechanism described by Guan, the Fe-C(ipso) is involved in the cycle.

In 2015, the group of Schneider showed the five-coordinated PNP-iron complex **Fe17** to release 1 equivalent of H_2 with formation of insoluble linear polyaminoboranes. Mechanistic studies suggested that catalyst deactivation proceeds via reaction with free BH_3 to a give an in borohydride complex; hence, addition of a bulky amine in solution resulted in high TON (330 with 0.05mol% of catalyst loading) for a well-defined iron complexes with release of 1 equivalent of H_2. Furthermore, **Fe17** is a bifunctional catalyst, with the involvement of N atom of non-innocent PNP ligand.

Again in 2015, the iron(II) trimethylphosphine hydride **Fe18** was employed by Baker et al.[73] in dehydrocoupling of AB and the soluble BCTB was isolated for the first time as key intermediate in the formation of borazine and polyborazylenes.

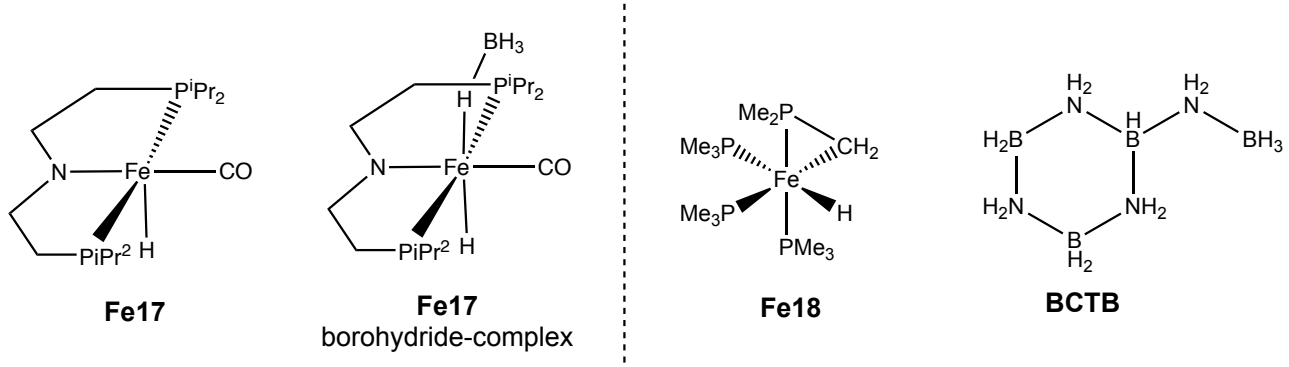

Figure 9. On the left, Schneider's PNP iron precatalyst **Fe17** and its deactivated borate-complex. On the right, the **Fe18** employed by Baker et al. in the identification of BCTB as key intermediate.

Webster et al.[74] recently described the iron(II)-β-diketiminate complex **Fe19** as good catalyst for dehydrocoupling of both phosphine- and amine-boranes at room

temperature with 1mol% of compound. In mechanistic studies with Me_2NBH_3 they were able to isolate an iron-chairlike complex, identified as catalyst resting state.

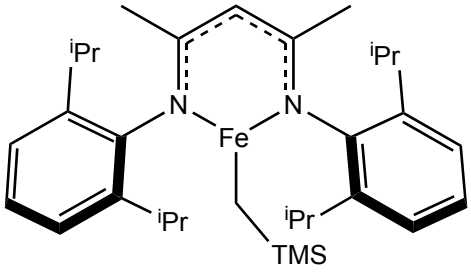

Fe18

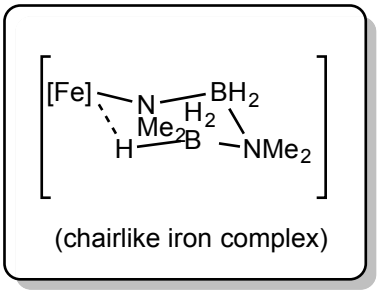

Figure 10. Fe(II) precatalyst described by Webster et al. for the dehydrocoupling of phosphine- and amine-boranes. On the right the isolated chairlike resting state of the catalyst.

Water oxidation

Production of new fuels and compounds of interest with renewable energy, needs a good supply of electrons and protons to form reduced products. One approach is the use of artificial photosynthesis, inspired by the natural processes, and water as a source of electrons and protons.[75,76] Water oxidation indeed is able to produce both of them together with molecular oxygen (O_2).

$$H_2O \rightarrow O_2 + 4H^+ + 4e^-$$

Water oxidation is a highly demanding reaction with unfavourable thermodynamics and slow kinetics, so the use of a catalyst is needed. Moreover, water splitting based on electrocatalysis usually involves high overpotentials, as a result of the slow kinetics. These poor rates of reaction are probably due to several intermediates needed to release all $4H^+/4e^-$ to fully oxidise water to O_2.

In order to exploit this high-energy reaction in a green chemistry outlook, many researchers began to develop new Water Oxidation Catalyst (WOC) to lower the kinetic barrier. Indeed, water splitting to molecular oxygen and hydrogen is an intriguing system, with high potential impact on the energy storage issue, since both oxygen and hydrogen can be then recombined in a fuel cell.[77]

Iron-based WOC.

Iron-based WOCs have been recently divided in two different classes by Thapper[78] depending on their behaviour:

I. Class I are six-coordinated iron complexes with two coordination sites occupied by labile ligands, which are *cis* to each other. These complexes react via O-O bond formation between the oxo-ligand on iron and water/hydroxyl ligand on cerium (involving Cerium Ammonium Nitrate, CAN, as oxidant).

II. Class II contains five- or six-coordinate iron complexes with one site available. The O-O bond formation mechanism involves a nucleophilic attack of water on a high valent Fe(V)-oxo system.

In 2010, Collins and Bernhard[79] reported five iron complexes bearing a tetraamido macrocyclic ligand (TAML) for water oxidation of Class I. The iron-TAML complexes were first synthesised in 1980 by Collin[80] for oxidation of organic compounds with H_2O_2 as oxidant: in that application deprotonated robust amido ligands were assessed as strong donor ligands that allowed high oxidation state iron. The least acid- and oxidatively-stable TAML complex (**Fe20A**) was unreactive in water oxidation, instead the other four catalysts displayed a fast activity depending on TAML substituents, with the most electron-withdrawing substituent (**Fe20E**) as the best active catalyst. The best TOF measured was > 1.3 s^{-1} after few seconds, then decreasing and being constant for hours. A same behaviour was described earlier by Elizarova et al.[81] with first-row transition metal tetrapyrrole catalysts, however none of these catalysts sustained the high activity for more than a few seconds, due to ligand dissociation and decomposition. An electrocatalytic version of TAML complex was developed in 2014 and displayed higher TON compared to the homogeneous one;[82] the catalyst was immobilised on a glassy carbon electrode.

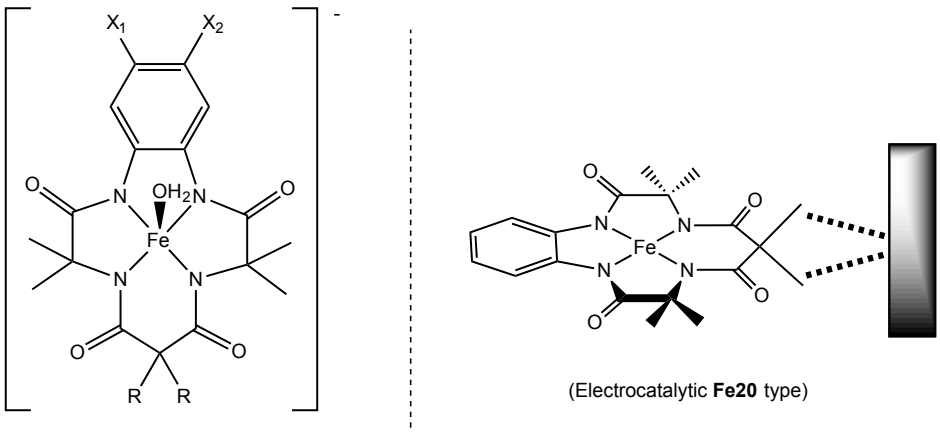

Fe20A $X_1=X_2=H$; $R=CH_3$
Fe20B $X_1=X_2=H$; $R=(CH_2)_2$
Fe20C $X_1=X_2=H$; R=F
Fe20D $X_1=NO_2$; $X_2=H$; R=F
Fe20E $X_1=X_2=Cl$; R=F

Figure 11. TAML-iron catalysts in water oxidation (left) and electrocatalytic version (right).

In 2011 Fillol and Costas described a series of tetraaza non-heme iron-based complexes.[83] In their study, a key aspect for activity of this system is the presence of two *cis* free coordination sites on the iron centre (Class I catalyst). One of the best iron catalyst **Fe21** gives high activity (TON>1050 and TOF=222h^{-1}) with sodium periodate ($NaIO_4$) as oxidant.

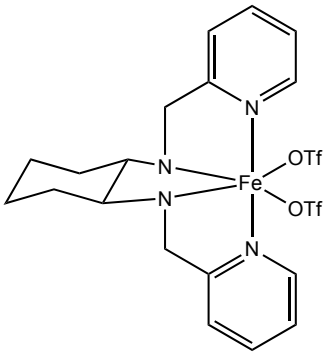

Fe21

Figure 12. Costat non-heme iron catalyst working with $NaIO_4$. OTf, triflate.

Later, Llobet, Fukuzumi and co-workers[84] studied a non-heme iron complex **Fe22** in different pH conditions providing insights on homogeneous vs heterogeneous catalyst behaviour (Scheme 22). In acidic condition, with CAN as oxidant, TONs of 80 were obtained. In solution an iron(IV)-oxo complex in competition with a ligand dissociation accompanied by CO_2 release was observed. Kinetic studies revealed also a homogeneous behaviour (Class I catalyst). At basic pH, in the light-driven water oxidation with $[Ru(bpy)_3]^{2+}$ as photosensitiser and $S_2O_8^{2-}$ as electron acceptor, a heterogeneous behaviour was observed: iron hydroxide nanoparticles, that acted as true catalyst, were released in water due to ligand dissociation.

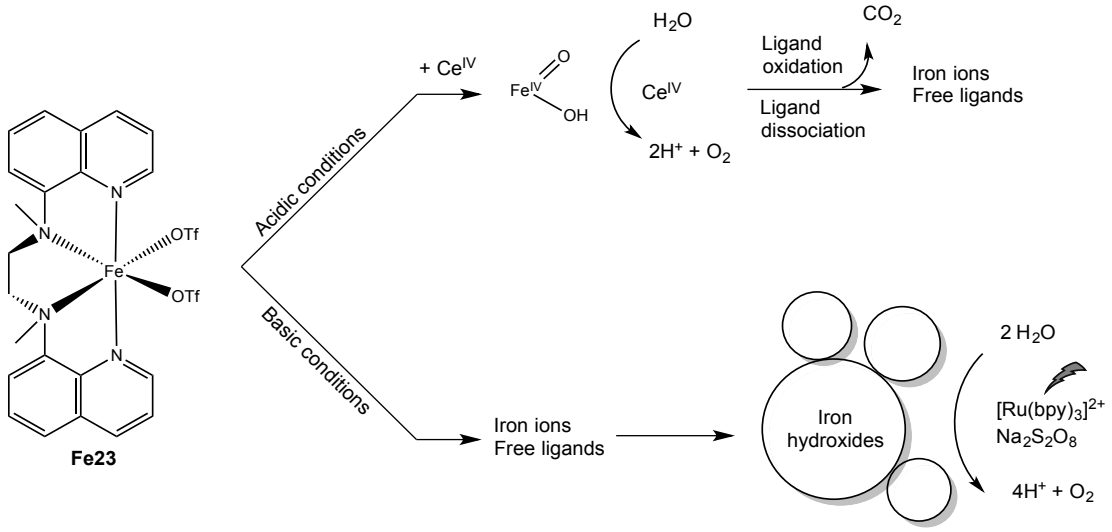

Scheme 20. Homogeneous vs. heterogeneous behaviour of **Fe22**. OTf, triflate; bpy, 2,2'-bipyridine.

In 2016 Thapper et al.[85] reported two iron complexes **Fe23** and **Fe24** bearing polypyridine ligand Py5OH (Scheme 23); also in this case, the pH of water solution discriminated between two different mechanisms. In acidic condition with CAN as oxidant **Fe24** displayed the best TON, whilst at slightly basic condition (pH=8) with $Ru(bpy)_3^{3+}$ as oxidant **Fe23** was the best. The two catalysts differ for the sixth ligand: **Fe23** coordinated a chloride, whilst **Fe24** methanol or acetonitrile (labile ligands). Under acidic condition, two *cis* sites with labile ligand are needed (Class I catalyst), since an intramolecular O-O bond formation was proposed. Therefore, **Fe23** with a coordination site permanently occupied by a chloride ligand showed poorer activity. **Fe24** instead, with already one labile ligand, could detach one pyridine group in order to create two *cis* empty coordination sites. Under neutral/basic conditions, only one coordination site was involved (Class II catalyst) due to a nucleophilic attack of water on a Fe(V)-oxo species. The activity was reversed, since **Fe23** was stabilised by the chloride ligand, which prevented decomposition of complex.

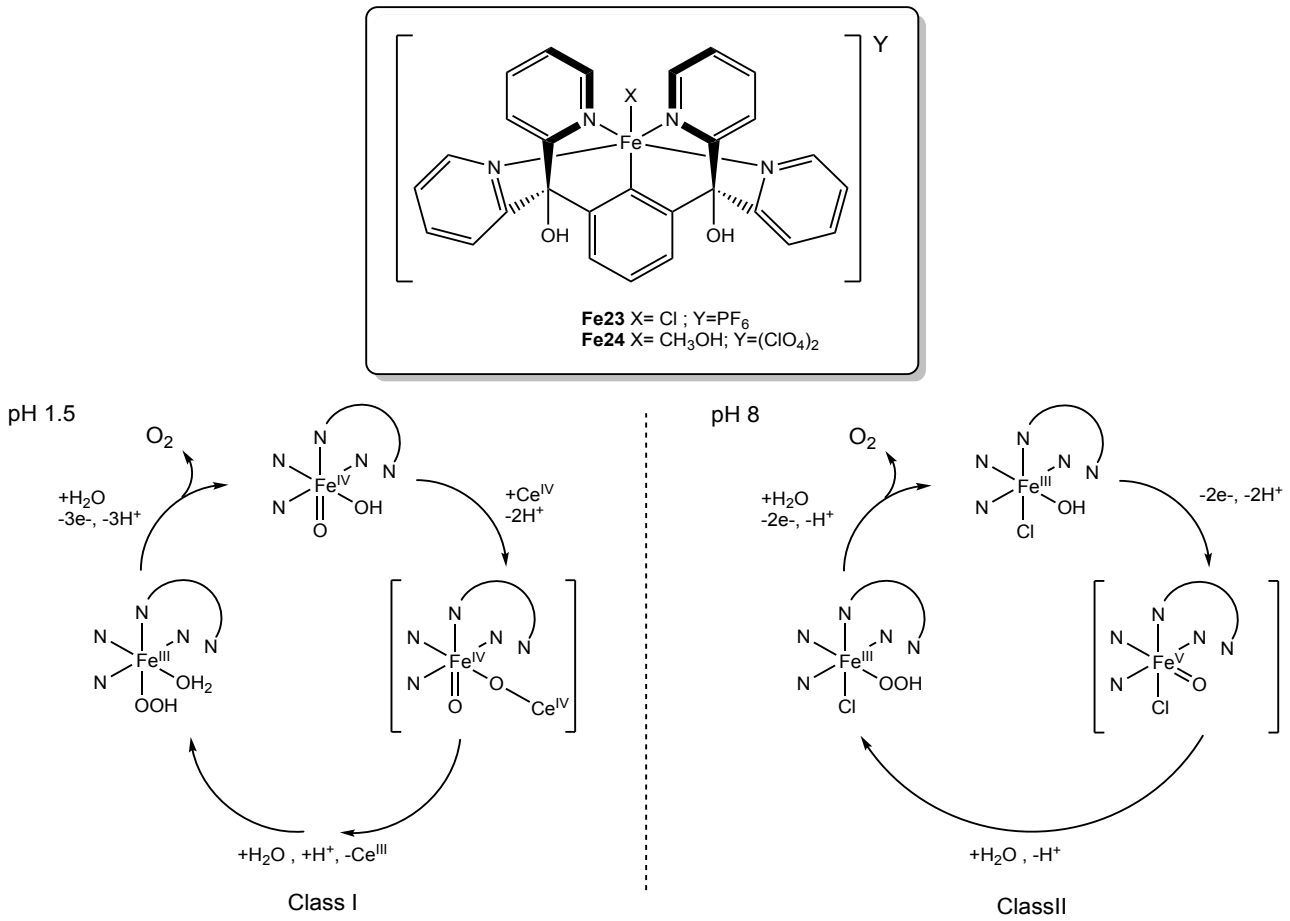

Scheme 21. Thapper and co-workers Py5OH-Fe complexes with Class I and II behaviours depending on pH conditions.

In the same year, Masaoka and co-workers[85] described a robust pentanuclear iron complex **Fe25** (Figure 13) with high activity (TOF=1900s^{-1}) compared to the other homonuclear iron WOCs. Electrochemical experiments showed six different oxidation states are involved in the mechanism between $Fe^{(II)}$ and $Fe^{(IV)}$ atoms, with Fe^{III}_5 the active species. Furthermore, the O-O bond formation was performed by two adjacent active iron sites (close to Class I catalyst). Drawbacks of this systems were the need of high overpotential (> 0.5V) and inability to operate in water rich solutions (acetonitrile/water mixture is needed to reach the high TOF).

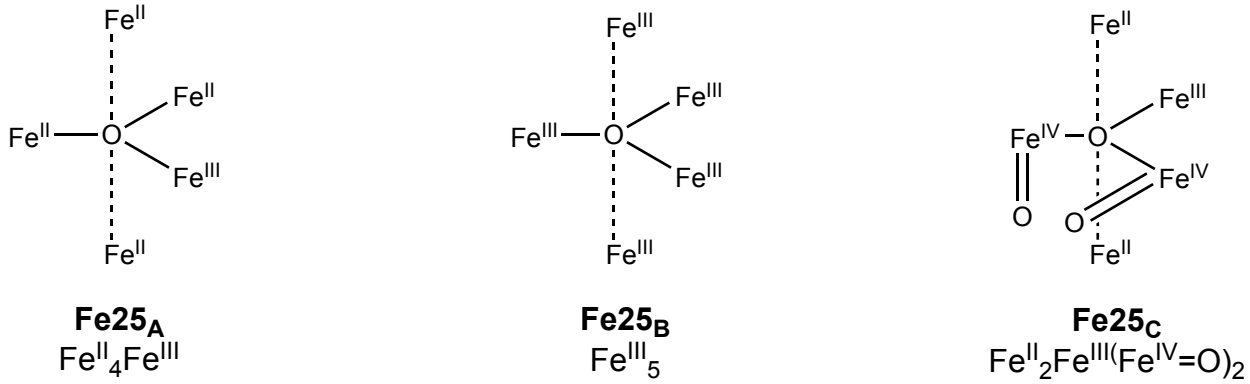

Figure 13. Pentanuclear iron complex as WOCs. **Fe25A** as the ground state, **Fe25B** as active form and **Fe25C**, in which the two adjacent FeIV-oxo sites are shown.

Bioinorganic.

The last decades have witnessed impressive advances in the elucidation of molecular mechanisms governing fundamental processes in biology and life sciences. This is in part due to a much better understanding of the structure of enzymes and metalloenzymes. Indeed, most of the enzymes are proteins and more than half contain metal ions in their structure; these ones are known as metalloenzymes. The metal is usually the active site of an enzyme, where the substrate is bound. Some inorganic elements were found to be essential in animals and plants such as Mg, Mn, Fe, Co, Ni, Cu, Zn and others. The science involved in studying these compounds is called bioinorganic chemistry.

After the discovery of Coenzyme B12 and its structure by D. Hodgkin,[86] it became clear the importance of organometallic species in nature. Since then, several groups have endeavoured to develop new organometallic compounds for homogeneous catalysis and for medicinal applications, inspired by natural occurring enzymes.

Herein, I report an example of natural enzyme to exploit in catalyst design, the hydrogenases, and some pharmaceutical organometallic compounds.

Hydrogenases

Some bacteria are able to use H_2 as reducing energy source, or protons from water as final acceptor of electrons, releasing H_2; these reactions are mediated by metalloenzymes called hydrogenases.[87]

Overall, hydrogenases reversibly catalyse the conversion of hydrogen into two protons and two electrons:

$$H_2 \rightleftarrows 2H^+ + 2e^-$$

There are three classes of hydrogenases: [NiFe]-hydrogenases, iron-only [FeFe]-hydrogenases and cluster-free [Fe]-hydrogenases. The last ones lack the typical FeS cubane centres and involve a different mechanism: the hydrogen uptake is coupled to the close co-factor methenyltetrahydromethanopterin (methenyl-H_4MPT), which accepts a hydride (equivalent of H^+ and $2e^-$). The other hydrogenases instead, need to transfer the electrons to distant electron acceptors *via* their redox active cluster co-factors (FeS cubanes). Crystal structures of active centres of both [NiFe]- and [FeFe]-hydrogenases have been determined (Figure 14).

In 1995, crystallographic studies on the active site of [NiFe]-hydrogenases **Fe26** from *Desulfovibrio gigas*,[88] showed a low-spin dicyanoiron(II) dicarbonyl centre bridged to a nichel tetrathiolate centre by an oxo- or hydroxyl-ligand and two thiolate groups from cysteine residues. The bridging oxo- or hydroxyl-group can be converted to water after H_2 addition. Different mechanisms based on collected data and involving hydride on Ni or Fe centres have been proposed.

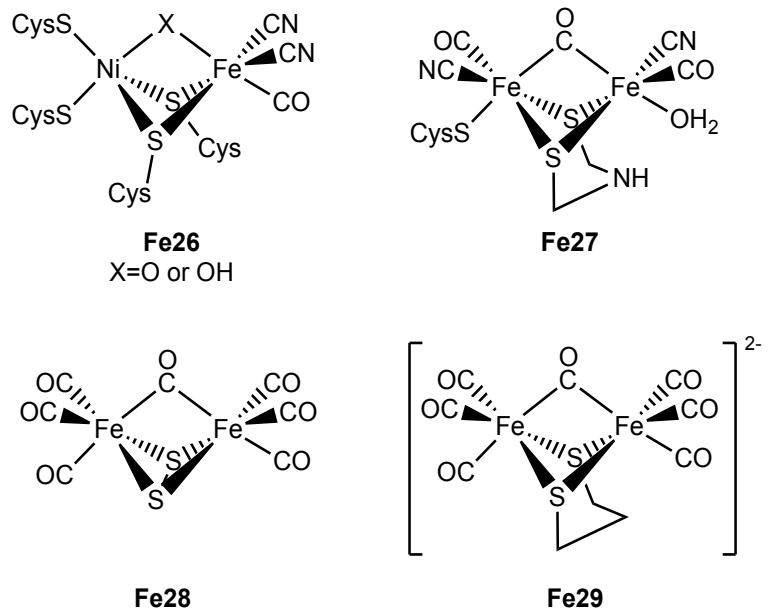

Figure 14. [NiFe] **Fe26** and [FeFe] **Fe27** hydrogenases described in crystallographic studies. **Fe29** is an example of a synthesised hydrogenases. Cys, cysteine residue.

In 1999, studies on the [FeFe]-hydrogenases active centre **Fe27** from *Clostridium pasteurianum*[89] showed two cyanoironcarbonyl groups bridged by a carbonyl and a 2-azapropane-1,3-dithiolate. The NH pendant group in proximity of the iron active site is believed to act as a base. One iron atom has a labile ligand (likely water) where H_2 might bind. The splitting of this H_2 intermediate is proposed to be heterolytic, in which the proton is transferred to the internal NH base.

Finally, a series of complexes that mimic the active site of hydrogenases have been reported[90]. An example, iron dimer **Fe29** has been synthesised starting from precursor **Fe28**, which is believed to be developed from iron sulphide, dissolved at deep-sea vents by CO, as a speculation of the origin of life.

Biomedical applications

Nowadays, organometallic compounds are receiving a growing interest in pharmacology and medicine. One of the first important discoveries in this field was the use of polymeric organoarsenical Salvarsan as first antisyphilitic by Enlirch,[91] who also won the Nobel Prize in 1908 for his work on foundations of chemotherapy. Antitumor drugs are indeed one of the most researched topic of last years.

The best-known anticancer drug is the cisplatin, cis-$[PtCl_2(NH_3)_2]$ **Pt1**, which binds strongly to DNA then inhibiting the cell growth. The cancer cells are more affected by

these drugs since they grow at a faster rate compared to the healthy cells. Two of the most employed platinum-based antitumor drugs are oxaliplatin **Pt2** and carboplatin **Pt3**.[92] Other metal-based organometallic drugs, such as **Ru1**, have also been investigated (Figure 15).[93]

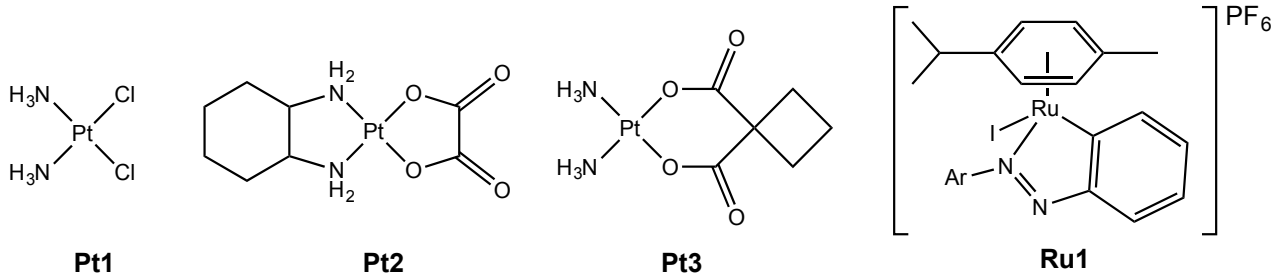

Figure 15. Anticancer drugs developed in the last few years based on platinum and ruthenium. PF_6, hexafluorophosphate.

Recently, iron(III) complexes bearing salen (bis(salicylidine)ethylenediamine) ligand and their derivatives were reported as active anticancer drugs. In general, salen-metal complexes induce oxidative DNA/RNA cleavage. Mandel et al.[94,95] demonstrated that salen **Fe30** and salphen **Fe31** (Figure 16) complexes induce nuclear fragmentation and human cellular apoptosis. Biological analyses suggested a mitochondrial pathway of apoptosis, since release of cytochrome c from mitochondria to cytosol was observed. Even though the mechanism is still not clear, the nature of the metal centre with substituents and bridging spacers in ligands play a crucial role in reactivity. Indeed, a screening of 14 different type of salen- and salphen-iron(III) complexes showed that cytotoxicity is highly influenced by substituents, which control the permeation through the cell membrane.

Failes and Hambley[96] reported a derivative of iron(III)-salen complex **Fe32** (Figure 16) bearing marimastat, which is a known matrix metalloproteinase (MMP) inhibitor. The iron complexes deliver the inhibitor at tumour sites, since the MMP are found to be overexpressed on tumour cell membranes and are implicated in the metastasised cancers. Upon reduction from Fe(III) to the more labile Fe(II) centre, **Fe32** releases the MMP inhibitor, whilst it is stable in non-reducing conditions (non tumour cells).

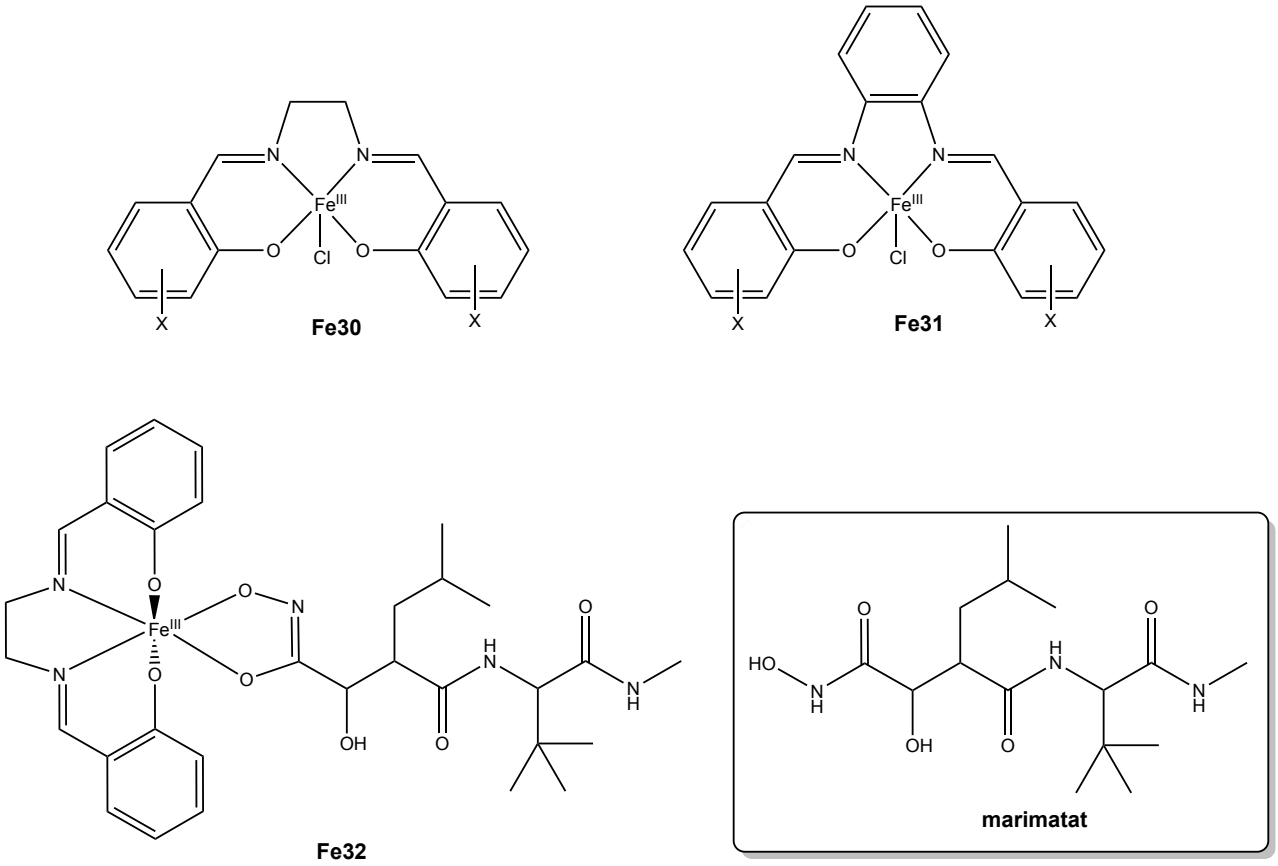

Figure 16. Salen- **Fe30** and salphen-iron(III) **Fe31** complexes and the marimastat derivative **Fe32**.

Chemically Modified Electrodes

Heterogenization of homogeneous organometallic complexes is an intriguing topic that has gained much interest in recent years. Heterogenization would allow one to exploit the high activity and selectivity of homogeneous catalysts, but with a straightforward separation from products, and easy recycling of the catalyst itself. Another possible application, that it is here taken into consideration, is the design of the Chemically Modified Electrodes (CMEs).

CMEs contain a conductive substrate modified with electroactive thin films, monolayers, or thick coatings.[97] Each modified electrode is designed for a particular application, which it is not possible for a bare conductive electrode. The bare electrode is often made of an inexpensive material (e.g. carbon), with glassy carbon among the most used substrates for modification. It is important that the layer or coating on the electrode surface is electroactive, this means that it can exchange electrons being oxidised or reduced.[98] Some examples of modified surfaces are: transfer of chemical properties from the modifier to the electrode; enhanced electrocatalytic activity and sensitivity; selectivity towards a specific analyte.

Concerning the active layer or coating, conductive polymers are a good choice, since the discovery by Shirakawa et al.[99] in 1970s that oxidised polyacetylene can reach high conductivity. In this field, the most interesting polymers were based on polyanilines, polypyrroles, polythiophenes, polyphenylenes and poly(p-phenylene vinylene)s. Of these, the new poly(3,4-ethylenedioxythiophene), known as PEDOT or PEDT, is the most successful (Figure 17).

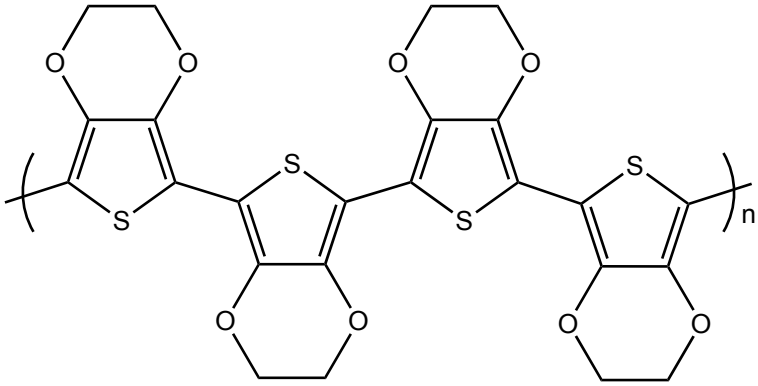

PEDOT

Figure 17. PEDOT polymer, a thiophene derivative.

PEDOT

In 1980s, scientists of Bayer AG[100] developed the thiophene derivative, known as PEDOT, to obtain a water soluble conductive polymer. The PEDOT was insoluble in water, but it featured other important properties: low oxidation potential, moderate band gap, good stability in the oxidised state, high conductivity and almost transparent in thin films. In order to get the water solubility, a water soluble polyelectrolyte, poly(styrene sulfonic acid) PSS, was employed as charge-balancer during polymerization, resulting in a PEDOT/PSS film. This combination is commercially known as BAYTRON P.

Synthesis of PEDOT layers might follow three different mechanisms:[101]

I. Oxidative chemical polymerization;
II. Electrochemical polymerization;
III. Transition metal-mediated coupling of dihalo-derivatives of monomer EDOT.

Among these, the electrochemical approach is not the best choice for bulk industrial production, since polymer is produced in very small amounts. Anyway, it is very useful in production of thin polymer layers and for studies of polymerization mechanism and

properties of the polymers: only small amounts of monomer are required; electrochemical analyses on properties are very rapid; precision and accuracy are high, then screening and comparison between different systems in the same conditions is easily carried out.

A series of different substituted EDOT derivatives have been reported in recent years; functional groups/chains can be coordinated to the EDOT monomer in order to get new features to exploit in CEMs.

Hydroxymethylated EDOT **EDT1** and its derivatives such as acrylate **EDT2** and glyme **EDT3** monomers[102] can be electro-polymerised in water with the same peak potential of EDOT; their corresponding PEDOT polymer are well soluble in common solvents.

The sulfonate-substituted **EDT4**[103] also polymerised in water and the pendant sulfonate group provided cation exchange properties.

Oligoethyleneglycol-substituted **EDT5** and **EDT6a-c** were described by Roncali et al.[104,105] and they were employed in sensor applications to detect mono- and di-valent cations, which can be easily complexed by the ethyleneoxy-arms (Figure 18).

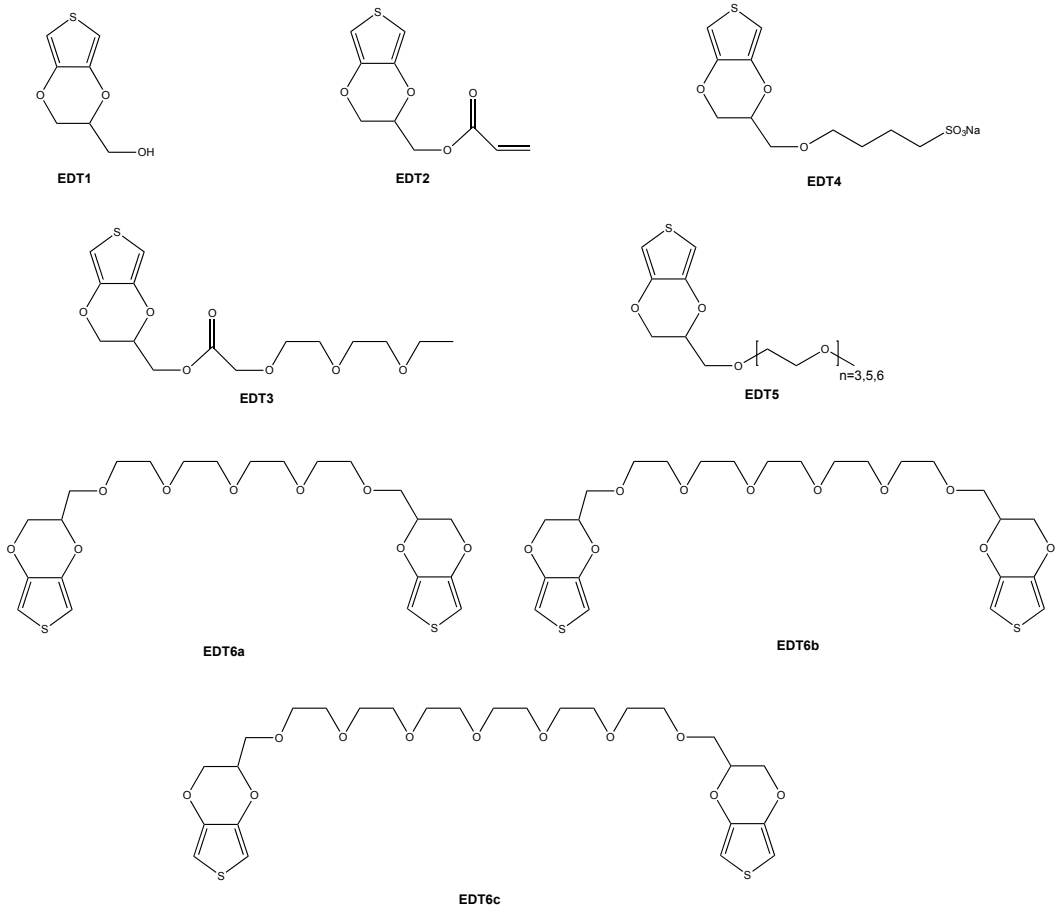

Figure 18. EDOT derivatives.

Furthermore, a PEDOT film has been recently functionalised with ferrocene (Scheme 24), that is a well-known and established redox mediator bearing an Fe^{II}/Fe^{III} couple. Scavetta et al.[106] reported a two-step procedure consisting of electrodeposition of EDOT-N_3 over an indium tin oxide electrode (ITO), followed by a copper-catalysed azide-alkyne cycloaddition of ethynylferrocene.

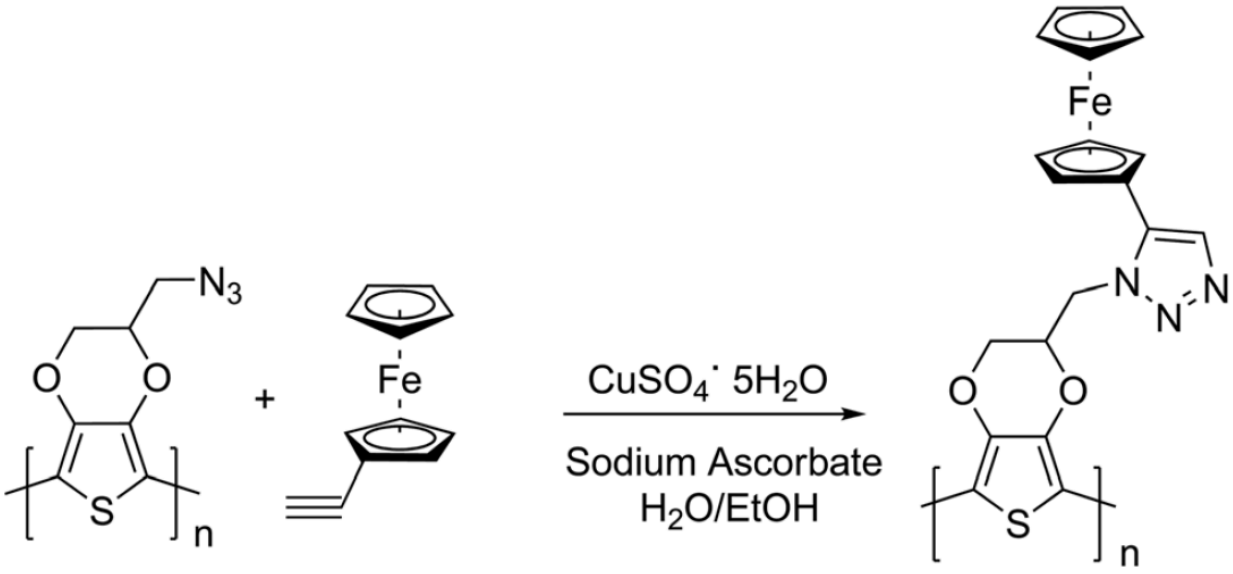

Scheme 22. PEDOT-Fc film as reported by Scavetta et el.

Topic

The main topic of this thesis concern the synthesis and reactivity of a new class of iron complexes bearing two ligands: cyclopentadienone (CpO), a well-known non-innocent ligand, and N-Heterocyclic carbene (NHC), an easy functionalised ligand, which is highly resistant toward decomposition.

As for the introduction, this work regards different areas of chemistry, as reported hereinafter. Iron compounds were evaluated as possible catalyst in different reactions, immobilise on an electrode and tested as drug against pancreatic cancer cells. A brief description of chapters is here described.

I. Chapter I, new class of iron complexes is prepared bearing both CpO and NHC ligands.
II. Chapter II, iron compounds are evaluated as transfer hydrogenation as well as alcohol oxidation catalysts.
III. Chapter III, iron compounds are evaluated as dehydrocoupling of ammonia-boranes catalysts.
IV. Chapter IV, electrochemical studies on iron complexes show the new iron-CpO-NHC system as good candidate as water oxidation catalyst (WOC).
V. Chapter V, electrochemical and DFT investigation about the activity of diiron complexes bearing carbyne and cyanide ligands, resembling the [Fe,Fe]-hydrogenase.
VI. Chapter VI, synthesis of EDOT modified iron complexes, exploiting NHC ligand as linker; afterwards, iron-EDOT monomers are employed to coat an electrode with a thin film of iron-PEDOT. The chemically modified electrode are assessed as glucose detector.
VII. Chapter VII, iron complexes bearing CpO and NHC ligands are evaluated as anticancer drug against pancreatic cancer cells.

References

[1] P. T. Anastas; J. C. Warner, «Green Chemistry: Theory and Practice,» *Oxford University Press: New York,* **1998***,* p. 30.

[2] C. K. Jørgensen; *Coord. Chem. Rev.*, **1966,** *1*, 164.

[3] A. Wanat; T. Schneppensieper; G. Stochel; R. v. Eldik; E. Bill; K. Wieghardt; *Inorg. Chem.*, **2002**, *41*, 1.

[4] P. J. Chirik; K. Wieghardt; *Science*, **2010**, *327*, 794.

[5] V. Lyaskovskyy; B. d. Bruin; *ACS Catal.*, **2012**, *2*, 270.

[6] L. Que; W. B. N. Tolman; *Nature*, **2008**, *455*, 333.

[7] B. L. Small; M. Brookhart; *J. Am. Chem. Soc.*, **1998**, *120*, 7143.

[8] K. T. Sylvester; P. J. Chirik; *J. Am. Chem. Soc.*, 2009, *131*, 8772.

[9] G. J. P. B. et. al.; *Chem. Commun.*, **1998**, *849*, 1998.

[10] B. L. Conley; M. K. Pennington-Boggio; E. Boz; T. J. Williams; *Chem. Rev.*, **2010**, *110*, 2294.

[11] H. J. Knölker; E. Baum; H. Goesmann; R. Klauss; *Angew. Chem. Int. Ed.*, 1999, *38*, 2064.

[12] G. N. Schrauzer; *J. Am. Chem. Soc.*, 1959, *81*, 5307.

[13] H.-J. Knölker; E. Baum; H. Goesmann; R. Klauss; *Angew. Chem. Int. Ed.*, 1999, *38*, 2064.

[14] C. P. Casey; H. Guan; *J. Am. Chem. Soc.*, **2007**, *129*, 5816.

[15] C. P. Casey; H. Guan; *J. Am. Chem. Soc.*, **2008**, 131, 2499.

[16] A. Quintard; J. Rodriguez; *Angew. Chem. Int. Ed.*, **2014**, 53, 4044.

[17] T.-T. Thai; D. S. Mõrel; A. Poater; S. Gaillard; J.-L. Renaud; *Chem. Eur. J.*, **2015**, *21*, 7066.

[18] D. S. Mérel; M. Elie; J.-F. Lohier; S. Gaillard; J.-L. Renaud; *ChemCatChem.*, **2013**, *5*, 2939.

[19] S. Moulin; H. Dentel; A. Pagnoux-Ozherelyeva; S. Gaillard; A. Poater; L. Cavallo; J.-F. Lohier; J.-L. Renaud; *Chem. Eur. J.*, **2013**, 19, 17881.

[20] A. Berkessel; S. Reichau; A. v. d. Höh; N. Leconte; J.-M. Neudörfl; *Organometallics,* **2011**, *30*, 3880.

[21] S. Díez-González; S. Nolan; *Coord. Chem. Rev.*, **2007**, *251*, 874.

[22] S. T. Liddle; I. S. Edworthy; P. L. Arnold; *Chem. Soc. Rev.*, **2007**, *36*, 1732.

[23] E. Fischer; A. Maasböl; *Angew. Chem. Int. Ed.*, **1964**, *3*, 580.

[24] R. Schrock; *J. Am. Chem. Soc.*, **1974**, *96*, 6796.

[25] H. Wanzlick; H.-J. Sch¨onherr; *Angew. Chem. Int. Ed.*, **1968**, *7*, 141.

[26] K. Öfele; *a) J. Organomet. Chem.*, **1968**, *12*, P42 b) *Angew. Chem. Int. Ed.,* **1970**, *9*, 739 c) *J. Organomet. Chem.*, **1970**, *22*, C9.

[27] A. A. III; R. Harlow; M. Kline; *J. Am. Chem. Soc.*, **1991**, *113*, 361.

[28] F. E. Hahn; M. C. Jahnke; *Angew. Chem. Int. Ed.*, **2008**, *47*, 3122.

[29] M. N. Hopkinson; C. Richter; M. Schedler; F. Glorius; *Science*, **2014**, *510*, 485.

[30] M. K. Denk; J. M. Rodeznoì; S. Gupta; A. J. Lough; *J. Organomet. Chem.*, **2001**, *242*, 617.

[31] L. Perrin; E. Clot; O. Eisenstein; J. Loch; R. Crabtree; *Inorg. Chem.*, **2001**, *40*, 5806.

[32] A. C. Tolman; *Chem. Rev.*, **1977**, *77*, 313.

[33] T. Dröge; F. Glorius; *Angew. Chem. Int. Ed.*, **2010**, *49*, 6940.

[34] D. J. Nelson; S. P. Nolan; *Chem. Soc. Rev.*, **2013**, *42*, 6723.

[35] A. C. Hillier; W. J. Sommer; B. S. Yong; J. L. Petersen; L. Cavallo; S. P. Nolan; *Organometallics*, **2003**, *22*, 4322.

[36] C. M. Crudden; D. P. Allen; *Coord. Chem. Rev.*, **2004**, 2*48*, 2247.

[37] W. A. Herrmann; *Angew. Chem. Int. Ed.*, **2002**, *41*, 1290.

[38] F. E. Hahn; L. Wittenbecher; D. L. Van; R. Fröhlich; *Angew. Chem. Int. Ed.*, **2000**, *39*, 541.

[39] H. M. J. Wang; I. J. B. Lin; *Organometallics*, **1998**, *17*, 97.

[40] H. Jacobsena; A. Correab; A. Poaterb; C. Costabile; L. Cavallo; *Coord. Chem. Rev.*, **2009**, *253*, 867.

[41] M.-T. Lee; C.-H. Hu; *Organometallics*, **2004**, *23*, 976.

[42] C. Bolm; J. Legros; J. L. Paih; L. Zani; *Chem. Rev.*, **2004**, *104*, 6217.

[43] D.Wang; D. Astruc; *Chem. Rev.*, **2015**, *115*, 6621.

[44] E. Knoevenagel; B. Bergdolt; *Chem. Ber.*, **1903**, *36*, 2857.

[45] A. Verley; *Bull. Soc. Chim. Fr.*, **1925**, *37*, 537.

[46] H. Meerwein; R. Schmidt; *Liebigs Ann. Chem.*, **1925**, *444*, 221.

[47] G. K. Chuah; S. Jaenicke; Y. Z. Zhu; S. H. Liu; *Curr. Org. Chem*, **2006**, *10*, 1639.

[48] M. Kitamura; M. Tokunaga; R. Noyori; *J. Am. Chem. Soc.*, **1995**, *117*, 2931.

[49] A. Fujii; S. Hashiguchi; N. Uematsu; T. Ikariya; R. Noyori; *J. Am. Chem. Soc.*, **1996**, *118*, 2521.

[50] N. Uematsu; A. Fujii; S. Hashiguchi; T. Ikariya; R. Noyori; *J. Am. Chem. Soc.*, **1996**, *118*, 4916.

[51] R. Noyori; *Angew. Chem. Int. Ed.*, **2002**, *41*, 2008.

[52] C. Bianchini; E. Farnetti; M. Graziani; M. Peruzzini; A. Polo; *Organometallics*, **1993**, *12*, 3753.

[53] S. Enthaler; B. Hagemann; G. Erre; K. Junge; M. Beller; *Chem. Asian J.*, **2006**, *1*, 598.

[54] S. Enthaler; G. Erre; M. K. Tse; K. Junge; M. Beller; *Tetrahedron Lett.*, **2006**, *47*, 8095.

[55] C. P. Casey; H. G. J.; *J. Am. Chem. Soc.*, **2007**, *129*, 5816.

[56] C. P. Casey; H. Guan; *J. Am. Chem. Soc.*, **2008**, *131*, 2499.

[57] A. A. Mikhailine; R. H. Morris; *Inorg. Chem.*, **2010**, *49*, 11039.

[58] P. O. Lagaditis; A. J. Lough; R. H. Morris; *J. Am. Chem. Soc.*, **2001**, *133*, 9662.

[59] W. Zuo; S. Tauer; D. E. Prokopchuk; R. H. Morris; *Organometallics*, **2014**, *33*, 5791.

[60] W. Zuo; A. J. Lough; Y. F. Li; R. H. Morris; *Science*, **2013**, *342*, 1080.

[61] S. Zhou; S. Fleischer; K. Junge; S. Das; D. Addis; M. Beller; *Angew. Chem. Int. Ed.*, **2010**, *49*, 8121.

[62] V. V. K. M. Kandepi; J. M. S. Cardoso; E. Peris; B. Royo; *Organometallics*, **2010**, *29*, 2777.

[63] T. Hashimoto; S. Urban; R. Hoshino; Y. Ohki; K. Tatsumi; F. Glorius; *Organometallics*, **2012**, *31*, 4474.

[64] G. Wienhöfer; F. A. Westerhaus; R. V. Jagadeesh; K. Junge; H. Junge; M. Beller; *Chem. Comm.*, **2012**, *48*, 4827.

[65] G. Wienhöfer; I. Sorribes; A. Boddien; F. A. Westerhaus; K. Junge,;H. Junge; R. Llusar; M. Beller; *J. Am. Chem. Soc.*, **2011**, *133*, 12875.

[66] A. Rossin; M. Peruzzini; *Chem. Rev.*, **2016**, *116*, 8848.

[67] H. C. Johnson; T. N. Hooper; A. S. Weller; *Top. Organomet. Chem.*, **2015**, *49*, 153.

[68] S. Bhunya; P. M. Zimmerman; A. Paul; *ACS Catal.*, **2015**, *5*, 3478.

[69] V. Pons; R. T. Baker; N. K. Szymczak; D. J. Heldebrant; J. C. Linehan; M. H. Matus; D. J. Grant; D. A. Dixon; *Chem. Comm.*, **2008**, 6597.

[70] R. T. Baker; J. C. Gordon; C. W. Hamilton; N. J. Henson; P.-H. Lin; S. Maguire; M. Murugesu; B. L. Scott; N. C. Smythe; *J. Am. Chem. Soc.*, **2012**, *134*, 5598.

[71] J. R. Vance; A. Schäfer; A. P. M. Robertson; K. Lee; J. Turner; G. R. Whittell; I. Manners; *J. Am. Chem. Soc.*, **2014**, *136*, 3048.

[72] P. Bhattacharya; J. A. Krause; H. Guan; *J. Am. Chem. Soc.*, **2014**, *136*, 11153.

[73] H. A. Kalviri; F. Gärtner; G. Ye; I. Korobkov; R. T. Baker; *Chem. Sci.*, **2015**, *6*, 618.

[74] N. T. Coles; M. F. Mahon; R. L. Webster; *Organometallics*, **2017**, *36*, 2262.

[75] A. J. Bard; M. A. Fox; *Acc. Chem. Res.*, **1995**, *28*, 141.

[76] T. J. Meyer; *Acc. Chem. Res.*, **1989**, *22*, 163.

[77] J. D. Blakemore; R. H. Crabtree; G. W. Brudvig; *Chem. Rev.*, **2015**, *115*, 12974.

[78] B. Das; A. Orthaber; S. Ott; A. Thapper; *ChemSusChem*, **2016**, *9*, 1178.

[79] W. C. Ellis; N. D. McDaniel; S. Bernhard; T. J. Collins; *J. Am. Chem. Soc.*, **2010**, *132*, 10990.

[80] T. J. Collins; *Acc. Chem. Res.*, **2002**, *35*, 782.

[81] G. L. Elizarova; L. G. Matvienko; N. V. Lozhkina; V. N. Parmon; *React. Kinet. Catal. Lett.*, **1984**, *26*, 67.

[82] E. L. Demeter; S. L. Hilburg; N. R. Washburn; T. J. Collins; J. R. Kitchin; *J. Am. Chem. Soc.*, **2014**, *136*, 5603.

[83] J. L. Fillol; Z. Codola; I. Garcia-Bosch; L. Gomez; J. J. Pla; M. Costas; *Nat. Chem.*, **2011**, *3*, 807.

[84] D. Hong; S. Mandal; Y. Yamada; Y.-M. Lee; W. Nam; A. Llobet; S. Fukuzumi; *Inorg. Chem.*, **2013**, *52*, 9522.

[85] M. Okamura; M. Kondo; R. Kuga; Y. Kurashige; T. Yanai; S. Hayami; V. K. K. M. Okamura; M. Kondo; R. Kuga; Y. Kurashige; T. Yanai; S. Hayami; V. K. K. Praneeth; M. Yoshida; K. Yoneda; S. Kawata; S. Masaoka; *Nature*, **2016**, *530*, 465.

[86] J. A. K. Howard; *Nature Rev. Molec. Cell Biol.*, **2003**, *4*, 891.

[87] R. H. Crabtree; The organometallic chemistry of the transition metals, Wiley, Sixth Ed., **2014**.

[88] A. Volbeda; M.-H. Charon; C. Piras; E. Hatchikian; M. Frey; J. FontecillaCamps, *Nature*, **1995**, *373*, 580.

[89] J. Peters; W. Lanzilotta; B. Lemon; L. Seefeldt; *Science*, **1998**, *282*, 1853.

[90] D. M. Heinekey; *J. Organometal. Chem.*, **2009**, *694*, 2671.

[91] A. Piro; A. Tagarelli; G. Tagarelli; *Int. Rev. Immunol.*, **2008**, *27*, 1.

[92] Y. Jung; S. J. Lippard; *Chem. Rev.*, **2006**, *106*, 1387.

[93] G. Sava; A. Bergamoa; P. J. Dyson; *Dalton. Trans.*, **2011**, *40*, 9069.

[94] K. I. Ansari; S. Kasiri; J. D. Grant; S. S. Mandal; *J. Biomol. Screening*, **2011**, *16*, 26.

[95] T. S. Lange; C. McCourt; R. K. Singh; K. K. Kim; A. P. Singh; B. S. Luisi; O. Alpturk; R. M. Strongin; L. Brard; *Drug Des. Dev. Ther.*, **2009**, *3*, 17.

[96] T. W. Failes; T. W. Hambley; *J. Inorg. Biochem.*, **2007**, *101*, 396.

[97] M. Sajid; M. K. Nazal; M. Mansha; A. Alsharaa; S. M. S. Jillani; C. Basheer; *Trends in Anal. Chem.*, **2016**, *76*, 15.

[98] A. J. Bard; *Chem. Educ.*, **1983**, *60*, 302.

[99] H. Shirakawa; E. J. Lewis; A. G. MacDiarmid; C. K. Chiang; A. J. Heeger; *Chem. Commun.*, **1977,** 578.

[100] Bayer AG, *Eur. Patent 339 340*, **1988**.

[101] L. Groenendaal; F. Jonas; D. Freitag; H. Pielartzik; J. R. Reynolds; *Adv. Mater. 2000*, **2000**, *7*, 481.

[102] D. M. Welsh; A. Kumar; J. R. Reynolds; *Polym. Prepr.*, **1997**, *38*, 320.

[103] O. Stephan; P. Schottland; P. Y. L. Gall; C. Chevrot; *J. Chim. Phys. Phys.-Chim. Biol.*, **1998**, *95*, 1168.

[104] S. Sadki; J. Roncali; *Electrochem. Commun.*, **2000**, *2*, 72.

[105] I. Perepichka; E. Levillain; M. Sallé; J. Roncali; *Chem. Mater.*, **2002**, *14*, 449.

[106] E. Scavetta; R. Mazzoni; F. Mariani; R. G. Margutta; A. Bonfiglio; M Demelas; S. Fiorilli; M. Marzocchi; F. Fraboni; *J. Mater. Chem. B.*, **2014**, *2*, 2861.

Synthesis and reactivity of N-Heterocyclic Carbene Iron complexes

1.1 Abstract

Novel iron complexes bearing both cyclopentadienone and *N*-heterocyclic carbene ancillary ligands have been obtained by a straightforward synthesis from $Fe_2(CO)_9$. The preparation represents a rare example of silver transmetallation involving iron. The reaction is general and occurs in the presence of variously functionalized NHC and cyclopentadienones. The reactivity of the new iron species is then discussed.

1.2 Introduction

Iron is the most abundant transition metal in Earth's crust; it is cost effective and environmentally benign. Furthermore, its low toxicity and involvement in several biological processes make iron one of the most important elements in nature.[1] For a long time, noble metals such as Pd, Rh, Ir, Ru have dominated the field of homogeneous catalysis and only in the last decade has the use of iron complexes in catalysis witnessed a strong acceleration.[2] In particular, iron cyclopentadienone complexes have recently received special attention due to their easy preparation from simple and cheap materials, air–water stability and, most important, their catalytic features arising from the presence of a non-innocent ligand.[3]

One important aspect in coordination chemistry is the control and fine-tuning of electronic and steric properties of the ligand sphere. Good candidates for achieving fine control are *N*-heterocyclic carbenes (NHC), ligands of widespread use for coordination compounds and catalysis.[4] NHC ligands are easily prepared and, due to the robust bond formed with most metal centers, are highly resistant toward decomposition. Easy accessibility and steric/electronic tunability are further important features of NHCs. Indeed, a series of reports in the last few years have shown that, in addition to the intrinsic interest in iron-NHC chemistry, such compounds do have considerable potential for unique and wide-ranging applications including: novel coordination chemistry, homogeneous catalysis, and bio-mimetic chemistry.[5] Developments in homogeneous catalysis involving iron-NHC complexes are represented by cross-coupling Kochi reactions, C-C bond formation reactions,

hydrosilylation,[6] allylic alkylation, C–X bond formation (X = B, N, Mg, S), reduction reactions, transfer hydrogenation[7] and cyclization reactions.[1]

In principle by combining NHC and cyclopentadienone ligands on transition metal complexes, the properties of both ligands should be exploited allowing the design of novel metal/cyclopentadienone bifunctional catalysts in which steric and electronic properties, solubility and the introduction of substituents suitable for heterogenisation should be finely tuned.

With this aim in mind, a straightforward approach towards Ru(0)-NHC complexes has been recently communicated by the group in which I performed my PhD,[8] based on a dimeric Ru(0) cyclopentadienone dicarbonyl dimer (**3**). Cleavage of **3** in the presence of the silver carbene precursor **2** provided access to a new class of ruthenium complexes (Scheme 1).

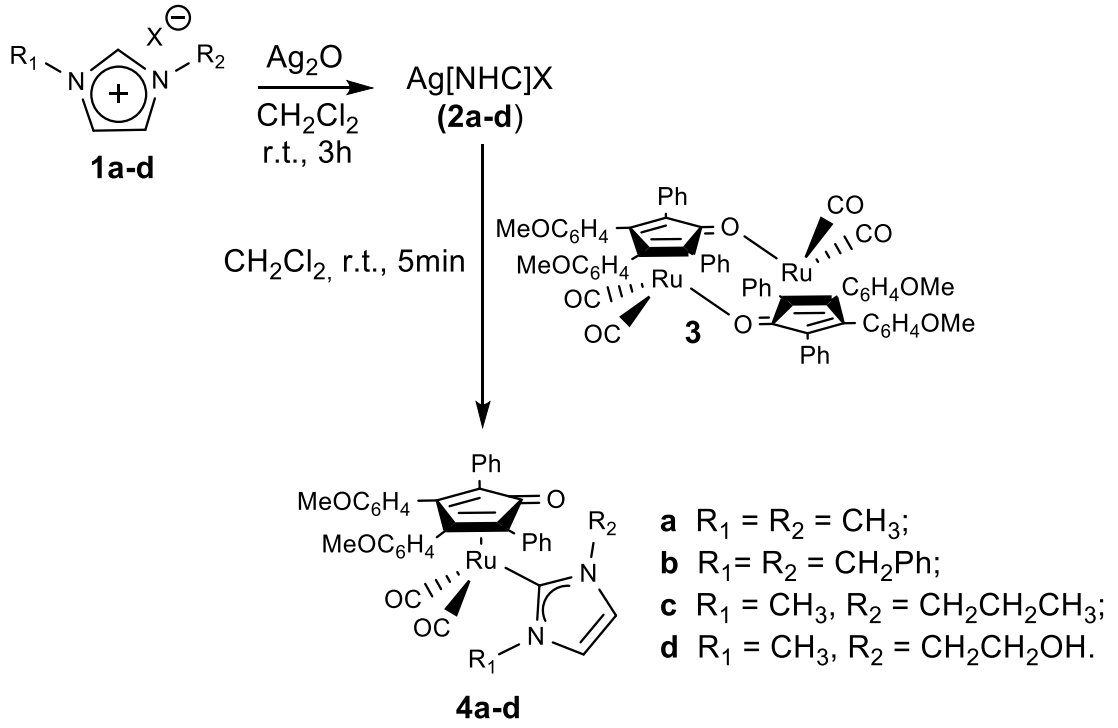

Scheme 1. Synthesis of dicarbonyl-cyclopentadienone-*N*-heterocyclic carbene ruthenium complexes (**4a-d**).

The reaction, clean and quantitative, can be also performed in one pot by adding all the reagents *in situ*. The same procedure has been successively extended to triazolylidene ligands and the corresponding complexes showed to be active in transfer hydrogenation and in oxidation of alcohol in the presence of additives such as cerium ammonium nitrate (CAN).[9]

In order to expand the scope of this reaction to iron, a cyclopentadienone triscarbonyl iron complex was chosen as precursor. Synthesis and reactivity of cyclopentadienone NHC iron complexes are described in this chapter.

1.3 Results and Discussion

1.3.1 Microwave-assisted synthesis.

Inspired by previous work on ruthenium,[10] we tried to take advantage of microwave irradiation for the synthesis of the triscarbonyl cyclopentadienone precursor (**5**) with significant reduction of the reaction time. Indeed, after screening different temperatures and times, best reaction conditions have been found at 140 °C, with a reaction time of 70 minutes. Under these conditions, the same efficiency was obtained as traditional heating at reflux for 18 h,[11] leading to a 50% yield.

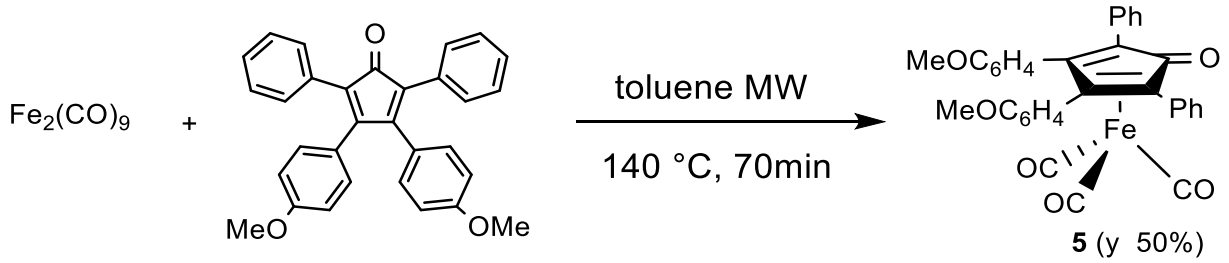

Scheme 2. Microwave assisted synthesis of triscarbonyl-(η^4-3,4-bis(4-methoxyphenyl)-2,5-diphenylcyclopenta-2,4-dienone)iron (**5**).

Suitable crystals of **5** were obtained with the double layer technique (dichloromethane/hexane). The crystal structure of **5** (Figure 1) closely resembles those previously reported for other $Fe(CO)_3$-cyclopentadienone complexes.[12] The X-ray crystal structure clearly illustrates the η^4 character of the bonding of the cyclopentadienone ligand. The average bonding distance from the iron to the tetracyclone ring carbons C(4)-C(7) is 2.11 Å and is markedly shorter than the distance to the ketonic carbon Fe(1)-C(3) [2.4074(19) Å].

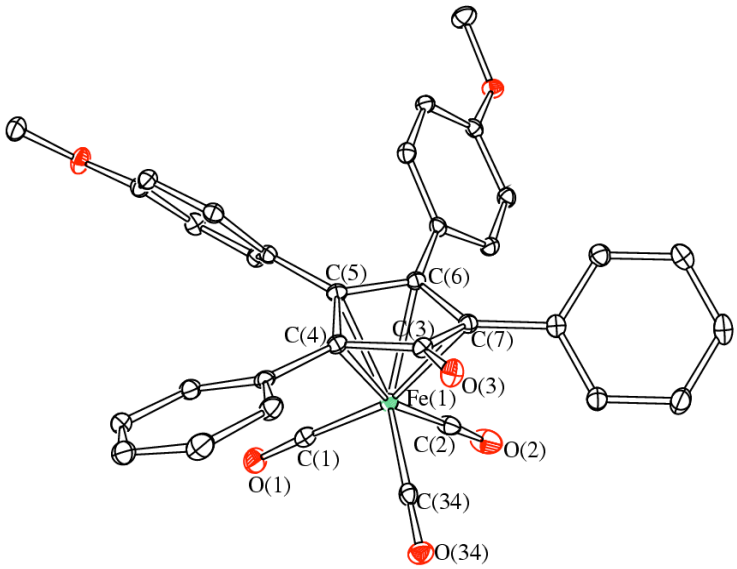

Figure 1. ORTEP drawing of **5**. Displacement ellipsoids are at the 30% probability level. H-atoms have been omitted for clarity. Selected bondlengths (Å): Fe(1)-C(1) 1.807(2), Fe(1)-C(2) 1.800(2), Fe(1)-C(34) 1.809(2), Fe(1)-C(3) 2.4074(19), Fe(1)-C(4) 2.1257(19), Fe(1)-C(5) 2.1065(19), Fe(1)-C(6) 2.1016(19), Fe(1)-C(7) 2.1027(19), C(3)-O(3) 1.230(2).

1.3.2 Transmetallation reaction.

After having optimized the preparation of **5**, one of the terminal carbonyls was replaced upon reaction with Me_3NO in acetonitrile, with the more labile acetonitrile ligand, leading to the formation of biscarbonyl-acetonitrile(η^4-3,4-bis(4-methoxyphenyl)-2,5-diphenylcyclopenta-2,4-dienone)iron (**6**). Complex **6** was treated with silver-NHC complexes, obtained *in situ* by reaction of imidazolium salts **1** and Ag_2O.[8] The latter reaction, performed in refluxing toluene, leads to the formation of the desired NHC complexes **7a-f** generally in good or excellent yields (50-80%, Scheme 3). The low yield (18%) observed for **7d** can be probably ascribed to the presence of an –OH group in the NHC side chain which could interact with the C=O group of cyclopentadienone and/or with the metal center with a detrimental influence on transmetallation.

Indeed, indication of an intramolecular hydrogen bond between the cyclopentadienone and –OH group in complex **7d** can be inferred from IR and ^{13}C NMR spectra. In the IR spectra the low-energy shift of the carbonyl band of **7d** [υ(CO) = 1576 cm^{-1}] compared with those of **7a-7c**, **7e**,**f** [υ(CO) = 1584-1587 cm^{-1}] suggests a η^4 to an η^5 coordination change of cyclopentadienone. Furthermore the ^{13}C-NMR shift of the C=O signal (**7a-**

7c, **7e,f**: 166-167 ppm vs. **7d**: 163 ppm) and the broadness of CH_2 signals in ^{1}H-NMR are in agreement with H-bond formation.

The same behaviour was observed for a similar ruthenium complex for which the hydrogen bond formation was also confirmed by X-ray diffraction.[8] To further confirm the role of –OH group in affecting the transmetallation to iron complexes the corresponding silver complex of the –OMe functionalized imidazolium salt **1f** has been reacted with **6** affording **7f** in 55% yield.

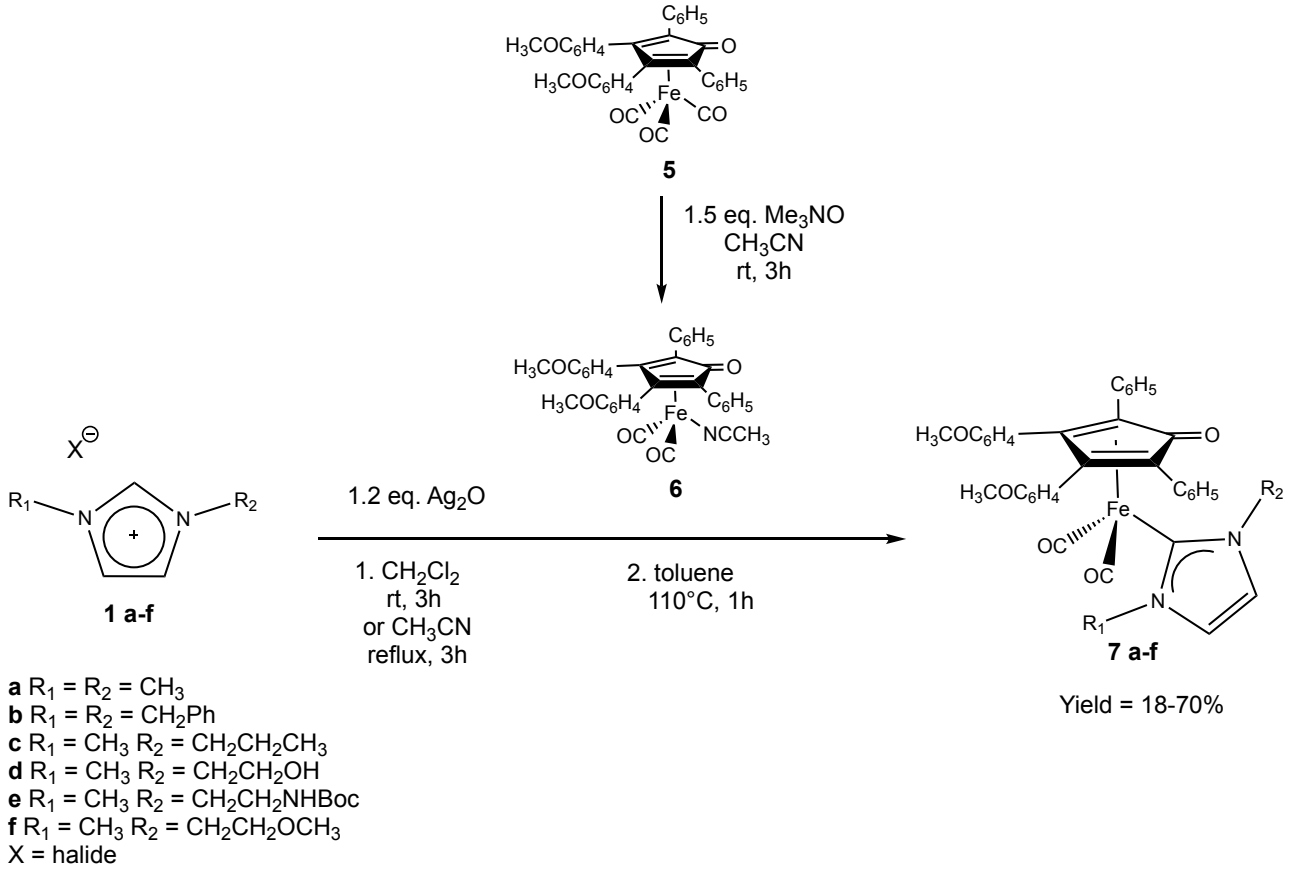

Scheme 3. Synthesis of dicarbonyl-cyclopentadienone-*N*-heterocyclic carbene iron complexes **7a-f**.

The reaction is general with non-bulky NHCs and tolerant of functional groups: in fact it occurs in the presence of a primary alcohol and amide in the lateral chain (**1d,e** to **7d,e**). The synthesis of **7a-f** has been followed by IR spectroscopy observing in all cases a lowering in the CO stretching frequencies (*e.g.* **7a**: υ(CO) = 1988, 1930 cm^{-1} *vs.* **5**: 2008, 1954 cm^{-1}) due to the strong NHC σ-donor properties. ^{13}C-NMRs (Figure 2) show a diagnostic signal for the Fe-$C_{carbene}$ within the range 182-185 ppm and molecular ions of complexes **7a-f** are detectable by ESI-MS. Complexes **7a-f** are air- and moisture-stable both in solid state and in solution and are soluble in the most common organic solvents.

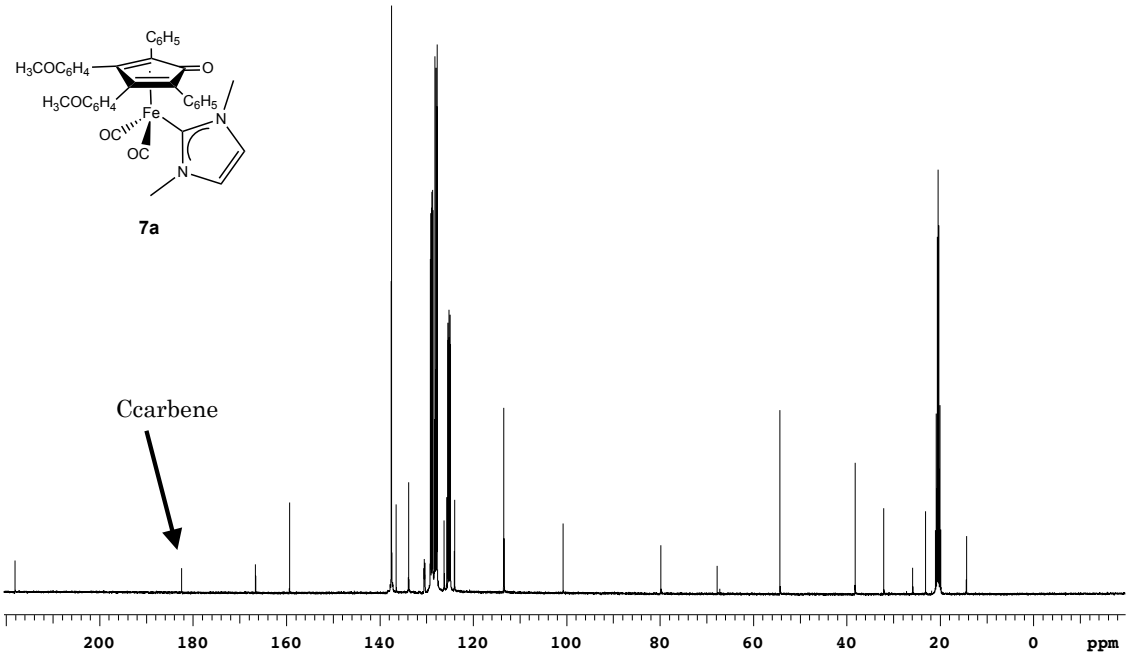

Figure 2. ^{13}C-NMR of **7a** in C_7D_8. In evidence the Fe-Ccarbene.

Complexes **7a**, **7b** and **7c** have been also characterised by X-ray diffraction studies. The molecular structure of **7a** is reported in Figure 3, whereas those of **7b** and **7c** are given in the Experimental Section (Figures 5 and 6). Their structures are similar to those previously reported for analogous Ru-complexes.[8] In particular, the Fe(1)-C(3) distance [2.348(3) Å in **7a**] is significantly longer than Fe(1)-C(4-7) [2.053(3)- 2.162(3) Å, average 2.118(6) Å in **7a**] and C(3)-O(3) [1.246(4) Å in **7a**] is essentially a double bond,[13] in agreement with C=O bond, absorptions around 1585 cm^{-1} were found in the IR spectra of complexes **7a-f**. The Fe(1)-C(34) bond [1.980(3) Å in **7a**] is in the typical range for the interaction between Fe(0) and a *N*-heterocyclic carbene.[7a]

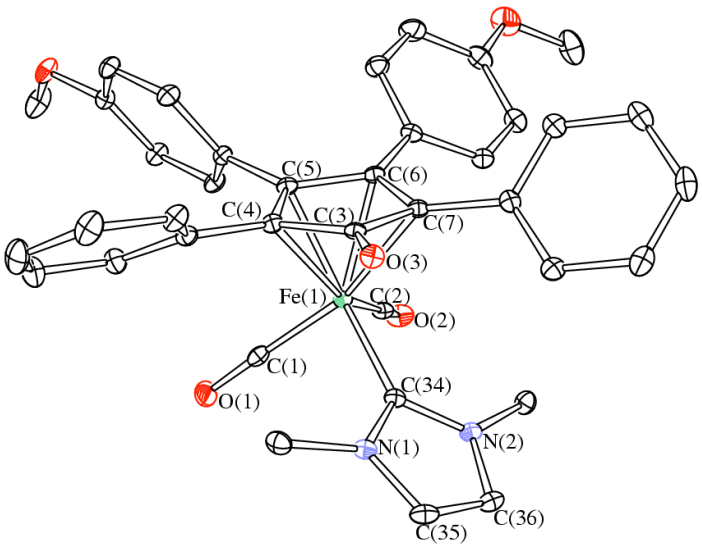

Figure 3. ORTEP drawing of **7a**. Displacement ellipsoids are at the 30% probability level. H-atoms have been omitted for clarity. Selected bond lengths (Å): Fe(1)-C(1) 1.754(3), Fe(1)-C(2) 1.765(3), Fe(1)-C(3) 2.348(3), Fe(1)-C(4) 2.162(3), Fe(1)-C(5) 2.053(3), Fe(1)-C(6) 2.099(3), Fe(1)-C(7) 2.156(3), Fe(1)-C(34) 1.980(3), C(3)-O(3) 1.246(4).

In order to further extend the ligand scope, the Knolker's cyclopentadienone triscarbonyl complex[14] has been obtained, exploiting microwave irradiation. As previously observed for **5**, the synthesis is by far faster than that reported in the literature affording **8** in good yield (83%). By treating **8** with Me_3NO in CH_3CN, the intermediate **9** has been obtained and employed as precursor for the synthesis of NHC complexes **10** by transmetallation with silver-NHC complexes prepared *in situ* (Scheme 4). Complexes **10a,b,d,e** have been completely characterized (see Experimental section). Noteworthy, –OH functionalized complex **10d** (y = 13 %) resembles the behavior of the congener **7d** further confirming an influence of the hydroxyl group on the reactivity of these complexes.

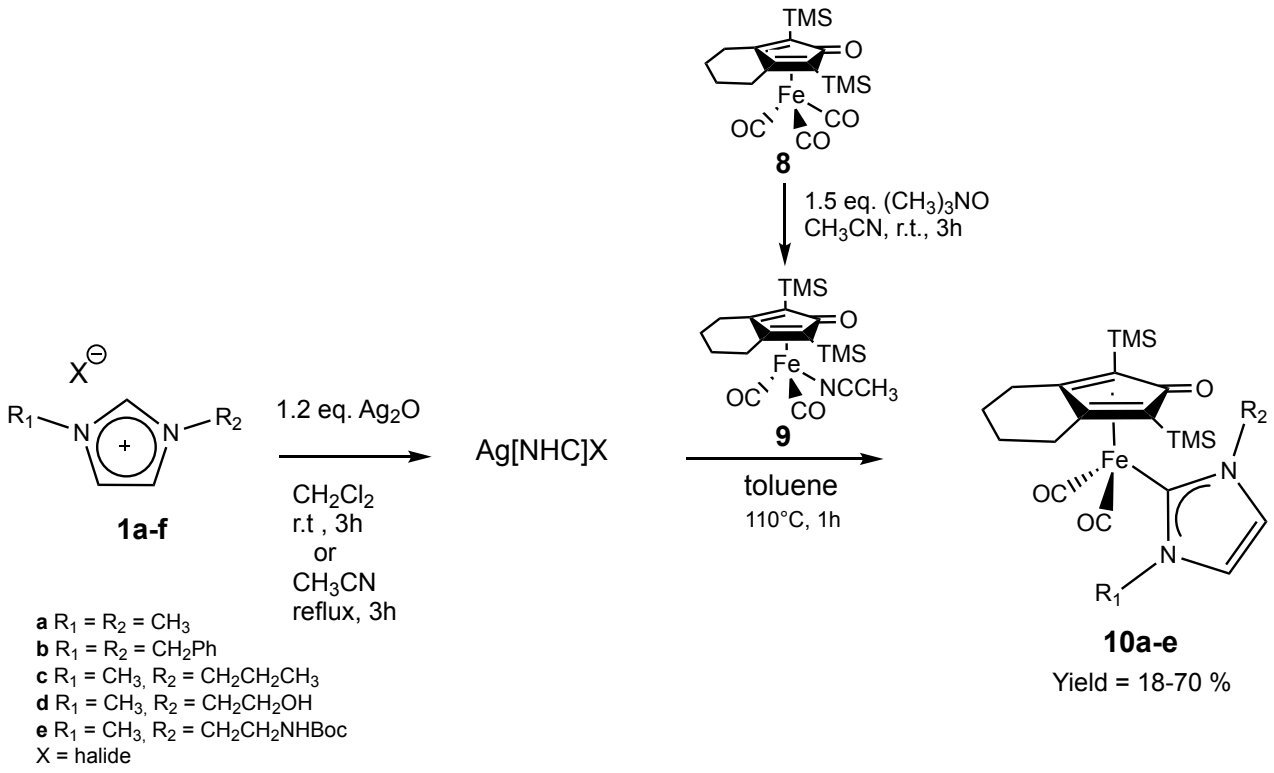

Scheme 4. Synthesis of dicarbonyl-cyclopentadienone-*N*-heterocyclic carbene iron complexes **10a-e.**

Complex **10a** has been characterized by X-ray diffraction and its structure is similar to **7a** apart from the different substituents on the cyclopentadienone ring.

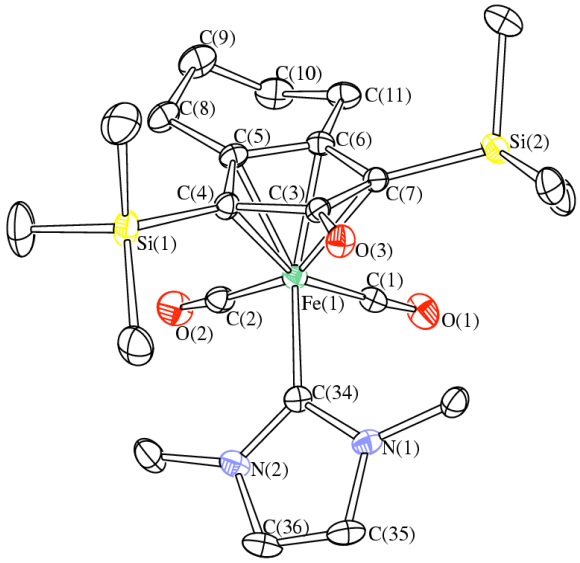

Figure 4. ORTEP drawing of **10a**. Displacement ellipsoids are at the 30% probability level. H-atoms have been omitted for clarity. Selected bond lengths (Å): Fe(1)-C(1) 1.747(3), Fe(1)-C(2) 1.754(3), Fe(1)-C(3) 2.359(2), Fe(1)-C(4) 2.153(3), Fe(1)-C(5) 2.091(3), Fe(1)-C(6) 2.067(2), Fe(1)-C(7) 2.177(2), Fe(1)-C(34) 1.996(3), C(3)-O(3) 1.250(3).

The reaction reported in Schemes 3 and 4 is one of the rare examples of transmetallation from silver complexes to first row transition metals, such as iron[1,15,16,17] and the first example in which transmetallation is employed in the

synthesis of piano stool complexes. Such complexes were initially obtained upon reaction of diamines with mononuclear ([FeCp($SnPh_3$)(CO)(CS)]) or dinuclear ([$Fe_2Cp_2(CO)_2$(μ-CO)(μ-C(SMe_2)(CN))]$^+$) thiocarbyne complexes.[18] An alternative route consists in the deprotonation of the imidazolium salts followed by reaction of the resulting carbene with an iron halide precursor (e.g. [FeCp$(CO)_2$I]).[19] Finally, an elegant synthetic approach, was described by Royo et al.[20] based on the formation of bidentate cyclopentadienyl functionalized iron(II)-NHC by direct reaction of the imidazolium proligands with $Fe_3(CO)_{12}$.

The disadvantage of the deprotonation method is that the generation of a free, often unstable, carbene intermediate requires special bases, rigorous air and moisture-free conditions and generally deliver the corresponding complexes with scarcely reproducible yields. On the other hand, transmetallation with silver complexes does not require any particular reaction condition and can be applied to a broad range of imidazolium salts bearing various *N*-substituents.

In our case transmetallation might be favoured by the presence of the non-innocent cyclopentadienone ligand, which can interact with silver[8] and labilize the silver-carbene bond. The valence of the iron centre might also have an influence on the reactivity, as suggested by the related complex [FeCp$(CO)_2(CH_3CN)]BF_4$, obtained reacting [FeCp$(CO)_2]_2$ with $AgBF_4$, that does not undergo transmetallation with silver-NHC complexes. Furthermore, a possible role for the NHC ligand donor properties should not be excluded, in addition to their steric effects (complex **6** is unreactive towards hindered silver-NHC such as 1,3-bis(2,6-diisopropylphenyl)imidazol-2-ylidene silver chloride). Indeed, NHCs with bulky substituents generally display better donor properties, as evaluated by TEP values (Tolman Electronic Parameters). A combination of these steric and electronic effects might increase both stability and inertness of the silver complexes intermediates and consequently disfavour carbene transmetallation.[21]

1.3.3 Reactivity: CO release.

The air- and water-stable iron-NHC complexes **7** and **10** displayed interesting properties concerning the CO release. In this discussion, the TMS-type **10** complexes are taken as model compounds.

The removal of one CO ligand is a main concern, since **10** features a saturated coordination around the metal centre. Hence, displacement of a CO with a more labile ligand as acetonitrile, might be a key step for potential application in catalytic or redox reactions. Removal of one CO might be achieved under oxidative (Me_3NO) or photochemical (UV irradiation) conditions.

Treating **10a** with an excess of Me_3NO (up to 5eq.) resulted in no reaction even in refluxing acetonitrile. Irradiation of **10a** solution in acetonitrile at about 325nm (UV light) led to extensive decomposition. Disappointed by the results and in an attempt to labilize the Fe-CO bond, reactions with strong protic acid were investigated: protonation of dienone has already been reported[9] to afford cationic products. Considering the non-innocent character of cyclopentadienone ligand, the positive charge might be localized either at the oxygen (A, Scheme 5) or at the iron centre (B, Scheme 5), inducing an iron(II) formal oxidation state and depletion of electron density from the metal centre, which is expected to reduce the strength of the Fe-CO bond. Upon the addition of CF_3SO_3H or HBF_4 (1 eq.) to a solution of **10a** in Et_2O, precipitation occurred, yielding a light-yellow solid in quantitative yield. The solid was identified as the corresponding iron salts **10a[CF_3SO_3H]** and **10a[HBF_4]**.

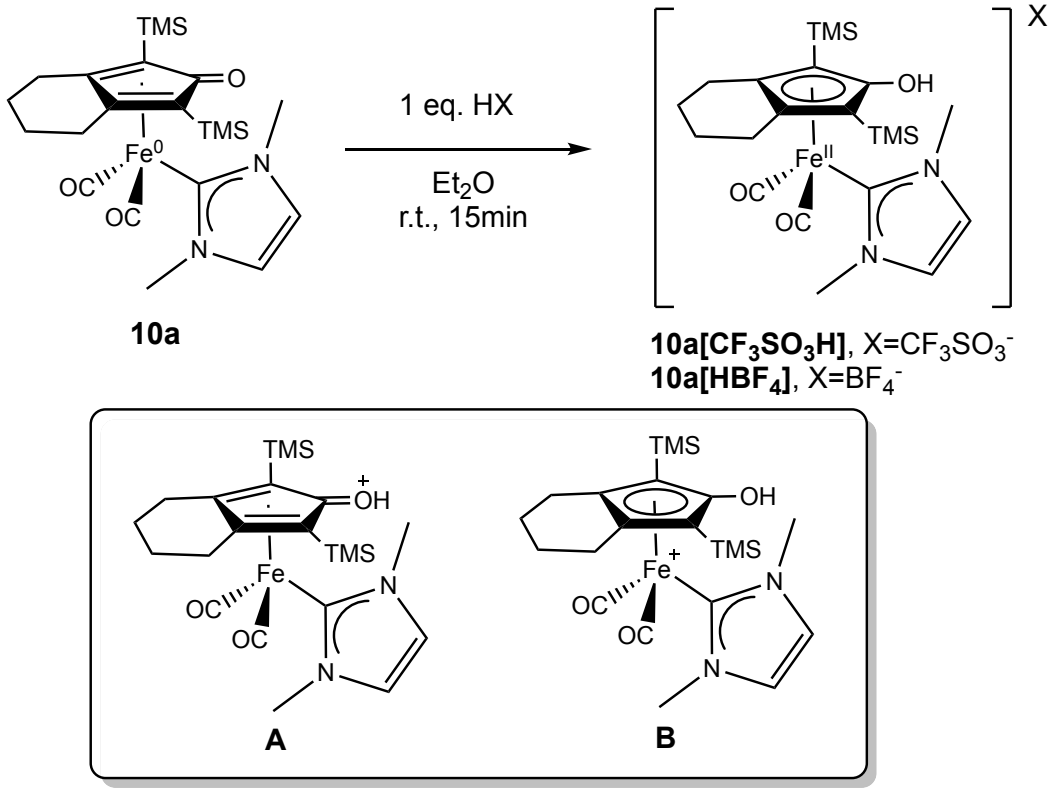

Scheme 5. Synthesys of iron salts **10a[X]**. On the bottom the possible representation of the cationic structure A and B.

IR spectroscopy analysis of the salt **10a[X]** showed a strong shift to high-energy field of the CO stretching frequencies (*e.g.* **10a**: υ(CO) = 1983, 1922 cm^{-1} *vs.* **10a[CF_3SO_3H]**: 2023, 1975 cm^{-1}) due to the formal oxidation of the iron centre and the ketone C=O stretching of the Cp=O disappeared. ^{13}C-NMRs gave further insights on the structure of the compound: coordination of the dienone ligand switching from η^4-cyclopentadienone to η^5-hydroxycyclopentadienyl, consistent with the shift to higher field resonance of the ketone-enol carbon (δ **10a**$_{C=O}$: 176ppm vs **10a[CF_3SO_3H]**$_{C-OH}$: 145ppm). The Fe-NHC carbon signal is also shifted to higher-energy field (δ($C_{carbene}$) **10a**: 184ppm vs **10a[CF_3SO_3H]**: 176 ppm).

A crystal structure of **10a[CF_3SO_3H]** was obtained by a single-crystal X-ray diffraction and confirmed the new coordination arrangement around the iron centre. Selected bond distance differences between **10a[CF_3SO_3H]** and **10a** are reported in Table 1: the Fe-CO bond is longer and in according with a reduced π-character of the bond; the Fe-C(3) bond distance is far shorter now, which is indicative of η^5-coordination of the hydroxycyclopentadyenil (Cp-OH); finally, C(3)-O(3) is a single bond[14], in accordance with Cp-OH.

Table 1. Selected bonds of **10a** and corresponding cationic salt **10a[CF_3SO_3H]**.

Bond	**10a (Å)**	**10a[CF_3SO_3H] (Å)**
Fe(1)-C(1)	1.747(3)	1.774(4)
Fe(1)-C(2)	1.754(3)	1.774(4)
Fe(1)-C(3)	2.359(2)	2.119(4)
Fe(1)-C(4)	2.153(3)	2.119(3)
Fe(1)-C(5)	2.091(3)	2.126(4)
Fe(1)-C(6)	2.067(2)	2.124(4)
Fe(1)-C(7)	2.177(2)	2.154(4)
Fe(1)-C(34)	1.996(3)	1.977(4)
C(3)-O(3)	1.250(3)	1.384(5)
C(1)-O(1)	1.155(4)	1.137(6)
C(2)-(O)2	1.153(4)	1.141(5)

Treating **10[HBF$_4$]** with Me_3NO (up to 5 eq.) yielded the neutral precursor **10a**, in that Me_3NO acted as a base, extracting the proton from the diene. Upon irradiation of a solution **10[HBF$_4$]** in acetonitrile, the bright yellow solution turned to deep red in a few minutes. The new reddish complex **11** is an unsaturated iron(II) compound, in which the free vacant site on the metal centre is occupied by acetonitrile. The species **11** is stable only a few minutes in air in acetonitrile solution, and must be handled with care under a nitrogen or argon atmosphere. ^{1}H-NMR (Figure 5) showed the splitting of hydroxycyclopentadyenil signals, which might be ascribable to the four-substituted iron centre: the CH_{3TMS} is now split in two, while the CH_2 resonances of the six-membered ring are now six separated multiplets.

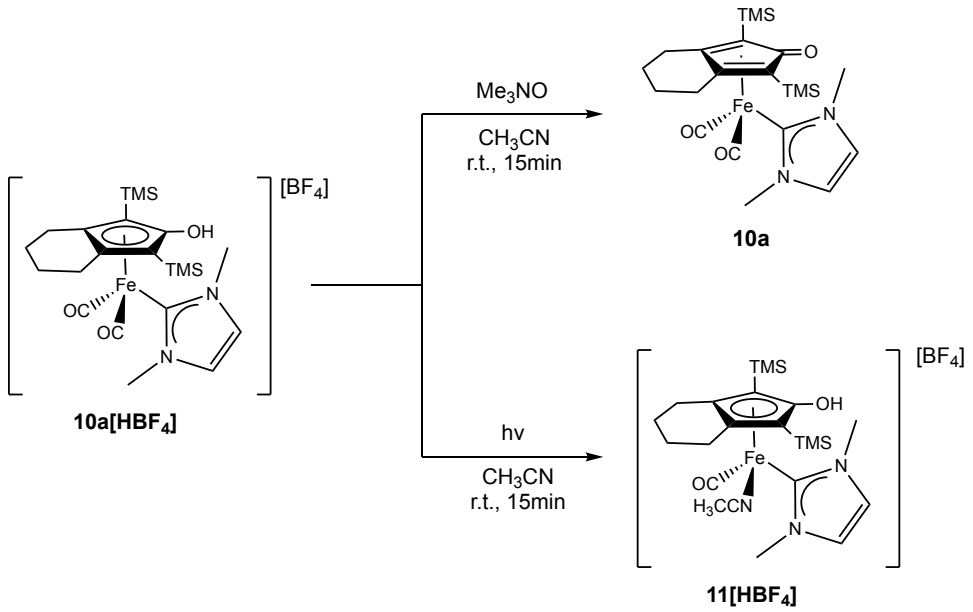

Scheme 6. Synthesis of **11** under UV irradiation.

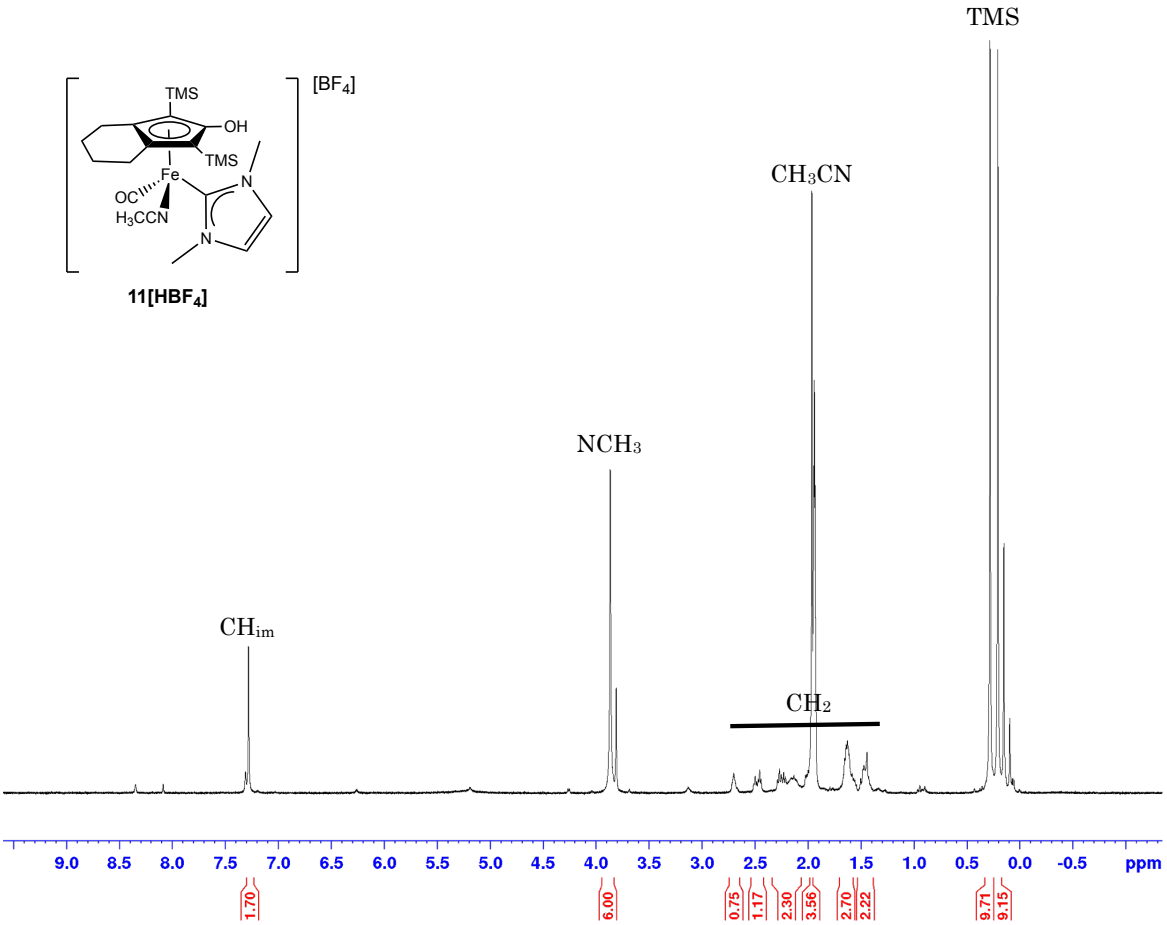

Figure 5. ^{1}H-NMR of compound **11** in CD_3CN.

Intrigued by the reactivity of the iron(II) species and wishing to obtain an iron(0) analogue, **11** was treated with Me_3NO, but a mixture, hard to purify, of the corresponding neutral carbonyl-acetronitrile-NHC iron(0) complex and the biscarbonyl-NHC **10a** was obtained. Thus, another neutral iron(0) **10g** (scheme 7) compound has been synthesised, bearing a chelating group on a lateral chain of the NHC ligand, which might be able to enhance the carbonyl displacement under UV irradiation.

1.3.4 The amino family.

The iron complex **10g**, bearing an amine as functional group on the NHC, is the deprotected derivative of **10e**: treating precursor with an excess of tetrafluoroboric acid (HBF_4) followed by neutralization, yielded the corresponding amino-complex **10g** in good yield (Scheme 7). The ^{1}H-NMR and ^{13}C-NMR spectra are comparable with the previous **10**-type compounds, and ESI-MS confirmed the structure.

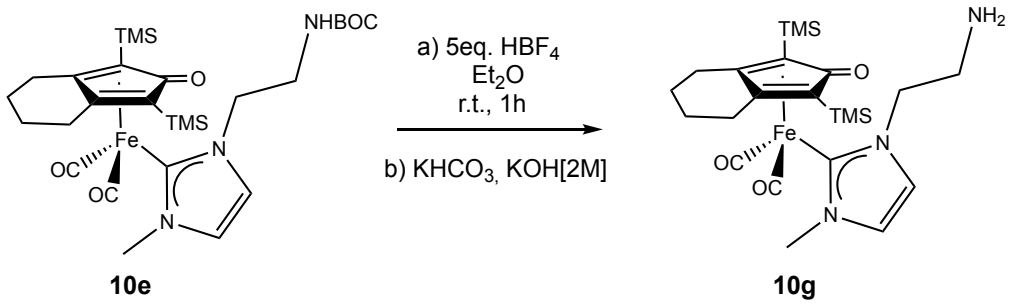

Scheme 7. Deprotection of NHBOC.

Upon irradiation for about 1 hour, a yellow solution of **10g** in toluene, turned deep red affording the corresponding chelated complex **12**. The reaction was followed by IR spectroscopy and compound **12** showed only one CO stretching frequency at 1879 cm^{-1}. As for the complex **11[HBF$_4$]**, in which four different ligands are bonded to the iron metal centre, signals in the ^{1}H-NMR are split due to the lower symmetry. ^{13}C-NMR showed four different quaternary C_{Cp} and a shift to respectively lower and higher fields of $C_{carbene}$ (δ **10g**: 185ppm vs **12**: 193 ppm) and C=O (δ **10g**: 176ppm vs **12**: 168 ppm).

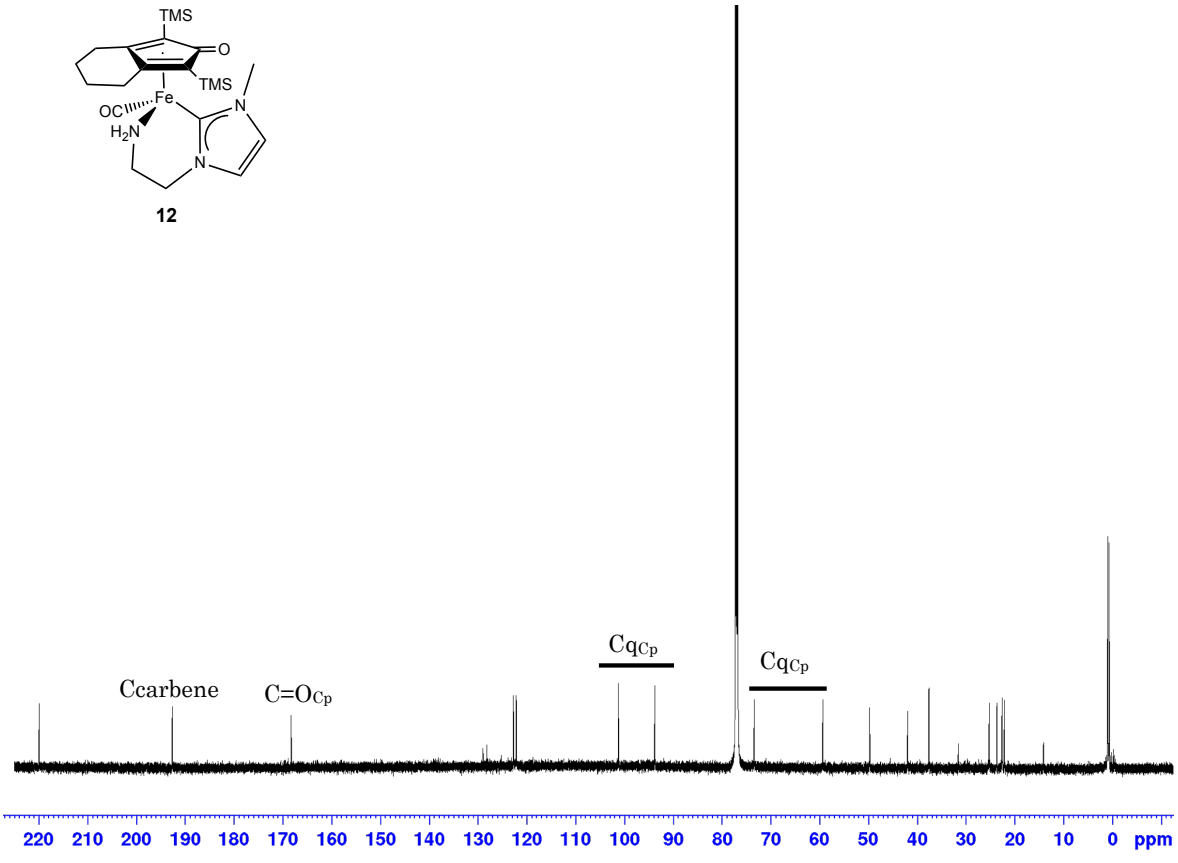

Figure 6. ^{13}C-NMR in $CDCl_3$ of **12**. CqCp, quaternary carbon of cyclopentadienone.

The molecular structure of **12**, as determined by X-ray crystallography (Figure 7), closely resembles that previously reported for the complex **10a**. Thus, the Fe(1)-C(2) distance [2.295(3) Å] is significantly longer that Fe(1)-C(3-6) [2.080(3)-2.160(3) Å] and C(2)-O(2) [1.268(4) Å] is essentially a double bond[13]. The Fe(1)-C(17) contact [1.945(3) Å] is in the typical range for the interaction between Fe(0) and a N-heterocyclic carbene[22]. The amino side-chain of the functionalized NHC ligand acts as a chelating agent on the iron centre, as evidenced by the close Fe(1)-N(3) contact [2.065(3) Å]. An intra-molecular hydrogen bond is present between the amino and ketone groups [N(3)-H(3b) 0.89 Å, H(3b)···O(2) 2.10 Å, N(3)···O(2) 2.854(4) Å, <N(3)H(3b)O(2) 141.9°].

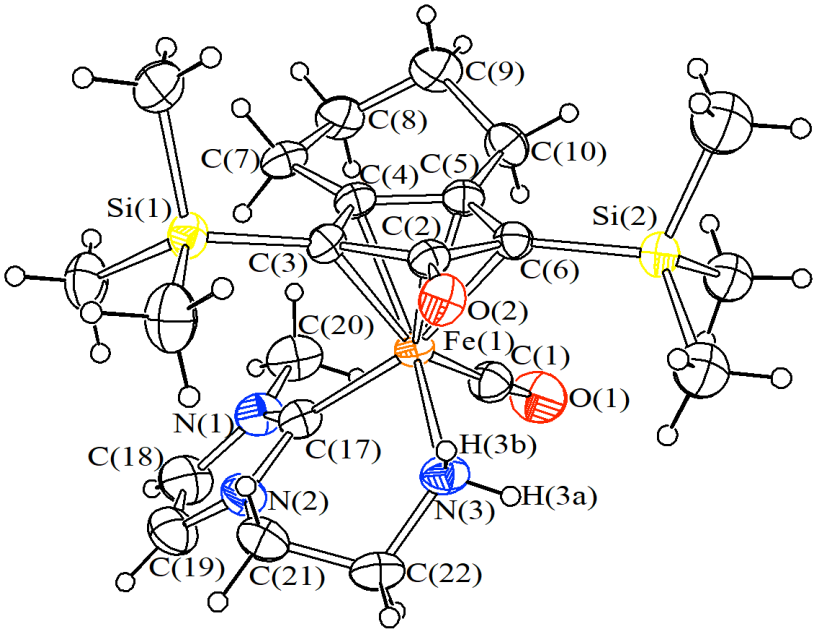

Figure 7. ORTEP drawing of **12**. Displacement ellipsoids are at the 30% probability level. Selected bond lengths (Å): Fe(1)-C(1) 1.733(4), Fe(1)-C(2) 2.296(3), Fe(1)-C(3) 2.160(3), Fe(1)-C(4) 2.079(3), Fe(1)-C(5) 2.075(3), Fe(1)-C(6) 2.131(6), Fe(1)-C(17) 1.946(3), Fe(1)-N(3) 2.065(3), C(3)-O(3) 1.268(4).

The new complex is stable at air at room temperature. The tendency of **10g** to undergo a carbonyl displacement is high, indeed even exposure to sun light promotes the reaction; this is clearly visible by a change from yellow to an orange solid (a mixture of yellow and red after a couple of days). On the contrary, a solution of **12** under CO atmosphere (1.5 atm) does not undergo the reverse transformation to **10g**, demonstrating the high stability of the chelated form.

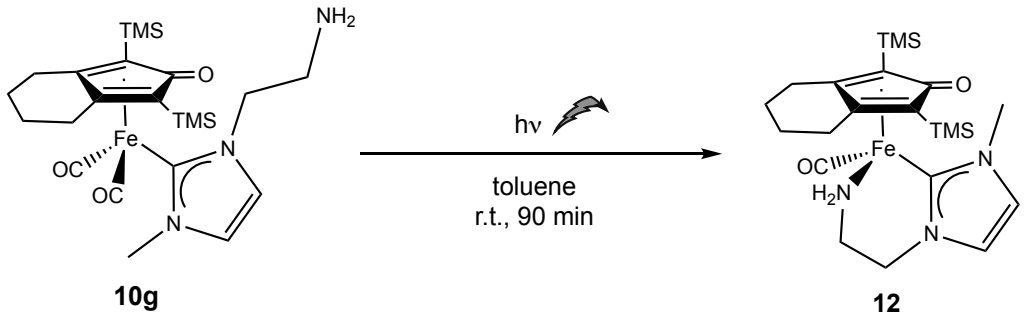

Scheme 8. Irradiation of **10g** in toluene leading to corresponding chelated compound **12**.

1.3.5 Water solubility of amino-substituted iron complexes.

Amino functionalized complex **10g** is also soluble in acidic water (35.4 mmol/L, acetic acid/acetate buffer solution, pH 4.74), but not in neutral or basic (e.g. disodium phosphate(DSP)/monopotassium phosphate(MKP) buffer solutions, pH 7.4) conditions. This behaviour might be due to an equilibrium between protonated species in solution involving the NH_2 group. IR of the acidic solution revealed the presence of **10g (**υ(CO) = 1981, 1921 cm^{-1}) and its corresponding mono-protonated hydroxycyclopentadienil (υ(CO) = 2031, 1986 cm^{-1}). Complex **10g** might undergo protonation in two different sites (Scheme 7): the C=O of cyclopentadienone ligand (**10g-II**) and the NH_2 on the NHC ligand (**10g-I**). Both the two functional groups might engage a hydrogen bond, leading to **10g-III** as an equilibrium between the two species. Indeed, only one protonated species is visible in the IR spectrum, then the equilibrium should be far to the right and **10g-III** is the only visible species at IR time-scale.

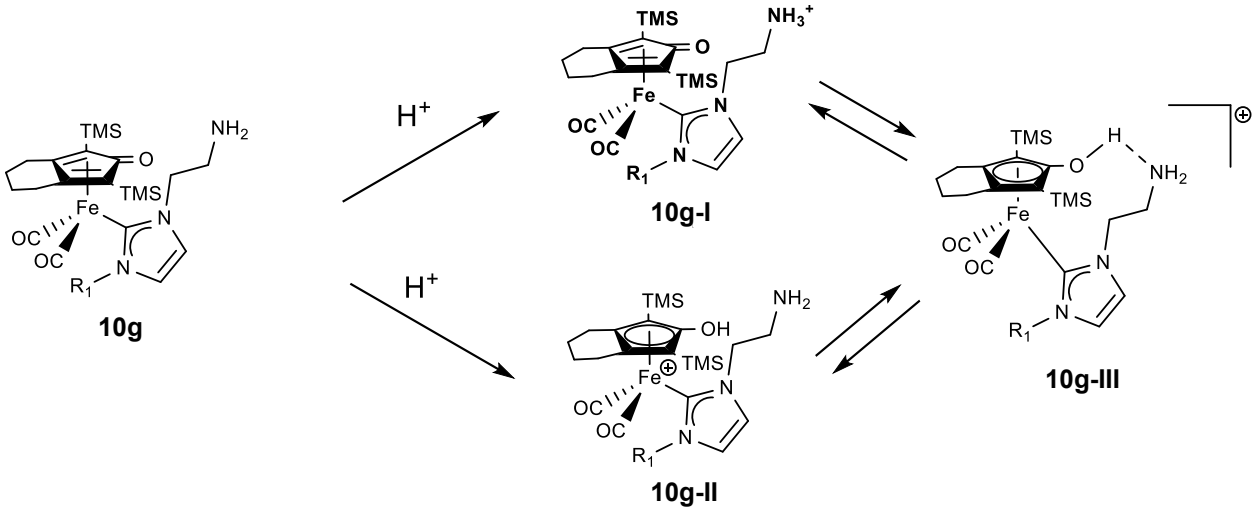

Scheme 9. The equilibrium in acidic water of **10g**.

In order to solve the water solubility problem at basic pH values, ionic complex **10h** was synthesised (Scheme 6). Triscarbonyl iron complexes bearing a ionic group on cyclopentadienone are already known in literatures and they have been successfully employed in water-based catalysis.[23] Following the same synthetic route, **10g** was treated with methyl iodide to yield the light yellow powder **10h**, which has been characterised by IR, NMR and ESI-MS. IR spectrum is comparable with **10x** iron complexes and ^{1}H-NMR confirmed methylation of N atom (DMSO-*d6*, $N(CH_3)_3$ δ: 3.22ppm). The new compound **10h** was indeed soluble in both buffer solutions.

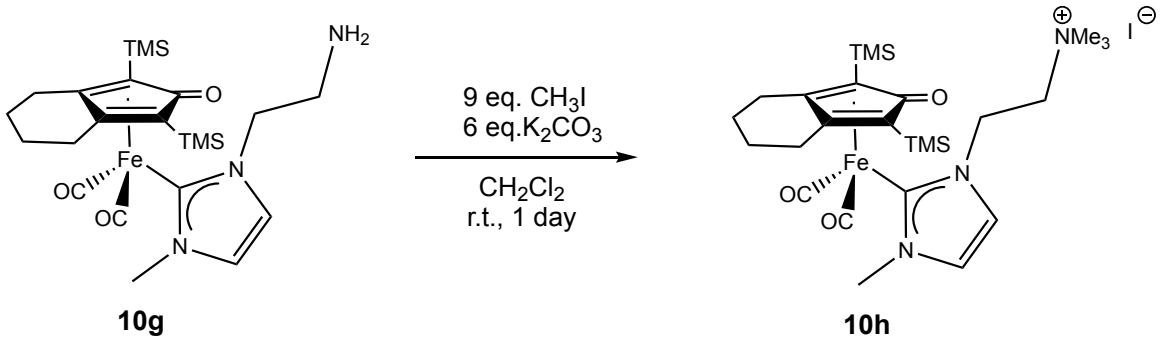

Scheme 10. Alkylation of **10g** and corresponding ammonium salt **10h**.

1.3.6 Mössbauer characterisation.

In order to estimate oxidation state of the iron centre, a Mössbauer characterisation is herein reported. In general, Mössbauer isomer shifts of Fe complexes are useful in providing a sensitive indication of metal s electron density. A decrease in the value of δ reflects an increase in s density which can be prompted by enhanced ligand σ donation (to metal s orbitals) or by greater retrodative π bonding from filled metal d orbitals to empty ligand orbitals.[24] Samples **8** and**10a** showed a Mössbauer spectrum characterised by an intense doublet centered near 0 velocity value. The best fitting was obtained by using a single doublet, with parameters as reported in Table 2. A δ value so close to 0 mm/s is representative of high s density on Fe nucleus and is comparable with other Fe(0) complexes, such as PNP-Fe(0) reported by Milstein.[25] Concerning **10a[HBF$_4$]**, the lower value of δ is in line with a low-spin Fe(II) shift.[26] Variations in the CpO substituents showed no significant differences between **7a** and **10a** hyperfine parameters.

The quadrupole splitting (Δ) is related to the symmetry of the system. Indeed, triscarbonyl precursor **8** showed lower value in comparison with NHC-featured iron

complexes, which is in line with a higher overall symmetry. Mössbauer spectra are reported in Figure 8.

Table 2. Room temperature Mössbauer parameters.

Sample	***δ*** ***(mm·s⁻¹)***	***Δ*** ***(mm·s⁻¹)***	***Γ*** ***(mm·s⁻¹)***	***A*** ***%***
7a	0.017±0.001	1.89±0.01	0.24±0.01	100
8	0.015±0.001	1.52±0.01	0.26±0.02	100
10a	0.019±0.003	1.89±0.01	0.23±0.01	100
10a[HBF4]	0.004±0.001	1.99±0.01	0.25±0.01	100

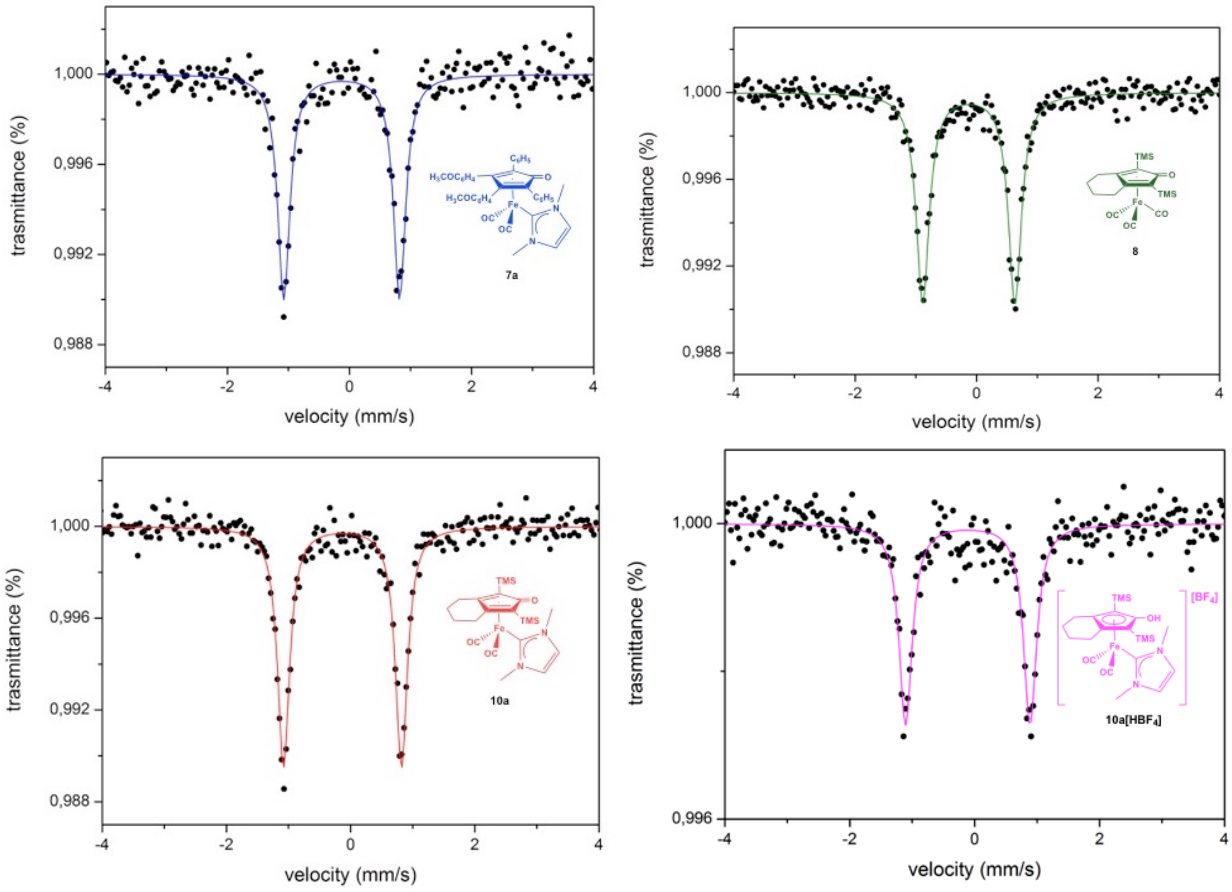

Figure 8. Mössbauer spectra at room temperature.

1.4 Conclusion

In summary a very efficient and rapid synthetic route for obtaining a new class of Fe(0) complexes, which contain both *N*-heterocyclic carbenes and cyclopentadienone ligands, has been developed. The synthetic approach takes advantage of transmetallation from silver-NHC complexes, which is a method rarely exploited in the case of iron-NHC complexes. Transmetallation could be favoured either by non-innocent cyclopentadienone ligand or by iron valence. Donor and steric properties of NHCs can also play a role.

The corresponding iron(II) salts are easily obtained by treating the precursor iron(0) with a strong acid. Furthermore, a second carbonyl ligand can be displaced in the iron(II) species or in the iron(0) compound with the appropriate NHC ligand, bearing $-NH_2$ functionality. In addition, the amino group on the NHC promotes water solubility, which is strongly pH dependant. Complete solubility is finally obtained with the insertion of a cationic NMe_3^+ on the lateral chain.

1.5 Experimental section

General data. All reactions were routinely carried out under a nitrogen atmosphere, using standard Schlenk techniques. Glassware was ovendried before use. Solvents: dichloromethane (CH_2Cl_2), tetrahydrofuran (THF), diethyl ether (Et_2O), petroleum ether referring to a fraction of bp 60-80 °C, acetonitrile (CH_3CN) were dried and distilled prior to use. Acetone has been degassed and stored under inert atmosphere on molecular sieves. Other solvents such as ethylacetate (EtOAc), chloroform, ethanol (EtOH), methanol (MeOH), heptane, toluene, $CDCl_3$, D_2O, CD_3CN (Sigma Aldrich) have been employed without further purification. Reagents: $Fe_2(CO)_9$ (Strem), methyl iodide, chloridric acid, silver oxide, 1-methylimidazole, 1,3 diphenylacetone, benzyl bromide,4,4'dimethoxybenzil (Alfa Aesar), potassium carbonate, sodium bicarbonate, disodium phosphate (DSP), monopotassium phosphate (MKP), sodium acetate, acetic acid trifluoroboric acid, trifluoromethanesulfonic acid have been employed as purchased.

1,3-dimethylimidazolium iodide (**1a[I]**),[27]1,3-dibenzylimidazolium bromide (**1b[Br]**),[28] 1-methyl-3-(2-hydroxyethyl)imidazolium chloride (**1d**),[29]mancabimime NHBoc (JOMC 2008)1,3-bis(2,6-diisopropylphenyl)imidazolium bromide (**1f[Br]**),[30] 1-methyl-3-(2-hydroxyethyl)imidazolium chloride (1, 1,3-dimethylimidazol-2-ylidene silver iodide (**2a[I]**),[31] 1,3-dibenzylimidazol-2-ylidene silver bromide (**2b[Br]**),[32]1-methyl-3-(2-hydroxyethyl)imidazol-2-ylidene silver chloride (**2d**),[33]1,3-bis(2,6-diisopropylphenyl)imidazol-2-ylidene silver bromide (**2f[Br]**),[34]1,3-di-(2,6-diisopropylphenyl)imidazol-2-ylidene copper chloride,[35]3,4-Bis(4-methoxyphenyl)-2,5-diphenylcyclopenta-2,4-dienone,[36] 1,8-bis(trimethylsilyl)octa-1,7-diyne[37] have been prepared following procedures reported in the literature.

The prepared derivatives were characterized by spectroscopic methods. The NMR spectra were recorded using Varian Inova 300 (^{1}H, 300.1; ^{13}C, 75.5 MHz), Varian Mercury Plus VX 400 (^{1}H, 399.9; ^{13}C, 100.6 MHz), Varian Inova 600 (^{1}H, 599.7; ^{13}C, 150.8 MHz) spectrometers at 298 K; chemical shifts were referenced internally to residual solvent peaks. Full ^{1}H- and ^{13}C-NMR assignments were done, when necessary, by gHSQC and gHMBC NMR experiments using standard Varian pulse sequences. Infrared spectra were recorded at 298 K on a Perkin-Elmer Spectrum 2000 FT-IR spectrophotometer. ESI-MS spectra were recorded on Waters Micromass ZQ

4000 with samples dissolved in MeOH or CH_3CN. Elemental analyses were performed on a Thermo-Quest Flash 1112 Series EA instrument. UV irradiation was performed by using a commercial Hg lamp.

Triscarbonyl-(η^4-3,4-bis(4-methoxyphenyl)-2,5-diphenylciclopenta-2,4-dienone)iron (5). In a 75 mL Teflon tube equipped with magnetic stirrer, 3,4-Bis(4-methoxyphenyl)-2,5-diphenylcyclopenta-2,4-dienone 0.53 g (1.2 mmol) and $Fe_2(CO)_9$ 0.728 g (2 mmol) were dissolved in 40 mL of toluene. The container was closed with a cap, equipped with a temperature sensor, and placed into microwave. The reaction was heated to 140 °C for 70 min. Upon removal of the solvent, the crude was purified to afford the yellow triscarbonyl-η^4-3,4-bis(4-methoxyphenyl)-2,5-diphenylcyclopenta-2,4-dienone)iron complex (**5**) by neutral alumina column chromatography using dichloromethane/ethyl acetate (100/0 to 0/100). Yield = 50%

Suitable crystals of **5** for X-ray diffraction were obtained by slow diffusion (CH_2Cl_2/Hexane). **5** has been analyzed by IR, ^{1}H-NMR, ^{13}C-NMR, ESI-MS and X-Ray diffraction. ^{1}H-NMR (399.9 MHz, $CDCl_3$): δ (ppm) 7.55-6.69 (m, 18H, C_{aryl}), 3.76 (s, 6H, -OCH_3). ^{13}C-NMR (150.8 MHz, $CDCl_3$, g-HSQC, g-HMBC): δ (ppm) 208.58 (CO), 169.75 (C=O, Cp), 159.58 (-*C*OCH_3), 133.05-121.56 (C_{aryl}), 113.40 (CH_{aryl}), 103.44 ($C_{2,5}$, Cp), 82.75 ($C_{3,4}$, Cp), 55.12 (-OCH_3). IR (CH_2Cl_2, cm^{-1}): (ν_{CO}) 2067, 2013, 1997; ($\nu_{C=O}$) 1636; ($\nu_{C=C}$) 1609, 1518. ESI-MS (m/z) (+): 585 $[M+H]^+$; 607 $[M + Na]^+$; 623 $[M+K]^+$. Anal. Calcd (%) for $C_{34}H_{24}O_6Fe$: C, 69.88; H, 4.14. Found: C, 65.97; H, 3.93.

Dicarbonyl-(η^4-3,4-bis(4-methoxyphenyl)-2,5-diphenylcyclopenta-2,4-dienone)(acetronitrile)iron (6). In a dried 15 mL Schlenk flask, triscarbonyl-(η^4-3,4-bis(4methoxyphenyl)-2,5-diphenylcyclopenta-2,4-dienone)iron (**5**) 0.145 g (0.249 mmol) and trimethylamine-N-oxide 0.028 g (0.374 mmol) were dissolved in 3 mL of anhydrous acetonitrile. Reaction mixture was stirred at room temperature and protected from light for 3 hours. A yellow precipitate appeared. The solid was filtered and washed with diethyl ether and hexane. Yield : 54%

5 has been analyzed by IR, ^{1}H-NMR, ^{13}C-NMR, ESI-MS. ^{1}H-NMR (399.9 MHz, C_7D_8): δ (ppm) 8.24-6.433 (m, 18H, CH_{aryl}); 3.10 (s, 6H, -OCH_3); 0.72 (s, 3H, -$NCCH_3$). ^{13}C-NMR (150.8 MHz, C_7D_8, g-HSQC, g-HMBC): δ (ppm) 214.21 (CO), 169.74 (C=O, Cp), 159.56 (-*C*OCH_3), 134.99-124.45 (C_{aryl}), 113.44 (CH_{aryl}), 101.41 ($C_{2,5}$, Cp), 81.31 ($C_{3,4}$, Cp),

54.32 (-OCH_3), 2.48 (CH_3, CH_3CN). IR (CH_2Cl_2, cm^{-1}): (ν_{CO}) 2008, 1954; ($\nu_{C=O}$) 1636; ($\nu_{C=C}$) 1608, 1515. ESI-MS (m/z) (+): 557 $[M\text{-}CH_3CN]^+$, 583 $[M\text{-}CH_3]^+$, 598 $[M+H]^+$. Anal. Calcd (%) for $C_{35}H_{27}NO_5Fe$: C, 70.36; H, 4.56. Found: C, 73.75; H, 4.35.

General procedure for the synthesis of dicarbonyl-η⁴-3,4-bis(4-methoxyphenyl)-2,5-diphenylcyclopenta-2,4-dienone)(NHC)iron complexes (7)

Imidazolium salts (**1**), silver oxide (1.2 eq.), tryscarbonyl-η⁴-3,4-bis(4-methoxyphenyl)-2,5-diphenylcyclopenta-2,4-dienone) iron precursor (**5**) and trimethylamine-N-oxide (1.5 eq.) were reacted in CH_3CN under inert atmosphere and with protection from light. After stirring the reaction for the time and at the temperature required in order to reach complete conversion to silver complexes (**2**), the solvent was removed under vacuo. then the solid dissolved in toluene. The reaction mixture was stirred for 1 hour at 110 °C. Upon removal of the solvent, the crude was purified to afford the dicarbonyl-η⁴-3,4-bis(4-methoxyphenyl)-2,5-diphenylcyclopenta-2,4-dienone)(NHC)iron complexes (**7**) by neutral alumina column chromatography using dichloromethane/ethyl acetate (100/0 to 0/100). Formation of the iron complexes (**7**) was verified by IR, ^{1}H-NMR, ^{13}C-NMR, ESI-MS and X-Ray crystal structure, when suitable crystals were available.

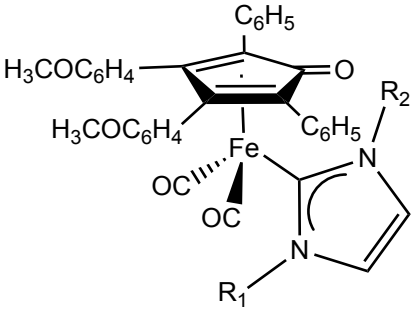

7a-f

a $R_1=R_2=CH_3$
b $R_1=R_2=Ch_2Ph$
c $R_1=CH_3$ $R_2=CH_2CH_2CH_3$
d $R_1=CH_3$ $R_2=CH_2CH_2OH$
e $R_1=CH_3$ $R_2=CH_2CH_2NHBOC$
f $R_1=CH_3$ $R_2=CH_2CH_2OCH_3$

Dicarbonyl-(η⁴-3,4-bis(4-methoxyphenyl)-2,5-diphenylcyclopenta-2,4-dienone)(1,3-dimethyl-ilidene)iron (7a). Triscarbonyl-(η⁴-3,4-bis(4-methoxyphenyl)-2,5-diphenylcyclopenta-2,4-dienone)iron (**5**) 0.150 g, (0.256 mmol), trimethylamine-N-oxide 0.029 g (0.384 mmol), 1,3-dimethylimidazolium iodide (**1a**) 0.057 g (0.256 mmol) and silver oxide 0.071 g (0.307 mmol), room temperature, 3h. Yield : 60%.

Suitable crystals of **7a** for X-Ray diffraction were obtained by slow diffusion (THF/Hexane). **7a** has been analyzed by IR, ^{1}H-NMR, ^{13}C-NMR, ESI-MS and X-Ray diffraction. ^{1}H-NMR (399.9 MHz, C_7D_8): δ (ppm) 8.33-6.50 (m, 18H, CH_{aryl}), 5.88 (s, 2H, CH_{NHC}) 3.10 (s, 6H, -OCH_3), 2.93 (s. 6H, -NCH_{3NHC}). ^{13}C-NMR (150.8 MHz, C_7D_8, g-HSQC, g-HMBC): δ (ppm) 218.11 (CO), 182.41 ($C_{carbene}$), 166.57 (C=O, Cp), 159.30 (-$COCH_3$), 123.96 (CH_{NHC}), 136.44-125.66 (CH_{aryl}), 113.39 (CH_{aryl}), 100.73 ($C_{2,5}$, Cp), 79.76 ($C_{3,4}$, Cp), 54.28 (-OCH3) 38.18 (-NCH_3). IR (CH_2Cl_2, cm^{-1}): (ν_{CO}) 1988, 1930; ($\nu_{C=O}$) 1585; ($\nu_{C=C}$) 1603, 1518. ESI-MS (m/z) (+): 653 $[M+H]^+$; 675 $[M + Na]^+$; 691 $[M+K]^+$. Anal. Calcd (%) for $C_{38}H_{32}N_2O_5Fe$: C, 69.95; H, 4.94. Found: C, 66.33; H, 4.63.

Synthesis of dicarbonyl-(η4-3,4-bis(4-methoxyphenyl)-2,5-diphenylcyclopenta-2,4-dienone)(1,3-dibenzylimidazole)iron (7b). Triscarbonyl-(η^4-3,4-bis(4-methoxyphenyl)-2,5-diphenylcyclopenta-2,4-dienone)iron (**5**) 0.030 g (0.005 mmol), trimethylamine-N-oxide 0.006 g (0.080 mmol), 1,3-dibenzylimidazolium bromide (**1b**) 0.016 g (0.005 mmol), and silver oxide 0.014 g (0.016 mmol), 80 °C, 3h. Yield : 70 %.

Suitable crystals of **7b** for X-Ray diffraction were obtained by slow diffusion (Toluene/Hexane). **7b** has been analyzed by IR, ^{1}H-NMR, ^{13}C-NMR, ESI-MS and X-Ray diffraction. 1H-NMR (399.9 MHz, C_7D_8) δ (ppm): 8.43-6.46 (m, 28H, CH_{aryl}), 6.06 (s, 2H, -CH_{NHC}), 5.15 (m, -CH_2), 4.50 (m, -CH_2) 3.06 (s, 6H, -OCH_3). ^{13}C-NMR (150.8 MHz, C_7D_8, g-HSQC, g-HMBC) δ (ppm): 217.43 (CO), 184.99 ($C_{carbene}$), 167.37 (C=O, Cp), 159.27 (-$COCH_3$), 137.34-123.15 (C_{aryl}), 127.78 (CH_{NHC}), 113.36 (CH_{aryl}), 101.31 ($C_{2,5}$, Cp), 80.08 ($C_{3,4}$, Cp), 54.57 (-CH_2), 54.22 (-OCH_3). IR (CH_2Cl_2, cm^{-1}): (ν_{CO}) 1989, 1933; ($\nu_{C=O}$) 1586; ($\nu_{C=C}$) 1603, 1518. ESI-MS (m/z) (+): 805 $[M+H]^+$; 827 $[M + Na]^+$; 843 $[M+K]^+$. Anal. Calcd (%) for $C_{50}H40N_2O_5Fe$: C, 74.63; H, 5.01. Found: C, 71.19; H, 4.65.

Dicarbonyl-(η4-3,4-bis(4-methoxyphenyl)-2,5-diphenylcyclopenta-2,4-dienone)(1-methyl-3-butyl-imidazol-ylidene)iron (7c). Triscarbonyl-(η^4-3,4-bis(4-methoxyphenyl)-2,5-diphenylcyclopenta-2,4-dienone)iron (**5**) 0.030 g (0.005 mmol), trimethylamine-N-oxide 0.006 g (0.075 mmol), 1-methyl-3-butyl-imidazolium bromide (**1c**) 0.011 g (0.005mmol) and silver oxide 0.014 g (0.006 mmol), 80°C, 3 hours. Yield : 50 %.

Suitable crystals of **7c** for X-Ray diffraction were obtained by slow diffusion (Toluene/Hexane). **7c** has been analyzed by IR, ^{1}H-NMR, ^{13}C-NMR, ESI-MS and X-Ray diffraction. ^{1}H-NMR (399.9 C_7D_8) δ (ppm): 8.97-7.13 (m, 18H, CH_{aryl}), 6.85 (d, H, -CH_{NHC}), 6.69 (d, H, -CH_{NHC}), 4.19 (m, 2H, $CH_{2\ NHC}$), 3.73 (s, 6H, -OCH_3), 3.60 (s. 6H, -$CH_{3\ NHC}$), 2.73 (m, 2H, $CH_{2\ NHC}$), 1.53 (t, 2H, $CH_{2\ NHC}$), 1.36 (t, 3H, $CH_{3\ NHC}$). ^{13}C-NMR (150.8 MHz, C_7D_8, g-HSQC, g-HMBC) δ (ppm): 216.04 (CO), 182.41 ($C_{carbene}$), 166.83 (C=O, Cp), 159.29 (-$COCH_3$), 129.18-121.65 (C_{aryl}), 124.54 (CH_{NHC}), 113.40 (CHa_{ryl}), 100.87 ($C_{2,5}$, Cp), 80.26 ($C_{3,4}$, Cp), 54.27 (-OCH_3), 50.39 (-NCH_2-), 38.22 (-NCH_3), 33.63 (-CH_2-), 25.83 (-CH_2-), 13.99(-CH_3). IR (CH_2Cl_2, cm^{-1}): (ν_{CO}) 1987, 1931; ($\nu_{C=O}$) 1587; ($\nu_{C=C}$) 1607, 1518. ESI-MS (m/z) (+): 695 $[M+H]^+$; 717 $[M + Na]^+$; 733 $[M+K]^+$. Anal. Calcd (%) for $C_{41}H_{38}N_2O_5Fe$: C, 70.90; H, 5.51. Found: C, 67.19; H, 5.13.

Dicarbonyl-(η4-3,4-bis(4-methoxyphenyl)-2,5-diphenylcyclopenta-2,4-dienone)[1-(2-hydroxyethyl))-3-methylilidene]iron (7d). Triscarbonyl-(η^4-3,4-bis(4-methoxyphenyl)-2,5-diphenylcyclopenta-2,4-dienone)iron 0.060 g (0.103 mmol), trimethylamine-N-oxide 0.012 g (0.155 mmol), 13-(2-hydroxyethyl)-1-methylimidazole chloride (**1d**) 0.016 g (0.103 mmol) and silver oxide 0.029 g (0.124 mmol), room temperature,3 h. Chromatography eluent: dichloromethane/ethyl acetate/MeOH (100/0/0 to 0/0/100). Yield : 18 %.

7d has been analyzed by IR, ^{1}H-NMR, ^{13}C-NMR, ESI-MS. ^{1}H-NMR (399.9 MHz, C_7D_8) δ (ppm): 8.10 (m, 18H, CH_{aryl}), 6.63 (s, 1H, CH_{NHC}), 6.07 (s, 1H, CH_{NHC}), (CH_2 not visible), 3.10 (s, 6H, -OCH_3), 2.90 (s, 3H, -NCH_3). ^{13}C-NMR (150.8 MHz, C_7D_8, g-HSQC, g-HMBC) δ (ppm): 218.60 (CO), 181.69 ($C_{carbene}$), 163.05.57 (C=O, Cp), 159.46 (-$COCH_3$) 134.80-125.37 (CH_{aryl}), 124.48 (CH_{NHC}), 121.99 (CH_{NHC}), 113.47 (CH_{aryl}), (not visible $C_{3,4}$, Cp), 69.25 (not visible $C_{2,5}$, Cp), 59.24 (-CH_2), 53.30(-OCH_3), 52.40 (-CH_2), 37.92 (-NCH_3). IR (CH_2Cl_2, cm^{-1}) (ν_{CO}) 1991, 1935; ($\nu_{C=O}$) 1576 (broad); ($\nu_{C=C}$) 1604, 1517. ESI-MS (m/z) (+): 683 $[M+H]^+$, 705 $[M+Na]^+$. Anal. Calcd (%) for $C_{39}H_{34}N_2O_6Fe$: C, 68.63; H, 5.02. Found: C, 65.35; H, 4.69.

Dicarbonyl-(η4-3,4-bis(4-methoxyphenyl)-2,5-diphenylcyclopenta-2,4-dienone)[1-(2-Boc-NH-ethyl)-3-methylilidene]iron (7e). Triscarbonyl-(η^4-3,4-bis(4-methoxyphenyl)-2,5-diphenylcyclopenta-2,4-dienone)iron (**5**) 0.150 g (0.257 mmol), trimethylamine-N-oxide 0.029 g (0.386 mmol), 1-(2-BocNH-ethyl-)-3-

methylimidazolium iodide (**1e**) 0.091 g (0.257 mmol) and silver oxide 0.071 g (0.308 mmol), room temperature,1 h. Yield : 52.6 %.

7e has been analyzed by IR, ^{1}H-NMR, ^{13}C-NMR, ESI-MS. ^{1}H-NMR (399.9 MHz, C_7D_8) δ (ppm): 8.10-6.48 (m, 18H, CH_{aryl}), 6.68 (s, H, CH_{NHC}), 5.98 (s, H, CH_{NHC}), 3.12 (s, 2H, -CH_2), 3.11 (s, 6H, OCH_3), 2.96 (s, 2H, CH_2), 2.79 (s, 3H, NCH_3), 1.45 (s. 9H, -$CH_{3\ BOC}$). ^{13}C-NMR (150.8 MHz, C_7D_8, g-HSQC, g-HMBC) δ (ppm): 217.63 (CO), 182.44 ($C_{carbene}$), 164.51 (C=O, Cp), 159.43(-$COCH_3$), 156.86 (C=O, BOC). 137.68-121.84 (C_{aryl}), 125.41 (CH_{NHC}), 121.84 (CH_{NHC}), 113.46 (CH_{Aryl}), 98.92 ($C_{2,5}$, Cp), 88.59 ($C_{3,4}$, Cp), 77.94 (C, BOC), 58.32 (CH_2), 54.38 (-OCH_3), 49.33 (NCH_2), 37.82(NCH_3), 28.66 (-CH_3, BOC). IR (CH_2Cl_2, cm^{-1}): (ν_{CO}) 1991, 1935; ($\nu_{C=O}$) 1576 (broad); ($\nu_{C=C}$) 1604, 1517. ESI-MS (m/z) (+) = 782$[M+H]^+$, 804 $[M+Na]^+$. Anal. Calcd (%) for $C_{44}H_{43}N_3O_7Fe$: C, 67.61; H, 5.54. Found: C, 63.95; H, 5.06.

Dicarbonyl-(η4-3,4-bis(4-methoxyphenyl)-2,5-diphenylcyclopenta-2,4-dienone)[1-(2-methoxyethyl)-3-methylilidene]iron (7f). Triscarbonyl-(η^4-3,4-bis(4-methoxyphenyl)-2,5-diphenylcyclopenta-2,4-dienone)iron (**5**) 0.060 g (0.100 mmol), trimethylamine-N-oxide 0.012 g (0.150 mmol), 13-(2-methoxyethyl)-1-methylimidazole chloride (**1f**) 0.016 g (0.103 mmol) and silver oxide 0.028 g (0.120 mmol, room temperature,1 h. Yield : 35 %.

7f has been analyzed by IR, ^{1}H-NMR, ^{13}C-NMR, ESI-MS. ^{1}H-NMR (399.9 MHz, C_7D_8) δ (ppm): 8.29-6.49 (m, 18H, CH_{aryl}), 6.95 (s, 1H, CH_{NHC}), 6.00 (s, 1H, CH_{NHC}), 3.86 (br, 2H, CH_2), 3.09 (s, 6H, -OCH_3), 2.92 (s, 3H, -NCH_3) 2.88 (s, 3H, -OCH_3), 2.08 (br, 2H, CH_2). ^{13}C-NMR (150.8 MHz, C_7D_8, g-HSQC, g-HMBC) δ (ppm): 218.05 (CO), 182.42 ($C_{carbene}$), 166.72 (C=O, Cp), 159.34 (-$COCH_3$) 136.23-125.61 (CH_{aryl}), 124.24 (CH_{NHC}), 123.53 (CH_{NHC}), 113.41 (CH_{aryl}), 100.83 ($C_{3,4}$, Cp), 79.97 ($C_{2,5}$, Cp), 72.72 (-CH_2), 58.17 (-OCH_3), 54.30 (-OCH_3), 50.73 (CH_2), 38.14 (-NCH_3). IR (CH_2Cl_2, cm^{-1}): (ν_{CO}) 1987, 1931; ($\nu_{C=O}$) 1586 (broad); ($\nu_{C=C}$) 1518. ESI-MS (m/z) (+) = 697 $[M+H]^+$, 719 $[M+Na]^+$. Anal. Calcd (%) for $C_{40}H_{36}N_2O_6Fe$: C, 68.97; H, 5.21. Found: C, 65.80; H, 4.99.

Triscarbonyl-(2,4-bis(trimethylsilyl)bicyclo[3.3.0]nona-1,4-dien-3-one)iron (8). In a 75 mL Teflon tube equipped with magnetic stirrer, 1,7-octadiyne 0.027 g (0.11 mmol) and $Fe_2(CO)_9$ 0.039 g (0.11 mmol) were dissolved in 40 mL of toluene. The container is closed with a cap, equipped with a temperature sensor, and placed into

microwave reactor. The reaction is heated to 140 °C for 140 min. Upon removal of the solvent, the crude was purified to afford the yellow triscarbonyl-(2,4-bis(trimethylsilyl)bicyclo[3.3.0]nona-1,4-dien-3-one)iron (**8**) by neutral alumina column chromatography using dichloromethane/ethyl acetate (100/0 to 0/100). Yield = 83%

8 has been analyzed by IR, ^{1}H-NMR. ^{1}H-NMR (399.9 MHz, $CDCl_3$): δ (ppm) 2.56 (m, 4H, CH_2), 1.82 (m, 4H, CH_2), 0.27 (s, 18H, CH_3, TMS). IR (CH_2Cl_2, cm^{-1}): (ν_{CO}) 2063, 2004, 1987; ($\nu_{C=O}$). Anal. Calcd (%) for $C_{18}H_{26}O_6Fe$: C, 51.67; H, 6.26. Found: C, 49.08; H, 5.93.

Dicarbonyl-(2,4-bis(trimethylsilyl)bicyclo[3.3.0]nona-1,4-dien-3-one)[acetonitrile]iron (9). In a dried 15 mL Schlenk flask, triscarbonyl-(2,4-bis(trimethylsilyl)bicyclo[3.3.0]nona-1,4-dien-3-one)iron (**8**) 0.039 g (0.094 mmol) and trimethylamine-N-oxide 0.011 g (0.14 mmol) were dissolved in 3 mL of anhydrous acetonitrile. Reaction mixture was stirred at room temperature and protected from light for 3 hours. A yellow precipitate appeared. The solid was filtered and washed with diethyl ether and hexane. Yield : 78%.

9 has been analyzed by IR, ^{1}H-NMR. ^{1}H-NMR (399.9 MHz, CD_3Cl): δ (ppm) 2.28 (m, 4H, CH_2), 2.23 (s, 3H, CH_3), 1.56 (m, 4H, CH_2), 0.24 (s, 18H, CH_3, TMS). IR (CH_2Cl_2, cm^{-1}): (ν_{CO}) 1999, 1938. Anal. Calcd (%) for $C_{19}H_{29}NO_3Fe$: C, 52.89; H, 6.78. Found: C, 49.71; H, 6.37.

General procedure for the synthesis of dicarbonyl-(2,4-bis(trimethylsilyl)bicyclo[3.3.0]nona-1,4-dien-3-one)(NHC)iron complexes. (10) Same general procedure for complex **7**. Precursor is triscarbonyl-(2,4-bis(trimethylsilyl)bicyclo[3.3.0]nona-1,4-dien-3-one)iron (**8**).

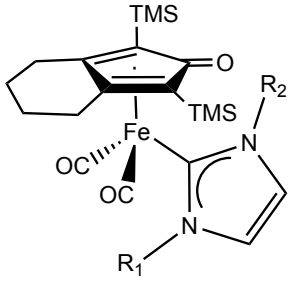

10a-h

a R_1=R_2=CH_3
b R_1=R_2=Ch_2Ph
c R_1=CH_3 R_2=$CH_2CH_2CH_3$
d R_1=CH_3 R_2=CH_2CH_2OH
e R_1=CH_3 R_2=CH_2CH_2NHBOC
g R_1=CH_3 R_2=$CH_2CH_2NH_2$
h R_1=CH_3 R_2=$CH_2CH_2NMe_3^+I^-$

Dicarbonyl-(2,4-bis(trimethylsilyl)bicyclo[3.3.0]nona-1,4-dien-3-one)[1,3-dimethyl-ilidene]iron (10a). Triscarbonyl-(2,4-bis(trimethylsilyl)bicyclo[3.3.0]nona-1,4-dien-3-one)iron (**8)** 0.035 g (0.084 mmol), trimethylamine-N-oxide 0.009 g (0.12 mmol), 1,3-dimethylimidazolium iodide 0.019 g (0.084 mmol) and silver oxide 0.035 g (0.084 mmol), room temperature, 3 h. Yield : 86 %

Suitable crystals of **10a** for X-Ray diffraction were obtained by slow diffusion (Toluene/Hexane). **10a** has been analyzed by IR, ^{1}H-NMR, ^{13}C-NMR, ESI-MS and X-Ray diffraction. ^{1}H-NMR (399.9 $CDCl_3$) δ (ppm): 6.98 (s, 2H, CH_{NHC}), 3.91 (s, 6H, CH_3), 2.45 (t, 4H, CH_2), 1.85-1.87 (m, 4H, CH_2), 0.174 (s, 18H, CH_3, TMS). ^{13}C-NMR (150.8 MHz, $CDCl_3$, g-HSQC, g-HMBC) δ (ppm): 217.00 (CO), 182.00 ($C_{carbene}$), (C=O, Cp) (not visible), 123.79 (CH_{NHC}), 103.72 ($C_{3,4q}$), 65.00 ($C_{2,5q}$), 39.94 (CH_3), 24.52 (CH_2), 22.55 (CH_2), 0.23 (CH_3, TMS). IR (CH_2Cl_2, cm^{-1}): (ν_{CO}) 1983, 1922. ESI-MS (m/z): 487 $[M+H]^+$, 509 $[M+Na]^+$, 525 $[M+K]^+$. Anal. Calcd (%) for $C_{22}H_{34}N_2O_3Si_2Fe$: C, 54.31; H, 7.04. Found: C, 51.82; H, 6.72.

Dicarbonyl-(2,4-bis(trimethylsilyl)bicyclo[3.3.0]nona-1,4-dien-3-one)[1,3-dibenzylimidazol-lilidene]iron (10b). Triscarbonyl-(2,4-bis(trimethylsilyl)bicycle-[3.3.0]nona-1,4-dien-3-one)iron (**8**) 0.077 g (0.018 mmol), trimethylamine-N-oxide 0.021 g (0.28 mmol), 1,3-dibenzylimidazolium bromide 0.060 g (0.018 mmol) and silver oxide 0.051 g (0.022 mmol), 80 °C 3 h. Yield : 20%.

10b has been analyzed by IR, ^{1}H-NMR, ^{13}C-NMR, ESI-MS. ^{1}H-NMR (399.9 $CDCl_3$) δ (ppm): 7.42-7.18 (10H, CH_{aryl}), 6.82 (s, 2H, CH_{NHC}), 5.6 (br, 4H, NCH_2), 2.49 (m, 4H, CH_2), 1.78-1.72 (m, 4H, CH_2), 0.19 (s, 18H, CH_3, TMS). ^{13}C-NMR (150.8 MHz, $CDCl_3$, g-HSQC, g-HMBC) δ (ppm): 216.14 (CO), 186.32 ($C_{carbene}$), 177.02 (C=O, Cp), 136.30 (C_{aryl}), 128.75 (CH_{aryl}), 127.88 (CH_{aryl}), 126.81(CH_{aryl}), 123.30 (CH_{aryl}), 103.91 ($C_{3,4q}$), 70.12 ($C_{2,5q}$), 55.15 (-NCH_2-), 23.94 (CH_2), 22.04 (CH_2), 0.98 (CH_3, TMS). IR (CH_2Cl_2, cm^{-1}): (ν_{CO}) 1986, 1924. ESI-MS (m/z): 639 $[M+H]^+$, 661 $[M+Na]^+$, 677 $[M+K]^+$. Anal. Calcd (%) for $C_{34}H_{42}N_2O_3Si_2Fe$: C, 63.93; H, 6.63. Found: C, 61.22; H, 6.21.

Dicarbonyl-(2,4-bis(trimethylsilyl)bicyclo[3.3.0]nona-1,4-dien-3-one)[1-(2-hydroxyethyl))-3-methylilidene]iron (10c). Triscarbonyl-(2,4-bis(trimethylsilyl)-bicyclo[3.3.0]nona-1,4-dien-3-one)iron (**8**) 0.048 g (0.103 mmol), trimethylamine-N-oxide 0.012 g (0.155 mmol), 3-(2-hydroxyethyl)-1-methylimidazole chloride 0.020 g

(0.103 mmol) and silver oxide 0.037 g (0.160 mmol), room temperature, 3 h. Chromatography eluent: dichloromethane/ethyl acetate/MeOH (100/0/0 to 0/0/100). Yield = 12.8 %

10c has been analyzed by IR, ^{1}H-NMR, ^{13}C-NMR, ESI-MS. ^{1}H-NMR (399.9 $CDCl_3$) δ (ppm): 7.27 (d, 1H, -CH_{NHC}), 7.04 (d, 1H, -CH_{NHC}), 4.33 (t, CH_2, NHC), 4.00 (t. 2H, -CH_2, NHC), 3.83 (s, 3H, -NCH_3), 2.52-2.45 (m, 4H, CH_2), 1.85-1.75 (m, 4H, CH_2), 0.18 (s, 18H, CH_3, TMS). ^{13}C-NMR (150.8 MHz, $CDCl_3$, g-HSQC, g-HMBC) δ (ppm): 217.68 (CO), 183.60 ($C_{carbene}$), 171.22 (C=O, Cp), 126.63 ($C_{3,4}$, Cp), 124.28 (CH_{NHC}), 120.91 (CH_{NHC}), 75.27 ($C_{2,5}$, Cp), 59.06 (-CH_2-), 52.66 (-CH_2-), 40.24 (-NCH_3), 25.01 (-CH_2-, Cp), 22.43 (-CH_2-, Cp), 0.21 (CH_3, TMS). IR (CH_2Cl_2, cm^{-1}): (ν_{CO}) 1986, 1926. ESI-MS (m/z): 517 $[M+H]^+$, 539 $[M+Na]^+$. Anal. Calcd (%) for $C_{23}H_{36}N_2O_4Si_2Fe$: C, 53.48; H, 7.02. Found: C, 50.54; H, 6.67.

Dicarbonyl-(2,4-bis(trimethylsilyl)bicyclo[3.3.0]nona-1,4-dien-3-one)[1-(2-BocNH-ethyl)-3-methylilidene]iron (10e). Triscarbonyl-(η^4-3,4-bis(4-methoxy-phenyl)-2,5-diphenylcyclopenta-2,4-dienone)iron 0.082 g (0.197 mmol), trimethylamine-N-oxide 0.022 g (0.296 mmol), 1-(2-BocNH-ethyl-)-3-methylimidazolium iodide 0.070 g (0.197 mmol) and silver oxide 0.055 g (0.236 mmol), room temperature, 1 h. Yield = 52.3 %.

10d has been analyzed by IR, ^{1}H-NMR, ^{13}C-NMR, ESI-MS. ^{1}H-NMR (399.9 $CDCl_3$) δ (ppm): 7.19 (s, 1H, -CH_{NHC}), 6.98 (s, 1H, -CH_{NHC}), 6.41 (br, 1H, NH), 4.33 (t, CH_2, NHC), 3.85 (s, 6H, -NCH_3), 3.65 (t. 2H, -CH_2, NHC), 2.47 (t, 4H, CH_2), 1.83-1.77 (m, 4H, CH_2), 1.35 (s, 9H, CH_3, BOC), 0.17 (s, 18H, CH_3, TMS). ^{13}C-NMR (150.8 MHz, $CDCl_3$, g-HSQC, g-HMBC) δ (ppm): 217.61 (CO), 184.56 ($C_{carbene}$), 174.08 (C=O, Cp), 156.66 (C=O, BOC), 123.91 (CH_{NHC}), 121.17 (CH_{NHC}), 103.26 ($C_{3,4}$, Cp), 78.80 (Cq, BOC), 73.31 ($C_{2,5}$, Cp), 49.55 (-NCH_2-), 40.16 (-NCH_3), 38.73 (-NCH_2-), 28.32 (CH_3, BOC), 24.87 (-CH_2), 22.47 (-CH_2), 0.29 (CH_3, TMS) IR (CH_2Cl_2, cm^{-1}): (ν_{CO}) 1982, 1922. Anal. Calcd (%) for $C_{28}H_{46}N_3O_5Si_2Fe$: C, 54.53; H, 7.52. Found: C, 51.53; H, 7.10.

Synthesis of dicarbonyl-(2,4-bis(trimethylsilyl)bicyclo[3.3.0]nona-1,4-dien-3-one)[1-(2-aminoethyl)-3-methylilidene]iron (10g). In a dried 25 mL Schlenk flask, dicarbonyl-(2,4-bis(trimethylsilyl)bicyclo[3.3.0]nona-1,4-dien-3-one)[1-(2-BocNH-ethyl)-3-methylilidene]iron (0.058 g, 0.094 mmol) was dissolved in Et_2O (2 mL) and

HBF_4 (0.071 mL, 0.515 mmol) was added dropwise. Reaction mixture was stirred at room temperature for 1 hour. The precipitate was dissolved in CH_2Cl_2 and the excess of HBF_4 neutralized with a saturated solution of sodium carbonate (pH=7-8). Aqueous phase was extracted with dichloromethane and washed with potassium idroxide solution (1.5 M, 3x10mL). Organic phase was dried with sodium sulfate and filtrated. Solvent was removed to leave a yellow solid. Yield = 73.4 %. ^{1}H-NMR (399.9 MHz, $CDCl_3$) δ (ppm): 7.20 (d, 1H, -CH_{im}), 7.02 (d, 1H, -CH_{im}), 4.31 (t, CH_{2im}), 3.92 (s, 6H, -NCH_3), 3.13 (t. 2H, -CH_{2im}), 2.44 (m, 4H, CH_2), 1.85-1.76 (m, 4H, CH_2), 0.16 (s, 18H, CH_{3TMS}); ^{13}C-NMR (150.8 MHz, $CDCl_3$) δ (ppm): 217.43 (CO), 184.94 (C_{carb}), 176.28 (C_1=O, Cp), 124.13 (CH_{im}), 122.10 (CH_{im}), 103.89 ($C_{3,4}$, Cp), 71.45 ($C_{2,5}$, Cp), 53.87 (-NCH_2-), 42.49 (-NCH_2-), 40.16 (-NCH_3), 24.56 (-CH_2), 22.53 (-CH_2), 0.24 (CH_{3TMS}). IR (CH_2Cl_2, cm^{-1}) ν (CO) 1982 cm^{-1}, 1922 cm^{-1}. ESI-MS (m/z): 459 $[M+H-2CO]^+$, 488 $[M+H-CO]^+$, 516$[M+H]^+$, 538 $[M+Na]^+$. Anal. Calcd (%) for $C_{23}H_{37}FeN_3O_3Si_2$: C, 53.58; H, 7.23; N, 8.15. Found: C, 53.69; H, 7.24; N 8.14.

Synthesis of dicarbonyl-(2,4-bis(trimethylsilyl)bicyclo[3.3.0]nona-1,4-dien-3-one)[1-(2-N,N,N-trimethyl-aminoethyl)-3-methylilidene]iron iodide (10h). In a dried 25 mL Schlenk flask, dicarbonyl-(2,4-bis(trimethylsilyl)bicyclo[3.3.0]nona-1,4-dien-3-one)[1-(2-BocNH-ethyl)-3-methylilidene]iron (0.097 g, 0.187 mmol) and potassium carbonate (0.116 g, 0.842 mmol) were dissolved in CH_2Cl_2 (2 mL) and methyl-iodide (0.105 mL, 1.683 mmol) was added dropwise. Reaction mixture was stirred at room temperature for 1 day. Solution were filtered and solvent removed under vacuum. The crude was purified to afford the yellow iron complex by column chromatography on neutral alumina using dichloromethane/methanol (40:5). Quantitative yield._^{1}H-NMR (399.9 MHz, DMSO-*d6*) δ (ppm): 7.63 (s, 1H, -CH_{im}), 7.60 (s, 1H, -CH_{im}), 4.66 (t, CH_{2im}), 3.88 (s, 3H, -NCH_3), 3.69 (t. 2H, -CH_{2im}), 3.22 (s, 9H, CH_3), 2.41-2.20 (m, 4H, CH_2), 1.82-1.73 (m, 4H, CH_2), 0.082 (s, 18H, CH_{3TMS}). ^{13}C-NMR (150.8 MHz, DMSO-*d6*) δ (ppm): 217.67 (CO), 182.84 (C_{carb}), 177.64 (C_1=O, Cp), 126.04 (CH_{im}), 123.61 (CH_{im}), 105.27 ($C_{3,4}$, Cp), 68.32 ($C_{2,5}$, Cp), 63.52 (-NCH_2), 53.22(-N^+CH_3), 44.13 (-NCH_2), (-NCH_3, not visible), 23.79 (-CH_2), 22.05 (-CH_2), 0.03 (CH_{3TMS}). IR (CH_2Cl_2, cm^{-1}) ν (CO) 1978, 1917._ESI-MS (m/z) = 682 $[M+H]^+$, 720 $[M+K]^+$, 149 $[I]^-$. Anal. Calcd (%) for $C_{26}H_{44}FeN_3O_3Si_2$: C, 45.55; H, 6.47; N, 6.13. Found: C, 45.73; H, 6.49; N 6.14.

Dicarbonyl-(2,4-bis(trimethylsilyl)bicyclo[3.3.0]nona-1,4-dienyl)(1,3-dimethyl-ilidene)iron triflate (10a[CF_3SO_3H]). Dicarbonyl-(2,4-bis(trimethylsilyl)bicycle-[3.3.0]nona-1,4-dien-3-one)[1,3-dimethyl-ilidene]iron complex (**10a**) 0.020g (0.035mmol) was dissolved in 5 mL of diethyl ether under inert atmosphere. 3.3 µL of HCF_3SO_3 (solution at 98% in CH2Cl2) were subsequently added. The reaction mixture was stirred for 10 minutes at room temperature, then the precipitate obtained was filtered, washed with 10 ml of hexane and died under vacuum. The yellow solid obtained was identified as **10a[CF_3SO_3H]** by IR, ^{1}H-NMR, ^{13}C-NMR, ^{19}F-NMR, ESI-MS. ^{1}H-NMR (399.9 MHz, $CDCl_3$) δ (ppm): 7.28(s, 2H, CH_{NHC}), 3.39 (s. 6H, -NCH_3). 2.41 (m, 4H, CH_2), 1.79 (m, 4H, CH_2), 0.29 (s, 18H, CH_3, TMS). ^{13}C-NMR (150.8 MHz, $CDCl_3$, g-HSQC, g-HMBC): δ (ppm) 214.16 (CO), 170.93 (Ccarbene), C-OH not visible, 126.26 (CH_{NHC}), 104.00 ($C_{2,5}$, Cp), 82.43 ($C_{3,4}$, Cp), 39.87 (-NCH_3), 23.79 (CH_2, 2C), 21.97 (CH_2, 2C), 0.99 (CH_3, TMS, 6C). ^{19}F-NMR (282.4 MHz, $CDCl_3$) δ (ppm): -78.18 (CF_3SO_3).IR (CH_2Cl_2, cm^{-1}): (vCO) 1949 cm^{-1}.

Dicarbonyl-(2,4-bis(trimethylsilyl)bicyclo[3.3.0]nona-1,4-dienyl)(1,3-dimethyl-ilidene)iron tetrafluoroborate (10a[HBF_4]). Dicarbonyl-(2,4-bis(trimethylsilyl)bicyclo[3.3.0]nona-1,4-dien-3-one)[1,3-dimethyl-ilidene]iron complex (**10a**) 0.020g (0.035mmol) was dissolved in 5 mL of diethyl ether under inert atmosphere. 3.3 µL of $HBF_4{\cdot}Et_2O$ were subsequently added. The reaction mixture was stirred for 10 minutes at room temperature, then the precipitate obtained was filtered, washed with 10 ml of hexane and died under vacuum. The yellow solid obtained was identified as **10a[CF_3SO_3H]** by IR, ^{1}H-NMR, ^{13}C-NMR, ^{19}F-NMR, ESI-MS. ^{1}H-NMR (399.9 MHz, CD_3CN) δ (ppm): 7.26(s, 2H, CH_{NHC}), 3.85 (s. 6H, -NCH_3). 2.44-2.21 (m, 4H, CH_2), 1.93 (s, 3H, NCH_3), 1.60 (m, 4H, CH_2), 0.26 (s, 9H, CH_3, TMS), 0.19 (s, 9H, CH_3, TMS). ^{13}C-NMR (150.8 MHz, CD_3CN): δ (ppm) 222.44 (CO), 179.93 (Ccarbene), 145.21 (C-OH), 126.44 (CH_{im}, 2C), 102.75, 96.38 ($C_{2,5}$, Cp, 2C), 75.53, 66.97 ($C_{3,4}$, Cp, 2C), 40.35 (-NCH_3), 23.56, 23.44 (CH_2, 2C), 22.49, 22.46 (CH_2, 2C), 0.46, 0.35 (CH_3, TMS, 6C). ^{19}F-NMR (282.4 MHz, $CDCl_3$) δ (ppm): -151.21 (BF_4). IR (CH_2Cl_2, cm^{-1}): (vCO) 1952cm^{-1}.

Synthesis of carbonyl-(2,4-bis(trimethylsilyl)bicyclo[3.3.0]nona-1,4-dien-3-one)[1,3-dimethylilidene][acetonitrile]iron tetrafluoroborate(11[HBF_4]). In a dried 50 mL Schlenk flask, Dicarbonyl-(2,4-bis(trimethylsilyl)bicyclo[3.3.0]nona-1,4-dienyl)(1,3-dimethyl-ilidene)iron tetrafluoroborate (0.030 g, 0.096 mmol) was dissolved in acetonitrile (15 mL). The reaction solution was irradiated under UV (325 nm) at room temperature for 15 minutes. Solvent was removed in vacuo and the red crude was washed with hexane several times. Quantitative yield. ^{1}H-NMR (400 MHz, CD_3CN) δ(ppm): 7.26 (s, 2H, CH_{im}), 3.84 (s, 3H, CH_3), 2 2.43-2.23 (br, 4H, CH_2), 1.94 (not visible, 3H, NCH_3) 1.60 (br, 4H, CH_2), 0.26 (s, 9H, CH_{3TMS}), 0.19 (s, 9H, CH_{3TMS}); ^{13}C-NMR (150.8 MHz, CD_3CN) δ(ppm): 222.44 (CO), 179.93 (C_{carb}), 145.21 (C-OH_{Cp}), 126.44 (CH_{im}), 102.75 (C_q), 96.38 (C_q) 75.53 (C_q), 66.97 (C_q), 40.35 (NCH_3), 23.44 (CH_2), 22.49 (CH_2), 0.46 (CH_{3TMS}), 0.35 (CH_{3TMS}). IR (CH_2Cl_2, cm^{-1}): v 1879. ESI-MS (m/z): 488$[M+H]^+$, 510 $[M+Na]^+$. Anal. Calcd (%) for $C_{22}H_{37}FeN_3O_2Si_2$: C, 54.19; H, 7.65; N, 8.62. Found: C, 54.29; H, 7.64; N 8.63.

Synthesis of carbonyl-(2,4-bis(trimethylsilyl)bicyclo[3.3.0]nona-1,4-dien-3-one)[1-(2-aminoethyl)-3-methylilidene]iron (12). In a dried 50 mL Schlenk flask, dicarbonyl-(2,4-bis(trimethylsilyl)bicyclo[3.3.0]nona-1,4-dien-3-one)[1-(2-aminoethyl)-3-methylilidene]iron (0.040 g, 0.096 mmol) was dissolved in toluene (40 mL). The reaction solution was irradiated under UV (325 nm) at room temperature for 90 minutes. Solvent was removed in vacuo. The red solid was re-dissolved in acetonitrile and washed with hexane several times. Yield: 65%. ^{1}H-NMR (400 MHz, $CDCl_3$) δ(ppm): 6.91 (s, 2H, CH_{im}), 3.91-3.81 (m, 2H, CH2), 3.83 (s, 3H, CH_3), 3.28 (m, 1H, CH2), 3.01(m, 1H, CH2), 2.47-2.16 (m, 4H, CH_2), 1.65-1.56 (m, 4H, CH_2), 0.17 (s, 9H, CH_{3TMS}), -0.02 (s, 9H, CH_{3TMS}); ^{13}C-NMR (150.8 MHz, $CDCl_3$) δ(ppm): 220.00 (CO), 192.71 (C_{carb}), 168.33 (C=O_{Cp}), 122.78 (CH_{im}), 122.19 (CH_{im}), 101.24 (C_q), 93.79 (C_q) 73.41 (C_q), 59.37 (C_q) 49.74 (CH_2), 41.92 (CH_2), 37.60 (CH_3), 25.25 (CH_2), 23.66 (CH_2), 22.55 (CH_2), 22.11 (CH_2), 0.90 (CH_{3TMS}), 0.64 (CH_{3TMS}). IR (CH_2Cl_2, cm^{-1}): v 1879. ESI-MS (m/z): 488$[M+H]^+$, 510 $[M+Na]^+$. Anal. Calcd (%) for $C_{22}H_{37}FeN_3O_2Si_2$: C, 54.19; H, 7.65; N, 8.62. Found: C, 54.29; H, 7.64; N 8.63.

Mössbauer spectroscopy. Room Temperature Mössbauer spectroscopy was performed on a conventional constant acceleration spectrometer mounting a Rh

matrix ^{57}Co source, nominal strength 1850 MBq. The hyperfine parameters isomer shift (δ), quadrupole splitting (Δ), full linewidth at half maximum (Γ), were expressed in mms^{-1} while internal the relative area (A) in %. were obtained by means of standard least-squares minimization techniques. The spectra were fitted to Lorentzian line shapes with the minimum number of components. δ is quoted to α-Fe, using a 4-lines calibration

X-ray Crystallography. Crystal data and collection details for **5·0.5C$_6$H$_{14}$**, **7a·thf·C$_6$H$_{14}$**, **7b**, **7c** and **10a** are reported in Table X. The diffraction experiments were carried out on a Bruker APEX II diffractometer equipped with a CCD detector using Mo–Kα radiation. Data were corrected for Lorentz polarization and absorption effects (empirical absorption correction SADABS).[38] Structures were solved by direct methods and refined by full-matrix least-squares based on all data using F^2.[39] All hydrogen atoms were fixed at calculated positions and refined by a riding model. All non-hydrogen atoms were refined with anisotropic displacement parameters.

The C_6H_{14} molecule of **5·0.5C$_6$H$_{14}$** is located on an inversion center.

The C_6H_{14} and THF molecules of **7a·thf·C$_6$H$_{14}$** are disordered and, therefore, they have been split into two positions each and refined isotropically using one occupancy parameter per disordered group. The disordered molecules have been restrained to have similar geometries (SAME line in SHELXTL; s.u. 0.02) and similar *U* parameters (SIMU line in SHELXTL; s.u. 0.01). Restraints to bond distances were applied as follow (s.u. 0.02): 1.53 Å for C–C and 1.43 Å for C–O in THF and C_6H_{14}.

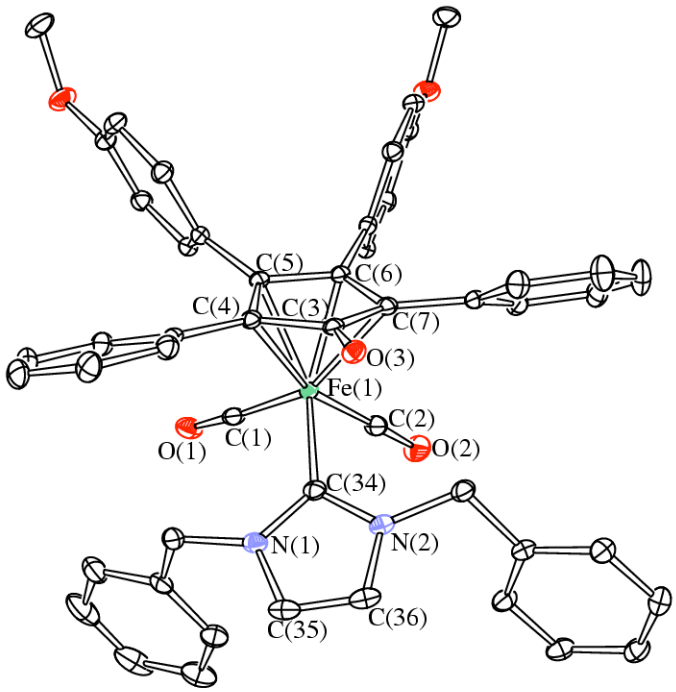

Figure 9. ORTEP drawing of **7b**. Displacement ellipsoids are at the 30% probability level. H-atoms have been omitted for clarity. Selected bondlengths (Å): Fe(1)-C(1) 1.7678(18), Fe(1)-C(2) 1.7671(17), Fe(1)-C(3) 2.3784(16), Fe(1)-C(4) 2.1442(15), Fe(1)-C(5) 2.0912(15), Fe(1)-C(6) 2.0766(15), Fe(1)-C(7) 2.1758(16), Fe(1)-C(34) 2.0138(17), C(3)-O(3) 1.2444(19).

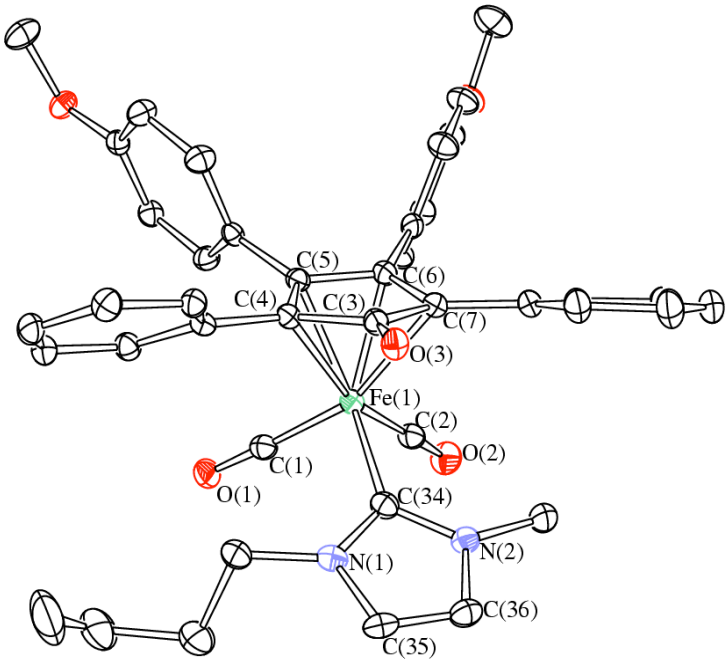

Figure 10. ORTEP drawing of **7c**. Displacement ellipsoids are at the 30% probability level. H-atoms have been omitted for clarity. Selected bondlengths (Å): Fe(1)-C(1) 1.764(3), Fe(1)-C(2) 1.766(4), Fe(1)-C(3) 2.392(3), Fe(1)-C(4) 2.161(3), Fe(1)-C(5) 2.079(3), Fe(1)-C(6) 2.082(3), Fe(1)-C(7) 2.168(3), Fe(1)-C(34) 2.000(3), C(3)-O(3) 1.240(4).

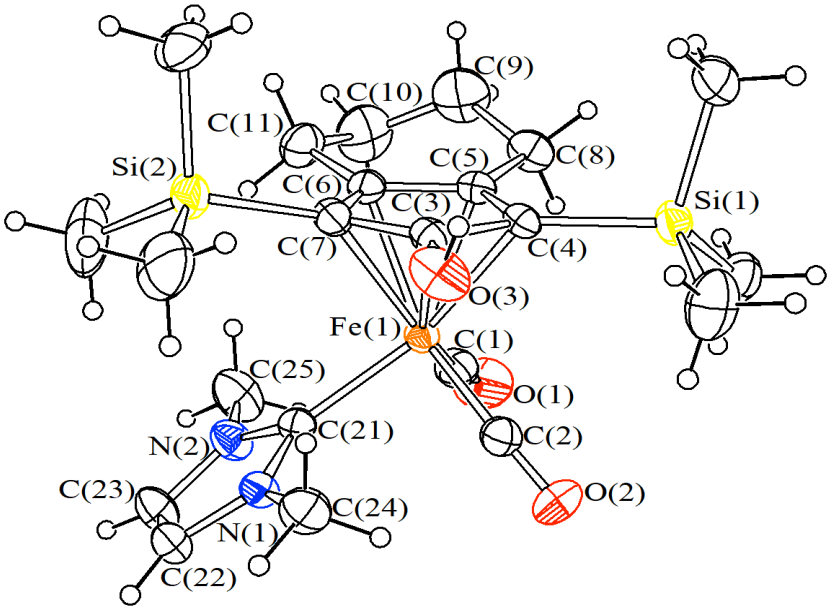

Figure 11. ORTEP drawing of **10a[CF_3SO_3H]**. Displacement ellipsoids are at the 30% probability level. Selected bondlengths (Å): Fe(1)-C(1) 1.774(4), Fe(1)-C(2) 1.774(4), Fe(1)-C(3) 2.119(4), Fe(1)-C(4) 2.119(4), Fe(1)-C(5) 2.126(4), Fe(1)-C(6) 2.124(4), Fe(1)-C(7) 2.154(4), Fe(1)-C(21) 1.977(4), C(3)-O(3) 1.384(5).

Table 3. *Crystal data and experimental details for* ***5·0.5C_6H_{14}, 7a·thf·C_6H_{14}, 7b, 7c*** *and* ***10a***.

	5·0.5C_6H_{14}	**7a·thf·C_6H_{14}**
Formula	$C_{37}H_{31}FeO_6$	$C_{48}H_{54}FeN_2O_6$
Fw	627.47	810.78
T, K	100(2)	100(2)
λ, Å	0.71073	0.71073
Crystal system	Monoclinic	Monoclinic
Space group	$P2_1/n$	$P2_1/n$
a, Å	14.3553(2)	9.4831(7)
b, Å	11.8026(2)	23.5286(19)
c, Å	17.6616(3)	19.2990(16)
α, °	90	90
β, °	90.0710(10)	103.518(4)
γ, °	90	90
Cell Volume, Å^3	2992.40(8)	4186.8(6)
Z	4	4

D_c, g cm^{-3}	1.393	1.286
μ, mm^{-1}	0.552	0.412
F(000)	1308	1720
Crystal size, mm	0.22·0.18·0.14	0.25·0.21·0.16
θ limits, °	1.83–25.03	1.73–26.00
Reflections collected	42504	64046
Independent reflections	5268 [R_{int}= 0.0285]	8231 [R_{int}= 0.0740]
Data / restraints /parameters	5268 / 0 / 397	8231/ 121 / 505
Goodness on fit on F^2	1.024	1.023
R_1 (I> 2σ(I))	0.0335	0.0641
wR_2 (all data)	0.0881	0.1870
Largest diff. peak and hole, e Å^{-3}	1.714 / –0.278	1.401 / –0.827

	7b	**7c**	**10a**
Formula	$C_{50}H_{40}FeN_2O_5$	$C_{41}H_{38}FeN_2O_5$	$C_{22}H_{34}FeN_2O_3Si_2$
Fw	804.69	694.58	486.54
T, K	100(2)	100(2)	100(2)
λ, Å	0.71073	0.71073	0.71073
Crystal system	Monoclinic	Monoclinic	Triclinic
Space group	$P2_1/n$	$P2_1/n$	$P\bar{1}$
a, Å	14.8500(8)	12.7360(4)	8.3374(2)
b, Å	15.3813(8)	17.9148(5)	10.1477(3)
c, Å	17.4682(10)	15.2500(4)	15.9325(4)
α, °	90	90	75.869(2)
β, °	101.570(3)	95.190(2)	77.444(2)
γ, °	90	90	76.216(2)
Cell Volume, Å^3	3908.9(4)	3465.22(17)	1251.27(6)
Z	4	4	2
D_c, g cm^{-3}	1.367	1.331	1.291
μ, mm^{-1}	0.439	0.483	0.723

F(000)	1680	1896	516
Crystal size, mm	0.19·0.15·0.12	0.16·0.13·0.10	0.18·0.16·0.11
θ limits, °	1.65–27.00	1.76–26.00	1.34–27.00
Reflections collected	64623	39892	21430
Independent reflections	8525 [R_{int}= 0.0444]	6797 [R_{int}= 0.0844]	5441 [R_{int}= 0.0497]
Data / restraints /parameters	8525 / 0 / 523	6797 / 18 / 442	5441 / 0 / 279
Goodness on fit on F^2	1.015	1.040	1.016
R_1 (I> 2σ(I))	0.0336	0.0472	0.0399
wR_2 (all data)	0.0866	0.1309	0.0987
Largest diff. peak and hole, e Å^{-3}	0.370 / –0.428	0.584 / –0.488	0.281 / –0.232

	10a[CF_3SO_3H]	**12**
Formula	$C_{23}H_{35}F_3FeN_2O_6SSi_2$	$C_{23}H_{39}Cl_2FeN_3O_2Si_2$
Fw	636.62	572.50
T, K	293(2)	293(2)
λ, Å	0.71073	0.71073
Crystal system	Orthorhombic	Triclinic
Space group	*Pca*2$_1$	*P*-1
a, Å	18.3460(7)	9.6755(3)
b, Å	9.1757(4)	11.2825(4)
c, Å	18.0764(7)	14.1021(4)
α, °	90	72.664(2)
β, °	90	80.181(2)
γ, °	90	88.247(2)
Cell Volume, Å^3	3042.93(2)	1477.65(8)
Z	4	2
D_c, g cm^{-3}	1.390	1.313
μ, mm^{-1}	0.699	0.812

F(000)	1328	604
Crystal size, mm	0.15·0.13·0.11	0.15·0.13·0.10

1.6 Notes and References

[1] K. Riener, S. Haslinger, A. Raba, M. P. Hogerl, M. Cokoja, W. A. Herrmann and F. E. Kuhn, *Chem. Rev.*, 2014, **114**, 5215.

[2] (a) C. Bolm, J. Legros, J. Le Paih, and L. Zani, *Chem. Rev.* 2004, **104**, 6217; (b) B. D. Sherry and A. Fürstner, *Acc. Chem. Res.*, 2008, **41**, 1500; (c) A. Correa, O. Garcia Mancheño and C. Bolm, *Chem. Soc. Rev.*, 2008, **37**, 1108; (d) S. Gaillard and J.-L. Renaud, *ChemSusChem*, 2008, **1**, 505; (e) S. Enthaler, K. Junge and M. Beller, *Angew. Chem., Int. Ed.*, 2008, **47**, 3317; (f) W. M. Czaplik, M. Mayer, J. Cvengroš and A. J. von Wangelin, *ChemSusChem*, 2009, **2**, 396; (g) R. H. Morris, *Chem. Soc. Rev.*, 2009, **38**, 2282; (h) A. Fürstner, *Angew. Chem., Int. Ed.*, 2009, **48**, 1364; (i) B. A. F. Le Bailly and S. P. Thomas, *RSC Adv.*, 2011, **1**, 1435; (l) K. Junge, K. Schröder and M. Beller, *Chem. Commun.*, 2011, **47**, 4849; (m) K. Gopalaiah, *Chem. Rev.*, 2013, **113**, 3248.

[3] (a) A. Quintard and J. Rodriguez, *Angew. Chem. Int. Ed.*, 2014, **53**, 4044; (b) C. P. Casey and H. Guan, *J. Am. Chem. Soc.* 2007, **129**, 5816; (c) S. Fleischer, S. S. Zhou, K. Junge and M. Beller, *Angew. Chem. Int. Ed.,* 2013, **52**, 5120; (d) C. P. Casey and H. Guan, *Organometallics*, 2012, **31**, 2631; (e) C. P. Casey and H. Guan, *J. Am. Chem. Soc.,* 2009, **131**, 2499.

[4] For selected reviews on NHCs: (a) W. A. Herrmann, *Angew. Chem., Int. Ed.,* 2002, **41**, 1290; (b) R. H. Crabtree, *J. Organomet. Chem.*, 2005, **690**, 5451; (c) S. Díez-González and S. P. Nolan, *Coord. Chem. Rev.*, 2007, **251**, 874; (d) O. Kühl, *Chem. Soc. Rev.*, 2007, **36**, 592; (e) S. T. Liddle, I. S. Edworthy and P. L. Arnold, *Chem. Soc. Rev.*, 2007, **36**, 1732; (f) F. E. Hahn and M. C. Jahnke, *Angew. Chem., Int. Ed.,* 2008, **47**, 3122; (g) S. Díez-González, N. Marion and S. P. Nolan, *Chem. Rev.*, 2009, **109**, 3612; (h) H. Jacobsen, A. Correa, A. Poater, C. Costabile and L. Cavallo, *Coord. Chem. Rev.*, 2009, **253**, 687; (i) O. Kühl, *Coord. Chem. Rev.*, 2009, **253**, 2481; (l) L. A. Schaper, S. J. Hock, W. A. Herrmann and F. E. Kühn, *Angew. Chem., Int. Ed.*, 2013, **52**, 270; (m) D. J. Nelson and S. P. Nolan, *Chem. Soc. Rev.,* 2013, **42**, 6723; (n) M. N. Hopkinson, C. Richter, M. Schedler and F. Glorius, *Nature*, 2014, **510**, 485; (o) S. P. Nolan, *N-Heterocyclic Carbenes: Effective Tools for Organometallic Synthesis*, Wiley VCH, 2014.

[5] M. J. Ingleson and R. A. Layfield, *Chem. Commun.*, 2012, **48**, 3579.

[6] (a) D. Bezier, J.-B. Sortais and C. Darcel, *Adv. Synth. Catal.*, 2013, **355**, 19; (b) S. Warratz, L. Postigo, and B. Royo, *Organometallics*, 2013, **32**, 893; (c) J. M. S. Cardoso, A. Fernandes, B. de P. Cardoso, M. D. Carvalho, L. P. Ferreira, M. J. Calhorda and B. Royo, *Organometallics*, 2014, **33**, 5670; (d) R. Lopes, J. M. S. Cardoso, L. Postigo and B. Royo, *Catal Lett*, 2013, **143**, 1061; (e) J. M.S. Cardoso, R. Lopes and B. Royo *J. Organomet. Chem.*, 2015, **775**, 173.

[7] (a) V. V. K. M. Kandepi, J. M. S. Cardoso, E. Peris, and B. Royo, *Organometallics*, 2010, **29**, 2777; (b) T. Hashimoto, S. Urban, R. Hoshino, Y. Ohki, K. Tatsumi and F. Glorius, *Organometallics*, 2012, **31**, 4474.

[8] C. Cesari, S. Conti, S. Zacchini, V. Zanotti, M. C. Cassani and R. Mazzoni, *Dalton Trans.*, 2014, **43**, 17240.

[9] C. Cesari, R. Mazzoni, H. Müller-Bunz and M. Albrecht, *J. Organomet. Chem.*, 2015, **793**, 256.

[10] C. Cesari, L. Sambri, S. Zacchini, V. Zanotti and R. Mazzoni, *Organometallics*, 2014, **33**, 2814

[11] S. Moulin, H. Dentel, A. Pagnoux-Ozherelyeva, S. Gaillard, A. Poater, L. Cavallo, J.-F. Lohier, and J.-L. Renaud, *Chem. Eur. J.*, 2013, **19**, 17881.

[12] H. K. Gupta, N. Rampersad, M. Stradiotto, M. J. McGlinchey, *Organometallics*, **2000**, *19*, 184-191; T. Rukachalsirkul, S. Arabl, F. Harstock, N. J. Taylor, A: J. Carty, *Organometallics*, **1984**, *3*, 1587-1589; G. G. Cash, R. C. Pettersen, *Inorg. Chem.*, **1978**, *17*, 650-653; I. emme, T. Labahn, A. de Meijere, *Eur. J. Org. Chem.*, **2006**, 399-404.

[13] H. Allen, O. Kennard, D. G. Watson, L. Brammer A. G. Orpen and R. Taylor, *J. Chem. Soc., Perkin Trans.*, 1987, **2**, S1-S19.

[14] (a) H.-J. Knolker, J. Heber and C. H. Mahler, *Synlett*, 1992, 1002; (b) H.-J. Knolker and J. Heber, *Synlett,* 1993, 924; (c) H.-J. Knolker, E. Baum and R. Klauss, *Tetrahedron Lett.*, 1995, **36**, 7647; (d) H.-J. Knolker, H. Goesmann and R. Klauss, *Angew. Chem. Int. Ed.,* 1999, **38**, 702.

[15] Require electrochemical conditions: B. Liu, Y. Zhang, D. Xu and W. Chen, *Chem. Commun.*, 2011, **47**, 2883.

[16] Polydentate ligands: a) B. Liu, Q. Xia and W. Chen, *Angew. Chem. Int. Ed.*, 2009, **48**, 5513. b) Z. Lu, S. A. Cramer and D. M. Jenkins, *Chem. Sci.*, 2012, **3**, 3081.

[17] A. Raba, M. Cokoja, S. Ewald, K. Riener, E. Herdtweck, A. Pothig, W. A. Herrmann and F. E. Kuhn, *Organometallics*, 2012, **31**, 2793

[18] Dinuclear piano stool iron complexes: V. Zanotti, S. Bordoni, L. Busetto, L. Carlucci, A. Palazzi, R. Serra, V. G. Albano, M. Monari and F. Prestopino, *Organometallics*, 1995, **14**, 5232; first mononuclear piano stool complex: M. H. Quick and R. J. Angelici, *J. Organomet. Chem.*, 1978, **160**, 231.

[19] (a) P. Buchgraber, L. Toupet, and V. Guerchais, *Organometallics,* 2003, **22**, 5144; (b) L. Mercs, G. Labat, A. Neels, A. Ehlers, and M. Albrecht, *Organometallics*, 2006, **25**, 5648; (c) L. Mercs, A. Neels, H. Stoeckli-Evans and M. Albrecht, *Dalton Trans.*, 2009, 7168.

[20] J. M. S. Cardoso and B. Royo, *Chem. Commun.*, 2012, **48**, 4944.

[21] (a) D. G. Gusev, *Organometallics*, 2009, **28**, 6458; (b) R. Tonner and G. Frenking, *Organometallics*, 2009, **28**, 3901; (c) A. Furstner, M. Alcarazo, H. Krause and C. W. Lehmann, *J. Am. Chem. Soc.*, 2007, **129**, 12676.

[22] V. V. K. M. Kandepi; J. M. S. Cardoso; E. Peris; B. Royo; *Organometallics*, **2010**, *29*, 2777.

[23] D. S. Mérel, M. Elie, J-F. Lohier, S. Gaillard, and J.-L. Renaud, *ChemCatChem*, **2013**, *5*, 2939.

[24] B. V. Johnson; P. J. Ouseph; J. D. Hsieh; A. l. Steinmetz; J. E. Shade; *Inorg. Chem.*, **1979**, *18*, 1796.

[25] B. Butschke; K. L. Fillman; T. Bendikov; L. J. W. Shimon; Y. Diskin-Posner; G. Leitus; S. I. Gorelsky; M. L. Neidig; D. Milstein; *Inorg. Chem.*, **2015**, *54*; 4909.

[26] E. I. Solomon; A. B. P. Lever; *Mössbauer Spectroscopy in Inorganic Electronic Structure and Spectroscopy*, Wiley: New York, **2006**; *Vol. I.*

[27] a) A. M.Oertel, V.Ritleng, L.Burr, C.Harwig and M. J.Chetcuti, *Organometallics,* **2011**, *30*, 6685; b) L. B.Benac, E. M.Burgess, L.Burr and A. J.Arduengo, *Organic Syntheses, Coll.*, **1990**, **7**, 195; **1986**, *64*, 92.

[28] S.Patil, J.Claffey, A.Deally, M.Hogan, B.Gleeson, L. M.Menéndez Méndez, H.Müller-Bunz, F.Paradisi and M.Tacke, *Eur. J. Inorg. Chem.,* **2010***,7*, 1020.

[29] L.C. Branco, J.N.Rosa, J.J. Moura Ramos andC.A.M.Afonso, *Chem. Eur. J.*, **2002**, *8*, 3671.

[30] a) L.Jafarpour, E.D.Stevens and S.P.Nolan, *J. Organomet. Chem.*, **2000**, *606*, 49; b)A.J.Arduengo, R.Krafczyk, H. A.Schmutzler, J.Craig, R.Goerlich, W.J.Marshall and M.Unverzagt,*Tetrahedron*, **1999**,*55*, 14523.

[31] W.Chen and F.Liu, *J. Organomet. Chem.*,**2003**, *673*, 5.

[32] S. Patil, A. Deally, F. Hackenberg, L. Kaps, H. Muller-Bunz, R. Schobert and M. Tacke*Helv. Chim. Acta*, **2011**, *94*, 1551.

[33]S. Hameury, P. de Frémont, P. -A. R. Breuil,H. Olivier-Bourbigou and P. Braunstein, *Dalton Trans.*, **2014**, *43*, 4700.

[34] D. V. Partyka and N. L. Deligonul, *Inorg. Chem.*,**2009**, *48*, 9463.

[35] J. Chun, H. S. Lee, I. G. Jung, S. W. Lee, H. J. Kim, and S. U. Son, *Organometallics,* **2010**, *29*, 1518.

[36] K. R. J.Thomas, M.Velusamy, J. T.Lin, C. H.Chuen and Y. T.Tao, *J. Mater.Chem.*,**2005**,*15*, 4453.

[37] L. M. Bushnell, E. R. Evitt, and R. G. Bergman, *J. Organomet. Chem.*, **1978**, *157*, 445.

[38] Sheldrick, G. M. *SADABS*, Program for empirical absorption correction, University of Göttingen, Germany, **1996**

[39] Sheldrick, G. M. *SHELX97*, Program for crystal structure determination, University of Göttingen, Germany, **1997**

Reactivity study of NHC cyclopentadienone iron complexes in transfer hydrogenation and alcohol oxidation

2.1 Abstract

The well-defined carbene iron complexes **10a** and **10a[HCF$_3$SO$_3$]** were evaluated as transfer hydrogenation catalysts with poor results. Also the corresponding **11a[HBF$_4$],** in which a coordination site was more easily accessible, was tested without interesting results. Finally, alcohol oxidation, that is the reverse reaction, was studied with better but still limited results.

2.2 Introduction

Since the review on iron catalysis by Bolm[1] in 2004, the field has witnessed a tremendous activity. Reduction and hydrogenation reactions play a major but not exclusive role, and new insights were recently reviewed by Renaud[2] and by Beller et al.[3]

As already described in the main introduction, several research groups based their recent works on transfer hydrogenation mediated by iron catalysts. In the field of transfer hydrogenation our group recently developed novel ruthenium complexes for bifunctional catalysis[4] by combining cyclopentadienones, which cooperates with the metal center in catalytic redox reactions,[5] with *N*-heterocyclic carbenes (NHC),[6] that are versatile and valuable ligands due to their easy preparation and the tunability of electronic and steric properties (some examples in Figure 1).[7] Indeed, NHCs are effective tools for the rational design of transition metal catalysts.[8] The cationic complexes **4[HX]** with the less coordinating anion $CF_3SO_3^-$, resulted in a higher catalytic activity in the transfer hydrogenation of the model substrate 4-fluoroacetophenone without the need of additives leading to a conversion of 93% corresponding to the yield in 24h. On the other hand, neutral complexes **4** were inactive under the conditions described in Figure 1 and needed to be activated by an oxidatant, such as cerium ammonium nitrate (CAN) in order to favour the release of CO (conversion = yield up to 87%).[4b] Noteworthy, the insertion of a pyridine substituent on the NHC side chain further improves the catalytic activity due to the presence of a second cooperative ligand containing a basic nitrogen (y > 99% in 24h).

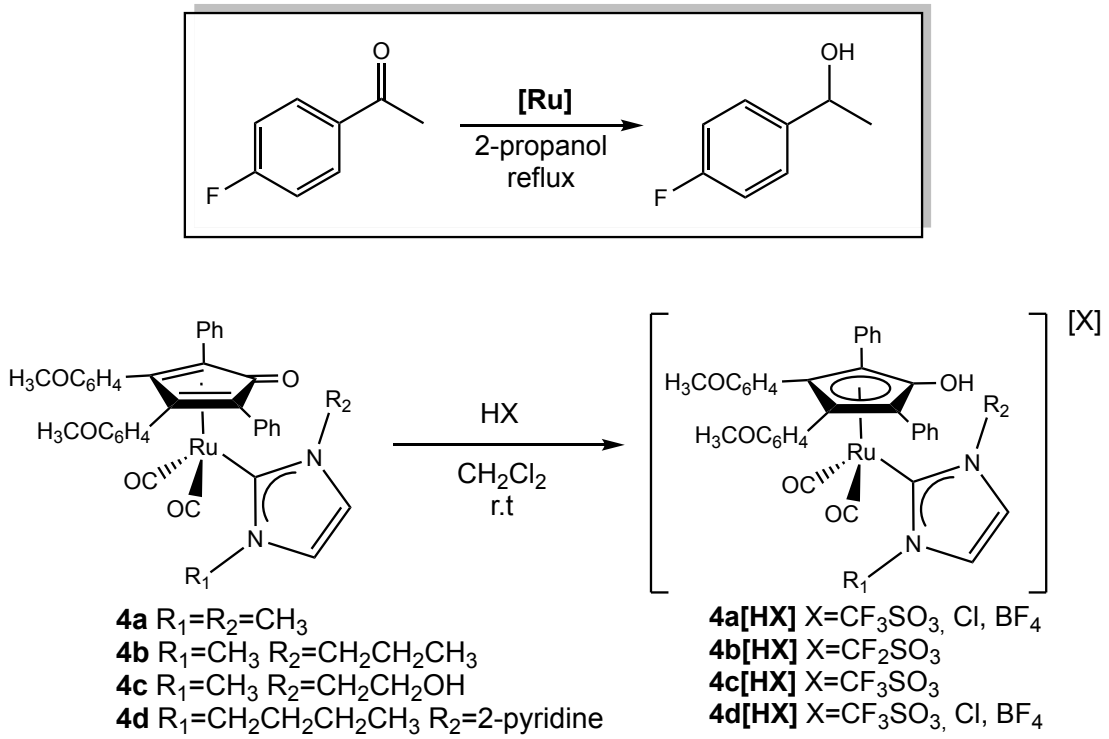

Figure 1. Transfer hydrogenation of 4-fluoroacetophenone catalyzed by **[Ru]** = **4a-c** and **4a-c[HX]** complexes at 80°C in ^{i}PrOH as solvent and hydrogen source, **[Ru]** = 5mol%.

Iron-based corresponding complexes of **10** and **10[HX]** have been already described in chapter I and herein their application in transfer hydrogenation and comparison with ruthenium analogues is discussed. A comparison with the cyclopentadienone iron bis-carbonyl-acetonitrile complex, reported in the literature and active in redox reaction, will be also presented and discussed.[9]

2.3 Results and Discussion

2.3.1 Transfer hydrogenation

Iron complexes **10** and **10[HX]** were evaluated as catalyst precursors for transfer hydrogenation (TH) of 4-fluoroacetophenone as model substrate. The TH, as already described in the introduction, is a hydrogenation reaction based on hydrogen donors instead of H_2 as the source of hydrogen. In this specific case, the donor is 2-propanol under refluxing condition.

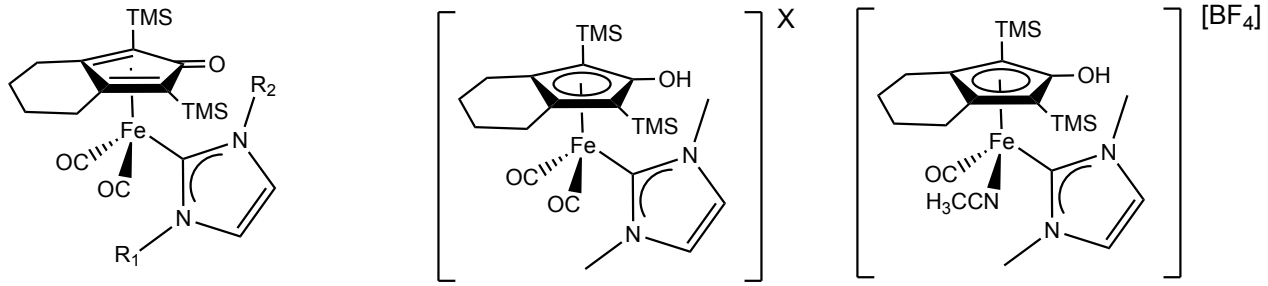

10a R_1=R_2=CH_3
10g R_1=CH_3 R_2=$CH_2CH_2NH_2$

10a[CF_3SO_3H], X=$CF_3SO_3^-$
10a[HBF_4], X=BF_4^-

11a[HBF_4]

Figure 2. Iron complexes evaluated in transfer hydrogenation of 4-fluoroacetophenone.

Catalytic runs were performed in order to compare the reactivity of iron to that of analogous ruthenium complexes **4** and **4[HX]**. Furthermore, the role of additives in the activation of iron complexes has been investigated.

Table 1 summarises all attempts and shows that NHC iron family is not a suitable pre-catalyst in the transfer hydrogenation reaction of 4-fluoroacetophenone.

On the other hand, the catalytic test with the analogue biscarbonyl-acetonitrile iron **9** (Entry 16) led to almost complete conversion after 24h as expected. The activation of the complex in this latter case can be ascribed to the lability of acetonitrile ligand, which provides a vacant site on the iron centre upon heating. Since NHC ligand is a good donor, in the NHC-derived iron complexes **10** and **10[HX]**, CO removal, which is necessary in order to create unsaturation on the metal centre, is not easily obtained, neither by heating, nor by UV irradiation, as described in the previous chapter (paragraph 1.3.3). Also the Ru-based precatalysts was activated only upon oxidation of the metal either by treatment with CAN (entry 1) or by protonation (entry 2), but unfortunately the same does not happen for the iron analogues. Treatment **10a** with CAN (entry 4) resulted in fast decomposition, whilst Me_3NO (entry 5) left **10a** unreacted. Addition of several bases (entry 6,7,8) was unsuccessful; the same low

conversion of entry 6 was achieved in a blank experiment with only NaOH as catalyst, revealing the pointlessness of **10a**. The amino derivative **10g** was employed as precatalyst without any additive (entry 12) and upon 1 hour of UV irradiation (entry 13): in both entries conversion was null and the complex was recovered as the chelated derivative **12** (see Chapter 1) at the end of reaction. Most likely, **12g** is a high stable form of **10g**, therefore it might be imagined as a resting state.

Table 1. Catalytic transfer hydrogenation of 4-fluoroacetophenone with iron.[a]

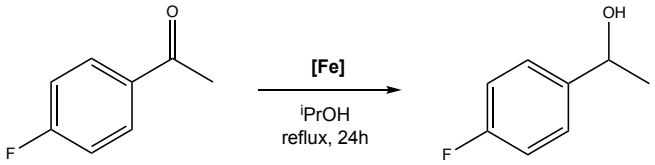

Entry	[Fe]	Additive	Conversion (%) 24h
1	**4a-[Ru]**	CAN[b]	61
2	**4a[HCF_3SO_3]-[Ru]**	---	93
3	**10a**	---	0
4	**10a**	CAN[b]	0
5	**10a**	Me_3NO[c]	0
6	**10a**	NaOH[d]	30
7	**10a**	KOH[d]	3
8	**10a**	Na_2CO_3[d]	0
9	**10a[HCF_3SO_3]**	---	0
10	**10a[HBF_4]**	---	0
11	**10a[HCF_3SO_3]**	hυ[e]	0
12	**10g**	---	0
13	**10g**	hυ	0
14	**11a[HBF_4]**	---	3.7
15	**11a[HBf_4]**	KOH[f]	15
16	**9**[g]	---	96

[a]General conditions: iron complex (5mol% Fe), iPrOH (1mL), T=82°C; conversion determined by ^{19}F-NMR spectroscopy. [b]CAN(Cerium Ammonium Nitrate) 1 mol. equiv. per iron centre. [c]Me_3NO 1.5 mol. equiv. per iron centre. [d]NaOH, KOH and Na_2CO_3 4 mol. equiv. per iron centre. [e]Irradiation @hυ for 1h, then stirring at r.t. [f]KOH 1 mol. equiv. per iron centre. [g]**9** is $CpFe(CO)_2(NCCH_3)$.

Also the **10a[HX]** iron(II) protonated species was evaluated as precatalyst but showed no activity in the TH of 4-fluoroacetophenone. UV irradiation of **10a[HCF$_3$SO$_3$]** for 1 hour, followed by refluxing or stirring at room temperature in 2-propanol resulted in extensive decomposition.

Finally, the carbonyl-acetonitrile-NHC derivative **11a[HBF$_4$]** was evaluated in TH. In spite of the presence of a labile ligand (CH_3CN) very poor conversions either without additive or with addition of KOH as base, were observed. At the end of reaction time the complex was not recovered since it decomposed very fast under reaction conditions (black precipitate). The behaviour of **11a[HBF$_4$]** suggests a significant change in the electronic structure of iron complexes compared to the triscarbonyl **5** and **8** or dicarbonyl-acetonitrile **6** and **9** precursors, which are active catalysts. The strong σ-donation of carbene might change the Lewis acidity of the iron centre, impairing the possibility of hydride abstraction under the condition employed.

2.3.2 Alcohol oxidation

The same carbene iron complexes have been also evaluated as catalyst precursor under oxidative conditions in the dehydrogenation of benzyl alcohol to benzaldehyde. Since it is the reverse of transfer hydrogenation the reaction could be favoured by the donation properties of NHC ligands. A screening of different solvents and additives was performed; the results are reported in Table 2.

The neutral iron complex **10a** did not display any catalytic activity in refluxing toluene, even in the presence of benzoquinone as oxidant. This additive with the analogous ruthenium complexes is able to regenerate the catalyst *in situ*, whereas it decomposes our iron compounds. Moreover, a catalytic test performed with the well-known triscarbonyl precursor (**8**) (entry 10) in the presence of BQ, confirmed that **8** is not able to convert the substrate but, as reported in the literature,[10] it needs an additive such as Me_3NO in order to exhibit catalytic activity.

On this basis, catalytic tests have been also performed in 1,4-dioxane as solvent with Me_3NO as additive, in these conditions low conversion has been observed: 4% with 7 mol% of Me_3NO, up to 10% with Me_3NO loading raised to 25 mol% (entries 3, 4). Increasing the catalyst loading to 10mol% with 25mol% of Me_3NO resulted in only 15%

conversion (entry 5). More catalytic runs have been carried out with the cationic complex **10a[HCF$_3$SO$_3$]** testing different solvents and additives: under all the applied reaction conditions a low conversion (11%) has been observed (entries 6, 7 ,8) and the presence of the carbene-free triscarbonyl iron(0) complex **8** has been detected at the end of the reaction. Using acetone as solvent (entry 9) no conversion has been reached but the complex **10a[CF$_3$SO$_3$]** has been recovered unaltered in the reaction crude, indicating that the complex is stable but not reactive under these conditions.

Table 2. Catalytic alcohol oxdidation of phenylethanol with iron.[a]

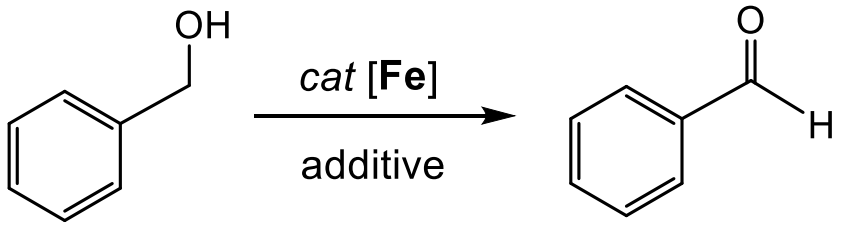

Entry	[Fe]	Solvent	Additive	conversion (%) 24h
1	**10a**	toluene	---	0
2	**10a**	toluene	BQ[b]	0
3	**10a**	1,4-dioxane	Me$_3$NO[c]	4
4	**10a**	1,4-dioxane	Me$_3$NO[d]	10
5	**10a**	1,4-dioxane	Me$_3$NO[e]	15
6	**10a[HCF$_3$SO$_3$]**	toluene	---	11
7	**10a[HCF$_3$SO$_3$]**	toluene	BQ[b]	11
8	**10a[HCF$_3$SO$_3$]**	1,4-dioxane	Me$_3$NO[c]	11
9	**10a[HCF$_3$SO$_3$]**	acetone	---	0
10	**8**	Toluene	BQ[b]	3

[a]General conditions: Iron complex (5 mol% Fe), solvent (1 mL), reflux; conversions determined by GC. [b]BQ 10 mol equiv. per iron centre. [c]Me$_3$NO 7 mol equiv. per iron center. [d]Me$_3$NO 25 mol equiv. per iron center. [e]catalyst loading increased to 10 mol% Fe.

With the aim of testing the complexes on more active substrates, the reactivity of **10a** and **10a[HCF$_3$SO$_3$]** has been extended to 1-phenylethanol. Indeed, secondary alcohols are more prone to oxidation.[11] Furthermore, in these experiments, the concentration of the substrate in the reaction mixture has been increased to 0.25 M. The catalytic results are reported in Table 3.

Table 3. Catalytic oxidation of 1-phenylethanol with iron.

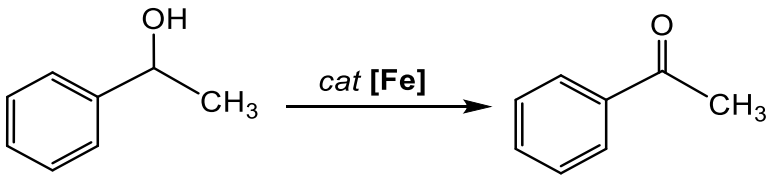

entry	***[Fe]***	*solvent*	*conversion 24h (%)*
1	**10a[HCF_3SO_3]**	toluene	33
2	**10a[HCF_3SO_3]**	acetone[b]	27
3	**10a**	acetone[b]	41[c]

[a]General conditions: Iron complex (5 mol% Fe), [substrate] = 0.25 M, solvent (1mL), reflux; conversions determined by GC; [b] test performed in a sealed glass ampoules equipped with a Young valve heating at 90°C; [c]yield ~ 20% the byproduct was identified as bis(alpha-methylbenzyl) ether.

The cationic complex **10a[CF_3SO_3]** under these conditions exhibits low catalytic activity in the oxidation of 1-phenylethanol both in toluene and acetone, leading to a conversion of 33% and 27% respectively (entry 1, 2). Furthermore, 41% conversion was observed using the neutral complex **28a** as catalyst precursor, even though the effective yield is lower (~ 20%) because of the formation of the bis(alpha-methylbenzyl) ether as by-product.

2.4 Conclusions

Carbene iron complex and its protonated derivative (**10a** and **10a[HCF_3SO_3]**) were evaluated in the transfer hydrogenation of 4-fluoroacetophenone with poor results. The complexes lacked reactivity even with several additives. The acetonitrile substituted **11a[HBF_4]** also performed unsatisfactorily, implying a change in the electronic structure of carbene-derived iron complexes compared to the active triscarbonyl **8** and biscarbonyl-acetonitrile **9** iron precursors.

Furthermore, iron compounds were evaluated in oxidation reverse conditions, that is alcohol oxidation to aldehyde and ketone. An improved reactivity was observed in the oxidation of 1-phenylethanol, but still not comparable with the triscarbonyl complex **8**.

In the light of these results, other reactions have been taken into consideration in order to exploit the features of carbene-iron complexes and will be described in following chapters.

2.5 Experimental Section

General data. All reactions were routinely carried out under a nitrogen atmosphere, using standard Schlenk techniques. Glassware was ovendried before use. Solvents: dichloromethane (CH_2Cl_2), tetrahydrofuran (THF), diethyl ether (Et_2O), petroleum ether referring to a fraction of bp 60-80 °C, acetonitrile (CH_3CN) were dried and distilled prior to use. Acetone has been degassed and stored under inert atmosphere on molecular sieves. Other solvents such as ethylacetate (EtOAc), chloroform, ethanol (EtOH), methanol (MeOH), heptane, toluene, $CDCl_3$, D_2O, CD_3CN (Sigma Aldrich) have been employed without further purification. Reagents: $Fe_2(CO)_9$ (Strem), methyl iodide, chloridric acid, silver oxide, 1-methylimidazole, 1,3 diphenylacetone, benzyl bromide, 4,4'dimethoxybenzil (Alfa Aesar) have been employed as purchased.
1,3-dimethylimidazolium iodide (1a),[12] 1-(2-BocNH-ethyl)-3-methylimidazolium iodide (1e)[13] 1,3-dimethylimidazol-2-ylidene silver iodide (2a),[14] 3,4-Bis(4-methoxyphenyl)-2,5-diphenylcyclopenta-2,4-dienone,[15] 1,8-bis(trimethylsilyl)octa-1,7-diyne[16] have been prepared following procedures reported in the literature.
The prepared derivatives were characterized by spectroscopic methods. The NMR spectra were recorded using Varian Inova 300 (^1H, 300.1; ^{13}C, 75.5 MHz), Varian Mercury Plus VX 400 (^1H, 399.9; ^{13}C, 100.6 MHz), Varian Inova 600 (^1H, 599.7; ^{13}C, 150.8 MHz) spectrometers at 298 K; chemical shifts were referenced internally to residual solvent peaks. Full ^1H-, ^{13}C- and ^{19}F-NMR assignments were done, when necessary, by gHSQC and gHMBC NMR experiments using standard Varian pulse sequences. Infrared spectra were recorded at 298 K on a Perkin-Elmer Spectrum 2000 FT-IR spectrophotometer. ESI-MS spectra were recorded on Waters Micromass ZQ 4000 with samples dissolved in MeOH or CH_3CN. Elemental analyses were performed on a Thermo-Quest Flash 1112 Series EA instrument.

General procedure for transfer hydrogenation. Complex (12.5 µmol, 5% mol), additive (1 eq or more. when needed) and *i*PrOH (1 mL) were stirred at reflux for 5 min. Then 4-fluoroacetophenone (36 µL, 300 µmol) was added and samples were taken at regular intervals. Aliquots (ca. 0.05mL) were diluted with $CDCl_3$ (0.5 mL) and conversions were determined by ^{19}F-NMR spectroscopy.

General procedure for alcohol oxidation. Complex (12.5 µmol, 5% mol), and solvent (1 mL) were stirred at reflux for 5min. Then substrate (30 µL, 250 µmol) was added and samples were taken at regular intervals and injected in the GC.

2.6 Notes and References

[1] C. Bolm, J. Legros, J. Le Paih and L. Zani, *Chem. Rev.*, **2004**, *104*, 6217.

[2] S. Gaillard, and J.-L. Renaud, *ChemSusChem*, **2008**,*1*, 505.

[3] K. Junge, K. Schröder, and M. Beller, *Chem. Commun.*, **2011**, *47*,4849,

[4] (a) C. Cesari, R. Mazzoni, H. Muller-Bunz and M. Albrecht, *J. Organomet. Chem.*, 2015, **793**, 256; (b) C. Cesari, A. Cingolani, C. Parise, S. Zacchini, V. Zanotti, M.C. Cassani and R. Mazzoni, *RSC Adv.*, 2015, **5**, 94707.

[5] (a) M. C. Warner, C. P. Casey and J.-E. Backvall, *Top. Organomet. Chem.*, 2011, **37**, 85; (b) B. L. Conley, M. K. Pennington-Boggio, E. Boz and T. J. Williams, *Chem. Rev.*, 2010, **110**, 2294; (c) T. Pasini, G. Solinas, V. Zanotti, S. Albonetti, F. Cavani, A. Vaccari, A. Mazzanti, S. Ranieri and R. Mazzoni, *Dalton Trans.*, 2014, **43**, 10224; (d) C. Cesari, L. Sambri, S. Zacchini, V. Zanotti and R. Mazzoni, *Organometallics*, 2014, **33**, 2814 and reference cited therein

[6] (a) C. Cesari, S. Conti, S. Zacchini, V. Zanotti, M. C. Cassani and R. Mazzoni, *Dalton Trans.*, 2014, **43**, 17240; (b) A. Cingolani, C. Cesari, S. Zacchini, V. Zanotti, M.C. Cassani and R. Mazzoni, *Dalton Trans.*, 2015, **44**, 19063.

[7] For reviews, see: a) F. E. Hahn and M. C. Jahnke, *Angew. Chem. Int. Ed.*, 2008, **47**, 3122; b) M. Melaimi, M. Soleilhavoup and G. Bertrand, *Angew. Chem. Int. Ed.*, 2010, **49**, 8810. c) L. Benhamou, E. Chardon, G. Lavigne, S. Bellemin-Laponnaz and V. Cesar, *Chem. Rev.,* 2011, **111**, 2705. d) L. A. Schaper, S. J. Hock, W. A. Herrmann and F. E. Kühn, *Angew. Chem. Int. Ed.*, 2013, **52**, 270.

[8] For selected reviews , see: a) D. Bourissou, O. Guerret, F. P. Gabbai and G. Bertrand, *Chem. Rev.*, 2000, **100**, 39; b) W. A. Herrmann, *Angew. Chem. Int. Ed.*, 2002, **41**, 1290; c) C. M. Crudden, and D. P. Allen, *Coord. Chem. Rev.,* 2004, **248**, 2247; d) M. Poyatos, J. A. Mata and E. Peris, *Chem. Rev.*, 2009, **109**, 3677; e) O. Schuster, L. Yang, H. G. Raubenheimer and M. Albrecht, *Chem. Rev.*, 2009, **109**, 3445; f) L. Mercs and M. Albrecht, *Chem. Soc. Rev.,* 2010, **39**, 1903; (g) M. N. Hopkinson, C. Richter, M. Schedlerand F. Glorius, *Nature*, 2014, **510**, 485; (h) S. P. Nolan, *N-Heterocyclic Carbenes: Effective Tools for Organometallic Synthesis* 2014, Wiley VCH.

[9] T. N. Plank; J. L. Drake; D. K. Kim; T. W. Funka; *Adv. Synth. Catal.*, **2012**, *354*, 597.

[10] A. Quintard and J. Rodriguez, *Angew. Chem. Int. Ed.*, **2014**, *53*, 4044; (b) C. P. Casey and H. Guan, *J. Am. Chem. Soc.* **2007**, *129*, 5816; (c) S. Fleischer, S. S. Zhou, K. Junge and M. Beller, *Angew. Chem. Int. Ed.,* **2013**, *52*, 5120; (d) C. P. Casey and H. Guan, *Organometallics*, **2012**, *31*, 2631; (e) C. P. Casey and H. Guan, *J. Am. Chem. Soc.,* **2009**, *131*, 2499.

[11] S. A. Moyer, T. W. Funk, *Tetrahedron Lett.*, 2010, **51**, 5430–5433.

[12] (a) A. M. Oertel, V. Ritleng, L. Burr, C. Harwig and M. J. Chetcuti, *Organometallics*, **2011**, *30*, 6685; (b) L. B. Benac, E. M. Burgess, L. Burr and A. J. Arduengo, *Organic Syntheses, Coll.*, **1990**, *7*, 195; **1986**, *64*, 92.

[13] L. Busetto, M. C. Cassani, C. Femoni, A. Macchioni, R. Mazzoni and D. Zuccaccia, *J. Organomet. Chem.*, **2008**, *693*, 2579.

[14] W. Chen and F. Liu, *J. Organomet. Chem.*, **2003**, *673*, 5.

[15] K. R. J. Thomas, M. Velusamy, J. T. Lin, C. H. Chuen and Y. T. Tao, *J. Mater. Chem.*, **2005**, *15*, 4453.

[16] L. M. Bushnell, E. R. Evitt, and R. G. Bergman, *J. Organomet. Chem.*, **1978**, *157*, 445.

NHC-Knölker type iron complexes as ammonia-borane dehydrocoupling catalysts

3.1 Abstract

NHC-iron complexes previously synthesised and described were employed as ammonia-borane dehydrocoupling catalysts. Neutral Fe(0) complex **10a** showed poor reactivity compared to the corresponding Fe(II) salt **10a[CF_3SO_3H]**, which reached full conversion after 2h (10mol% Fe) under UV irradiation. Analysis of dehydrogenation solution revealed a mixture of borazine and corresponding cross-linked polymer, together with other linear/branched polyaminoboranes. Interestingly, performing the reaction in an open-vessel led to complete conversion to borazine, which is not detected after 4h due to its volatility. Employing the acetonitrile substituted Fe(II) **11a[CF_3SO_3H]** species led to complete conversion to insoluble polyaminoboranes under very mild conditions (no irradiation, room temperature), proving that different mechanisms were involved under different reaction conditions.

3.2 Introduction

Ammonia-borane (AB) has recently drawn attention as hydrogen storage material due to its high H_2 content.[1] The "hydrogen economy" as replacement of fossil fuel-based economy is an attractive approach inside the green chemistry field. As described in the main introduction, H_2 features many issues such as transportation and storage due to its intrinsic physical properties, hence the need of finding a good chemical storage material that is safe and able to release efficiently hydrogen under mild conditions. AB as storage compound is one possibility and the use of metal-catalysed dehydrocoupling is a good choice considering the mild conditions required to release hydrogen. Depending on the reactivity of metal catalyst, it can release 1eq. or >1 eq. of H_2 per mole of AB, obtaining several byproducts (Scheme 1, e.g. BCTB, CTB, borazine, insoluble polyaminoboranes). In order to discriminate between different behaviours, catalysts have been classified into two main groups:[2,3] Type I, which are able to release 1 eq. of H_2 and are selective for insoluble polyaminoboranes, and Type II, that can release more than 2eq. of H_2 with formation of cyclic products, borazine and polyborazylenes. Among all borane-byproducts, borazine is the most dangerous, since it is a poison for catalyst

and PEM fuel cells (Proton Exchange Membrane), and a volatile liquid that can contaminate the H_2 flow. Thus tuning the selectivity of catalysts is a main issue in AB dehydrocoupling. Other byproducts might be considered as useful new BN-containing polymeric materials, even though the mechanism of polymerisation it is still not known and hard to understand.[4]

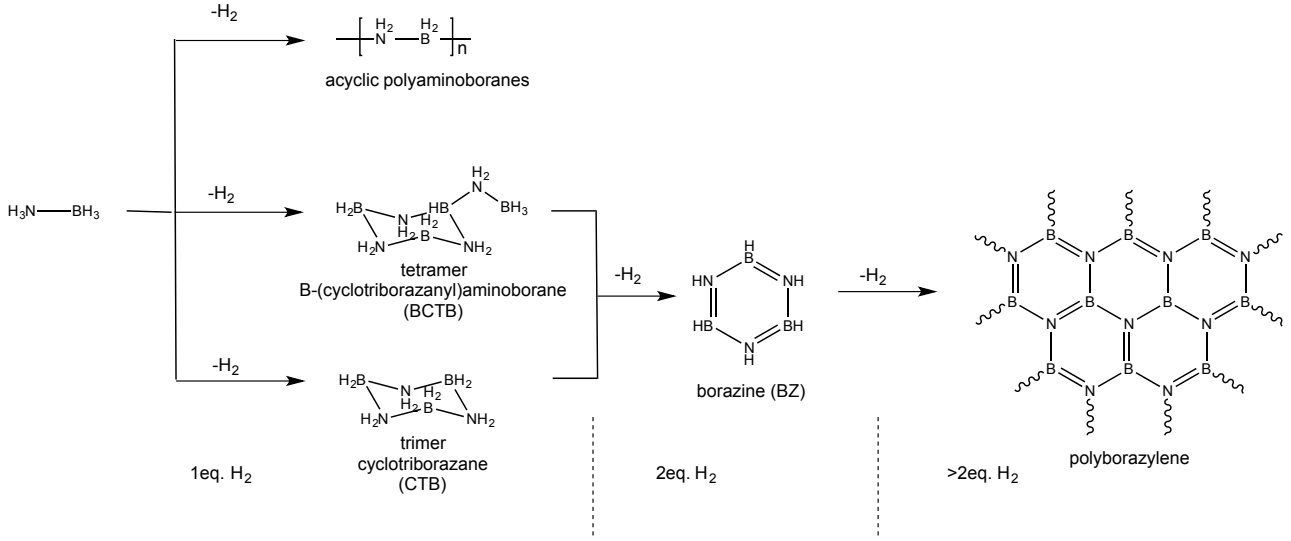

Scheme 1. Major byproducts of dehydrocoupling of ammonia-borane.

In this chapter, NHC-cyclopentadienone iron complexes described in Chapter I were evaluated as potential catalysts for the metal-catalysed ammonia-borane dehydrocoupling. Data and description presented in this chapter are the result of a collaboration with the group of Prof. Tom R. Baker from Center for Catalysis Research and Innovation (CCRI) at the University of Ottawa, Canada. The complexes taken into account are **10a**, **10g**, **10a[CF_3SO_3H]** and **11a[CF_3SO_3H]** (Figure 1). In the field of cylclopentadienone complexes, the Shvo's ruthenium dimer has been already employed in AB dehydrocoupling and described by Williams et al.[5] The ruthenium dimer is able to release up to 2 equivalents of H_2 per mole of AB and the ^{11}B-NMR spectrum of end reaction solution revealed only borazine as final byproduct. Mechanistic studies revealed two deactivation pathways: amine coordination to the metal centre or borazine hydroboration of the cyclopentadienone moiety.

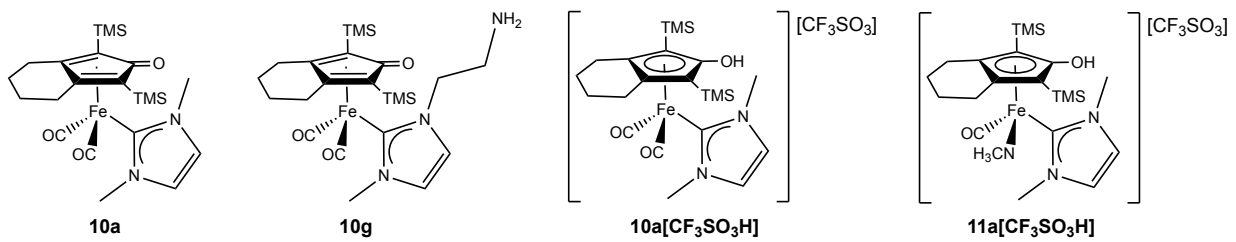

Figure 1. Iron complexes employed in this work.

3.3 Results and Discussion

Iron complexes **10a** and **10a[CF_3SO_3H]** were evaluated as catalyst precursors for ammonia-borane (AB) dehydrocoupling. Treatment of NH_3BH_3 (AB) solution in THF with **10a** and **10a[CF_3SO_3H]** (10mol% Fe) at room temperature for 2 hours led to poor formation of trimer B-(cyclotriborazanyl)amine-borane (BCTB), as indicated by ^{11}B-NMR spectroscopy. At about -43ppm was clearly visible a quintuplet with a $J_{B\text{-}H}$=80 HZ, which is typical of borohydride (BH_4^-) anion. Upon warming up at 60°C for 24 hours, a significant conversion was detected for both complexes (81% for **10a** and 82% for **10a[CF_3SO_3H]**), although to a detriment of selectivity: insoluble polymer was visible in solution and BCDB and borazine were detected by ^{11}B-NMR.

Since the cationic Fe(II) species **10a[CF_3SO_3H]** undergoes easily CO release upon photoirradiation (see Chapter I), a solution of AB in THF containing 10mol% of **10a[CF_3SO_3H]** was irradiated with a common Hg lamp (125W). Molecular H_2 evolution was visible after a few seconds and complete conversion was detected in about 50min (Figure 2). Analysis of reaction mixture with ^{11}B-NMR revealed a mix of trimer cyclotriborazane (CTB, ^{11}B-NMR: δ=-12.0 ppm), polymer (broad at ^{11}B-NMR: δ=-5.6 ppm) and borazine (^{11}B-NMR: δ=30.9 ppm). After a night at room temperature without irradiation, all CTB disappeared, likely converted to borazine and further dehydrogenated to polyborazylenes (broad ^{11}B-NMR: δ=31.2-26.1 ppm). At about δ=-37.1 ppm (^{11}B-NMR) a quartet ($J_{B\text{-}H}$=86Hz) was detectable throughout all experiment and it was assigned to carbene-BH_3 complex, as comparable to literature values,[6,7] showing a partial decomposition of **10a[CF_3SO_3H]**. The ^{1}H-NMR spectrum at 50 min showed several hydride signals (δ=-11.5 ppm (br), δ=-13.6 ppm (s), δ=-13.8 ppm(s), δ =-18.8 ppm(br)), which disappeared after the night except the one at δ=-11.5 ppm.

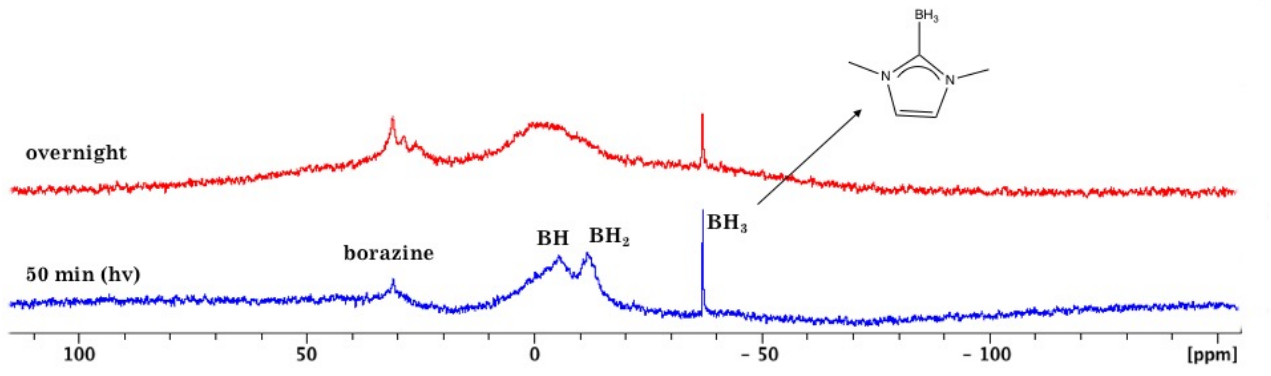

Figure 2. $^{11}B\{^1H\}$-NMR spectrum (THF) showing the reaction mixture with **10a[CF_3SO_3H]** after 50 min of irradiation (blue) and after stirring overnight at room temperature (red).

In order to shed some light on selectivity, reaction was performed in an open vessel under nitrogen atmosphere. Irradiation of the solution led to a complete conversion of ammonia-borane and after 4 hours no boron species were detected by ^{11}B-NMR spectroscopy in solution (Figure 3). Unlike the closed vessel reaction, formation of borazine was not preceded by polyaminoboranes formation (no broad signals around ^{11}B-NMR: δ=-5.6 ppm); indeed borazine is a volatile liquid (bp 53°C) and an open vessel setting might shift the equilibrium to the borazine as final product. As for the closed vessel, the quartet at δ=-37.1 ppm (^{11}B-NMR) assigned to NHC-BH_3 was clearly visible throughout all reaction time. In ^{1}H-NMR spectrum the only signal visible after 4h was the broad peak at δ=-11.5 ppm, this hydride is probably due to an Fe-H complex.

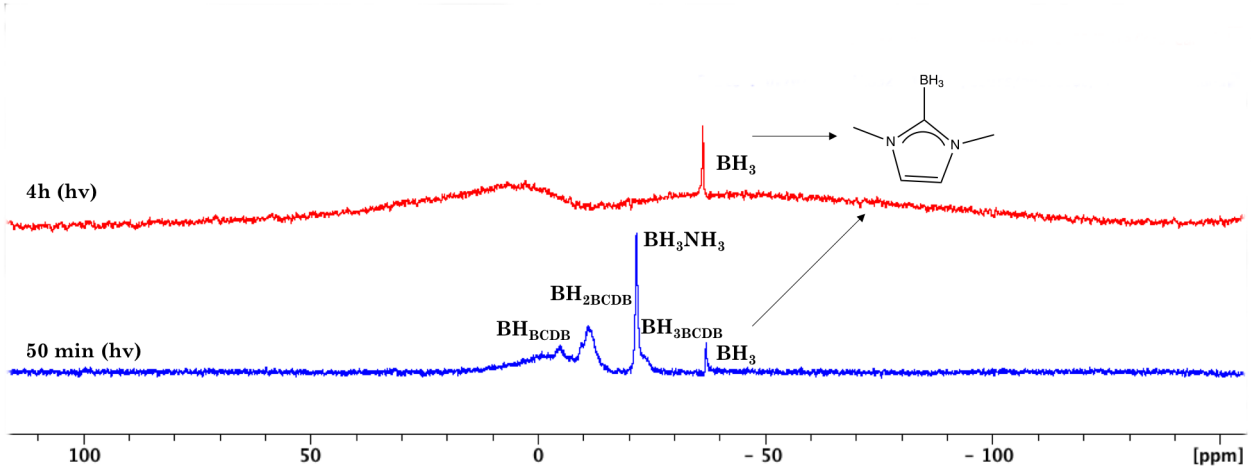

Figure 3. $^{11}B\{^{1}H\}$-NMR spectrum (THF) showing the reaction mixture with **10a[CF_3SO_3H]** in open vessel after 50 min of irradiation (blue) and after 4 h (red).

Also the corresponding neutral complex **10a** was evaluated as photocatalyst. Irradiating a solution of AB in THF led to poor reactivity compared to the cationic **10a[CF_3SO_3H]**. Indeed, ammonia-borane reagent was still detected together with a mixture of BCTB, insoluble polyaminoboranes and borazine after 4 hours.

Given the good results with **10a[CF_3SO_3H]** under photocatalytic conditions, the acetonitrile substituted Fe(II) derivative **11a[CF_3SO_3H]** was evaluated as precatalyst, in order to avoid any pre-activations (thermal or irradiation) of the solution mixture. In complex **11a[CF_3SO_3H]** one carbonyl ligand has been replaced by a labile acetonitrile. Hence, treatment of AB solution (THF) with **11a[CF_3SO_3H]** 10mol% at room temperature led to instantaneous H_2 evolution with formation of insoluble polyaminoboranes. Complete conversion was achieved after stirring for 4 hours (Figure 4). No signals were detected by ^{11}B-NMR of NHC-BH_3 species at about δ=-37.1 ppm,

suggesting that the very mild conditions avoid decomposition of the iron complex due to decoordination of NHC. ^{1}H-NMR showed a low signal of an hydride (^{1}H-NMR: s, δ=-13.9 ppm), likely a resting state of the catalyst. **11a[CF_3SO_3H]** performed quantitative conversion down to 2mol% of catalyst loading. Furthermore, **11a[CF_3SO_3H]** showed high selectivity to polyaminoboranes, hence it can be classified as Type I catalyst, which releases up to one equivalent of H_2 per equivalent of AB.

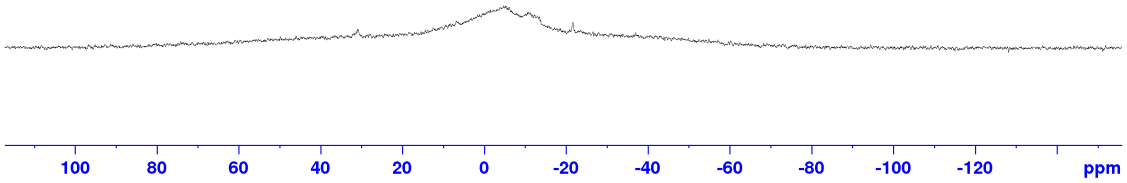

Figure 4. ^{11}B{^{1}H}-NMR spectrum (THF) showing the reaction mixture with **11a[CF_3SO_3H]** after 2h. No soluble B compounds were detected.

Finally, also Fe(0) **10g** was evaluated as precatalyst fo AB dehydrocoupling. In previous Chapter I, it has been discussed the ability of **10g** to undergo CO release even being a Fe(0) species. This feature is due to the NH_2 functional group on lateral chain of the NHC, which is able to chelate and stabilise the iron centre. Treatment of AB solution in THF with 10mol% **10g** under irradiation led to a low activity with a mixture of BCTB, borazine and ammonia-borane after 4 hours (Figure 5). At ^{11}B-NMR a quintuplet (J_{B-H}=82 Hz) was visible at δ=-39.4 ppm, suggesting a BH_4^- species in solution, whilst in ^{1}H-NMR a hydride was visible at δ=-13.9 ppm (br). Reaction solution turned red after a few minutes of irradiation, revealing the presence of the corresponding chelated iron species **12**, as seen in previous experiments (see Chapter I). Complex **12** is a stable compound and it might be a resting state of the catalyst, thus NH_2 itself is a poison inhibiting the activity of **10g** in AB dehydrocoupling.

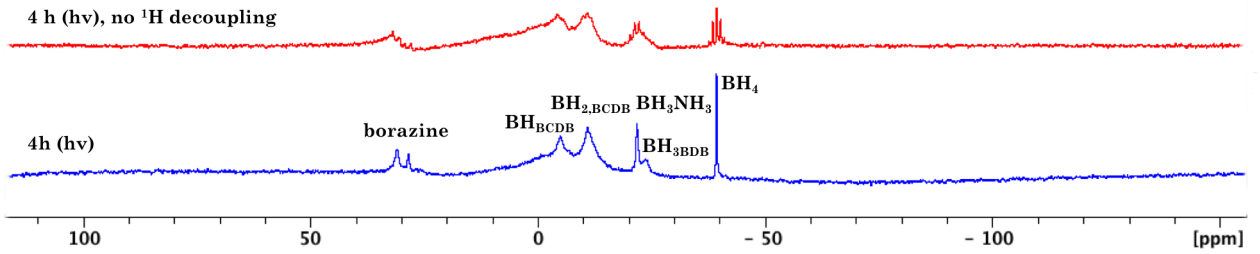

Figure 5. $^{11}B\{^{1}H\}$-NMR spectrum (THF) showing the reaction mixture with **10g** after 4h of irradiation (blue) and without ^{1}H decoupling (red).

3.4 Conclusions

In summary, we found that on photoirradiation Fe(II) **10a[CF_3SO_3H]** is a good catalyst for dehydrocoupling of ammonia-borane, performing a complete conversion in about 2h with 10mol% Fe loading. The catalyst is selective in formation of soluble BCTB followed by borazine as end-product. That is typical of Type II catalysts, which are able to release >1eq. of H_2 per AB. Drawbacks are the need for photoactivation, borazine as end-product, since it is a well-known poison for fuel cells due to its volatility, and decomposition of the catalyst by releasing of NHC. Indeed, a NHC-BH_3 species was detected by ^{11}B-NMR.

Treatment of AB solution with the acetonitrile substituted Fe(II) derivative **11a[CF_3SO_3H]**, led to complete conversion in 4h under very mild condition (room temperature). Avoiding irradiation of solution resulted in no decomposition of iron complex by NHC decoordination (no NHC-BH_3 evidence by ^{11}B-NMR). **11a[CF_3SO_3H]** showed selectivity for insoluble polyaminoboranes, typical of Type I catalysts, implying different reaction mechanisms involved depending on reaction conditions (irradiation vs. room temperature). Furthermore, **11a[CF_3SO_3H]** performed complete conversion with a loading as low as 2mol%.

Finally, also NH_2 functionalised Fe(0) **10g** was evaluated as catalyst, but poor conversions compared to previous compounds were observed, likely due to the NH_2 ability to chelate the iron centre, hence acting as a poison.

Although this is a preliminary study, several interesting results were obtained concerning NHC-iron compounds and further studies will be conducted to shed some light on mechanism and to enhance the stability under reaction conditions.

3.5 Experimental Section

General data. All reactions were routinely carried out under a nitrogen atmosphere, using standard Schlenk techniques or Glovebox. Glassware was ovendried before use. Solvents: dichloromethane (CH_2Cl_2), tetrahydrofuran (THF), diethyl ether (Et_2O), petroleum ether referring to a fraction of bp 60-80 °C, acetonitrile (CH_3CN) were dried and distilled prior to use. Acetone has been degassed and stored under inert atmosphere on molecular sieves. Other solvents such as ethylacetate (EtOAc), chloroform, ethanol (EtOH), methanol (MeOH), heptane, toluene, $CDCl_3$, D_2O, CD_3CN (Sigma Aldrich) have been employed without further purification. NH_3BH_3 (ammonia- borane, Sigma Aldrich) was sublimated before use. Reagents: sodium tetraphenilborate and boron trifluoride diethyl ether have been employed as purchased.
The NMR spectra were recorded using Varian Inova 300 (^1H, 300.1; ^{13}C, 75.5 MHz), Varian Mercury Plus VX 400 (^1H, 399.9; ^{13}C, 100.6 MHz), Varian Inova 600 (^1H, 599.7; ^{13}C, 150.8 MHz) spectrometers at 298 K; chemical shifts were referenced internally to residual solvent peaks. Infrared spectra were recorded at 298 K on a Perkin-Elmer Spectrum 2000 FT-IR spectrophotometer. ESI-MS spectra were recorded on Waters Micromass ZQ 4000 with samples dissolved in MeOH or CH_3CN. Elemental analyses were performed on a Thermo-Quest Flash 1112 Series EA instrument. UV irradiation was performed by using a commercial Hg lamp (125 W).

Ammonia-borane dehydrocoupling. In a typical experiment a THF solution of AB (0.4 mL) is added to a NMR tube. A solution of the corresponding iron complex (0.1 mL) have been added and the NMR tube sealed. For experiments that required heating, the NMR tube was placed in a heating block. For experiments that required photoactivation, the NMR tube was exposed to Hg-lamp (125 W). C_6D_6 has been used as lock solvent. Reactions have been monitored by ^{11}B-NMR, $^{11}B\{^1H\}$-NMR and ^1H-NMR.

Open-vessel ammonia-borane dehydrocoupling. The same setup as for the general dehydrocoupling, but the NMR tube is left open inside a glovebox nitrogen atmosphere.

Synthesis of 10a,10g, 10a[CF_3SO_3H] and 11a[CF_3SO_3H]. Same procedure described in Chapter I, experimental section.

3.6 Notes and References

[1] A. Rossin; M. Peruzzini; *Chem. Rev.*, **2016**, *116*, 8848.

[2] S. Bhunya; P. M. Zimmerman; A. Paul; *ACS Catal.*, **2015**, *5*, 3478.

[3] V. Pons; R. T. Baker; N. K. Szymczak; D. J. Heldebrant; J. C. Linehan; M. H. Matus; D. J. Grant; D. A. Dixon; *Chem. Comm.*, **2008**, 6597.

[4] W. C. Ewing; A. Marchione; D. W. Himmelberg; P. J. Carroll; L. G. Sneddon; *J. Am. Chem. Soc.*, **2011**, *133*, 17093.

[5] X. Zhang; L. Kam; R. Trerise; T. J. Williams; *Acc. Chem. Res.*, **2017**, *50*, 86.

[6] Wang, Y.; Quillian, B.; Wei, P.; Wannere, C. S.; Xie, Y.; King, R. B.; Schaefer, III, H. F.; Schleyer, P. v. R.; Robinson, G. H.; *J. Am. Chem. Soc.*, **2007**, *129*, 2412.

[7] D. P. Curran; A. Solovyev; M. M. Brahmi; L. Fensterbank; M. Malacria; E. Lacôte; *Angew. Chem. Int. Ed.*, **2011**, *50*, 10294.

Cyclopentadienone-NHC iron system as water oxidation catalyst

4.1 Abstract

The cyclopentadienone-NHC iron complexes described in Chapter I are characterised by Cyclic Voltammograms (CVs) in CH_3CN solution. CVs show an interesting anodic monoelectronic process (Fe^0/Fe^I), which is associated to the coordination of NHC to the iron centre. A preliminary screening of iron compounds in THF/water mixture upon addition of base (KOH), showed electrocatalytic activity as water oxidation catalysts (WOCs). The reactivity is general for the cyclopentadienone-carbene system, even with differently substituted ligands.

4.2 Introduction

The quest of new renewable and environmentally benign energy sources has driven the research towards the design of new catalysts and reactions not relying only on precious metals and fossil fuels. Two of the most abundant green resources of our planet are sunlight and water, which inspired growing efforts in developing artificial photosynthesis.[1,2] Artificial photosynthesis is the sunlight-driven splitting of water to molecular hydrogen (H_2) and oxygen (O_2). The bottleneck of the entire process is the water oxidation to O_2, since it is an uphill four-electron reaction and it is both thermodynamically and kinetically demanding.

$$2H_2O \rightarrow O_2 + 4H^+ + 4e^- \qquad E^0 = 1.23V\ vs.NHE$$

Hence the need of finding highly efficient, selective and stable water oxidation catalysts (WOCs). The term "molecular catalysts" instead of homogeneous catalysts better describes the chemistry around these classes of WOCs, since not all molecular WOCs are truly homogeneous systems, as they might involve heterogeneous species derived by strong oxidation and pH-dependant conditions. A recent study of Fukuzumi et al.[3] clearly described the water oxidation catalysed by nonheme iron complex $Fe(BQEN)(OTf)_2$ (BQEN = N,N'-dimethyl-N,N'-bis(8-quinolyl)cyclohexanediamine, OTf = CF_3SO_3-) at different pH conditions. Under acidic conditions the iron catalyst acts as homogeneous WOC with iron(IV)-oxo as active species, whilst iron hydroxide

nanoparticles were spotted under basic conditions, then acting as heterogeneous system.

Several molecular WOCs have been described in recent years, which have been inspired by nature's oxygen-evolving core of photosystem II, a Mn_4CaO_5 cluster responsible for O-O bond formation.[4,5] Mechanistic studies provide potential tools to better understand the reaction pathways of molecular WOCs, thus improving the design of catalysts to widen the bottleneck of water oxidation. Mechanistic insights on the O-O bond formation revealed that radical oxo coupling (ROC) as well as water nucleophilic attack (WNA) pathways are both possible (Scheme 1), and the computational work on a $[Ru{=}O(bda)L_2]^+$ (bda = 2,2'-bipyridine-6,6'-dicarboxylate) provided general guidelines for the design of a system in order to operate by a ROC mechanism.[6] In general, a ROC mechanism is more desirable since the lower activation energy required for radical coupling, compared to water nucleophilic attack pathway to generate the metal-peroxide intermediate.[7]

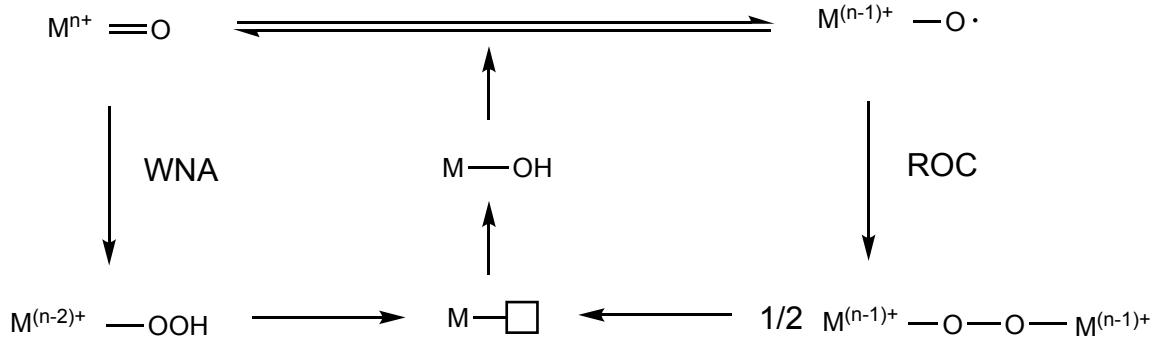

Scheme 1. Illustration of the two possible mechanism involving molecular water oxidation catalyst: water nucleophilic attack with generation of metal-peroxide intermediate (WNA) and radical oxo coupling (ROC).

The three most employed elements for molecular WOCs are manganese, ruthenium and iridium,[8] followed by a few examples of cobalt and iron catalysts.[9] As a rule, metal centres of molecular WOCs are chelated by strong N or O donor atoms, which prevent ligand dissociation and decomposition.[10]

Here, we present a new class of iron WOC based on cyclopentadienone(CpO) and N-heterocyclic carbene (NHC) ligands. Both ligands are able to stabilise the iron centre under harsh conditions, a key aspect in the water oxidation catalysis: the NHC being a strong σ–donor[11] and CpO a known non-innocent ligand,[12,13] capable of metal-ligand cooperation in catalysis and behaving as electron storage. Data and description presented in this chapter are the result of a collaboration with the group of Prof. Erika

Scavetta (Dr. Isacco Gualandi) from the Department of Industrial Chemistry "Toso Montanari".

4.3 Results and Discussion

N-heterocyclic carbene (NHC) cyclopentadienone (CpO) iron complexes **10a**, **10g**, **10i**, **7a**, **14a**, **14g** (Scheme 2) have been investigated by cyclic voltammetry in CH_3CN and as water oxidation catalysts (WOCs). Cyclic voltammograms (CVs) of the studied complexes in a mixture of THF/H_2O have been recorded in the presence of increasing amounts of potassium hydroxide (KOH). Catalytic activity in water oxidation is evidenced by the appearance of an irreversible wave that grows with increasing base concentrations.

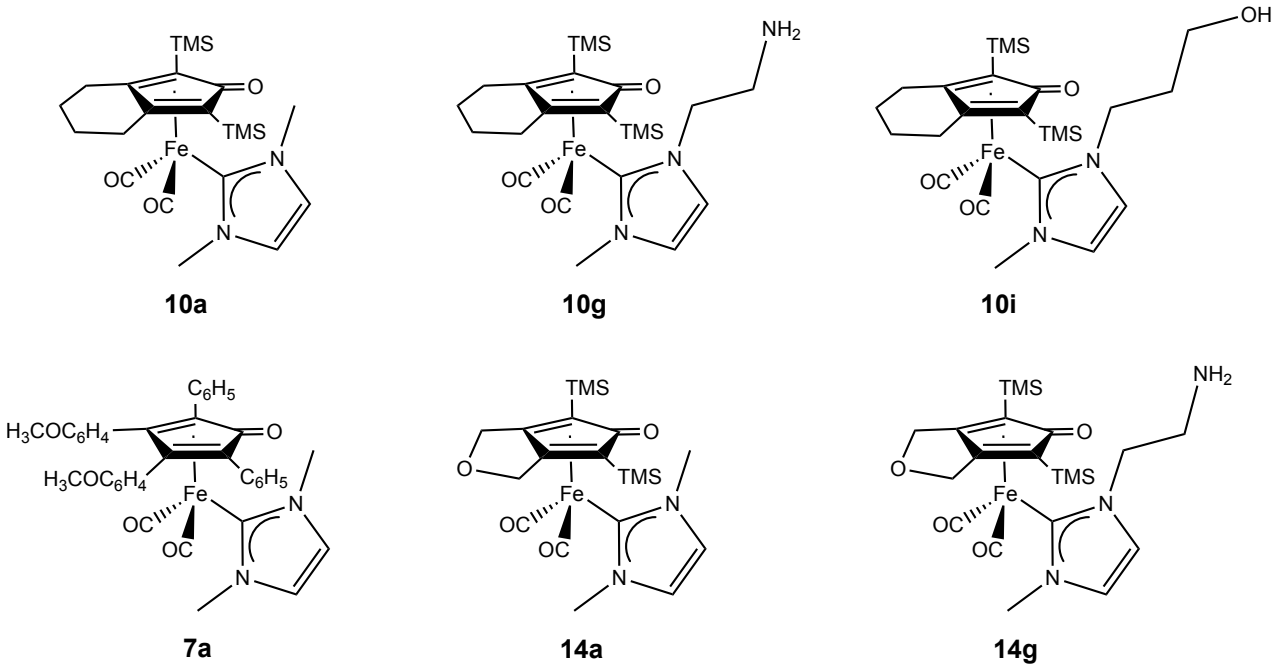

Scheme 2. NHC-Cp iron complexes evaluated as WOCs in this study.

4.3.1 Synthesis of WOC iron complexes.

Iron complexes bearing different substituted NHC ligands **10a**, **10g** and **10i** and different CpO ligands **7a**, **14a** and **14g** have been synthesised following the procedure described in Chapter 1. Complexes **10a**, **10g**, **10i** and **7a** were already reported in the previous chapters, whilst **14a** and **14g** are here described. **14g** was obtained by deprotection of **14e**, as for the **10g** analogue. **14a** and **14e** were obtained by transmetallation of the corresponding imidazolium salts **1** to the triscarbonyl precursor

13 (Scheme 3), by means of silver oxide (Ag_2O) as transfer reagent. Reaction was followed by IR spectroscopy and products **14a** and **14e** showed the same CO stretching pattern of analogues **10** and **7**. In general, CO frequencies of **14** are higher than **10** and comparable with **7** as shown in Table 1, which is in accordance with the withdrawing character of the furan ring of CpO ligand.

Table 1. IR stretching frequencies of **7a**, **10a** and **14a**.

Complex	**7a**	**10a**	**14a**
CO (cm^{-1})	1988/1930	1983/1922	1991/1931

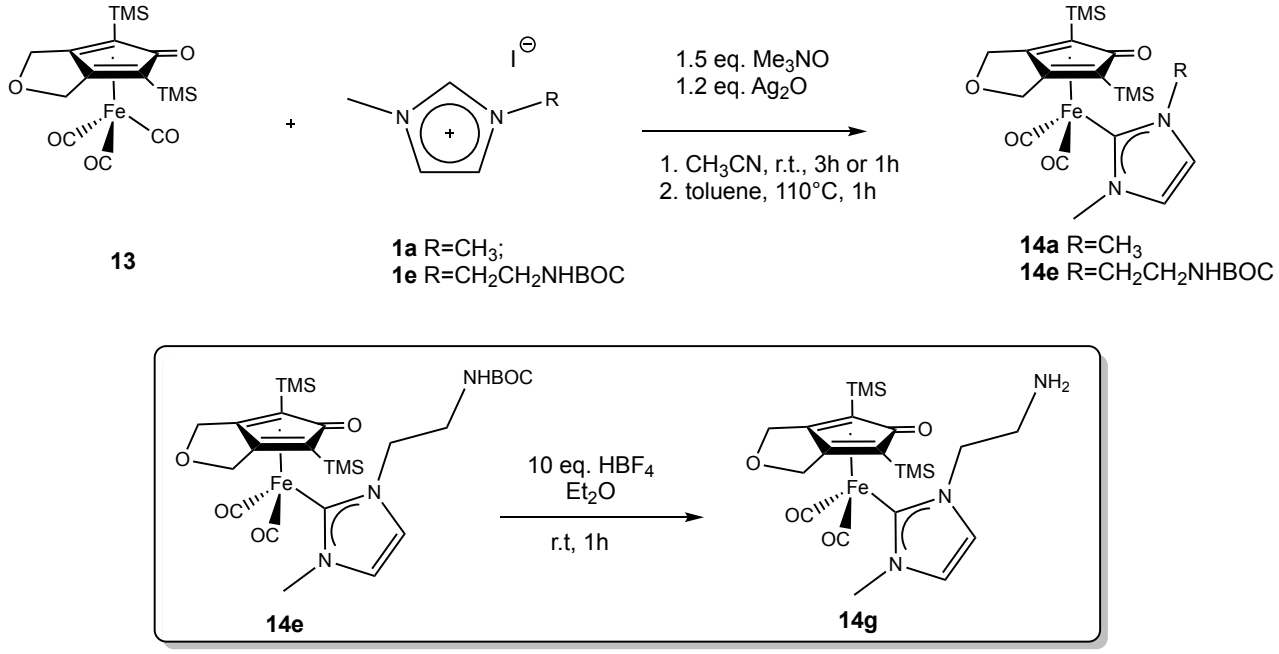

Scheme 3. Transmetallation reaction leading to complexes **14**. Box: deprotection of **14e**.

NHC iron complexes were characterised by ^{1}H-NMR, ^{13}C-NMR and ESI-MS. ^{1}H-NMR spectra were consistent with those of the previously reported **7** and **10**, and ^{13}C-NMRs show the diagnostic signal of Fe-$C_{carbene}$ ($\delta(C_{carbene})$ **14a**: 182 ppm, **14e**: 183 ppm). The molecular structure of **14g**, as determined by X-ray crystallography (Figure 2) closely resembles that previously reported in Chapter 1 for the complex **10a**. In particular, the Fe(1)-C(3) distance [2.376(3) Å] is significantly longer than Fe(1)-C(4-7) [2.072(3)-2.171(3) Å, average 2.118(6) Å] and C(3)-O(3) [1.241(4) Å] is essentially a double bond.[14]

The Fe(1)-C(21) bond [1.977(3) Å] is in the typical range for the interaction between Fe(0) and a *N*-heterocyclic carbene.[15]

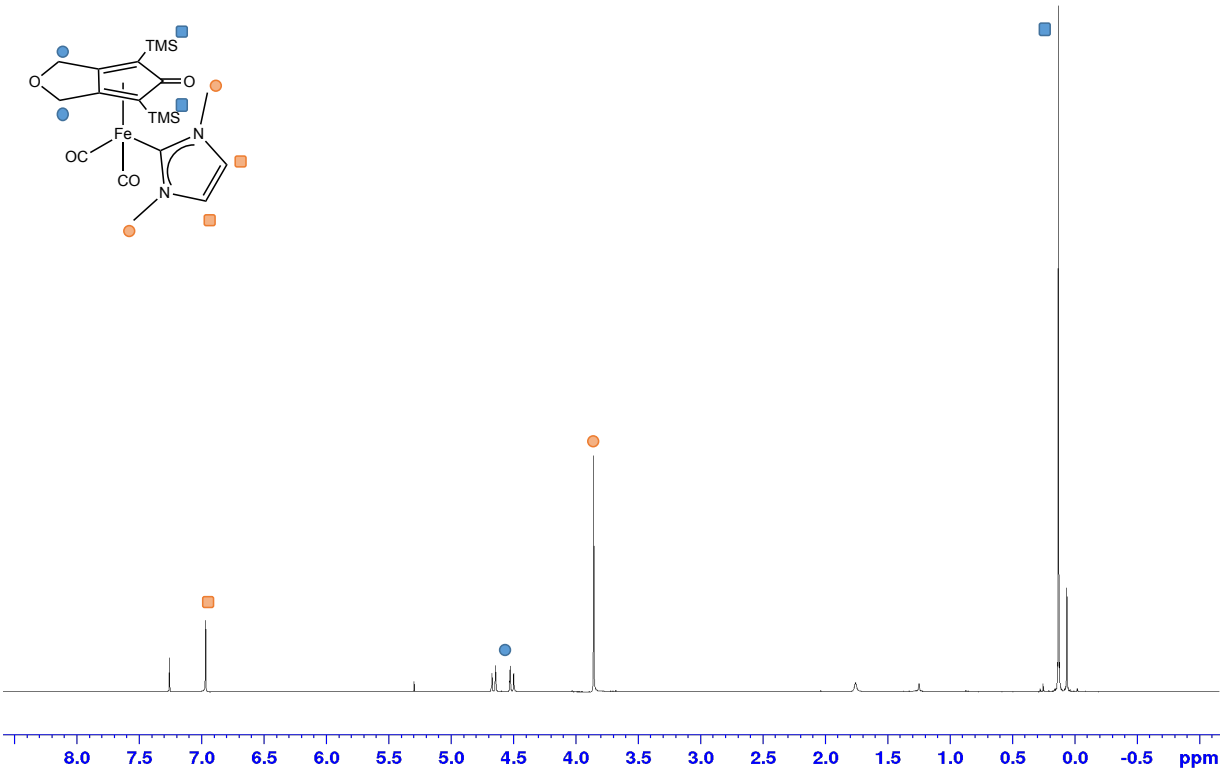

Figure 1. ^{1}H-NMR of **14a** with attributions.

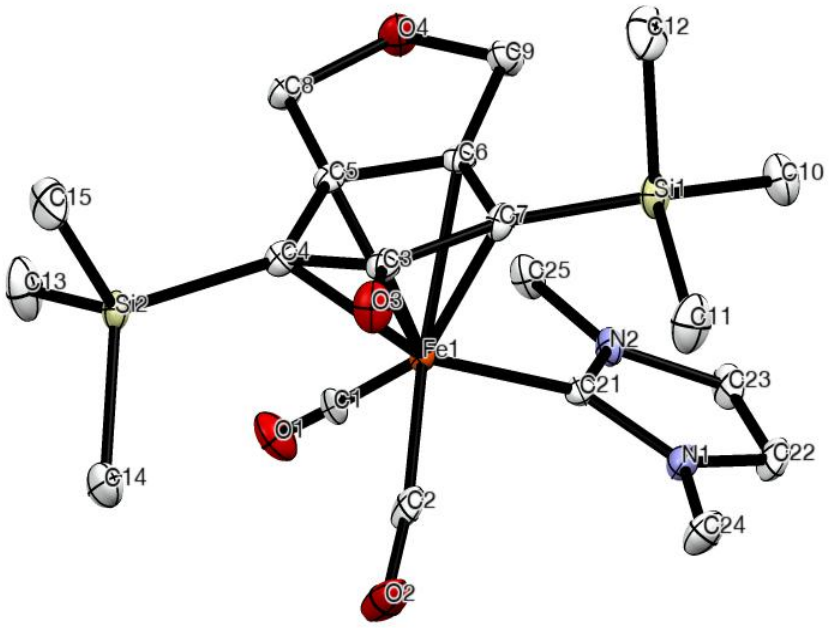

Figure 2. ORTEP drawing of **14a**. Displacement ellipsoids are at the 30% probability level. H-atoms have been omitted for clarity. Selected bond lengths (Å): Fe(1)-C(1) 1.767(4), Fe(1)-C(2) 1.778(3), Fe(1)-C(3) 2.376(3), Fe(1)-C(4) 2.139(3), Fe(1)-C(5) 2.0972(3), Fe(1)-C(6) 2.073(3), Fe(1)-C(7) 2.171(3), Fe(1)-C(21) 1.977(3), C(3)-O(3) 1.241(4).

Treating precursor **14e** with an excess of tetrafluoroboric acid (HBF_4) followed by neutralization, yielded the corresponding amino-complex **14g** in good yield (Scheme 3, bottom). Complex **14e** needs more than 5 eq. of acid addition compared to **10e** or **7e** in order to complete the reaction, likely due to the furan ring on the CpO ligand, which is prone to protonation, hence removing acid from reaction solution. Characterisation of **14e** (NMR, IR and ESI-MS) confirmed the structure with a NH_2 functional group on the later chain (See Experimental).

4.3.2 Electrochemical characterisation.

NHC-CpO iron complexes were characterised by cyclic voltammetry in CH_3CN containing Bu_4NPF_6 (0.1M). The CV (Figure 2, left) of complex **10a** displays one reversible redox process in the anodic region with formal potentials of +0.54 V versus ferrocenium/ferrocene (Fc+/Fc). The process represents the oxidation of the starting complex and involves one electron, as suggested by ΔEp=77mV, hence a Fe^0/Fe^+ redox couple.

Interestingly, CV (Figure 2, right) of triscarbonyl precursor **8** reveals an irreversible redox process at +1.15 V and two processes in the cathodic side at -2.08 V and -2.60 V, both irreversible. This demonstrates that NHC ligand provides intriguing redox processes at Cp iron complexes, stabilising the iron centre with a Fe^+ oxidation state. Moreover, since the oxidation involves electron abstraction from the HOMO we can suppose that the HOMO should involve NHC ligand.

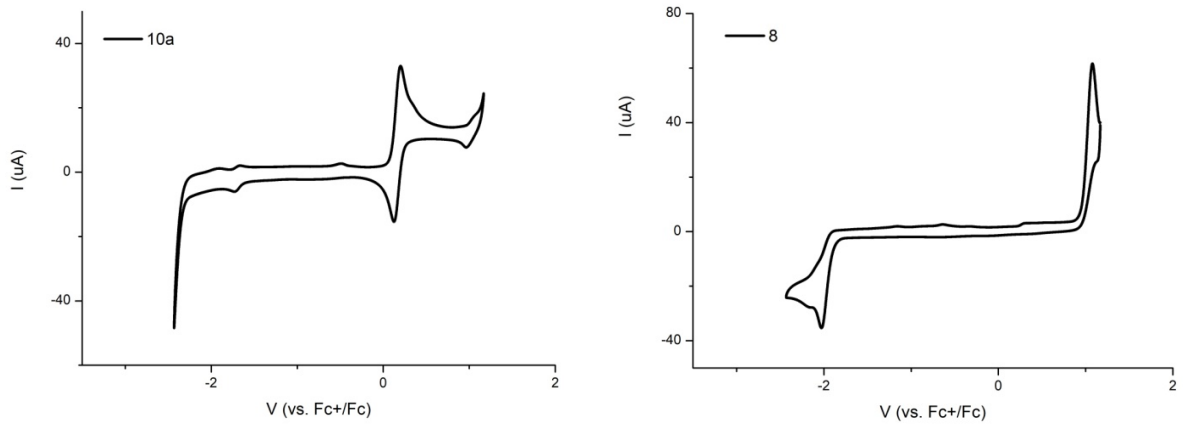

Figure 3. CVs recorded in 2mM solution in CH_3CN of **10a** (left) and **8** (right). Scan rate: 50mV/s.

Compounds **10i** and **14a** display the same behaviour and the relevant redox processes are reported in Table 2 (See Experimental Section for CVs).

The NH_2 complex **10g** shows an irreversible process in the cathodic region at -2.25 V, and two irreversible waves at +0.40 V and +0.97 V on the anodic side. The presence of two anodic irreversible waves might be due to the NH_2 group, which undergoes a chemical reaction after the first electrochemical oxidation step (EC mechanism). The analogue compound **14g** behaves similarly and redox processes are comparable (Table 2).

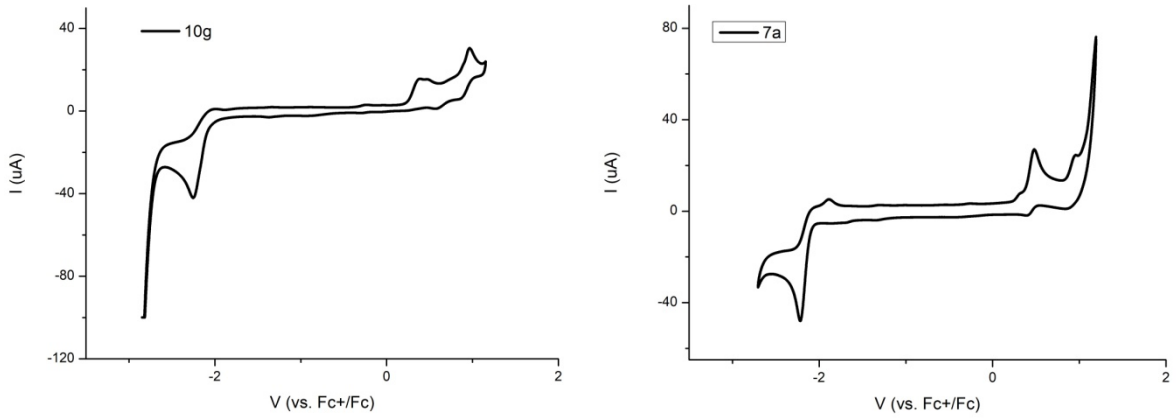

Figure 4. CVs recorded in 2mM solution (CH_3CN) of **10g** (left) and **7a**(right). Scan rate: 50mV/s.

Table 2. Formal potential of redox processes involved in NHC-Cp iron complexes.[a]

	E_{red}°' (V vs. Fc+/Fc)	**E_{ox}°' (V vs. Fc+/Fc)**
7a	-2.23*	+0.48*/+0.97*,**
10a	-	+0.16
10g	-2.25*	+0.40*/+0.97*,**
10i	-2.41*	+0.19
14a	-2.41*	+0.31
14g	-2.42*	+0.35*

[a] E_{ox}°' refers to anodic process and E_{red}°' to cathodic process. Single asterisk (*) indicates that the process is irreversible (peak potential is given) and double asterisk (**) indicates the second peak of the wave.

Finally, complex **7a** shows two irreversible redox processes in the anodic region at +0.48 V and +0.97 V, and one irreversible one on the cathodic side at -2.23 V. The different behaviour with respect to congeners **10a** and **14a**, might be ascribable to the differently substituted cyclopentadienone ligand. Indeed, both **7a** and **14** bear a more electron-withdrawing substituent on the CpO ligand compared to **10a**. Phenyl groups have

stronger withdrawing ability compared to cyclic ether of **14a**, thus **7a** showed higher oxidation and reduction potentials compared to the other two congeners.
Furthermore, reduction potentials of dimethyl-NHC **7a**, **10a** and **14a** are strongly influenced by electron withdrawing ability of functional groups of Cp ligand. Since reduction should add electrons to LUMO orbital, we can suppose that LUMO must involve the CpO ligand, whilst HOMO the NHC.

4.3.3 Electrocatalytic activity.

A preliminary screening of catalytic activity for iron compounds is herein reported. Electrocatalytic properties were studied recording CVs in a mixture of THF/H_2O (4:1), since iron complexes are not completely soluble in water, in the presence of increasing amounts of potassium hydroxide (KOH).
A scan without any KOH in solution confirmed the same redox waves described in the characterisation paragraph with CH_3CN as solvent, but at slightly shifted potential (Table 3).

Table 3. Formal potential of redox processes involved in NHC-Cp iron complexes in THF/H_2O.[a]

	E_{ox}°' (V vs. Fc+/Fc)
7a	+0.55
10a	+0.28
10g	+0.42*/+0.64*,**
10i	+0.29
14a	+0.40
14g	+0.50*

[a] E_{ox}°' refers to anodic process and E_{red}°' to cathodic process. Single asterisk (*) indicates that the process is irreversible (peak potential is given) and double asterisk (**) indicates the second peak of the wave.

In order to shed some light on the second peak typical of NH_2 complexes **10g** and **14g** and the role of amino group, CVs of **10g** were recorded in a phosphate buffer aqueous solution at pH=2 (Figure 5). Under these conditions **10g** is completely soluble in water phase and the amino group is totally protonated, thus it is less likely involved in any side reactions. Indeed, CVs showed only one reversible redox process at +0.70 V, even at slow scan rates (5 mVs^{-1}), demonstrating that the NH_2 group is involved in the chemical reaction following the first oxidation state (EC mechanism).

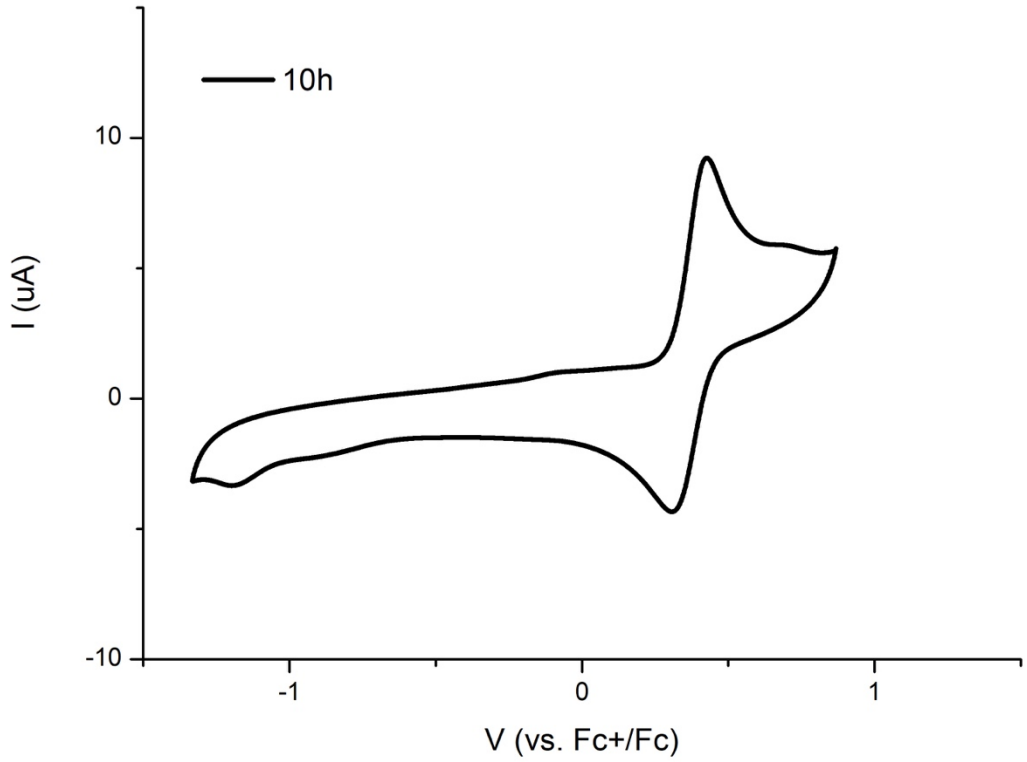

Figure 5. CVs in 2mM solution (H_2O, phosphate buffer pH=2) of **10g** at 50mVs^{-1}.

10a is chosen as reference compound to explain the catalytic behaviour of this class of iron complexes toward water oxidation. When CVs of **10a** were recorded in the presence of increasing amounts of base, an electrocatalytic behaviour was observed, as shown in Figure 6. In fact, the forward peak (positive I values) increases, indicating that the neutral form of the complex is regenerated by the catalytic reaction pathway (Scheme 4, A=reagent, B=product). At the same time, the backward peak decreases because the oxidized form of the complex is consumed by O_2 evolution.

$$Fe_{red} \longrightarrow Fe_{ox}$$

$$Fe_{ox} + A \longrightarrow Fe_{red} + B$$

Scheme 4. The oxidised form (Fe_{ox}), generated at the electrode, reacts with the reagent A (OH^-/H_2O) to leave product B (O_2) and neutral form (Fe_{red}).

The ratio between the currents in the presence (100 mM) and in the absence of potassium hydroxide, at a potential corresponding to the complex peak, was equal to 30. This value is so high as to rule out the possibility that the current is ascribable only to

other possible reactions involving **10a**. Plotting *i*cat/*i*pb (*i*cat=catalytic current, *i*b= blank current) over KOH concentration, we observed an increase of catalytic current upon subsequent addition of base, which is consistent with a base-dependent mechanism for water oxidation.[16]

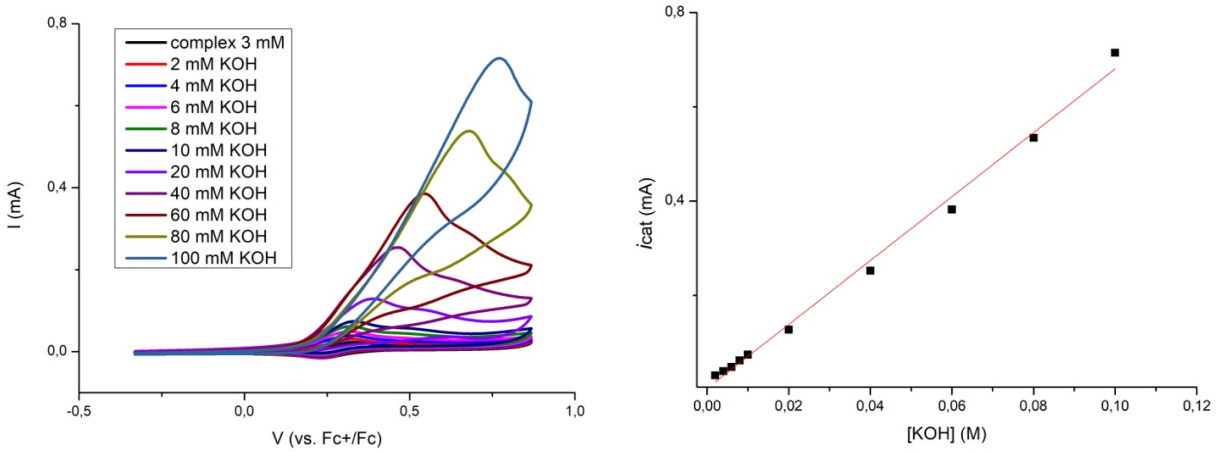

Figure 6. (Left) CVs in 3mM solution (THF/H_2O, 4:1) of **10a** with addition of KOH; scan rate: 50mVs^{-1}. (Right) Increasing current depending on base addition.

CVs showed a mixed behaviour between kinetic and diffusive conditions: presence of the peak-shape on CVs is typical of diffusive regime, whilst the shifting to more anodic region of peak potential with increasing amount of substrate is consistent with kinetic conditions. In our case, the substrate consumption phenomenon close to the electrode surface, then its decreasing concentration, causes its diffusion contribution to increase in the CV response, which deviate from the classical catalytic sigmoidal to a peak-shaped response.

To evaluate the catalytic activity of **10a** in terms of TOF, we used equation 1 below.[17] Indeed, even though we are not under purely kinetic conditions, the equation can be used as preliminary value to a rough estimate of the catalytic activity.

$$\frac{i_{cat}}{i_b} = 2.242 n_{cat} \left(\frac{K_{cat} RT}{F}\right)^{\frac{1}{2}} v^{-\frac{1}{2}} \qquad (1)$$

In the equation, n_{cat} is the number of electrons involved in the catalytic reaction, K_{cat} is the pseudo-first-order rate constant, R is the universal gas constant, T is the temperature, F is the Faraday constant and ν is the scan rate. From eq. 1 it can be calculated K_{cat}, which corresponds to TOF value of O_2 evolution at the potential of the used catalyst. Calculation for **10a** gives a TOF estimation of 53.65 s^{-1}.

Another parameter useful to evaluate the catalytic activity in voltammetry is the Catalytic Efficiency (C.E.) of the system,[18] which is given by

$$C.E. = \frac{i_{cat}/i_b}{C_B/C_{cat}}$$

In the equation, *i*cat is the catalytic current, *i*b is the blank current without substrate, C_B is the base concentration and C_{cat} is the catalyst concentration. Thus, C.E. varies between 0 and 1, with 1 the maximum efficiency. A plot of the ratio i_{cat}/i_b as a function of C_B/C_{cat} showed a linear relationship and the slope allowed to estimate C.E. for **10a** equal to 0.71.

Having analysed these results, we move to other complexes with different substituted NHCs **10g** and **10i**, and different cyclopentadienones **7a**, **14a** and **14g**. All complexes showed water oxidation activity upon addition of KOH to the solution. Corresponding CVs are reported in the Experimental Section. The slopes of the plots of *i*cat/*i*p, all TOF and C.E. values are reported in Table 4. In general, values are comparable between them as suggested by a diffusive regime, being **10i** with –OH the best among them. Furthermore, the reactivity as WOC is general for the NHC-Cp iron system and not dependant on selective functional groups on ligands.

Table 4. Slopes of *i*cat/*i*b with R^2 and TOF values for each iron compound.

Fe	**Slope(*i*cat/*i*b)**	**R^2(*i*cat/*i*b)**	**TOF**	**C.E.**
7a	212±8	0.98967	6.63	0.40
10a	(3.6±0.1)10^2	0.99119	54	0.71
10g	146±8	0.98226	0.165	0.29
10i	(3.7±0.1)10^2	0.99254	28	0.73
14a	200±5	0.9954	10.6	0.42
14g	231±1	0.99963	11.7	0.46

Finally, the role of KOH might be explained by two separate effects.

I. thermodynamic, by lowering the standard potential at which the O_2 evolution happens at that pH. Indeed, in water the following equation is valid: E=E°-0.0592pH, hence at basic pH conditions the oxygen will evolve at lower potential. In our THF/H_2O mixture, the OH- concentration will have the same effect on the

reaction potential. Without any base addition reaction did not take place, indeed the byproduct H^+ will lower pH in the absence of a buffer system and increase the reaction potential.

II. rate enhancements, as showed in Figure 6 for **10a** (right), in which is visible increasing of catalytic current (i_{cat}) versus concentration of KOH.

A base–enhanced catalysis has already been reported in a single-site Ru-based WOC[12,19], either in atom-proton transfer (APT) or proton-coupled electron transfer (PCET) pathways. The APT is involved in WNA mechanism (see Scheme 1), thus OH- acting either as proton acceptor base from water (eq. 2) or by direct nucleophilic attack on M=O (eq. 3). The PCET is involved in ROC mechanism (see Scheme 1) in the M-OH oxidation step to M=O, where OH- acts as proton bases in concert to electron transfer to the electrode (eq. 4).

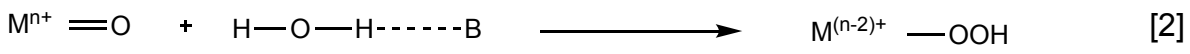

[2]

[3]

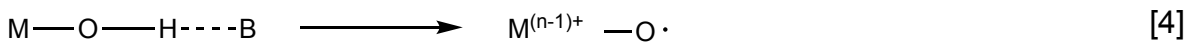

[4]

At this stage of the work, we are not still able to elucidate which mechanism is involved in this iron-based WOC, but mechanistic insight and further electrochemical studies are currently underway.

4.4 Conclusions

Organometallic NHC-CpO iron(0) complexes, without classic chelated N and O ligand, have been employed as water oxidation catalysts. A screening of different NHCs and CpO ligands showed that the activity is general for the carbene-cyclopentadienone iron system and not dependant on specific functional groups on ligands. Furthermore, catalytic properties arise from the presence of NHC ligand, in that measurements on the triscarbonyl precursor **8** (not containing NHCs) showed no redox waves in the anodic region and, consequently, no activity as WOC.

Preliminary screening of water oxidation activity in THF/water mixture showed that the NHC-CpO iron complexes have comparable activities. Plotting *i*cat/*i*p over base concentration and comparing slopes of all compounds, reveals that **10i** with an –OH on the longer-chain N-substituent is the best catalyst, followed by the simplest dimethyl-substituted **10a**.

Further studies are now underway in order to determine the catalytic activity and mechanistic insights to shed some light on the type of mechanism involved in the observed oxygen evolving reaction.

2.5 Experimental Section

General data. All reactions were routinely carried out under a nitrogen atmosphere, using standard Schlenk techniques. Glassware was ovendried before use. Solvents: dichloromethane (CH_2Cl_2), tetrahydrofuran (THF), diethyl ether (Et_2O), petroleum ether referring to a fraction of bp 60-80 °C, acetonitrile (CH_3CN) were dried and distilled prior to use. Acetone has been degassed and stored under inert atmosphere on molecular sieves. Other solvents such as ethylacetate (EtOAc), chloroform, ethanol (EtOH), methanol (MeOH), toluene, $CDCl_3$ (Sigma Aldrich) have been employed without further purification. Reagents: $Fe_2(CO)_9$ (Strem), methyl iodide, silver oxide, 1-methylimidazole, Bu_4NPF_6, potassium hydroxide, trifluoroboric acid have been employed as purchased.

1,3-dimethylimidazolium iodide,[20] NHBoc (JOMC 2008), 1-methyl-3-(2-hydroxyethyl)imidazolium chloride, 1,8-bis(trimethylsilyl)octa-1,7-diyne[21] have been prepared following procedures reported in the literature.

The prepared derivatives were characterized by spectroscopic methods. The NMR spectra were recorded using Varian Inova 300 (^1H, 300.1; ^{13}C, 75.5 MHz), Varian Mercury Plus VX 400 (^1H, 399.9; ^{13}C, 100.6 MHz), Varian Inova 600 (^1H, 599.7; ^{13}C, 150.8 MHz) spectrometers at 298 K; chemical shifts were referenced internally to residual solvent peaks. Infrared spectra were recorded at 298 K on a Perkin-Elmer Spectrum 2000 FT-IR spectrophotometer. ESI-MS spectra were recorded on Waters Micromass ZQ 4000 with samples dissolved in MeOH or CH_3CN. Elemental analyses were performed on a Thermo-Quest Flash 1112 Series EA instrument.

Triscarbonyl (2,4-bis(trimethylsilyl)-7-oxy-bicyclo[3.3.0]hepta-1,4-dien-3-one)iron (13).[22] In a 75 mL Teflon tube equipped with magnetic stirrer, (Oxybis(prop-1-yne-3,1-diyl))bis(trimethylsilane) 0.53 g (1.2 mmol) and $Fe_2(CO)_9$ 0.728 g (2 mmol) were dissolved in 40 mL of toluene. The container was closed with a cap, equipped with a temperature sensor, and placed into microwave. The reaction was heated to 140 °C for 70 min. Upon removal of the solvent, the product was purified to afford the yellow triscarbonyl-η^4-3,4-bis(4-methoxyphenyl)-2,5-diphenylcyclopenta-2,4-dienone)iron complex (**13**) by neutral alumina column chromatography using dichloromethane/ethyl acetate (100/0 to 0/100). Yield = 50%

13 has been analyzed by IR, ^{1}H-NMR. ^{1}H-NMR (399.9 MHz, $CDCl_3$): δ (ppm) 4.72 (m, 4H, CH_2), 0.24 (s, 186H, $CH_{3,TMS}$). IR (CH_2Cl_2, cm^{-1}): (ν_{CO}) 2067, 2013, 1997; ($\nu_{C=O}$) 1636; ($\nu_{C=C}$) 1609, 1518.

Dicarbonyl-(4,6-bis(trimethylsilyl)-1H-cyclopenta[c]furan-5(3H)-one)[1,3-dimethylilidene] iron (14a). In a dried 100 mL Schlenk flask, 1,3-dimethylimidazolium iodide (0.116 g, 0.52 mmol), silver oxide (0.132 g, 0.57 mmol), triscarbonyl-(4,6-bis(trimethylsilyl)-1H-cyclopenta[c]furan-5(3H)-one)iron (0.200 g, 0.48 mmol) and trimethylamine-N-oxide (0.054 g, 0.72 mmol) were added to reaction vessel and dissolved in acetonitrile (8 mL). Reaction mixture was stirred at room temperature and protected from light for 1 hour. Solvent was removed in vacuo. The solid was re-dissolved in toluene (20 mL) and left under reflux for 1 hour. At the end of reaction time, solvent was removed under vacuum and the product was purified to afford the yellow iron complex by column chromatography on neutral alumina using dichloromethane/ethyl acetate (100 to 100). Yield = 54 %

14a has been analyzed by IR, ^{1}H-NMR, ^{13}C-NMR and ESI-MS. ^{1}H-NMR (400 MHz, CD_3Cl) δ(ppm): 6.97 (s, 2H, CH_{im}), 4.67-4.50 (dd, 4H, CH2), 3.86 (s, 3H, NCH_3), 0.131 (s. 18H,-CH_{3TMS}). ^{13}C-NMR (150.8 MHz, CD_3Cl) δ (ppm): 216.11 (CO), 182.49 (C_{carb}), 181.05 (C=O, Cp), 124.05 (CH_{im}), 108.80 ($C_{2,5}$, Cp), 68.13 (CH_2) 63.42 ($C_{3,4}$, Cp), 39.22 (NCH_3), -0.69 (CH_{3TMS}). IR (CH_2Cl_2, cm^{-1}): (ν_{CO}) 1991, 1931; ($\nu_{C=O}$) cm^{-1}. ESI-MS (m/z): 475 $[M+H]^+$, 497 $[M+Na]^+$, 513 $]M+K]^+$.

Dicarbonyl-(4,6-bis(trimethylsilyl)-1H-cyclopenta[c]furan-5(3H)-one)[1,3-dimethylilidene] iron (14e). In a dried 100 mL Schlenk flask, 1,3-dimethylimidazolium iodide (0.200 g, 0.57 mmol), silver oxide (0.153 g, 0.66 mmol), triscarbonyl-(4,6-bis(trimethylsilyl)-1H-cyclopenta[c]furan-5(3H)-one)iron (0.220 g, 0.55 mmol) and trimethylamine-N-oxide (0.062 g, 0.83 mmol) were added to reaction vessel and dissolved in acetonitrile (10 mL). Reaction mixture was stirred at room temperature and protected from light for 1 hour. Solvent was removed in vacuo. The solid was re-dissolved in toluene (20 mL) and left under reflux for 1 hour. At the end of reaction time, solvent was removed under vacuum and the product was purified to

afford the yellow iron complex by column chromatography on neutral alumina using dichloromethane/ethyl acetate (100 to 100). Yield = 51 %

14g has been analyzed by IR, ^{1}H-NMR, ^{13}C-NMR and ESI-MS. ^{1}H-NMR (400 MHz, CD_3Cl) δ(ppm): 7.13 (s, 1H, CH_{im}), 7.10 (s, 1H, CH_{im}), 4.66-4.49 (dd, 4H, CH_2), 4.27 (t, 2H, CH_2) 3.84 (s, 3H, NCH_3), 3.50 (q, 2H, CH_2), 1.43 (s, 9H, BOC), 0.13 (s. 18H, CH_{3TMS}). ^{13}C-NMR (150.8 MHz, CD_3Cl) δ (ppm): 216.62 (CO), 182.62 (C_{carb}), 180.65 (C=O, Cp), 156.06 (C==, BOC), 124.57 (CH_{im}), 122.50 (CH_{im}), 108.76 ($C_{2,5}$, Cp), 79.83 (C_{BOC}), 68.07 (CH_2) 64.53 ($C_{3,4}$, Cp), 50.57 (CH_2), 40.79 (CH_2), 39.12 (NCH_3), 28.30 ($CH_{3,BOC}$), -0.74 (CH_{3TMS}). IR (CH_2Cl_2, cm^{-1}): (ν_{CO}) 1990, 1932; ($\nu_{C=O,BOC}$) 1712 cm^{-1}; ($\nu_{C=O}$) 1578 cm^{-1}. ESI-MS (m/z): 604 $[M+H]^+$, 626 $[M+Na]^+$, 642 $[M+K]^+$.

Dicarbonyl-(4,6-bis(trimethylsilyl)-1H-cyclopenta[c]furan-5(3H)-one)[1,3-dimethylilidene] iron (14g). In a dried 25 mL Schlenk flask, dicarbonyl-(4,6-bis(trimethylsilyl)-1H-cyclopenta[c]furan-5(3H)-one) [1-(2-BocNH-ethyl)-3-methylilidene]iron (0.146 g, 0.24 mmol) was dissolved in Et_2O (15 mL) and HBF_4 (0.16 mL, 1.2 mmol) was added dropwise. Reaction mixture was stirred at room temperature for 1 hour. The precipitate was filtered off and then dissolved in CH_2Cl_2, and the excess of HBF_4 neutralized with a saturated solution of sodium carbonate (pH=7-8). Aqueous phase was extracted with CH_2Cl_2 and washed with potassium hydroxide solution (2M, 3x10mL). Organic phase was dried with magnesium sulfate and filtrated. Solvent was removed to leave a yellow solid. Yield = 80.0 %

14i has been analyzed by IR, ^{1}H-NMR, ^{13}C-NMR and ESI-MS. ^{1}H-NMR (400 MHz, CD_3Cl) δ(ppm): 7.18 (s, 1H, CH_{im}), 6.99 (s, 1H, CH_{im}), 4.66-4.47 (dd, 4H, CH_2), 4.26 (t, 2H, CH_2)., 3.85 (s, 3H, NCH_3), 3.10 (t, 2H, CH_2), 0.12 (s. 18H, CH_{3TMS}). ^{13}C-NMR (150.8 MHz, CD_3Cl) δ (ppm): 216.47 (CO), 182.40 (C_{carb}), 181.03 (C=O, Cp), 124.39 (CH_{im}), 122.65 (CH_{im}), 108.94 ($C_{2,5}$, Cp), 68.11 (CH_2) 63.66 ($C_{3,4}$, Cp), 53.76 (CH_2), 42.94 (CH_2), 39.01 (NCH_3), -0.73 (CH_{3TMS}). IR (CH_2Cl_2, cm^{-1}): (ν_{CO}) ν_{CO}) 1991, 1933; ($\nu_{C=O}$) 1605 cm^{-1}. ESI-MS (m/z): 504 $[M+H]^+$, 526 $[M+Na]^+$.

Electrochemical Characterisation. Cyclic voltammograms were recorded at a scan rate of 0.05 V s^{-1} on a BAS-100A electrochemical analyser using a three-electrode cell: a glassy-carbon disk (0.071 cm^2) as the working electrode, a $Ag/AgNO_3$ (0.1 M) reference

electrode, and a platinum-wire counter electrode. All experiments were performed under a nitrogen atmosphere in CH_3CN containing 0.1 M $^nBu_4NPF_6$ at room temperature. Ferrocene (Fc) was the internal reference, and all potentials have been quoted relative to the Fc/Fc^+ couple set at 0.00 V.

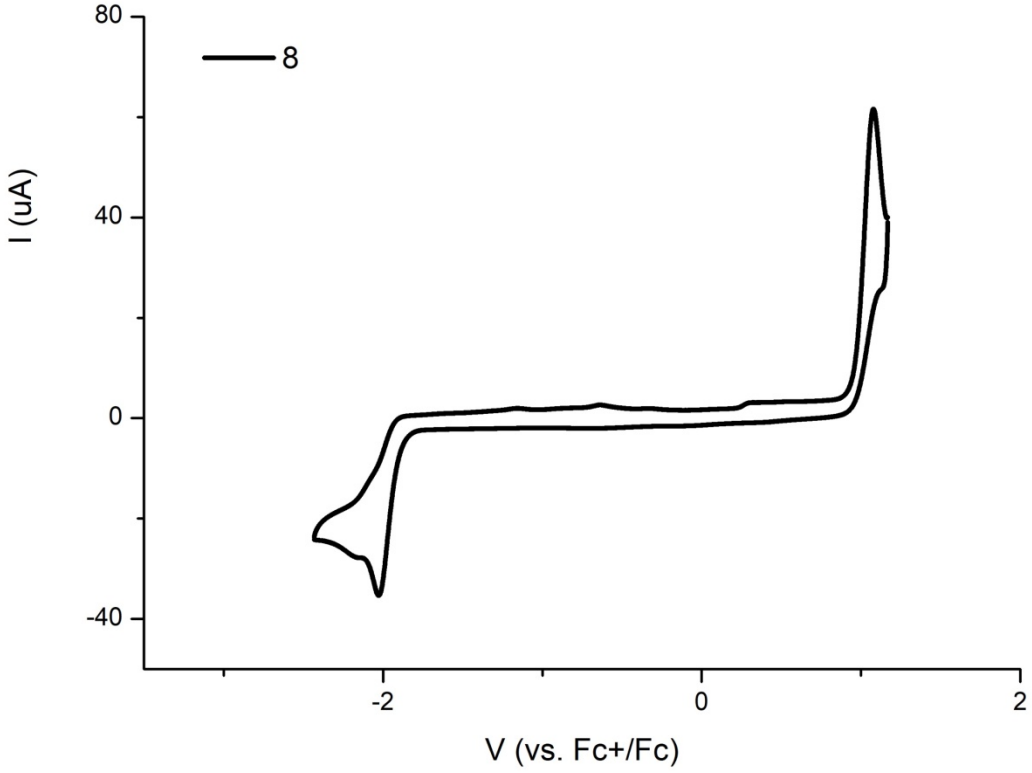

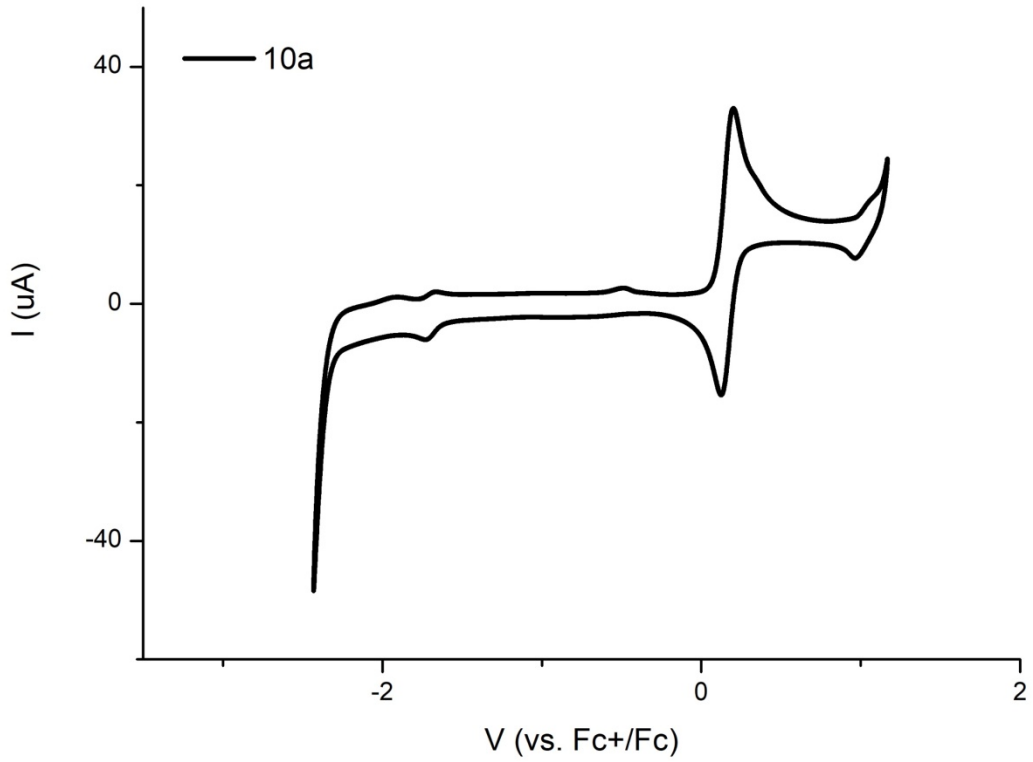
10a
40
0
-40
I (uA)
-2
0
2
V (vs. Fc+/Fc)

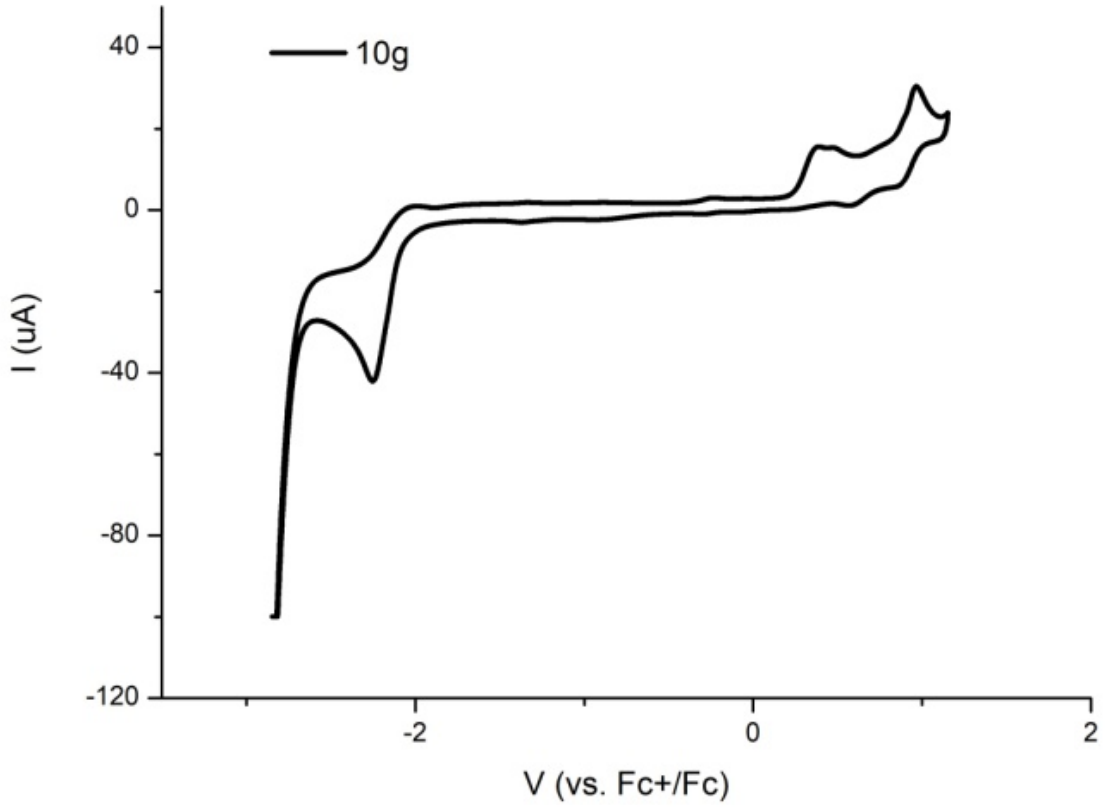
10g
40
0
-40
-80
-120
I (uA)
-2
0
2
V (vs. Fc+/Fc)

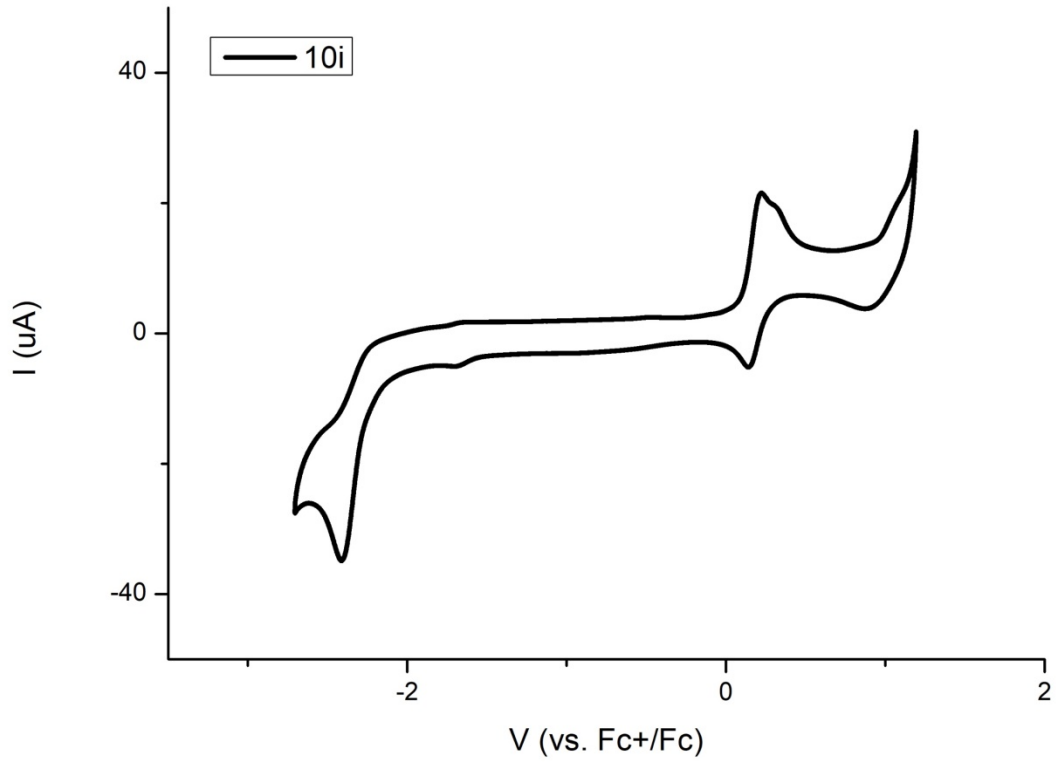
10i
40
0
-40
I (uA)
-2
0
2
V (vs. Fc+/Fc)

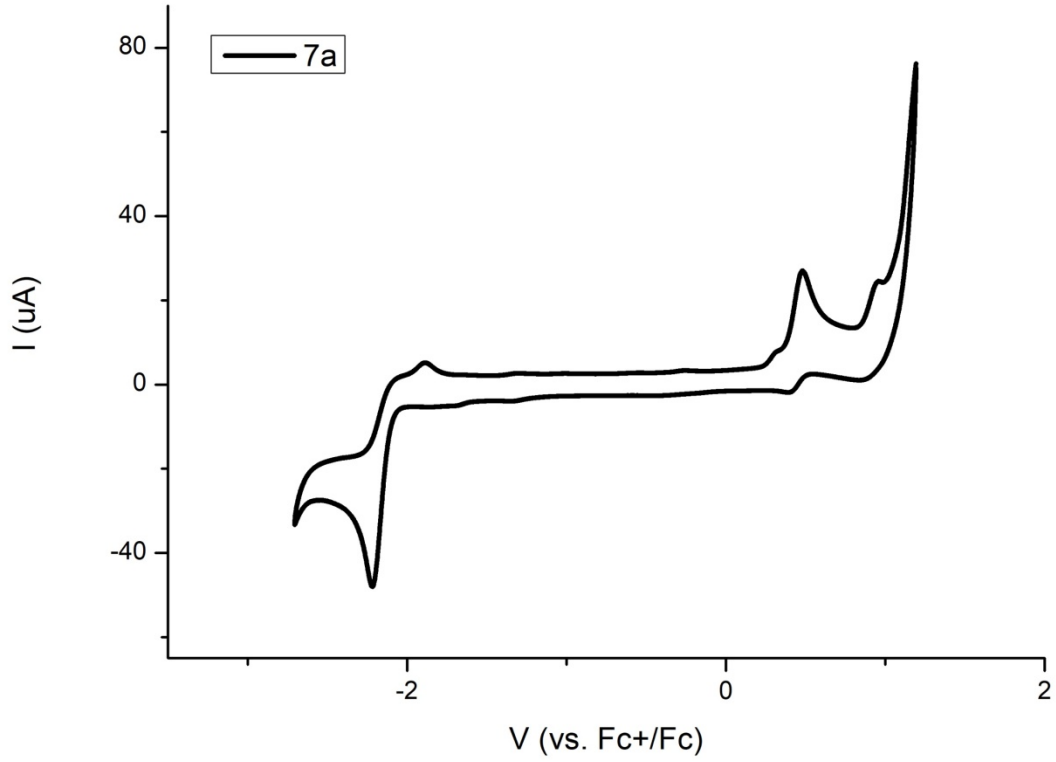
7a
80
40
0
-40
I (uA)
-2
0
2
V (vs. Fc+/Fc)

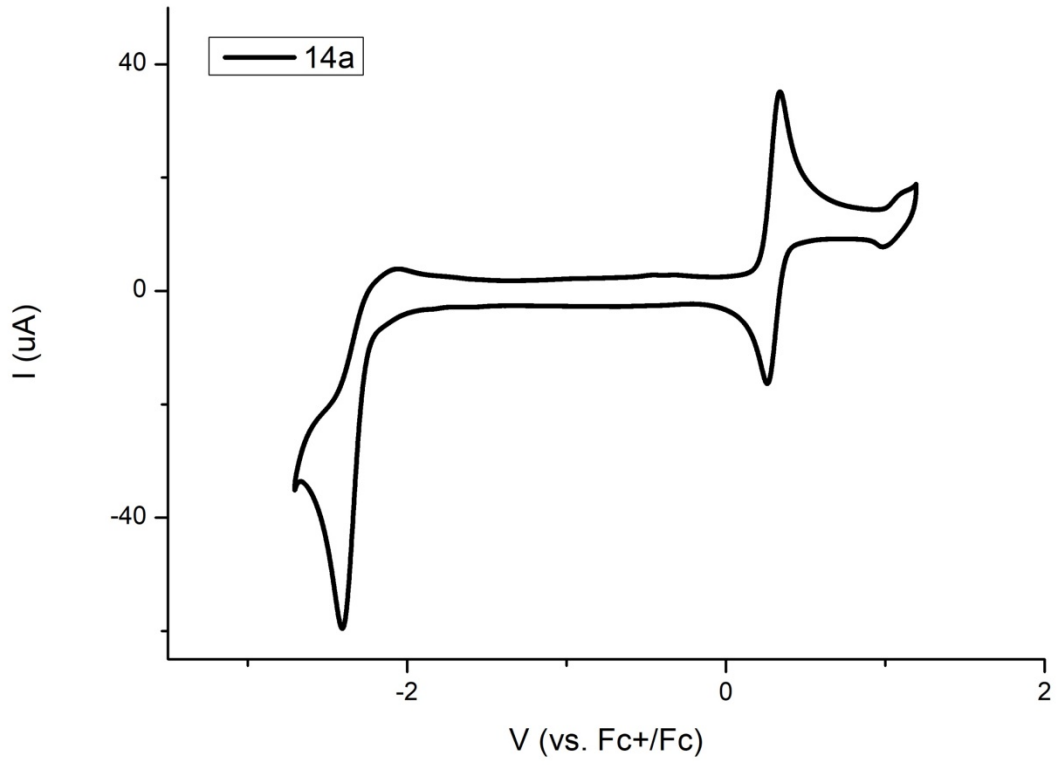
14a
40
0
-40
I (uA)
-2
0
2
V (vs. Fc+/Fc)

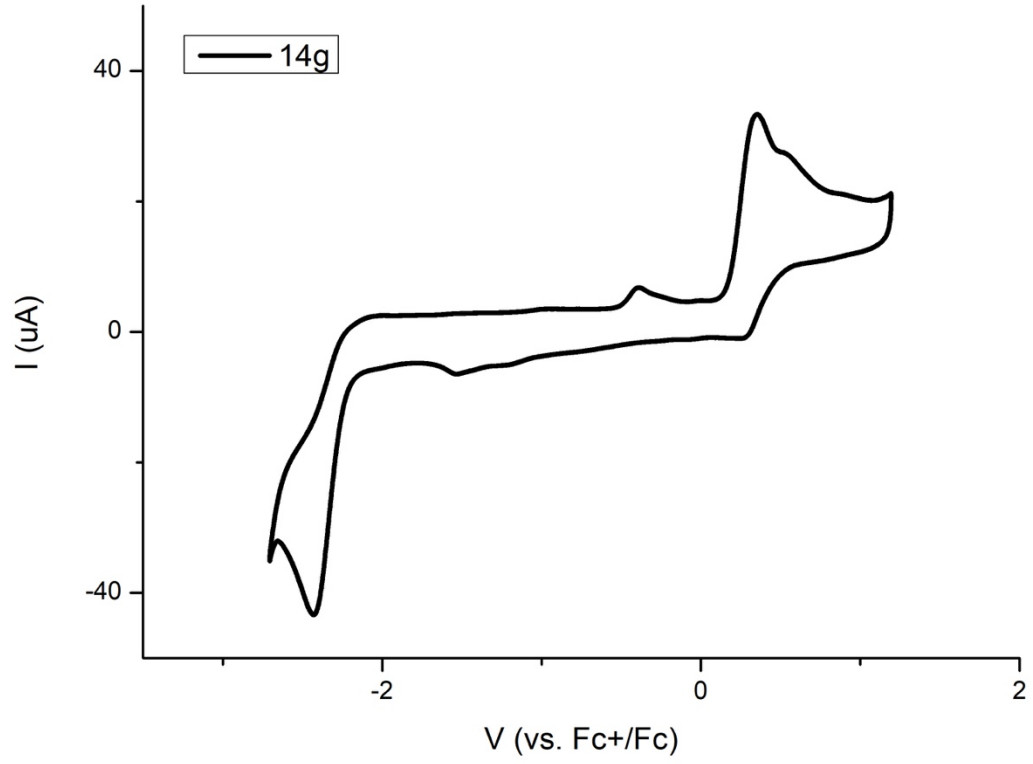
14g
40
0
-40
I (uA)
-2
0
2
V (vs. Fc+/Fc)

Electrocatalysis Studies. Cyclic voltammograms were recorded with the same setup of characterisation, but in THF/H_2O (4:1) mixture. Potassium hydroxide was added in molar equivalent increments via micropipette. All of the CVs have been recorded starting from the open circuit potential. Plot of *i*cat/*i*p over concentration of KOH showed the almost linear increment of current with base addition.

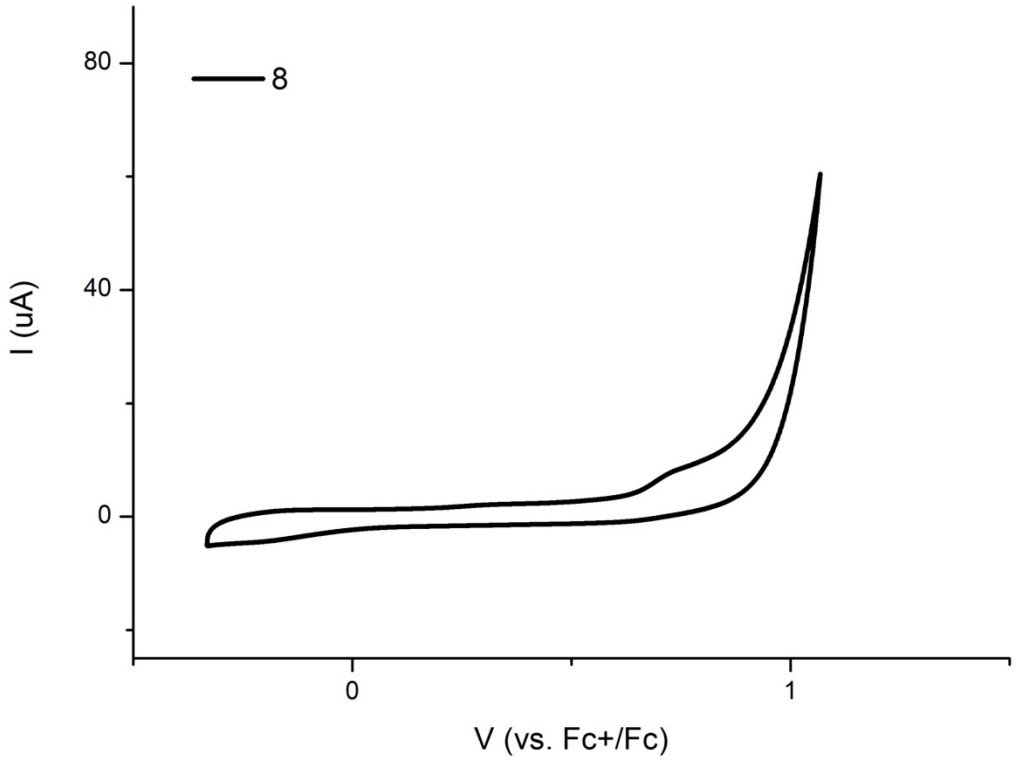

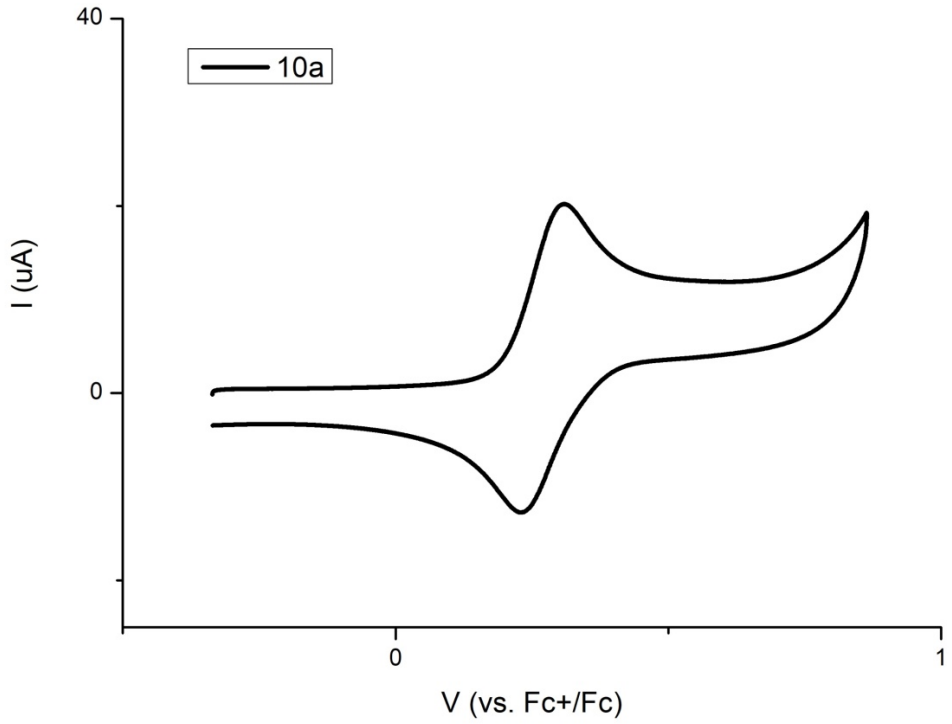
40
0
10a
I (uA)
0
1
V (vs. Fc+/Fc)

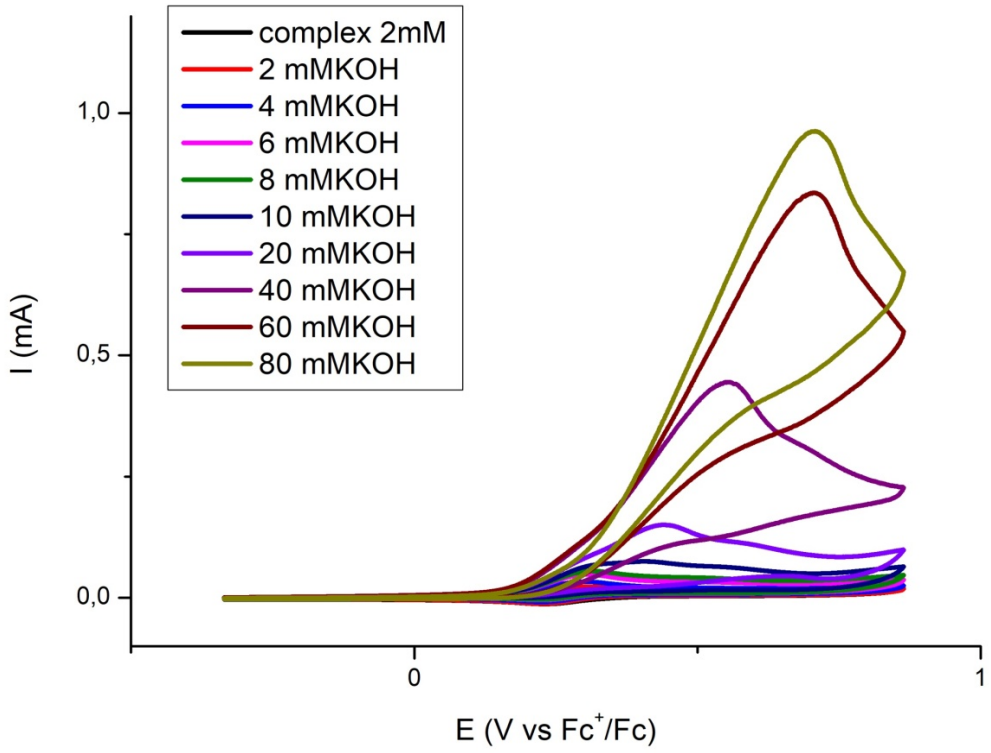
complex 2mM
2 mMKOH
4 mMKOH
6 mMKOH
8 mMKOH
10 mMKOH
20 mMKOH
40 mMKOH
60 mMKOH
80 mMKOH
1,0
0,5
0,0
I (mA)
0
1
E (V vs Fc+/Fc)

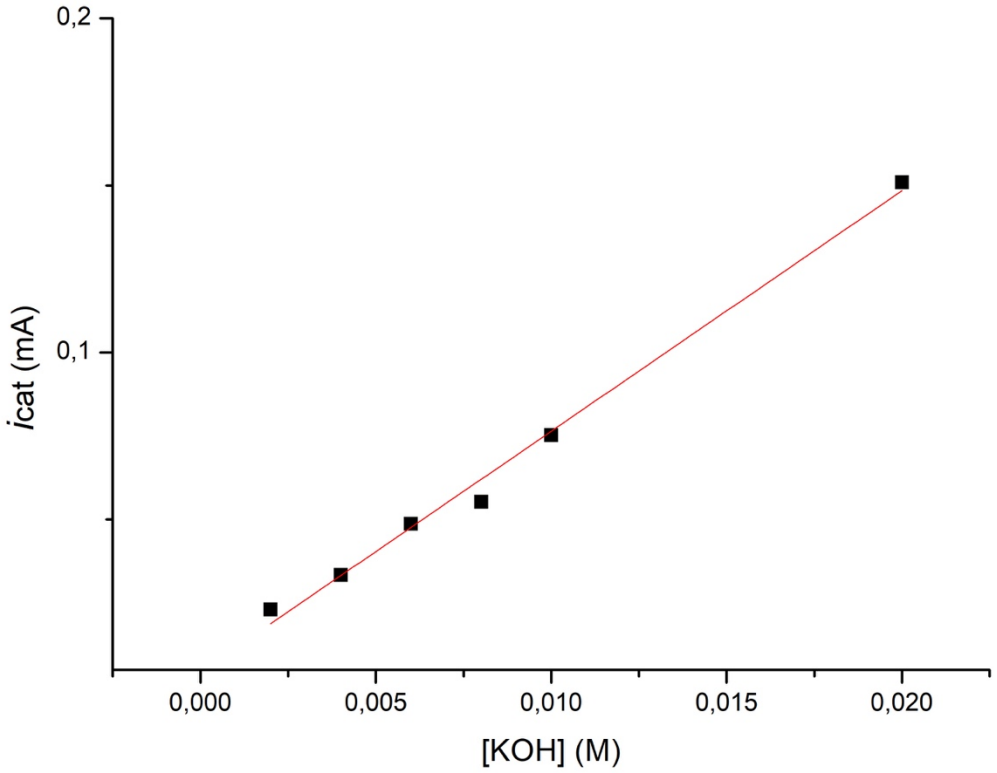
0,2
0,1
icat (mA)
0,000
0,005
0,010
0,015
0,020
[KOH] (M)

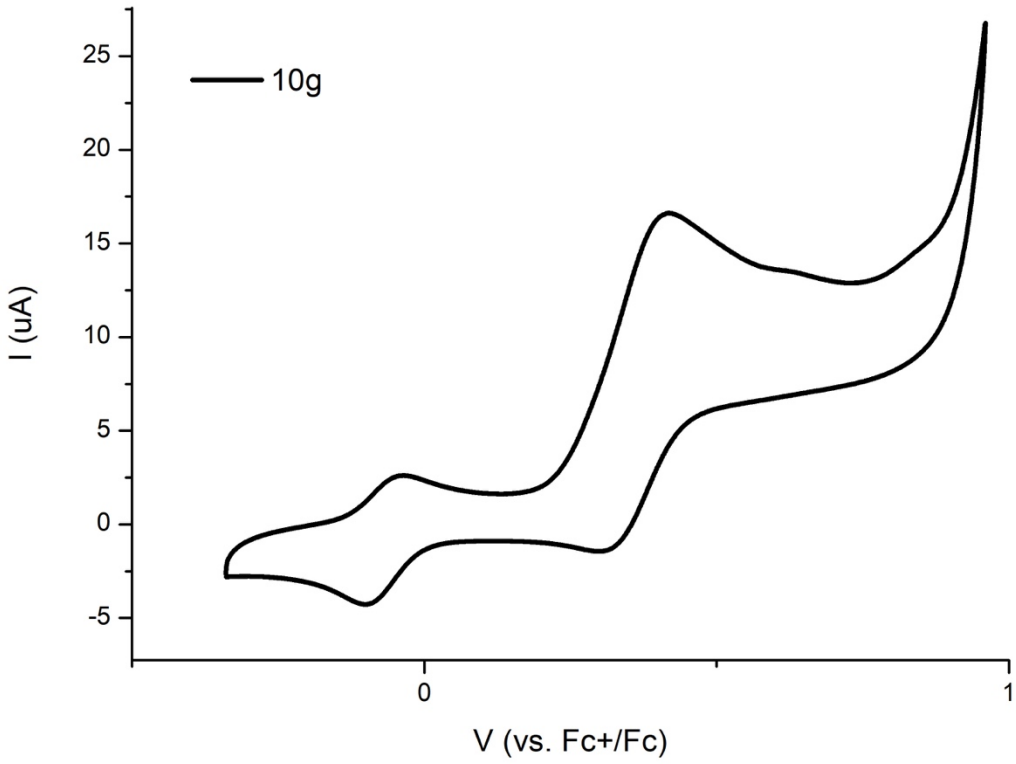
10g
25
20
15
10
5
0
-5
I (uA)
0
1
V (vs. Fc+/Fc)

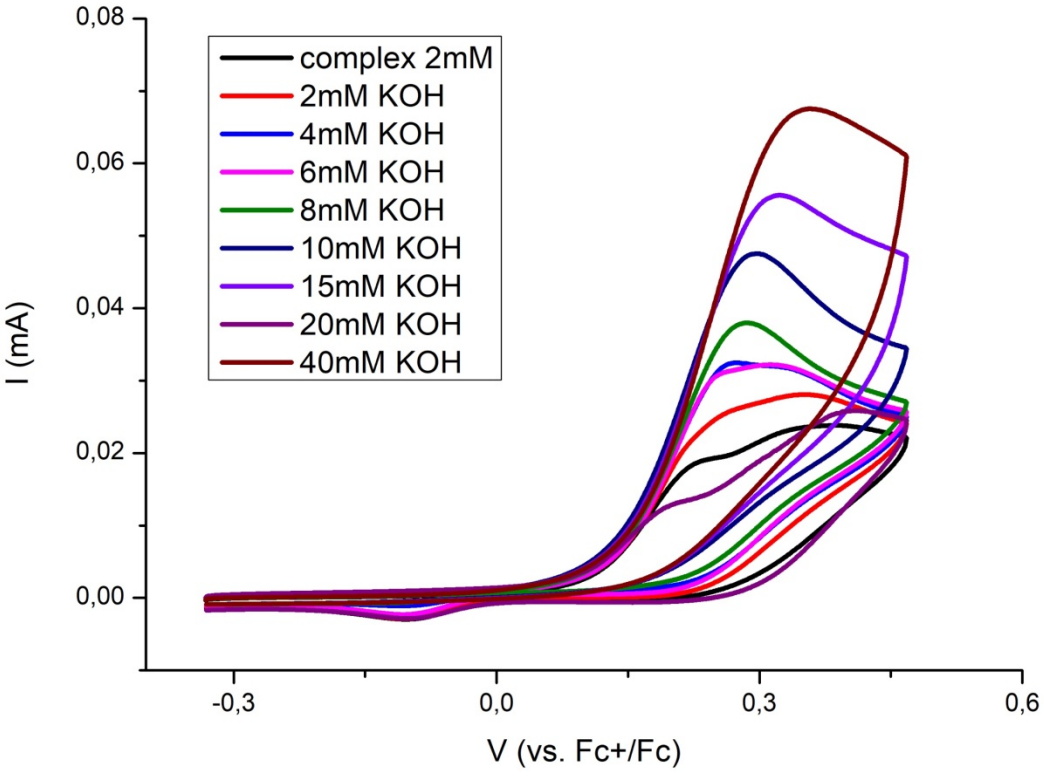
complex 2mM
2mM KOH
4mM KOH
6mM KOH
8mM KOH
10mM KOH
15mM KOH
20mM KOH
40mM KOH
I (mA)
V (vs. Fc+/Fc)
0,08
0,06
0,04
0,02
0,00
-0,3
0,0
0,3
0,6

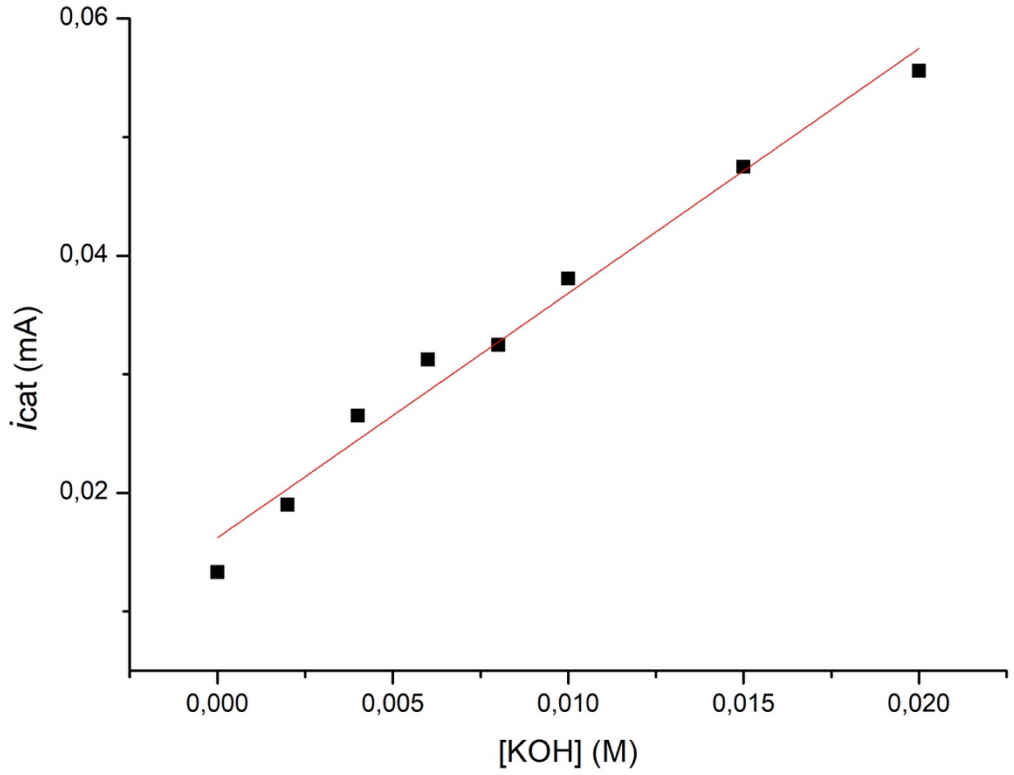
icat (mA)
[KOH] (M)
0,06
0,04
0,02
0,000
0,005
0,010
0,015
0,020

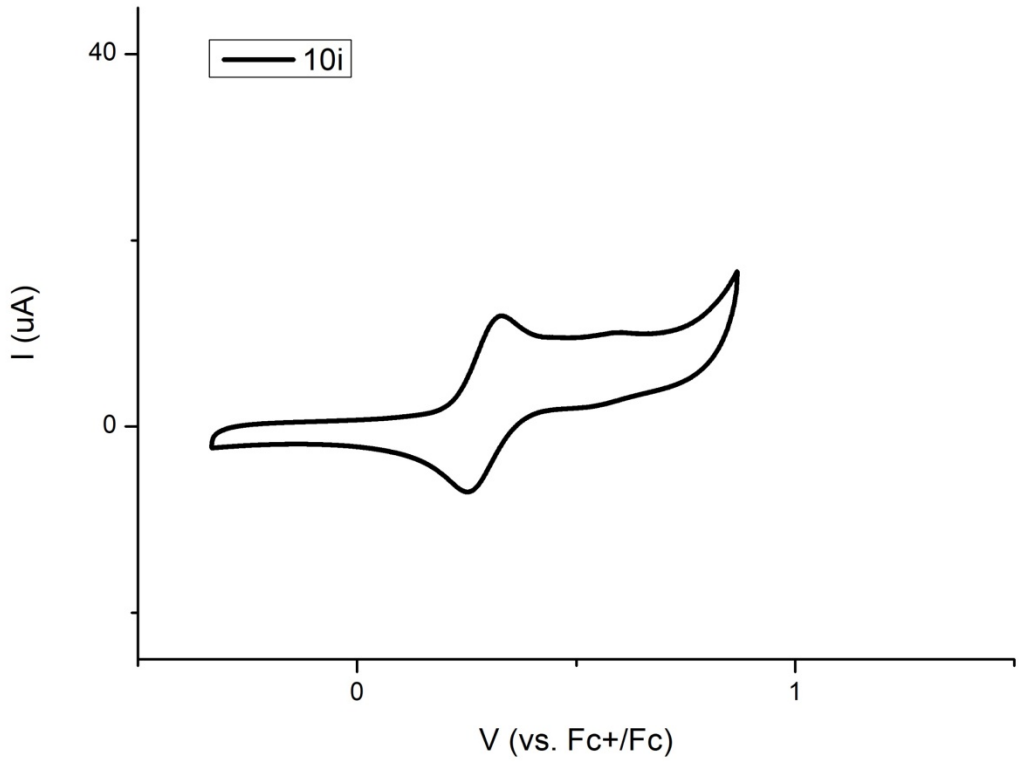
10i
40
0
I (uA)
0
1
V (vs. Fc+/Fc)

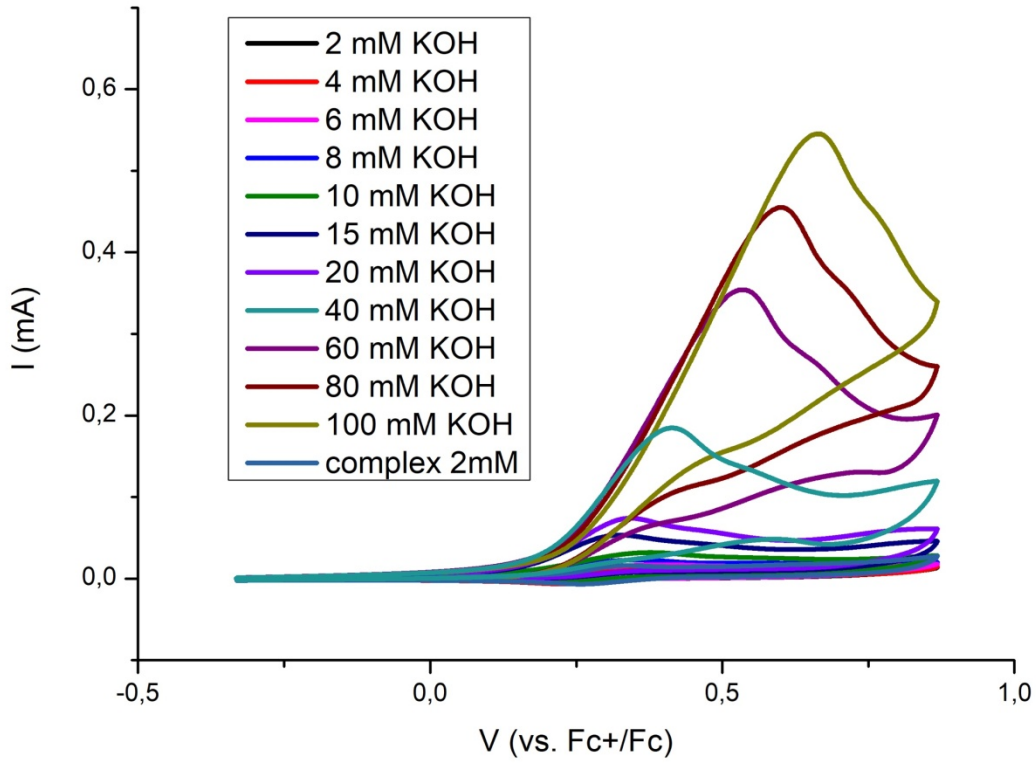
2 mM KOH
4 mM KOH
6 mM KOH
8 mM KOH
10 mM KOH
15 mM KOH
20 mM KOH
40 mM KOH
60 mM KOH
80 mM KOH
100 mM KOH
complex 2mM
0,6
0,4
0,2
0,0
I (mA)
-0,5
0,0
0,5
1,0
V (vs. Fc+/Fc)

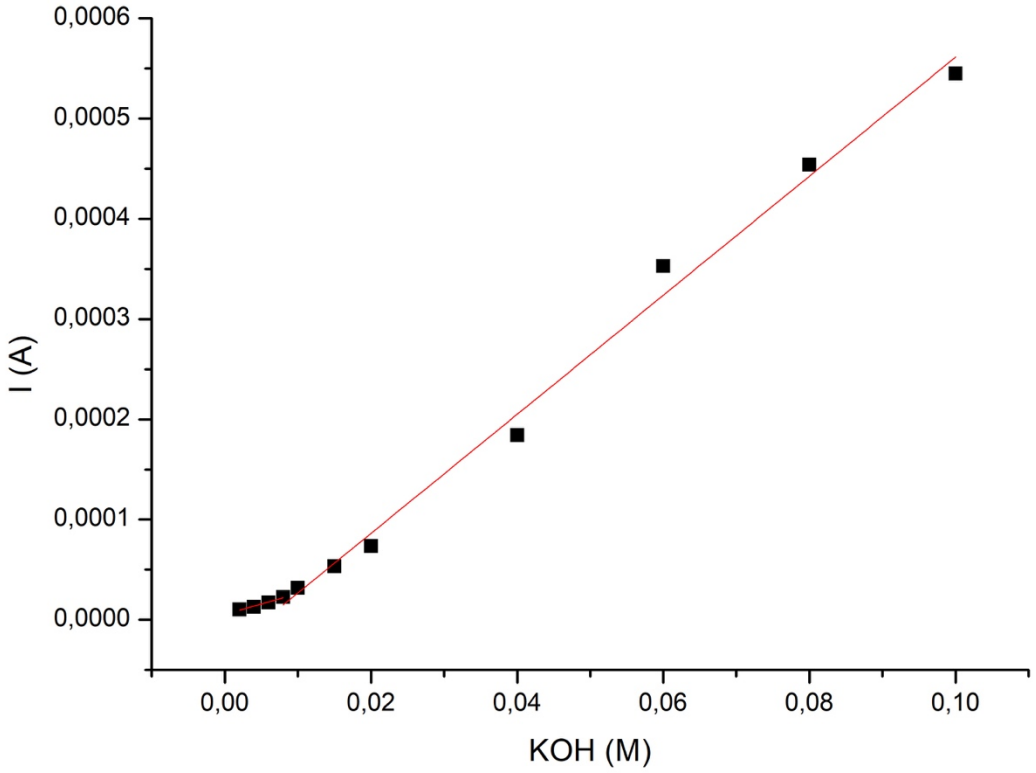
0,0006
0,0005
0,0004
0,0003
0,0002
0,0001
0,0000
I (A)
0,00
0,02
0,04
0,06
0,08
0,10
KOH (M)

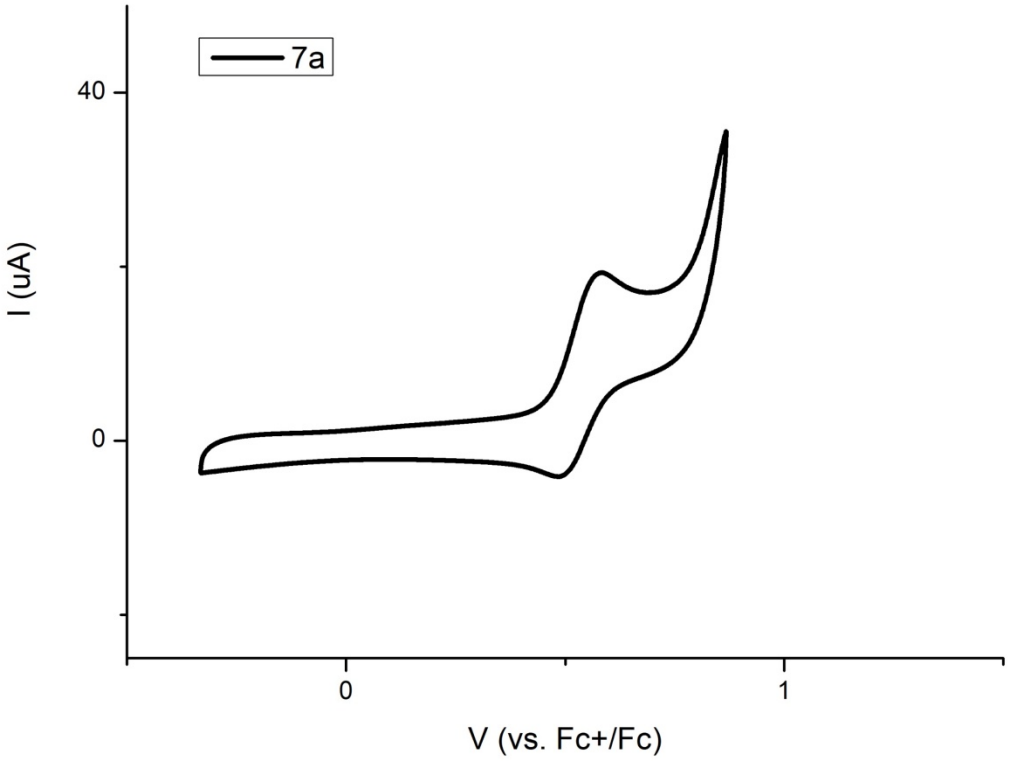
7a
40
0
I (uA)
0
1
V (vs. Fc+/Fc)

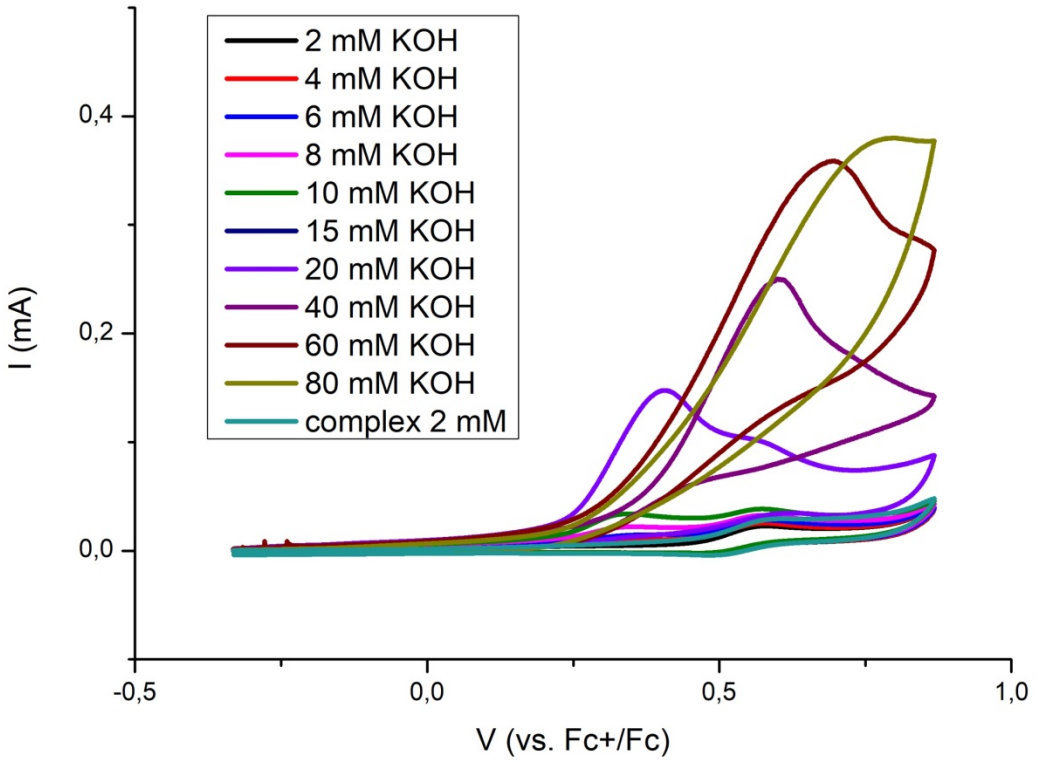
2 mM KOH
4 mM KOH
6 mM KOH
8 mM KOH
10 mM KOH
15 mM KOH
20 mM KOH
40 mM KOH
60 mM KOH
80 mM KOH
complex 2 mM
I (mA)
0,4
0,2
0,0
-0,5
0,0
0,5
1,0
V (vs. Fc+/Fc)

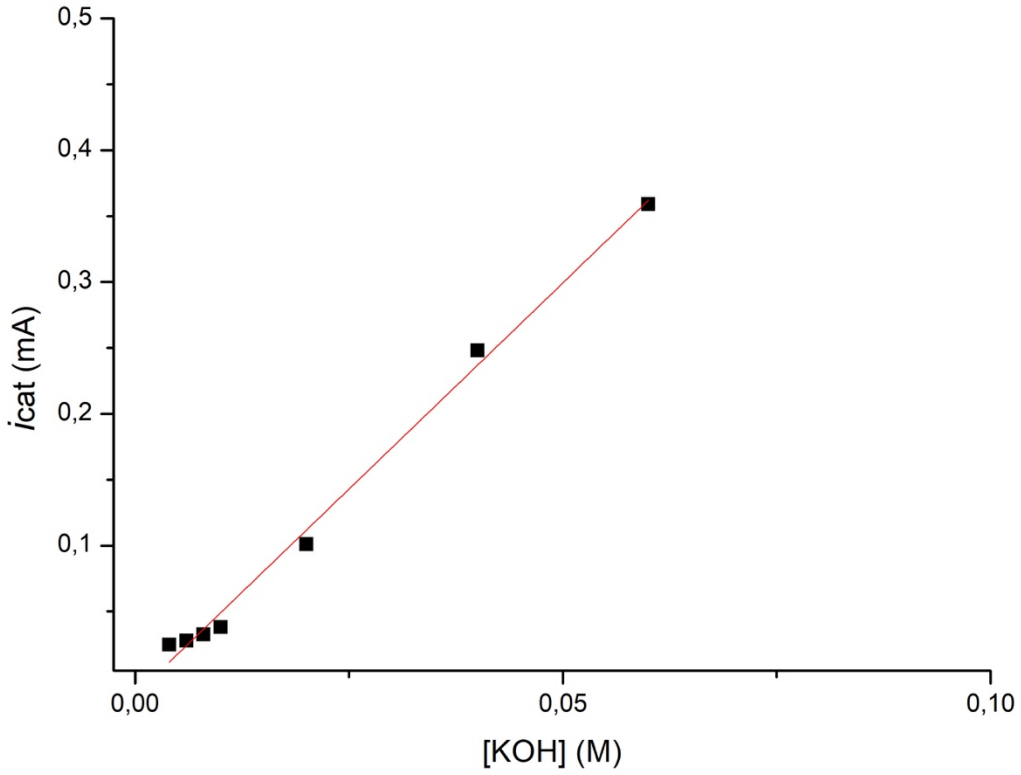
icat (mA)
0,5
0,4
0,3
0,2
0,1
0,00
0,05
0,10
[KOH] (M)

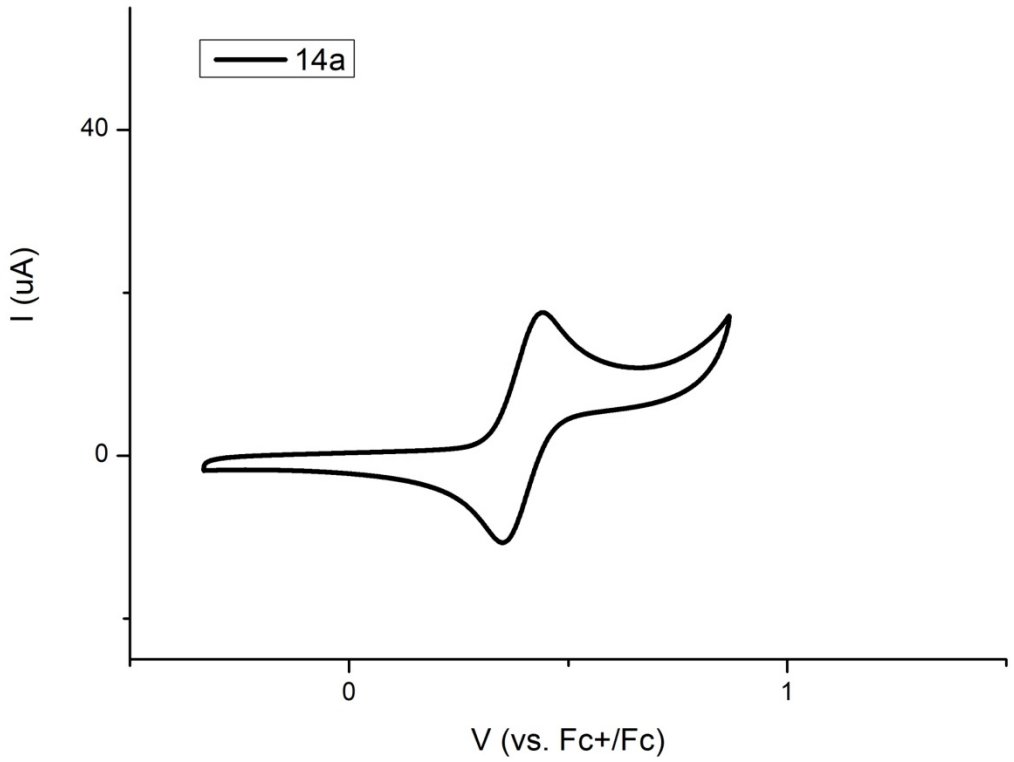
14a
40
0
I (uA)
0
1
V (vs. Fc+/Fc)

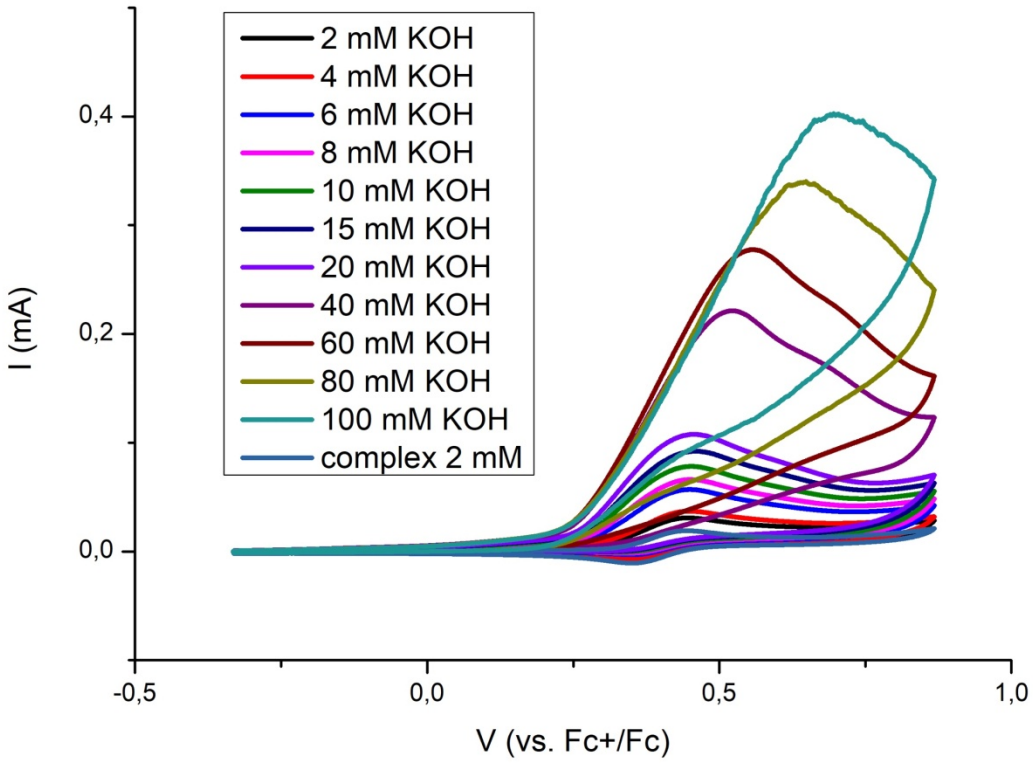
2 mM KOH
4 mM KOH
6 mM KOH
8 mM KOH
10 mM KOH
15 mM KOH
20 mM KOH
40 mM KOH
60 mM KOH
80 mM KOH
100 mM KOH
complex 2 mM
0,4
0,2
0,0
I (mA)
-0,5
0,0
0,5
1,0
V (vs. Fc+/Fc)

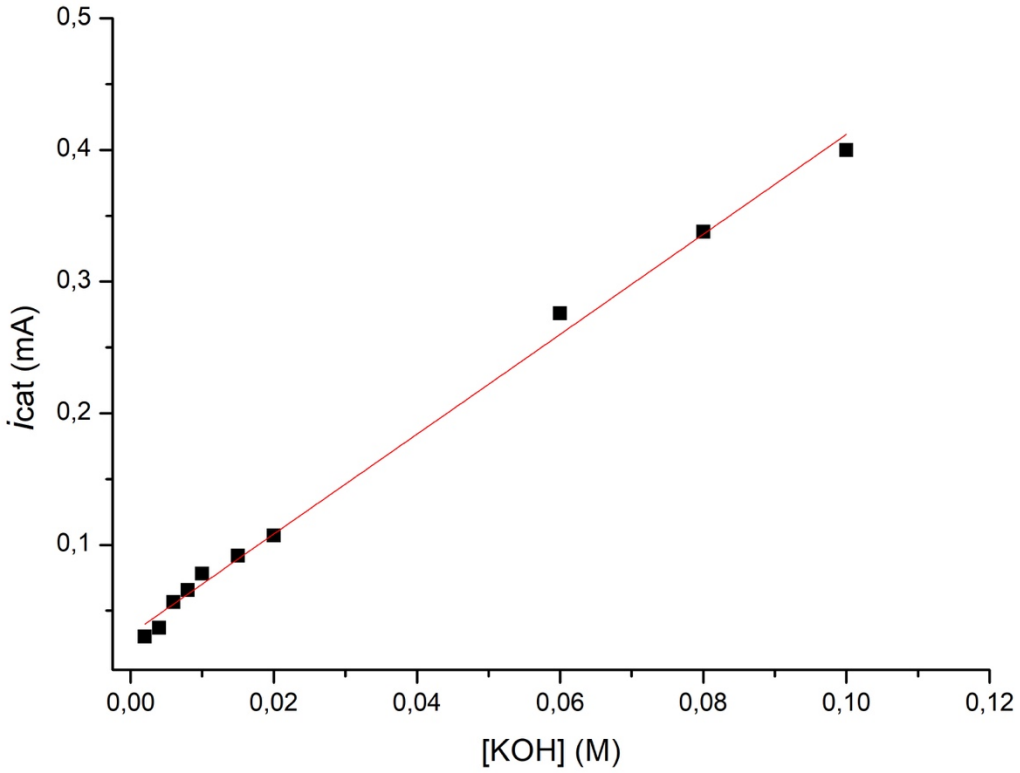
0,5
0,4
0,3
0,2
0,1
icat (mA)
0,00
0,02
0,04
0,06
0,08
0,10
0,12
[KOH] (M)

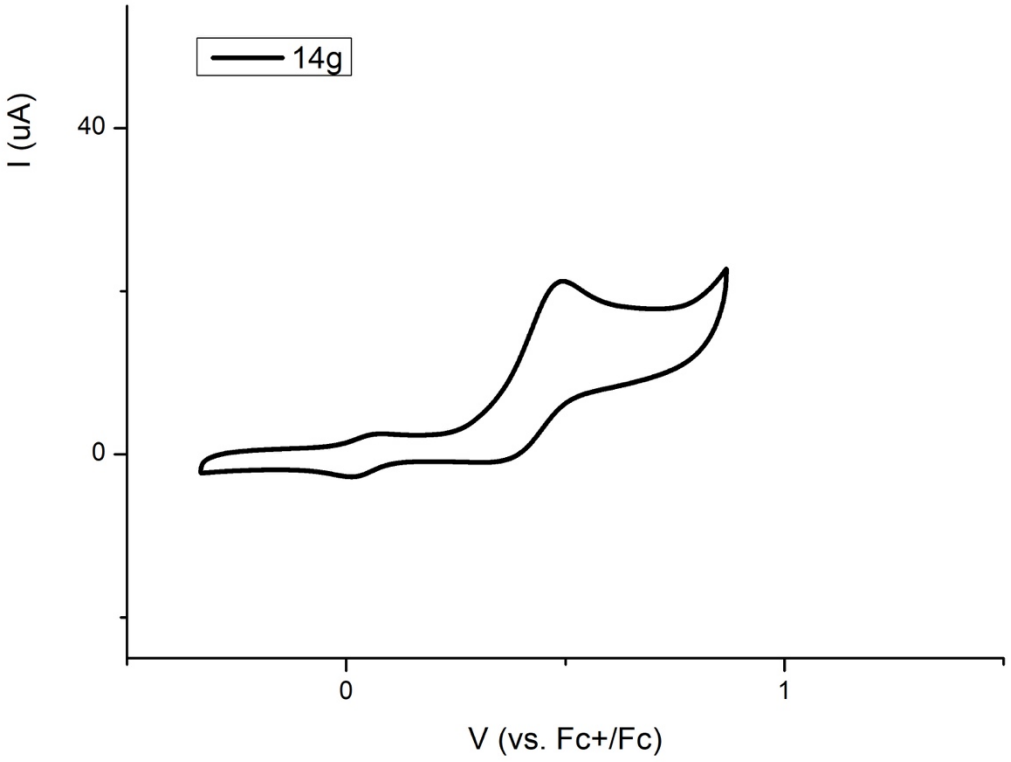
14g
40
0
I (uA)
0
1
V (vs. Fc+/Fc)

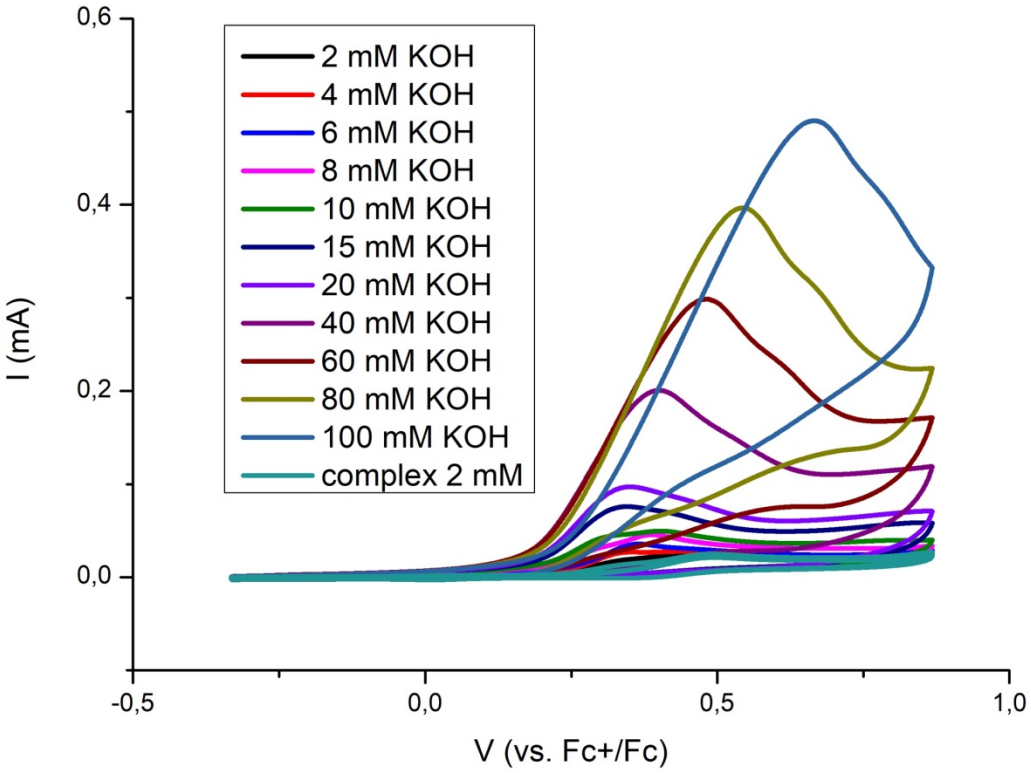
0,6
0,4
0,2
0,0
I (mA)
2 mM KOH
4 mM KOH
6 mM KOH
8 mM KOH
10 mM KOH
15 mM KOH
20 mM KOH
40 mM KOH
60 mM KOH
80 mM KOH
100 mM KOH
complex 2 mM
-0,5
0,0
0,5
1,0
V (vs. Fc+/Fc)

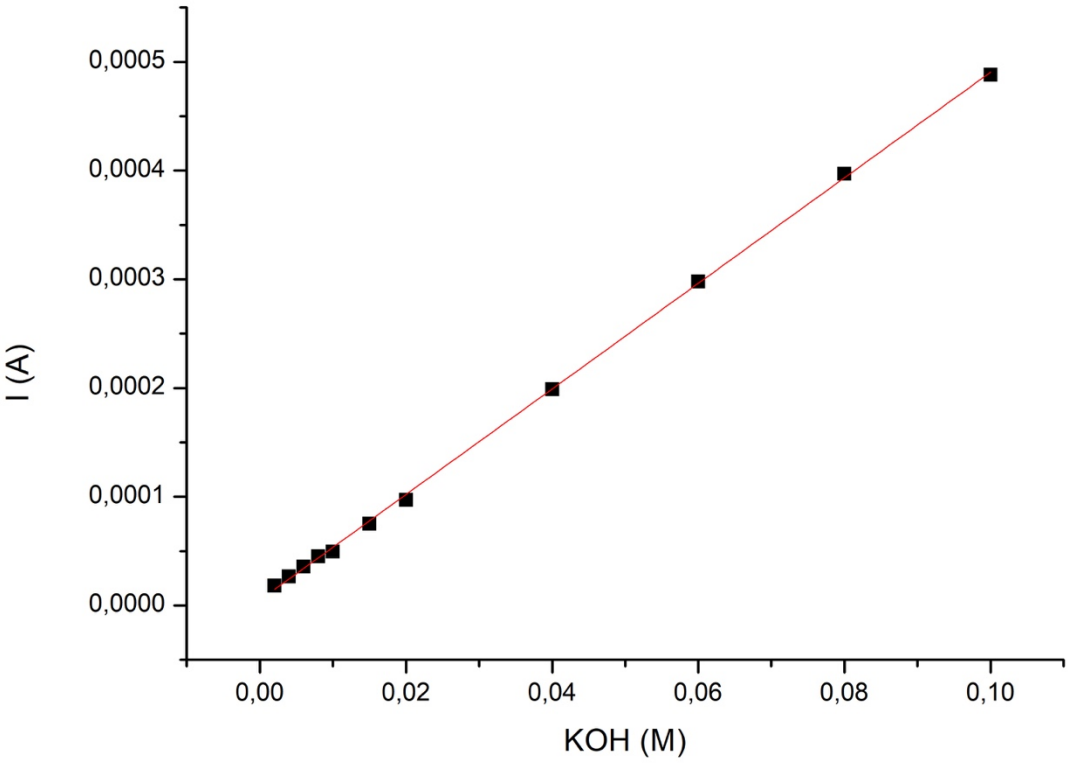
0,0005
0,0004
0,0003
0,0002
0,0001
0,0000
I (A)
0,00
0,02
0,04
0,06
0,08
0,10
KOH (M)

2.6 Notes and References

[1] A. J. Bard; M. A. Fox; *Acc. Chem. Res.*, **1995**, *28*, 141.

[2] T. J. Meyer; *Acc. Chem. Res.*, **1989**, *22*, 163.

[3] Hong, D.; Mandal, S.; Yamada, Y.; Lee, Y.-M.; Nam, W.; Llobet, A.; Fukuzumi, S.; *Inorg. Chem.*, **2013**, *52*, 9522.

[4] Y. Umena; K. Kawakami; J.-R. Shen; N. Kamiya; *Nature*, **2011**, *473*, 55.

[5] K. Kawakami; Y. Umena; N. Kamiya; J.-R. Shen; *J. Photochem. Photobiol. B: Biol.*, **2011,** *104*, 9.

[6] Fan, T.; Zhan, S.; Ahlquist, M. S. G.; *ACS Catal.*, **2016**, *6*, 8308.

[7] Hessels, J.; Detx, R. J.; Koper, M. T. M.; Reek, J. N. H.; *Chem. Eur. J.*, 10.1002/chem.201702850

[8] Cady, C. W.; Crabtree, R. H.; Brudvig, G. W.; *Coord. Chem. Rev.*, **2008**, *252*, 444.

[9] Blakemore, J. D.; Crabtree, R. H.; Brudvig, G. W.; *Chem. Rev.*, **2015**, *115*, 12974.

[10] Li, J.; Güttinger, R.; Moré, R.; Song, F.; Wan, W.; Patzke, G. R.; *Chem. Soc. Rev.*, **2017**, *46*, 6124.

[11] Hopkinson, M. N.; Richter, C.; Schedler, M.; Glorius, F.; *Nature*, **2014**, *510*, 485.

[12] B. L. Conley; M. K. Pennington-Boggio; E. Boz; T. J. Williams; *Chem. Rev.*, **2010**, *110*, 2294.

[13] A. Quintard; J. Rodriguez; *Angew. Chem. Int. Ed.*, **2014**, 53, 4044.

[14] H. Allen, O. Kennard, D. G. Watson, L. Brammer A. G. Orpen and R. Taylor, *J. Chem. Soc., Perkin Trans.*, 1987, **2**, S1-S19.

[15] V. V. K. M. Kandepi, J. M. S. Cardoso, E. Peris, and B. Royo, *Organometallics*, 2010, **29**, 2777.

[16] Z. Chen; J. J. Concepcion; X. Hu; W. Yang; P. H. Hoertz; T. J. Meyer; *PNAS*, **2010**, *107*, 7225.

[17] M. Okamura; M. Kondo; R. Kuga; Y. Kurashige; T. Yanai; S. Hayami; V. K. K. Praneeth; M. Yoshida; K. Yoneda; S. Kawata; S. Masaoka; *Nature*, **2016**, *530*, 465.

[18] G. A.N. Felton; C. A. Mebi; B. J. Petro; A. K. Vannucci; D. H. Evans; R. S. Glass; D. L. Lichtenberger; *J. Organomet. Chem.*, **2009**, *694*, 2681.

[19] N. Song; J. J. Concepcion; R. A. Binstead; J. A. Rudd; A. K. Vanucci; C. J. Dares; M. K. Coggins; T. J. Meyer; *PNAS*, **2015**, *112*, 4935.

[20] a) A. M.Oertel, V.Ritleng, L.Burr, C.Harwig and M. J.Chetcuti, *Organometallics,* **2011**, *30*, 6685; b) L. B.Benac, E. M.Burgess, L.Burr and A. J.Arduengo, *Organic Syntheses, Coll.*, **1990**, ***7***, 195; **1986**, *64*, 92.

[21] L. M. Bushnell, E. R. Evitt, and R. G. Bergman, *J. Organomet. Chem.*, **1978**, *157*, 445.

[22] S. Moulin; H. Dentel; A. Pagnoux-Ozheelyeva; S. Gaillard; A. Poater; L. Cavallo; J.-F. Lohier; J.-L. Renaud; *Chem. Eur. J.*, **2013**, *19*, 17881.

Beyond dithiolate paradigm in [FeFe] hydrogenase models: diiron complexes bearing hydrocarbyl ligands and mechanistic insight into the electrocatalytic H_2 production by $[Fe_2(CN)\{\mu\text{-}CN(Me)_2\}(\mu\text{-}CO)(CO)(Cp)_2]$.

5.1 Abstract

The role of cyanide ligand (CN^-) in the active electrocatalyst $[Fe_2(CN)\{\mu\text{-}CN(Me)_2\}(\mu\text{-}CO)(CO)(Cp)_2]$ (**13**) has been investigated. Replacement of CN^- with different sigma donor ligands (e.g benzylisocyanide, PPh_3 and N_3^-) showed no catalytic activity in hydrogen evolution from acetic acid. CVs (cyclic voltammograms) of the above compounds demonstrated an EC mechanism, implying a first reduction followed by protonation of diiron complexes with lack of hydrogen evolution.

DFT calculations have been used to investigate viable mechanisms of hydrogen evolution reaction (HER) electrocatalyzed by (**13**) in acetic acid. Molecular details underlying the proposed ECEC electrochemical sequence have been studied and the key functionalities of CN^- and amino-carbyne ligands have been elucidated. After the first reduction, CN^- works as a relay for the first proton from acetic acid to the carbyne, with such ligand serving as the main electron acceptor for both reduction steps. After the second reduction, a second protonation occurs at CN^- that forms a Fe(CNH) moiety, i.e., the acidic source for the H_2 generation. The role of cyanide has been supported by IR experiments, confirming that after a first reduction of **13**, the proton is not localized on the cyanide ligand. The hydride (formally $2e/H^+$), necessary for the heterocoupling with H^+ is thus provided by the $\mu\text{-}CN(Me)_2$ ligand and not by Fe centres, as occurring in typical $L_6Fe_2S_2$ derivatives modelling the hydrogenase active site.

5.2 Introduction

As discussed in the main introduction and in the previous chapter III, large-scale use of hydrogen as an alternative clean energy vector is an attractive but challenging issue in many aspects (e.g., production from renewable sources and storage).[1] One major issue for the development of both H_2 generation from water splitting and fuel cells is the

replacement of platinum (and other noble metals) with catalysts based on abundant and sustainable metals.[2] Natural hydrogenases, which are recognized as the most efficient catalysts for the conversion of protons and electrons into hydrogen, and the reverse reaction[3] have inspired a multitude of works aimed at the design and synthesis of structural and functional models.[4]

Due to their similarities with [FeFe]-hydrogenase active site **I** (Scheme 1), diiron dithiolato carbonyls **II** (Scheme 1) have been subject of intense research activities in the last decade which strongly contributed to better understand structural and mechanistic aspects of [FeFe]-H_2ases.[5,6] The cores of these diiron units, although rarely matching that of the enzyme subsite, are usually designed to mimic the natural systems, in that they contain dithiolate ligands, carbon monoxide, and cyanide. Based on the reasonable assumption that diiron complexes resembling the active site of natural [FeFe]-H_2ases might act as effective electrocatalyst for H_2 production, a huge number of diiron mimics have been designed by modification of the bridgehead group or substitution of carbonyls and cyanides, with other ligands.[7] Extension of the research field into a broader area involving diiron complexes not necessarily restricted to dithiolate mimics would potentially provide more chances to develop new and efficient catalysts. In other words, going beyond the "dithiolate paradigm", but still taking advantage of possible cooperative effects associated to the presence of two adjacent Fe atoms, could provide access to electrocatalytic H_2 production based on a mechanism not so strictly related to those of [FeFe]-H_2ases.

Based on this idea, we have recently investigated a number of diiron organometallic complexes containing cyclopentadienyls (η^5-C_5H_5, Cp), bridging and/or terminal CO, and bridging hydrocarbyl ligands such as: alkynyl, alkenyl, allyl, allenyl, vinyliminium **III,** and vinylalkylidene **IV** (Scheme 1) as potential electrocatalysts for H_2 production.[8] The presence of Cp ligands may produce effects comparable, at least in terms of electron donor ability, to those of other ligands (e.g. phosphines, isocyanides carbenes) generally used to replace CO in dithiolate mimics.[9] The most relevant change is the replacement of bridging dithiolate or aza-dithiolate ligands with bridging hydrocarbyl ligands, in that aza-dithiolate ligands are recognized to have a major role in H_2ases,[10] as well as in model systems.[11]

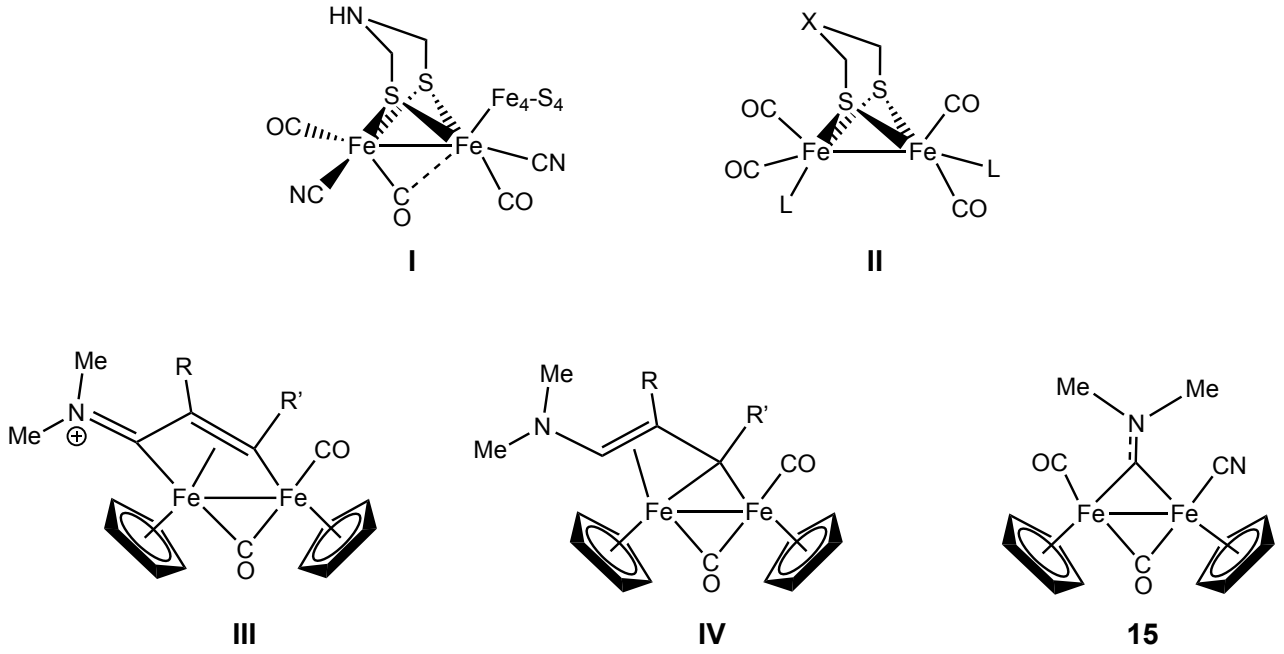

Scheme 1. [Fe,Fe]-H_2ase ***I*** occurring in nature, the synthetic diiron models **II** and new type and diiron complexes recently synthesized by Zanotti et al.

We found that in a limited number of cases, diiron complexes, namely those containing a bridging carbyne, (e.g. complex **15**) can act as electrocatalyst for H_2 generation affording results comparable to those of many common dithiolate systems. It was not clear why these, unlike other diiron hydrocarbyl complexes were effective in providing a catalytic pathway to proton reduction. In particular, it was surprising that complexes with most structured bridging ligands, incorporating π-extended systems and heteroatoms, such as vinyliminium **III** and vinylalkylidenes **IV**, in principle better candidates to mimic the behaviour of bridging azadithiolate, were ineffective as catalysts. Indeed, based on chemical and electrochemical evidence, we came to the conclusion that these bridging ligands were detrimental to catalysis in that reduction and protonation events occurred at the ligand, in place of the metal, therefore inhibiting a fundamental step in the sequence required to generate H_2. Our preliminary screening work also evidenced that only carbyne complexes containing a CN^- ligand gave significant catalytic activity. A reasonable but general explanation is that only a specific combination of ligands can provide a favourable electron density at the Fe-Fe core to favour metal protonation without shifting the reduction potentials to very negative values, which is disadvantageous.

In this chapter replacement of cyanide with isocyanide(**16**), phosphine(**17**) and azide(**18**) ligands, followed by screening of electrocatalytic behaviour have been carried

out in order to address the unique features of the cyanide group. DFT has been then used to shed some light on the H_2 evolution reactivity (HER) of **15**, through the characterization of possible reaction mechanisms associated with H_2 production at a molecular level. Data and description presented in this chapter are the result of a collaboration with the group of Prof. Giuseppe Zampella from the Department of Biotecnology and Biosciences at University of Milano-Bicocca.

5.3 Results and Discussion

Diiron complexes **16**, **17** and **18** with hydrocarbyl ligands have been investigated by cyclic voltammetry, which is the usual way to demonstrate electrocatalytic ability for hydrogen evolution.[12] Complex **17**[13] and **18**[14] have been obtained according to reported procedure, whilst synthesis of **16** is described in the Experimental Section. Cyclic voltammograms (CVs) of the studied complexes in CH_3CN have been recorded in the presence of increasing amounts of acetic acid (HOAc). Catalytic activity in hydrogen evolution is normally evidenced by the appearance of an irreversible wave that grows with increasing acid concentrations, whereas the position of the peak can be used to evaluate the overpotential.

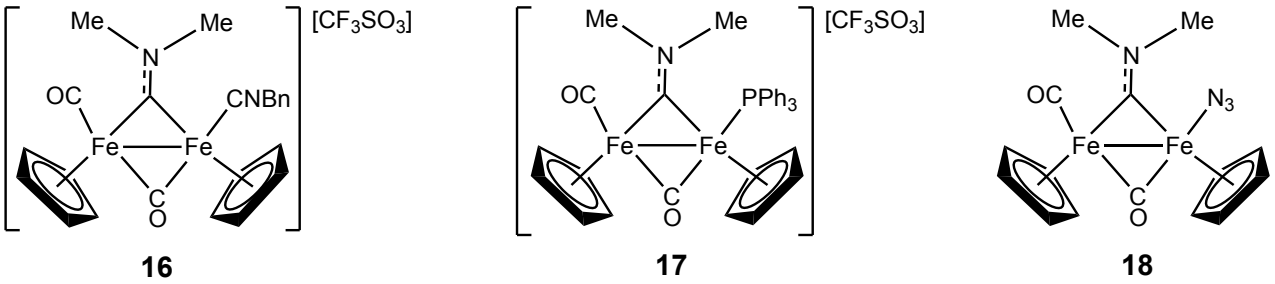

Scheme 2. Diiron complexes evaluated as electrocatalysts for proton reduction. Bn, benzyl. Ph, phenyl, N_3, azide.

5.3.1 Cyclic voltammograms of μ–alkylidyne complexes.

The aminoalkylidyne complexes selected for this work (Scheme 2) contain different ligands and substituents, which are expected to influence the redox and catalytic behaviour of the diiron complexes. The presence of the azide anionic ligand, likewise the cyanide, produces a neutral complex. The azide and isocyanide ligands have been selected in that they are close to cyanide as proton acceptor ability, indeed both can be protonated. On the contrary, coordinated phosphine lacks a protonation site, hence the bridging aminoalkylidyne is the best candidate to undergo protonation in this instance.

Furthermore, differences in electron donating and accepting ability of these ligands, might provide a favourable electron density on the Fe-Fe core.

The CV (Figure 1A) of complex **16** displays one irreversible redox process in the anodic region with formal potentials of +0.60 V. On the cathodic side complex **16** shows one reversible process at -1.71 V and an irreversible one at -2.46 V.

Electrocatalytic properties were studied recording CVs in the presence of increasing amounts of acetic acid (HOAc) (Figure 1B) in the cathodic region of the potential. No catalytic effect is observed at the peak current, and hydrogen evolution occurs at the same potentials recorded for the blank signal. The absence of catalytic activity for H_2 evolution, in spite of the reversible electron reduction at a relatively accessible potential, is probably a consequence of the fact that reduction and protonation events take place at the isonitrile ligand, which has not the same behaviour of cyanide ligand. In order to better understand this behaviour, we performed a controlled-potential electrolysis of **16** solution (2mM) in CH_3CN, which turned from yellow to dark brown, at 1-80 V (see Experimental Section).

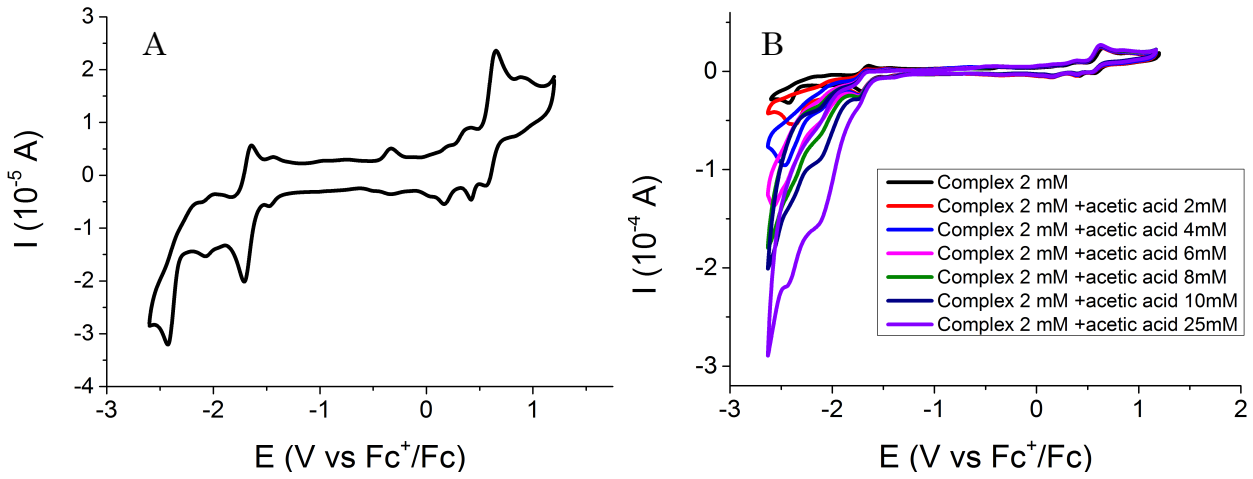

Figure 1. CVs recorded in a 2mM solution (in CH_3CN) of complex **16** in the absence (A) and in the presence (B) of acetic acid at different concentrations.

IR spectrum (Figure 2) of this solution showed a new broad signal at 2015 cm^{-1} and the disappearance of the μ–CO at 1815 cm^{-1}. After addition of 1 equivalent of glacial acetic acid under stirring, solution turned back to yellow and IR revealed a narrow signal at 2021 cm^{-1}. Disappearance of the μ–CO, and appearance of a new terminal-CO absorption suggest a shift of the CO from bridging to terminal. This, in turn, should be

associated to the protonation of the isocyanide ligand and change of its coordination from terminal to bridging.

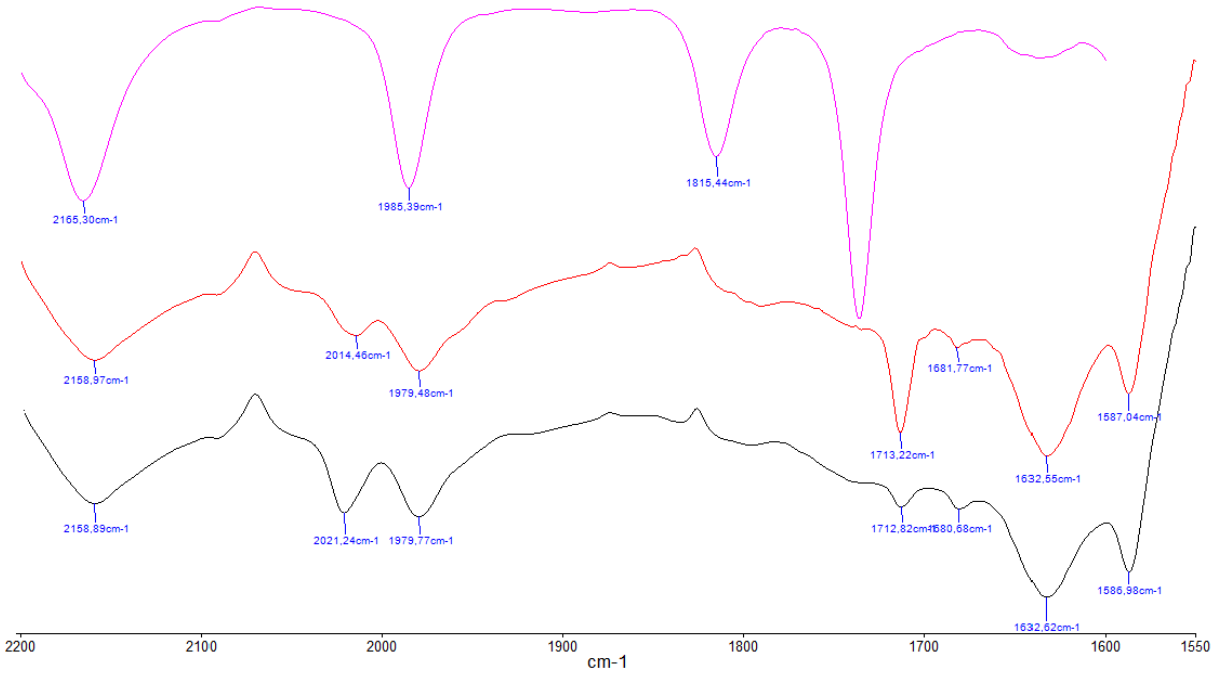

Figure 2. IR spectrum in solution (in CH_3CN) of complex **16** (violet), after controlled-potential electrolysis (red) and after acid addition (black). Value on x axis are in cm^{-1}.

The CV (Figure 3A) of complex **17** displays two irreversible redox processes in the anodic region with formal potentials of +0.45 and +0.77 V. On the cathodic side complex **17** shows four reversible processes at about -1.63, -1.72, -2.36 and -2.68 V.

Electrocatalytic properties of **17** were studied recording CVs in the presence of increasing amounts of acetic acid (HOAc) (Figure 3B) in the cathodic region of the potential. No catalytic effect is observed at the peak current, and hydrogen evolution occurs at the same potentials recorded for the blank signal. The redox processes at -1.63 and -1.72 V turned irreversible after acid addition, suggesting an EC mechanism in which an electrochemical reaction is followed by a chemical reaction. In this case protonation of carbyne might occur upon one electron reduction, without any catalytic activity.

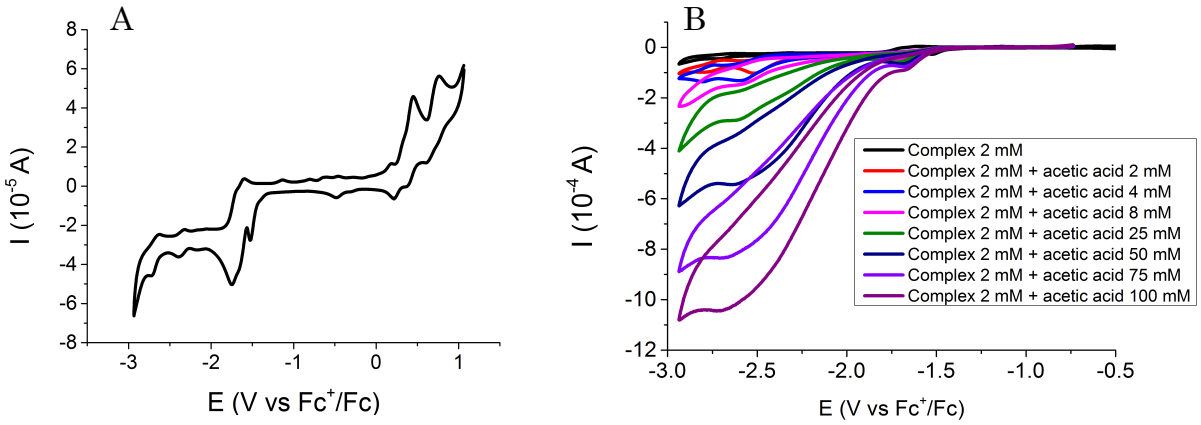

Figure 3. CVs recorded in a 2mM solution (in CH_3CN) of complex **17** in the absence (A) and in the presence (B) of acetic acid at different concentrations.

On the anodic side complex **18** (Figure 4A) shows one reversible redox process with formal potentials of -0.24 V. On the cathodic side CVs displays one reversible process at -1.63 V, probably involving two electrons.

Electrocatalytic properties were studied recording CVs in the presence of increasing amounts of acetic acid (HOAc) (Figure 4B) in the cathodic region of the potential. No catalytic effect is observed at the peak current, and hydrogen evolution occurs at the same potential recorded for the blank signal. The two electron redox process at -1.63 V turned irreversible after acid addition, suggesting, as for **17**, an EC mechanism involving a protonation at carbyne without any HER. Addition of a strong acid, such as triflic acid, CVs (Figure 4C) showed a shift of the anodic couple to a more anodic potential, likely involving a protonation of diiron complex at the azide ligand.

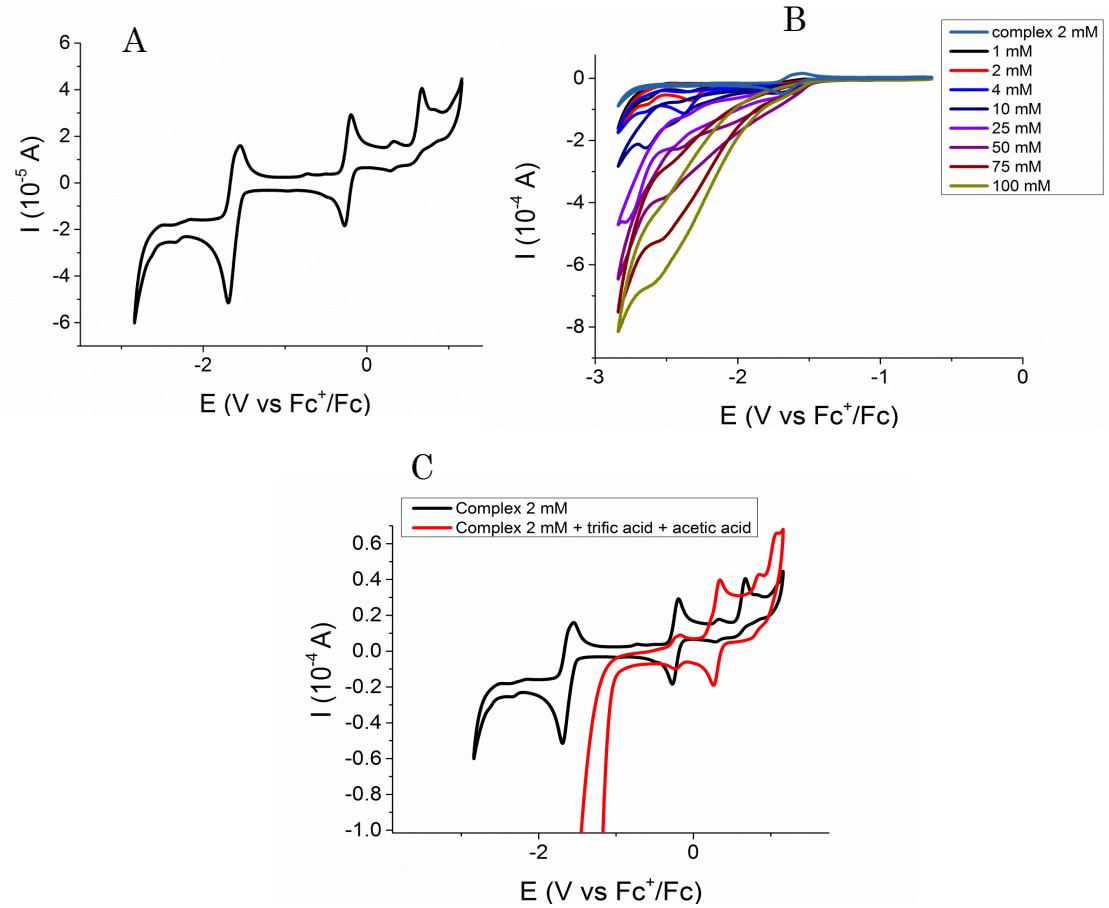

Figure 4. CVs recorded in a 2mM solution (in CH_3CN) of complex **18** in the absence (A), in the presence (B) of acetic acid at different concentrations and in the presence (C) of triflic acid.

5.3.2 Mechanistic dissection of the ECEC electrochemistry of HER.

DFT has been used in order to better understand the peculiar H_2 evolution reactivity of **15** bearing a cyanide ligand. Herein a summary of the overall mechanism is reported. The lowest energy pathway associated with the formation of the doubly-reduced/doubly-protonated **15HHa** is presented in Figure 5 (see Scheme 3 for pictures of compounds), and it can be summarized as follows: i) first one-electron reduction ii) first protonation, occurring at cyanide, iii) second one-electron reduction and migration of the proton from the cyanide to the aminocarbyne carbon atom. iv) second protonation, occurring at cyanide. After a second protonation **15HHa** has overall stored 2 electrons and 2 protons thus being activated for H_2 production. As **15HHa** does not feature a metal-hydride (that is normally the H^- source of the $H^- + H^+ \rightarrow H_2$ heterocoupling process) a transition state has been searched for along a reaction coordinate entailing the FeCN-H as H^+ donor and the μ-C(H)NMe_2 as H-to form dihydrogen. This would represent a case of HER electrocatalysis occurring by a ligand-based mechanism, which is compatible with

the absence of vacant coordination sites at the Fe_2 core. The activation barrier for the direct-intramolecular H-(carbene)/H+(CN) heterocoupling is high (37.8 kcal/mol; **TS(15HHa→15+H₂)**). However, including in the simulation an explicit acetic acid molecule working as proton shuttle, the activation energy is dramatically lowered (26.4 kcal/mol; **TS'(15HHa→15+H₂)**). Such value is in line with H_2 release near room temperature conditions. The assistance of acid molecules in proton migration processes has been recently reported in a study on $Fe_2\{\mu\text{-}CH_2(CH_2S)_2\}(CNR)_6$.[15] The optimized structure of the lowest energy TS for H_2 release (**TS'(15HHa → 15 +H₂)** is presented in Figure 6.

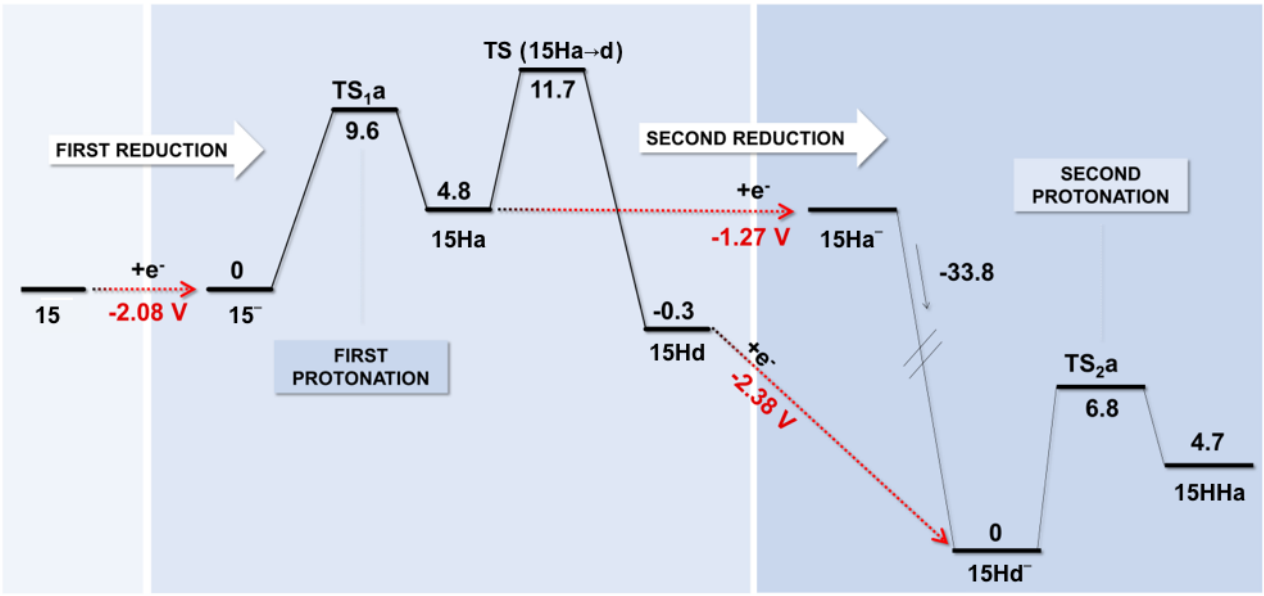

Figure 5. Summary of the lowest energy pathway associated with the formation of **15HHa**. Relative energies are in kcal/mol, reduction potentials in V.

The DFT mechanism herein proposed for HER emphasizes the general message that metal complexes have often the tendency to be first protonated at a site *which is not the metal itself,* but a weakly basic functional group in the metal coordination sphere, e.g. CN^- in **13**. In electron rich dithiolates such role is played by sulfur atoms, as demonstrated by Rauchfuss et al.[16] In most of biomimetic dithiolates, the accepted picture for HER entails a subsequent proton transfer occurring from the weak base to one metal center that forms either terminal or bridging metal-hydrides, prompted for H_2 formation, as evidenced by Gloaguen and Rauchfuss.[17] Remarkably, in the present

case study the proton shuttles from the cyanide to the aminocarbyne ligand rather than to Fe.

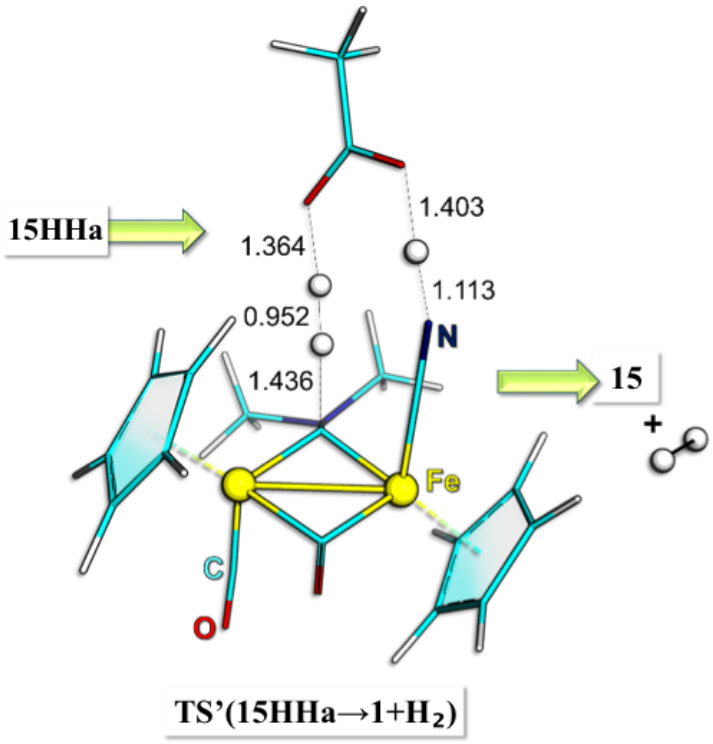

Figure 6. Representation of the H_2 release process from **15HHa**. Optimized structure of the involved transition state is also presented. Displayed distances are in Å.

The overall mechanism, summarized in Scheme 3, provides a picture compatible with a completely "ligand based" electrocatalysis, in which a clear non-innocent behaviour of ligands involves both redox and acid-base processes underlying HER. The ligand-based catalysis performed by **15** is in perfect agreement with its saturated valence 36e$^-$ $(Fe^I)_2$ core, thus working as a collecting point of reactants.[18] Nonetheless, besides providing a topological function of appropriately disposing the proximity of the reaction centers, Fe's take part in catalysis by tuning the ligand reactivity to favour HER. Actually, i) the Fe ions moderately drain electron density from cyanide (thus favouring proton trafficking between ligands, vide infra) and ii) help to localize the carbyne LUMO onto C, that is the exact catalytic site of reduction (vide infra).

Overall, the ligand-based reactivity of transition metal compounds is very well-documented in literature as well as the modifications brought about by ligand coordination to metal centers.[18]

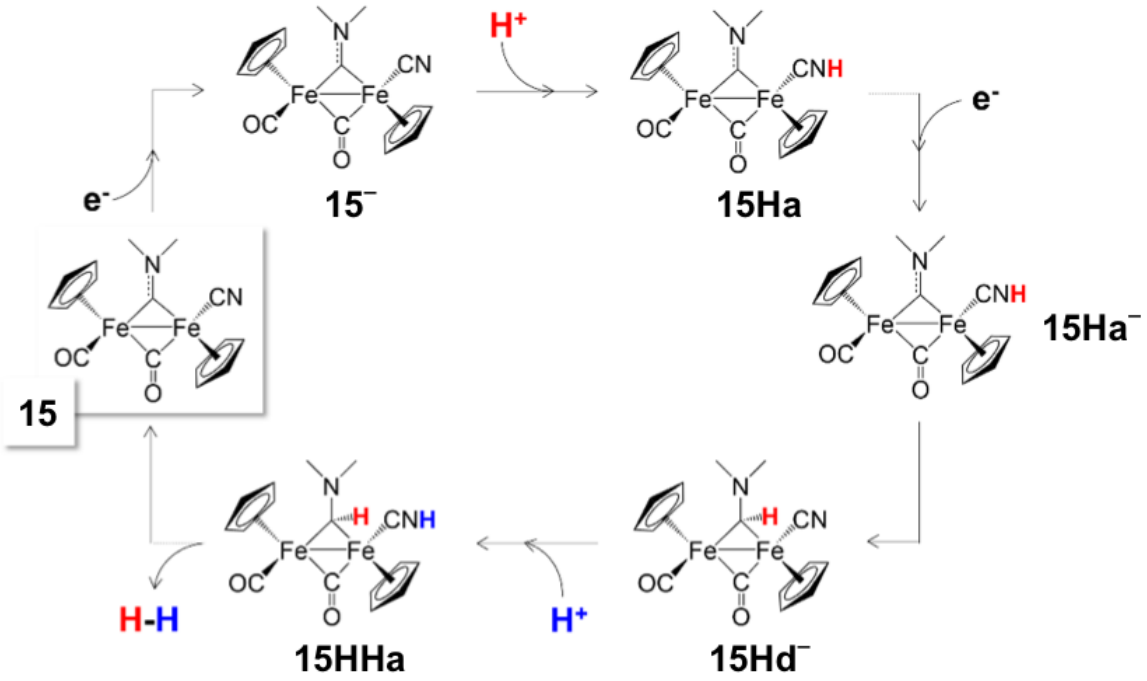

Scheme 3. Energetically viable pathway for proton reduction mediated by **15**.

According to DFT, H_2 is released directly from **15HHa**, with the "catalytic assistance" of an acid molecule as proton-shuttle (Figure 6). H_2 is thus generated through the combination of the acidic FeCN-H and of the carbenic-H. The fundamental role of these two ligands is detailed in the following.

5.3.3 The role of cyanide.

The DFT dissection of the catalytic mechanism presented above suggests that the activity of **15** is strictly related to the presence of a cyanide in the Fe coordination sphere. Indeed, on the one hand, the CN^- ligand provides a kinetically accessible protonation site, thus favoring a crucial step of catalytic HER. On the other hand, CN^- is not thermodynamically so basic to prevent H^+ from being subsequently conveyed to carbyne. This characteristic allows a facile proton migration during catalysis, that can be crucial for hydride formation. The proton-relay exerted by CN^- is interesting since it is unusual in typical diiron clusters modelling [Fe-Fe]-H_2ases, although even two cyanides are present in the enzyme cofactor. Indeed, in the Fe_2 core of the H-cluster, the role of proton relay from the outer environment to metal is not played by coordinated CN^- ions (anchored to the protein matrix through non-covalent interactions), but by the central nitrogen of the azadithiolate linker.

In the case of **15**, (without dithiolate coordinating the Fe_2 core), the CN^- presence is still a fundamental factor to observe HER, although through a chemistry that is probably completely different from all other H_2ase mimics. CN^- in **15** does not increase electron density at the Fe-Fe core, as demonstrated by the inspection of atomic partial charges. That is also consistent with the proposed "ligand based" electrocatalytic mechanism entailing no protonation of metal centers, an observation already supported by the saturated coordination sphere of Fe's in the complex. CN^- in **15** serves as a kinetically accessible basic site for H^+ that is sufficiently weak (in thermodynamic sense) to be able to subsequently release H^+ to carbyne. In this context, the metal plays a role by moderately withdrawing electron density from CN^- that, otherwise, would be too basic [NBO partial charges: [C(-0.3)-N(-0.7)] vs [Fe-C(-0.1)-N(-0.2)]. The simultaneous presence of both CN^- and carbyne ligands turns out to be thus essential because the proton affinity of the former is properly balanced to allow the proton release to the latter.

After the second reduction of the ECEC scheme, CN^- can be easily protonated and plays its second, crucial role in the entire catalytic cycle. In fact, it is directly involved in the H_2 formation process, acting as proton source in the $H^+ + H^- \rightarrow H_2$ process (through the transient assistance of an acetic acid molecule). All that makes **15** suited for HER catalysis.

The subtle role played by CN in the electrocatalyis of HER mediated by **15** is demonstrated by the experimental observation that replacing CN^- by another negatively charged ligand (N_3^-, complex **18)** completely abolished HER detection.

Indeed, the DFT investigation on the azido-Fe specie shows that the HN_3 is readily expelled by the Fe_2 scaffold (activation barrier associated with Fe-(HN_3) bond breaking is 2.0 kcal/mol, data not shown). Thus the inactivity of this species is fully justified and the double role played by CN further confirmed.

5.3.4 IR insight on cyanide.

In order to support the role of cyanide in **15**, two separate experiments were performed in solution and followed by IR spectroscopy: a strong acid (triflic acid) was first added to a solution of **15** and then to a solution of **15** previously reduced by means of controlled-potential electrolysis (as described for complex **16** in section 5.3.1).

The first experiment was performed in CH_2Cl_2 under nitrogen atmosphere. Triflic acid was added to a solution of **15** and then checked by IR (Figure 7). IR (Table 1) showed a broadening and a shift to lower frequency of the CN^- ligand, likely due to a protonation to CNH. Moreover, a shift to higher frequency of all CO signals (both terminal and bridged) occurred as a result of depletion of electron density from the iron core, confirming protonation of the iron dimer.

Table 1. IR frequencies of **13** before and after triflic acid addition.

Functional group	Before acid addition (cm^{-1})	After acid addition (cm^{-1})
CO	1980	1996
μ-CO	1804	1824
μ-CN	1579	1584
CN	2091	2049

In the second test, we performed a controlled-potential electrolysis of a solution 2mM (in CH_3CN) of **15**, followed by acid addition. The IR (Figure 7) revealed no evidence of CN protonation, since its frequency did not change. The right-side of recorded spectrum was noisy due to the presence of acid.

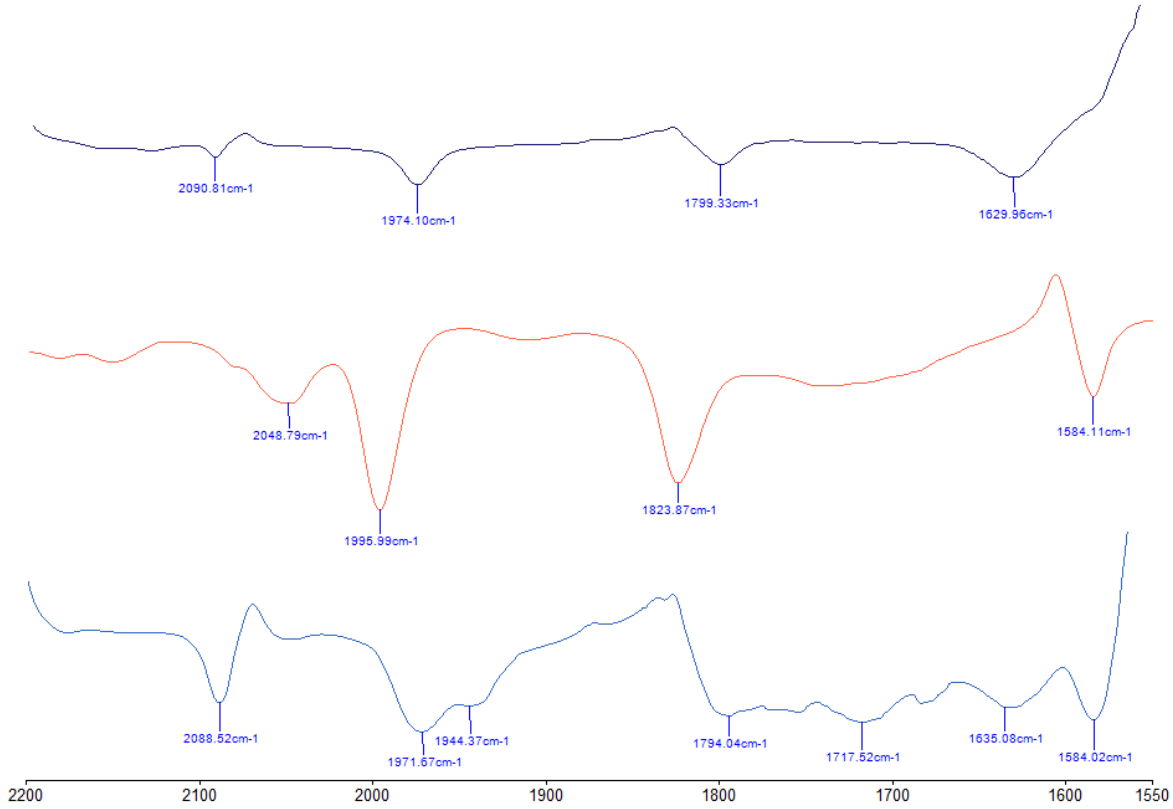

Figure 7. IR spectrum in solution (in CH_3CN) of complex **15** (dark, top), after acid addition (red) and after controlled-potential electrolysis followed by acid addition (blue, bottom). Value on x axis are in cm^{-1}.

Therefore, upon acid addition the cyanide ligand undergoes easily protonation. If the acid addition is preceded by reduction, there is no evidence of cyanide protonation by IR, confirming the mechanism well described by DFT calculation on **15**.

5.3.5 The role of carbyne.

The relative stability between the isomer featuring a protonated cyanide and the isomer with protonated carbyne is completely inverted upon double reduction.

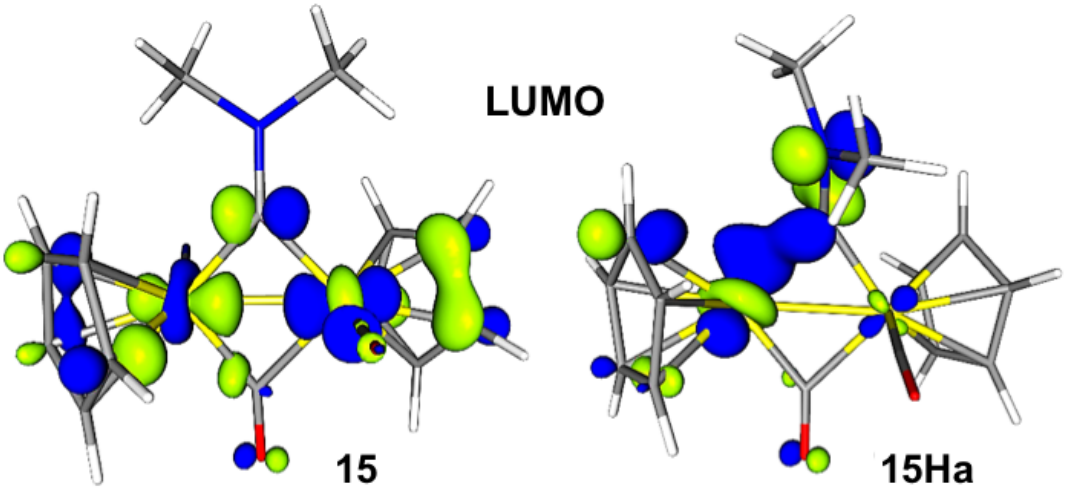

Figure 8. LUMO shapes of most stable isomers of **15** and **15Ha**.

The increasing stability of isomers with protonated carbyne upon reduction is due to a significant increase in the electron density on such ligand. Indeed, when considering the two reductive steps involved in catalysis **15**→**15**$^{-}$ and **15Ha** → **15Ha**$^{-}$, the variation of NBO charge at the carbyne ligand (Δq NBO: **15**→**15**$^{-}$ -0.17, **15Ha** → **15Ha**$^{-}$-0.20) is two-fold that at the cyanide (Δq NBO: **15**→**15**$^{-}$ -0.09, **15Ha** → **15Ha**$^{-}$-0.10), while the charge on metal centers (Δq NBO: **15**→**15**$^{-}$ -0.06/0.06, **15Ha** → **15Ha**$^{-}$-0.02/0.01) is almost the same independently from the redox state of the system. In addition, the LUMO (Figure 8) of **15** has a significant component of the carbyne C atom, through one of its *p* orbitals. The distribution of the LUMO (Figure 8) on the carbyne ligand becomes even more evident upon first protonation/reduction, in **15Ha**. As a result, going from **15** to **15Ha**$^{-}$ the carbyne ligand stores electron density and one proton to form a carbene with tetrahedral geometry and one C-H bond. The HER-type activity of this bond, (i.e., the hetero-coupling with H^{+}), however, is not dramatically high, as suggested by the activation barrier (26.4 kcal/mol) associated with the H_2 release.

5.4 Conclusions

Different diiron complexes bearing hydrocarbyl, CO and Cp ligands have been synthesized and investigated as electrocatalysts for H_2 production in order to better understand the peculiar reactivity of complex **15** bearing a CN ligand. Replacement of CN^- with different sigma donor ligands in all complexes taken into consideration did not display any hydrogen evolution reactivity (HER), but showed an EC mechanism likely involving a protonation of complexes without catalytic activity. These findings revealed that only a proper combination of ligands provide a favourable equilibrium of electron density on the diiron complexes, which do not feature dithiolate ligands.

DFT calculations on **15** suggest a ligand-based mechanism, in which μ-carbyne and terminal-CN ligands provide all acid-base and redox requisites necessary for the heterocoupling of hydrides and protons. The ligand-based mechanism found by DFT in the present investigation is fully consistent with the HER activity of **15** in spite of the saturated coordination environment of its metal centers.

A suggestion emerging from the present study to develop better performing variants of **15** concerns the design of a more efficient heterocoupling of hydride and proton. Synthetic modelling efforts should be put with the aim of achieving a closer H^-/H^+ spacing that could allow to get rid of the acid dependence. In fact, an intramolecular (or direct) proton shuttling process away from CN^- to H^- is expected to occur faster and more efficiently compared to an intermolecular (or mediated) one. Also, the incorporation of a highly versatile ligand such as carbyne in the Fe_2 scaffold, affords the opportunity to further explore the effects related to the switch between ligand-based and metal-based processes. In this context, the ability to control both the redox and protonation chemistry of HER represents a clear advantage in the design of more active and efficient catalyst.

In conclusion and to the best of our knowledge **15** represents the first example of electrocatalytically HER-competent catalysts that at the same time is: i) based on a non-precious dimetallic core (Fe_2), ii) dithiolate-free, iii) working with no (even transient) formation of Metal -H intermediates.

5.5 Experimental Section

General Data. All reactions were routinely carried out under a nitrogen atmosphere, using standard Schlenk techniques. Chromatography separations were carried out on columns of deactivated alumina (4% w/w water). Glassware was ovendried before use. Solvents: dichloromethane (CH_2Cl_2), tetrahydrofuran (THF), diethyl ether (Et_2O), petroleum ether referring to a fraction of bp 60-80 °C, acetonitrile (CH_3CN) were dried and distilled prior to use. Acetone has been degassed and stored under inert atmosphere on molecular sieves. Other solvents such as $CDCl_3$, D_2O, CD_3CN (Sigma Aldrich) have been employed without further purification. $Fe_2[\mu\text{-}CN(Me)_2](\mu\text{-}CO)(CO)(NCCH_3)(Cp)_2][CF_3SO_3]$ was synthesized according to reported procedures.[19]
The prepared derivatives were characterized by spectroscopic methods. The NMR spectra were recorded using Varian Inova 300 (^1H, 300.1; ^{13}C, 75.5 MHz), Varian Mercury Plus VX 400 (^1H, 399.9; ^{13}C, 100.6 MHz), Varian Inova 600 (^1H, 599.7; ^{13}C, 150.8 MHz) spectrometers at 298 K; chemical shifts were referenced internally to residual solvent peaks. Infrared spectra were recorded at 298 K on a Perkin-Elmer Spectrum 2000 FT-IR spectrophotometer. ESI-MS spectra were recorded on Waters Micromass ZQ 4000 with samples dissolved in MeOH or CH_3CN. Elemental analyses were performed on a Thermo-Quest Flash 1112 Series EA instrument.

Synthesis of $Fe_2[\mu\text{-}CN(Me)_2](\mu\text{-}CO)(CO)(CNBn)(Cp)_2][CF_3SO_3]$(16). In a dried 100 mL Schlenk, $Fe_2[\mu\text{-}CN(Me)_2](\mu\text{-}CO)(CO)(NCCH_3)(Cp)_2][CF_3SO_3]$ (0.040 g, 0.096 mmol) was dissolved in THF (15 mL). Benzylisocyanide (11.7 microL, 0.096 mmol) was added to the reaction mixture and left under reflux for 3 hours. Solvent was removed in vacuo. The solid was re-dissolved in dichloromethane (6 mL) and chromatographed through Al_2O_3. The final product was obtained using THF as eluent. Solvent was removed to leave a red solid. Yield: 91 %
14 has been analyzed by IR, ^1H-NMR, ^{13}C-NMR, ESI-MS. ^1H-NMR (400 MHz, $CDCl_3$) δ(ppm): 7.36 -7.08 (m, 5H, CH_{aryl}), 5.12 (s, 5H, Cp), 5.05 (s, 5H, Cp), 4.56 (br, 2H, CH_2), 4.15-4.08 (s, 6H, NCH_3). ^{13}C-NMR (150.8 MHz, $CDCl_3$) δ(ppm): 332.37 (μ-CN), 261.46 (μ-CO), 210.24 (CO), 157.23 (CN), 132.42-127.03 (CH_{aryl}), 88.73 (Cp), 88.45 (Cp), 54.04 (NCH_3), 53.78 (NCH_3), 49.11 (CH_2). IR (CH_3CN): (ν_{CN}) 2165, (ν_{CO}) 1985, ($\nu\mu\text{-}_{CO}$)1815 cm-

[1]. ESI-MS (m/z): 471[M]$^+$, 149 [OTf]$^-$. Anal. Calcd (%) for $C_{44}H_{43}N_3O_7Fe$: C, 67.61; H, 5.54. Found: C, 63.95; H, 5.06.

Synthesis of $Fe_2[\mu\text{-}CN(Me)_2](\mu\text{-}CO)(CO)(PPh_3)(Cp)_2][CF_3SO_3]$(17)[13]. In a dried 100 mL Schlenk, $Fe_2[\mu\text{-}CN(Me)_2](\mu\text{-}CO)(CO)(NCCH_3)(Cp)_2][CF_3SO_3]$ (0.147 g, 0.232 mmol) was dissolved in THF (15 mL). PPh_3 (0.42 mmol) was added to the reaction mixture and left under reflux for 3 hours. Solvent was removed in vacuo. The solid was re-dissolved in dichloromethane (6 mL) and chromatographed through Al_2O_3. The final product was obtained as a brown fraction using MeOH as eluent. Yield: 80 %

15 has been analyzed by IR, ^{1}H-NMR, ^{13}C-NMR. ^{1}H-NMR (400 MHz, $CDCl_3$) δ(ppm): 7.34 -7.21 (m, 15H, CH_{aryl}), 5.12 (s, 5H, Cp), 4.99 (s, 5H, Cp), 4.29 (br, 6H, NCH_3). ^{13}C-NMR (150.8 MHz, $CDCl_3$) δ(ppm): 328.50 (μ-CN), 267.32 (μ-CO), 210.65 (CO), 134.07 (ipso-Ph, $^1J_{PC}$=42.0 Hz), 133.32, 130.96, 128.84 (CH_{aryl}), 90.64, 89.19 (Cp), 56.40, 52.09 (NCH_3). IR (CH_2Cl_2): (ν_{CO}) 1986, ($\nu\mu\text{-}_{CO}$)1793 cm^{-1}.

Synthesis of $Fe_2[\mu\text{-}CN(Me)_2](\mu\text{-}CO)(CO)(N_3)(Cp)_2][CF_3SO_3]$(18)[14]. In a dried 100 mL Schlenk, $Fe_2[\mu\text{-}CN(Me)_2](\mu\text{-}CO)(CO)(NCCH_3)(Cp)_2][CF_3SO_3]$ (0.23 mmol) was dissolved in THF (15 mL). Chlorine azide ClN_3 (0.50 g, 7.69 mmol) was added to the reaction mixture and left under reflux for 3 hours. Solvent was removed in vacuo. The solid was re-dissolved in dichloromethane (6 mL) and chromatographed through Al_2O_3. The final product was obtained using THF as eluent. Yield: 65 %

16 has been analyzed by IR, ^{1}H-NMR, ^{13}C-NMR. ^{1}H-NMR (400 MHz, $CDCl_3$) δ(ppm): 4.74, 4.63 (s, 10H, Cp), 4.66, 4.24 (s, 6H, $N(CH)_3$). ^{13}C-NMR (150.8 MHz, $CDCl_3$) δ(ppm): 89.10, 86.6 (Cp), 52.80, 51.60 (NCH_3). IR (CH_2Cl_2): (ν_{N3}) 2033, (ν_{CO}) 1980, ($\nu\mu\text{-}_{CO}$)1800 cm^{-1}.

Electrochemical Studies. Cyclic voltammograms were recorded at a scan rate of 0.05 V s^{-1} on a BAS-100A electrochemical analyser using a three-electrode cell: a glassy-carbon disk (0.071 cm^2) as the working electrode, a $Ag/AgNO_3$ (0.1 M) reference electrode, and a platinum-wire counter electrode. All experiments were performed under a nitrogen atmosphere in CH_3CN containing 0.1 M $^nBu_4NPF_6$ at room temperature. Ferrocene (Fc) was the internal reference, and all potentials have been quoted relative to the Fc/Fc^+ couple set at 0.00 V. Glacial acetic acid was added in molar

equivalent increments via microsyringe. All of the CVs have been recorded starting from the open circuit potential. Bulk electrolysis was carried in a three-electrode cell with stirring at the appropriate potential, to reduce complex **15** and **16** (2 mM) during the first cathodic process using a rectangular GC electrode with a geometric area of 4.9 cm^2 and was stopped when the recorded current decreased to 5% of the initial value.

Computational details. DFT calculations have been carried out using Turbomole 7.1.1 suite of programs.[20] The GGA BP86-RI functional[21] has been used in conjunction with the split-valence polarized basis TZVP[22] on all atoms, thus explicitly considering also the core electrons of Fe. This computational scheme turned out to reliably model several features related to di-iron hydrogenase mimics.[23]

BP86 has also been reported to outperform the more popular B3LYP[24] in the theoretical reproduction of the redox potentials of Fe_2 complexes modelling hydrogenase, which is a crucial aspect when studying electrocatalytic behaviour of these compounds.[25] Results herein confirm the previously reported data (vide infra).

Nonetheless, the selected theory level has been herein further validated by comparing simulated structural parameters vs available XRD geometries and also theoretical vs experimental reduction potentials. Moreover, with the aim of corroborating the information emerging from our computations, the energy profiles associated with HER have been recomputed also by means of other functionals such as the aforementioned B3LYP, and the meta-GGA M06[2632] has been used to test possible better performance in reproducing structural parameters.

The solvent has been modelled according to the COSMO approach, that considers the solvent as a dielectric continuum (with $\varepsilon = 37.5$; acetonitrile).[27]

Transition state structures have been searched through an analytical hessian (or pseudo-Newton Raphson) procedure entailing an initial pre-optimization of a guess of transition state, continued through an eigen-vector following step.[28] Atomic partial charges have been evaluated by Natural Bond Orbital (NBO) methods.[29]

The Fc/Fc^+ redox potential (-4.87 V; acetonitrile) has been used as reference to scale the absolute reduction potentials. Indeed, computation of reduction potentials is based on the free energy difference (in solution) between reduced and oxidized species: $\Delta G°_{solv} = G°(ox)_{solv} - G°(red)_{solv}$, through the equation: $\Delta G°_{solv} = -nFE°$, where n is the number of

electrons involved in the reduction and *F* is the Faraday constant (23.061 kcal mol^{-1} V^{-1}). In order to obtain free energy, the KS-SCF electronic energy (E_{solv}) has been corrected by enthalpy and entropy contributions at 298.15 K and 1 bar (BP86 scaling factor = 0.9914). In some cases, the use of ΔE_{solv}, provided a better match to exp data than $\Delta G°_{solv}$ and the reasons of such apparent anomaly have been recently discussed and clarified in a paper on DFT modelling of the redox behavior of [FeFe]-hydrogenase models.[30]

2.6 Notes and References

[1] See for example: (a) Nocera, D. G. *Acc. Chem. Res.*, **2012**, *45*, 767. (b) Armaroli, N.; Balzani, V. *Chem. Sus. Chem.,* **2011**, *4*, 21. (c) Cook, T. R.; Dogutan, D. K.; Reece, S. Y.; Surendranath, Y.; Teets, T. S.; Nocera, D. G. *Chem. Rev.*, **2010**, *110*, 6474. (d) Armstrong, F. A.; Fontecilla-Camps, J. C. *Science*, **2008**, *321*, 498. (e) Turner, J. A. *Science*, **2004**, *305*, 972−974. (f) Lubitz, W.; Tumas, W. *Chem. Rev.*, **2007**, *107*, 3900.

[2] (a) Bullock, R. M. Catalysis Without Precious Metals; *Wiley-VCH:Weinheim*, Germany, **2010**. (b) Gray, H. B. *Nat. Chem.*, **2009**, *1*, 7.

[3] (a) Lubitz, W.; Ogata, H.; Rüdiger, O.; Edward Reijerse, E. *Chem.Rev.*, **2014**, *114*, 4081. (b) Fontecilla-Camps, J. C.; Amara, P.; Cavazza, C.; Nicolet, Y.; Volbeda, A. *Nature*, **2009**, *460*, 814.

[4] For a recent review see: Simmons, T. R.; Berggren, G.; Bacchia, M.; Fontecave, M.; Artero, V. *Coord. Chem. Rev.,* **2014**, *127*, 270.

[5] Schilter, D.; Camara, J. M.; Huynh, M. T.; Hammes-Schiffer, S.; Rauchfuss, T. B. *Chem. Rev*. **2016**, *116*, 8693.

[6] Gloaguen, F. *Inorg. Chem*. **2016**, *55*, 390.

[7] See for example :(a) Li, Y.; Rauchfuss, T.B. *Chem. Rev.* **2016**, *116*, 7043. (b) Capon, J.F.; Gloaguen, F.; Pétillon, F.Y.; Schollhammer, P.; Talarmin, J. *Coord. Chem. Rev.* **2009**, *253*, 1476. (c) Mejia-Rodriguez, R.; Chong, D.S.; Reibenspies, J.H.; Soriaga, M.P.; Darensbourg, M.Y. *J. Am. Chem. Soc.* **2004**, *126(38)*, 12004. (d) Cheah, M.H.; Tard, C.; Borg, S.J.; Liu, X.; Ibrahim, S.K.; Pickett, C.J.; Best, S.P. *J. Am. Chem. Soc.* **2007**, *129(36)*, 11085. (e) Harb, M.K.; Apfel, U.P.; Kubel, J.; Gorls, H.; Felton, G.A.N.; Sakamoto, T.; Evans, D.H.; Glass, R.S.; Lichtenberger, D.L.; El-Khateeb, M.; Weigand, W. *Organometallics* **2009**, *28(23)*, 6666.

[8] Mazzoni, R.; Gabiccini, A.; Cesari, C.; Zanotti, V.; Gualandi, I. Tonelli, D. *Organometallics* **2015**, *34*, 3228.

[9] Yang, D.; Li, Y.; Wang, B.; Zhao, X.; Su, L.; Chen, S.; Tong, P.; Luo,Y.; Qu, J. *Inorg. Chem*. **2015**, *54*, 10243.

[10] (a) Nicolet, Y.; de Lacey, A.L.; Vernede, X.; Fernandez, V.M.; Hatchikian, E.C.; Fontecilla-Camps, J.C. *J. Am. Chem. Soc.* **2001**, *123*, 1596. (b) Berggren, G.; Adamska,

A.; Lambertz, C.; Simmons, T.R.; Esselborn, J.; Atta, M.; Gambarelli, S.; Mouesca, J.M.; Reijerse, E.; Lubitz, W.; Happe, T.; Artero, V.; Fontecave, M. *Nature* **2013**, *499*, 66.

[11] See for example: (a) Tard, C.; Pickett, C.J. *Chem. Rev.* **2009**, *109*, 2245. (b) Wang, N.; Wang, M.; Liu, J.; Jin, K.; Chen, L.; Sun, L. *Inorg. Chem.*, **2009**, *48* (24), 11551. (c) Ezzaher, S.; Capon, J.F.; Gloaguen, F.; Petillon, F.Y.; Schollhammer, P.; Talarmin, J.; Kervarec, N. *Inorg. Chem.*, **2009**, *48*, 2. (d) Wang, Y.W.; Li, Z.M.; Zeng, X.H.; Wang, X.F.; Zhan, C.X.; Liu, Y.Q.; Zeng, X.R.; Luo, Q.Y.; Liu, X.M. *New J. Chem.* **2009**, *33*, 1780. (e) Olsen, M.T.; Rauchfuss, T.B.; Wilson, S.R. *J. Am. Chem. Soc.* **2010**, *132*, 17733. (f) Tschierlei, S.; Ott, S.; Lomoth, R. *Energy Environ. Sci.* **2011**, *4*, 2340. (g) Zheng, D.H.; Wang, N.; Wang, M.; Ding, S.D.; Ma, C.B.; Darensbourg, M.Y.; Hall, M.B.; Sun, L.C. *J. Am. Chem. Soc.* **2014**, *136*, 16817. (h) Arrigoni, F.; Mohamed Bouh, S.; De Gioia, L.; Elleouet, C.; Pétillon, F.Y.; Schollhammer, P.; Zampella, G. *Chem. Eur. J.* **2017**, *23*(18), 4364.

[12] Felton, G. A. N.; Mebi, C. A.; Petro, B. J.; Vannucci, A. K.; Evans, D. H.; Glass, R. S.; Lichtenberger, D. L. J. *Organomet. Chem.*, **2009**, *694*, 2681.

[13] Albano, V. G.; Busetto, L; Marchetti, F.; Monari, M.; Zacchini, S; Zanotti, V.; *Z. Naturforsch*, **2007**, *62b*, 427.

[14] Busetto, L; Marchetti, F; Zacchini, S.; Zanotti, V; *Inorg. Chim. Acta*, **2005**, *258*, 1204.

[15] Zhou, X.; Barton, B.E.; Chambers, G.M.; Rauchfuss, T.B.; Arrigoni, F.; Zampella G. *Inorg. Chem.*, **2016**, *55* (*7*), 3401.

[16] Zaffaroni, R.; Rauchfuss, T. B.; Gray, D. L.; De Gioia, L.; Zampella, G. *J. Am. Chem. Soc.* **2012**, *134*, 19260.

[17] Gloaguen, F.; Lawrence, J.D.; Rauchfuss, T.B. *J. Am. Chem. Soc.* **2001**, *123*, 9476.

[18] Wilkins, R.G. *Kinetics and Mechanism of Reactions of Transition Metal Complexes*, Ch. 6, 2nd thoroughly rev. ed., VCH Publishers, New York, **1991**.

[19] Albano, V. G.; Busetto, L.; Monari, M.; Zanotti, V. *Organomet. Chem.*, **2000**, *606*, 163.

[20] Ahlrichs, R.; Bar, M.; Haser, M.; Horn, H.; Kolmel, C. *Chem. Phys. Lett.* **1989**, *162*, 165.

[21] A) Becke, A. D. *Phys. Rev. A* **1988**, *38*, 3098-3100. B) Perdew, J. P. *Phys. Rev. B* **1986**, *33*, 8822.

[22] Schafer, A.; Huber, C.; Ahlrichs, R. *J. Chem. Phys.* **1994**, *100*, 5829.

[23] (a) Zampella, G.; Bruschi, M.; Fantucci, P.; Razavet, M.; Pickett, C. J.; De Gioia, L. *Chem. Eur. J.* **2005**, *11*, 509. (b) Tard, C.; Liu, X.; Ibrahim, S. K.; Bruschi, M.; De Gioia, L.; Davies, S. C.; Yang, X.; Wang, L.-S.; Sawers G.; Pickett, C. J. *Nature* **2005**, *433*, 610. (c) Boyke, C. A.; van der Vlugt, J. I.; Rauchfuss, T. B.; Wilson, S. R.; Zampella, G.; De Gioia, L. *J. Am. Chem. Soc.* **2005**, *127*, 11010. (d) Zampella, G.; Bruschi, M.; Fantucci, P.; De Gioia, L. *J. Am. Chem. Soc.* **2005**, *127(38)*, 13180. (e) Zampella, Giuseppe; Fantucci, Piercarlo; De Gioia, Luca *J. Am. Chem. Soc.* **2009**, *131(31)*, 10909. (f) Chouffai, D.; Zampella, G.; Capon, J-F.; De Gioia, L.; Le Goff, A.; Petillon, Francois Y.; Schollhammer, P.; Talarmin, J. *Organometallics* **2012**, *31(3)*, 1082.

[24] A) Ref. 22A. B) Lee, C., Yang, W., Parr, R.G., *Phys. Rev. B*, **1988**, *37*, 785-789. C) Becke, A.D., *J. Chem. Phys.*, **1993**, *98*, 5648.

[25] Roy, L.E.; Batista, E.R.; Hay, P.J. *Inorg. Chem.* **2008**, *47*(29), 9228.

[26] . Zhao, Y.; Truhlar, D. G. *Theor. Chem. Acc.*, **2008**, *120*, 215.

[27] A) Klamt, A. *J. Phys. Chem.* **1995**, *99*, 2224-2235. B) Klamt, A. *J. Phys. Chem.* **1996**, *100*, 3349.

[28] Jensen, F. *Introduction to Computational Chemistry*; John Wiley & Sons Ltd.-Baffins Lane: Chichester, England.

[29] . WIREs Comput Mol Sci **2012**, 2: 1–42 doi: 10.1002/wcms.51

[30] Filippi, G.; Arrigoni, F.; Bertini, L., De Gioia, L.; Zampella, G. *Inorg Chem.* **2015**, *54 (19)*, 9529.

NHC-iron complexes as redox mediators: immobilisation and glucose amperometric detection.

6.1 Abstract

This chapter reports on the synthesis of two new NHC-iron complexes **19-C11** and **19-C3** bearing an EDOT monomer in lateral chain. VMPP (Vetro Modificato PEDOT:PSS = Modified Glass PEDOT:PSS) electrodes have been coated with **19-Cx** and EDOT monomers in order to obtain a homogeneous film. The coated electrodes have been characterized by ATR-IR, showing successful copolymerisation, by cyclic voltammetry (CV), which is dominated by the reversible response of NHC-iron complexes, and by SEM-EDS, which provides the average copolymerisation ratio of 19-C_x/PEDOT (1/6 for **19-C11** and 1/7 for **19-C3**). A layer of the enzyme glucose oxidase (GOx) was applied over the film and the electrocatalytic performance of the devices was assessed by analysing glucose in phosphate buffer solution. Both sensors presented comparable activity, among which **19-C3** was the best with a linear range between 3 and 51 mM and a mean sensitivity of 7.5 μA M^{-1} cm^{-2}.

6.2 Introduction

Heterogenization, as stated in main introduction, is a good tool to exploit the high activity and specific properties of homogeneous complexes, and also exploit some advantages of heterogeneous catalysts (e.g. easy catalyst recovery). In this chapter, focus will be on design of a Chemically Modified Electrode (CME) bearing iron-NHC complexes described in Chapter 1. Data and description presented in this chapter are the result of a collaboration with the group of Prof. Erika Scavetta (Dr. Isacco Gualandi and Federica Mariani) from the Department of Industrial Chemistry "Toso Montanari". Chemically modified electrodes are widely employed in electroanalytical chemistry and an important goal is to strongly anchor redox mediators on the electrode surface (eg. covalent bonding). A redox mediator assists electron transfer between the electrode and a substrate or an active redox site, such as a redox enzyme. Ferrocene (Fc) and its derivatives are well known as electron mediators[1] due to their good electrochemical reversibility, regeneration at low potential, and generation of stable redox forms.

Ferrocenes can catalyse the oxidation or reduction of many small molecules, such as peroxides,[2] DNA,[3] glucose and AA (amino acids).[4] However, ferrocenes are generally insoluble in aqueous solutions and difficult to adsorb strongly on the electrode surface,[5] thus hindering a stable modified electrodes. To improve the attachment to the electrode surface, many immobilization methods, including cross-linking gels or polymers, have been developed.[6] In the last few years, poly(3,4-ethylenedioxythiophene) (PEDOT) has received great attention in the development of modified electrodes, due to its low-energy band gap[7] which makes it suitable for electro-optical applications. Moreover, the presence of ethylenedioxy substituents in the 3 and 4 positions of the polythiophenic ring makes it regiochemically better defined than the unsubstituted polythiophene. PEDOT can be prepared by several chemical or electrochemical routes, both in aqueous and organic media; electrochemical polymerization methods allow one to obtain PEDOT-coated electrodes by employing a small amount of monomer and short polymerization times.[8] The EDOT electropolymerization in aqueous media can be achieved using suitable water-soluble polyelectrolytes as emulsifiers. In particular, good results have been obtained when the polymerization is carried out in the presence of the polyelectrolyte poly(styrene-4-sulfonate) ($(PSS)^{n-}$). In this way, a film of PEDOT:PSS can be synthesized, in which the $(PSS)^{n-}$ polyanion is incorporated into the polymer to compensate for the positively charged PEDOT. The PEDOT:PSS system has been proven to produce films and micro-structured systems with facile electrochemistry, high-ionic conductivities, good electrochemical stability and a capacitance suitable for practical use in electrochemical supercapacitors.[9] Moreover, thanks to its good features, PEDOT:PSS has been recently employed for the fabrication of all-plastic electrochemical transistors (OECTs).[10] For these reasons, PEDOT:PSS has been chosen as a polymeric matrix to covalently bind ferrocene, in order to develop an amperometric sensor, which exploits the ferrocene redox mediator properties and the high conductivity of PEDOT:PSS. Within this field the same groups involved in this work have already described the synthesis and application of a ferrocene clicked PEDOT:PSS coated electrode employed in dopamine amperometric detection.[11] Indium tin oxide (ITO) electrodes have been coated with PEDOT:PSS that has been ferrocene-functionalized, by a two-step procedure consisting of the electrodeposition of PEDOT-N_3 followed by copper-catalysed azide–alkyne cycloaddition of ethynylferrocene. The coated electrodes

have been characterized by XPS, AFM, and cyclic voltammetry (CV). The electrocatalytic performance of the device has been assessed by analysing 3,4-dihydroxyphenyl ethylamine, also commonly known as dopamine (DA). The sensor presents a linear range between 0.01 and 0.9 mM, a mean sensitivity of 196 mA M^{-1} cm^{-2} and a limit of detection (LoD) of 1 mM.

With this background in mind, cyclopentadienone NHC-iron **10a** (described in Chapter 1) has been characterised by CV, which showed a reversible redox anodic couple located at potentials of +0.53 V and +0.63V (vs. SCE). Since the one-electron couple Fe(0)-Fe(I) closely resembles the one of ferrocene Fe(II)-Fe(III), a new procedure to anchor type-**10** iron complexes to a PEDOT:PSS film has been developed. The new procedure takes advantage of NHC ligand, which can be easily functionalised[12,13] on nitrogen atoms compared to the ferrocene and exploited as linker for immobilization of homogeneous complexes on solid supports.[14] VMMP (Vetro Modificato PEDOT:PSS = Modified Glass PEDOT:PSS) electrodes have been coated with PEDOT:PSS, that has been successively co-polymerised with two different iron-PEDOT monomers. Carbonyldiimidazolium has been exploited as coupling reagent between the NHC-iron complex and EDOT-OH. The coated electrodes have been characterised by XPS, SEM-EDS and cyclic voltammetry. Their performance has been assessed by analysing dopamine(DA) and glucose(Glu).

6.3 Results and Discussion

Two iron-EDOT monomers with a different chain-length linker have been synthesised in order to evaluate any influence in electrodeposition yield or in activity towards substrates. Herein, two distinctive synthesises are reported.

6.3.1 19-C_{11}

Complex **19-C_{11}** was synthesised in a multi-step route (Scheme 1): functionalization of the imidazolium salt by a coupling with an EDOT-OH monomer, followed by synthesis of the correspondent NHC-iron complex **19-C_{11}**.

New imidazolium salt **1g** was characterized by ^{1}H-NMR, ^{13}C-NMR and ESI-MS; the structure with eleven CH_2 groups as lateral chain was confirmed by single crystal X-Ray Diffraction (see Experimental Section). 1,1'-Carbonyldimidazolium (CDI) was exploited as coupling reagent between the –OH groups of **1g** and **EDOT-OH** in order to

get the corresponding imidazolium salt **EDOT-Im** bearing an EDOT on lateral chain. **19-C11** was then prepared following the reported general procedure in Chapter 1, consisting of a transmetallation reaction from a silver-NHC intermediate to the iron complex precursor $FeCpO(CO)_2(NCCH_3)$ **8** (described in chapter 1 paragraph 1.3.2) , employing the **EDOT-Im** as carbene precursor.

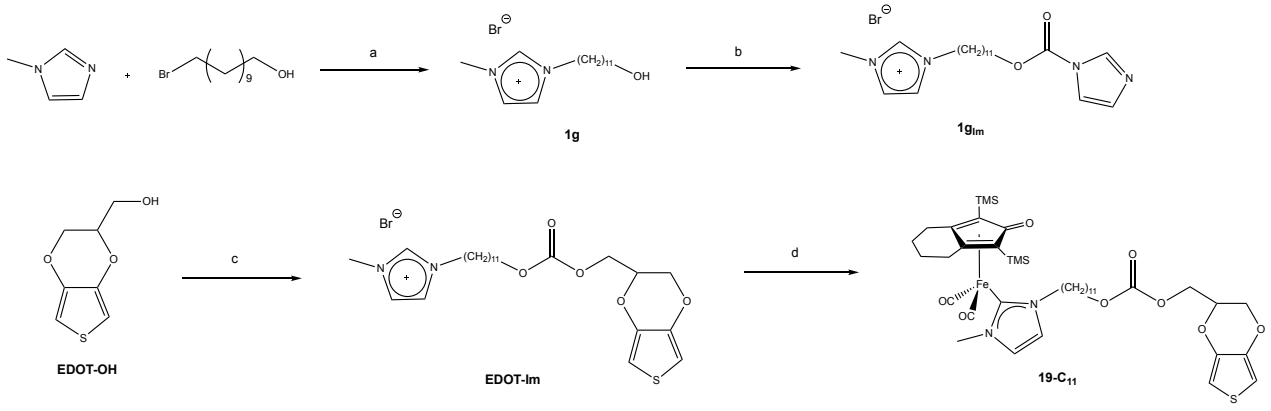

Scheme 1. a) neat, r.t., 6d, y=98%. b) 3 eq. CDI, CH_2Cl_2, r.t., 4h, y=98%. c) i) KO^{t}Bu, CH_3CN, reflux, 3h; ii) **1g$_{im}$**, CH_3CN, r.t, 19h, y=42%. d) i) **8**, 1.5eq. Me_3NO, 1.2eq. Ag_2O, CH_3CN, r.t.,1h; ii) toluene, reflux, 1h, y=50%.

The synthesis of **19-C11** has been followed by IR spectroscopy (Figure 1, top) observing a lowering in the CO stretching frequencies (**19-C11**: υ(CO) = 1982, 1921 cm^{-1} vs. **8 :** υ(CO) = 1999, 1938 cm^{-1}) due to the strong NHC σ-donor properties, and the presence of the C=O stretching of carbonyl group at 1747 cm^{-1} typical of a carbonate moiety. ^{1}H-NMR (Figure 1, bottom) shows signals assigned to CHs of imidazolium ring at 7.01 ppm, to CHs linked to S atom of EDOT at 6.35 ppm and to the alkyl chain at 1.25 ppm. ^{13}C-NMR shows the diagnostic signals for the Fe-$C_{carbene}$ at 184 ppm, the carbonate carbon at 155 ppm and the pattern from the iron skeleton and from the EDOT group (See Experimental for details). ESI-MS analysis confirmed the molecular weight of the compound allowing the identification of **19-C11** molecular ion at (m/z): 841 $[M+H]^+$, 863 $[M+Na]^+$, 525 $[M+K]^+$.

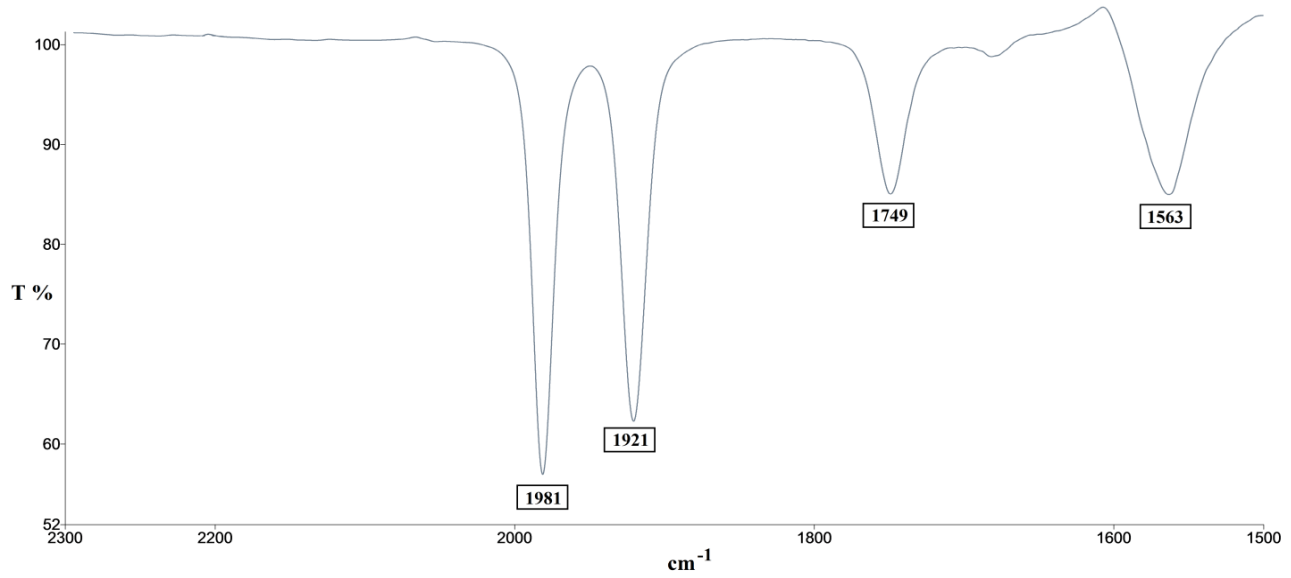

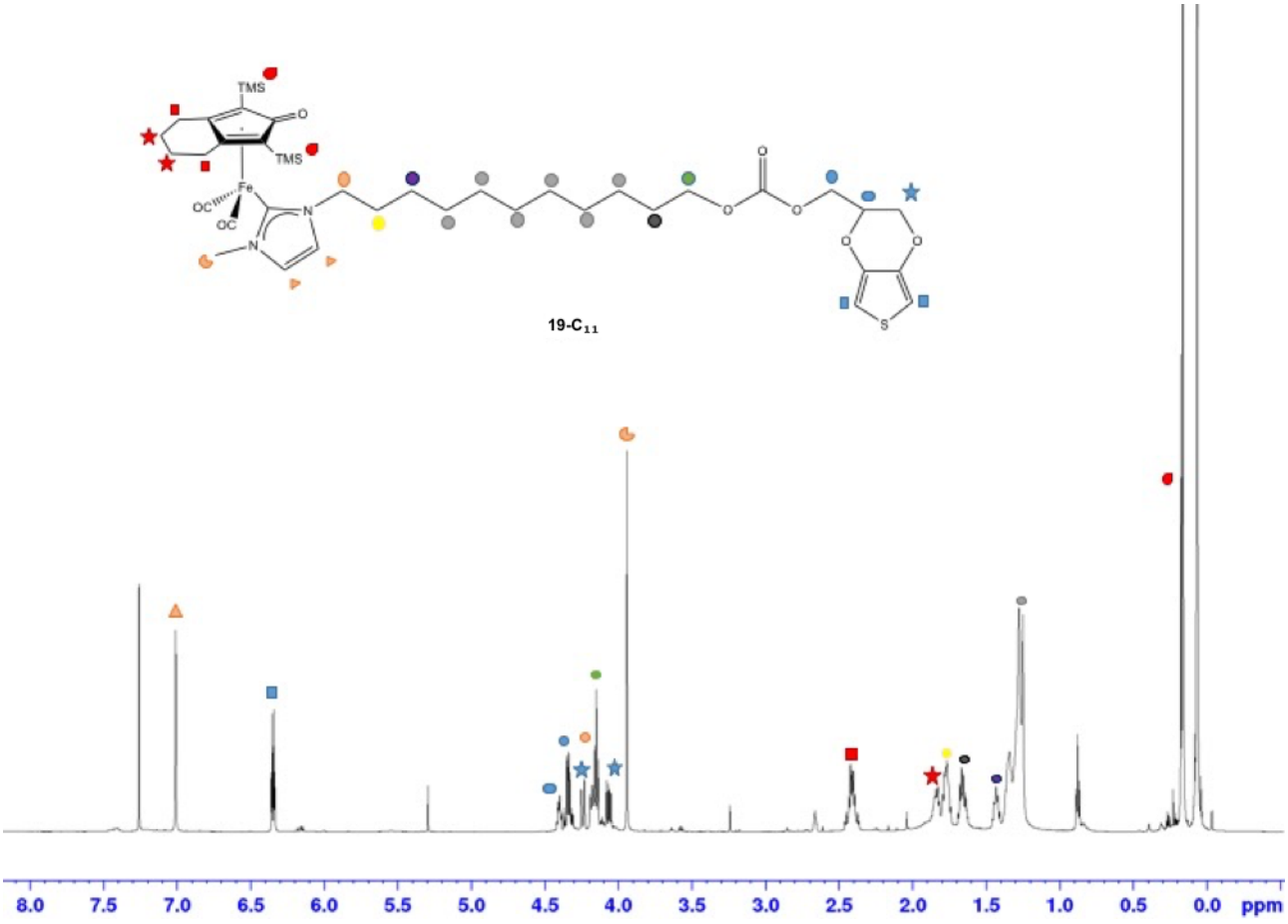

Figure 1. Top: IR spectrum in CH_2Cl_2. Bottom: ^{1}H-NMR of **19-C$_{11}$** in $CDCl_3$.

6.3.2 19-C$_3$

Compound bearing three CH_2 on lateral chain **19-C$_3$**, has been synthesised following a slightly different route (Scheme 2): transmetallation reaction of the NHC ligand from

the –OH functionalized silver intermediate to the iron precursor **8**, followed by functionalization of the carbene by coupling with EDOT-OH monomer. Iron complex **10i** was prepared following the same procedure described in chapter 1. The IR shows the typical set of CO stretching frequencies of carbene-iron complex of type **10**. ^{13}C-NMR shows the diagnostic signals for the Fe-$C_{carbene}$ at 183 ppm and ESI-MS confirmed the formation of the complex: (m/z) = 531 $[M+H]^+$. **10i** was then coupled to an EDOT-OH molecule exploiting CDI, as for the previous **19-C11**, leading to the EDOT-iron monomer **19-C3**. **19-C3** was investigated by IR, ^{1}H-NMR, ^{13}C-NMR (see experimental) and characterization compared to the analogue **19-C11**.

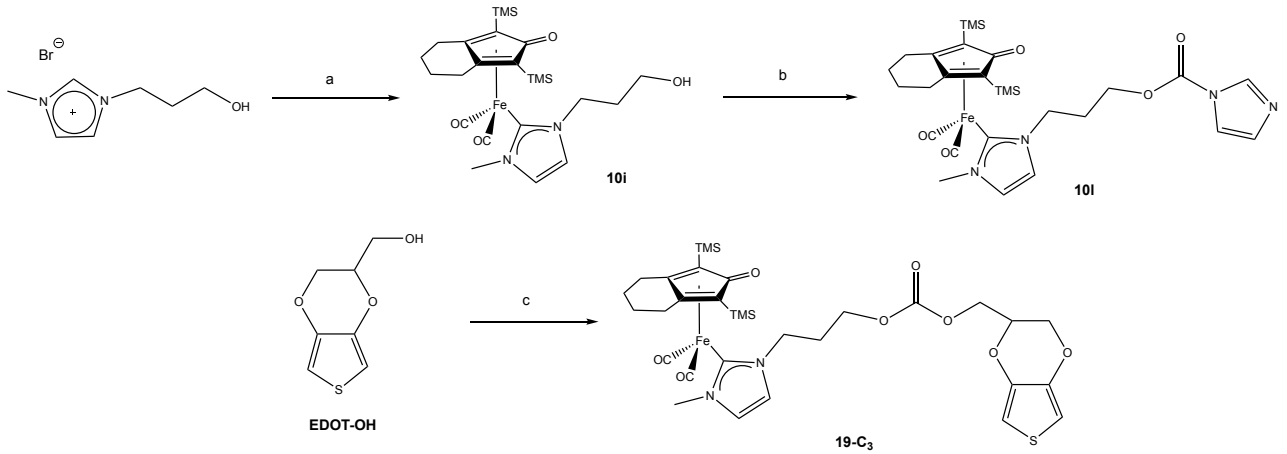

Scheme 2. a) i) **8**, 1.5eq. Me_3NO, 1.2eq. Ag_2O, CH_3CN, r.t.,1h; ii) toluene, reflux, 1h, y=30% b) 3 eq. CDI, CH_2Cl_2, r.t., 4h, y=98%. c) i) KO^{t}Bu, CH_3CN, reflux, 1h; ii) **10l**, CH_3CN, r.t, 19h, y=53%.

6.3.3 Electrochemical copolymerisation

Both iron compounds were copolymerised with EDOT on a VMPP surface (see Experimental). The use of co-monomer EDOT is necessary to obtain a regular film, due to the steric hindrance of the large iron-NHC tail close to the EDOT propagation centre. **19-Cx** were electrocopolymerized by cyclic voltammetry (one cycle in the potential range between 0.0 and +1.5 V at a scan rate of 0.05 V s^{-1}) from a 10 mM solution of **19-Cx** and EDOT containing 0.1mM $LiClO_4$ as the supporting electrolyte. Electropolymerisation with more than one cycle (e.g. 4 and 10) resulted in poor stability of the iron on the film. The best ratio between the two monomers was identified as **19-Cx**/EDOT 1:1 in order to obtain a homogeneous layer of copolymer over the surface. Figure 2 shows the CVs obtained during the growth of **19-C11** (red line) and **19-C3** (black line) copolymers on VMPP substrates. CV showed that the peak current in **19-C11** is at more anodic potential compared to **19-C3**, this is likely due to a different diffusion rate from the

solution to the electrode of the iron species. Diffusion might be influenced by the length of alkyl chain and in this case the longer chain in **19-C$_{11}$** results in a lower diffusione rate.

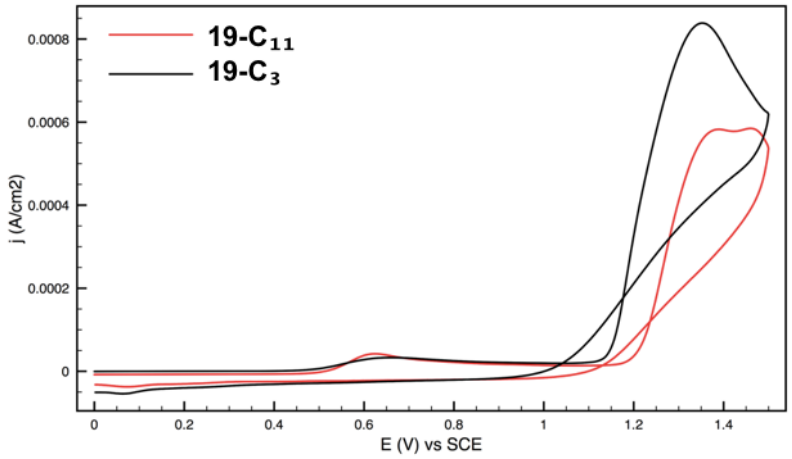

Figure 2. CV obtained on VMPP electrode in 0.1mM $LiClO_4$ in CH_3CN solution containing 10mM 17-C_{11}/EDOT(1:1) (red line) and 17-C_3/EDOT(1:1) (black line).

6.3.4 Characterisation of the 19-Cx/PEDOT coated VMMP electrode

Both coated electrodes were characterised by CV in 0.1 mM $LiClO_4$ aqueous solution, Figure 3 shows a comparison between the CV curves.

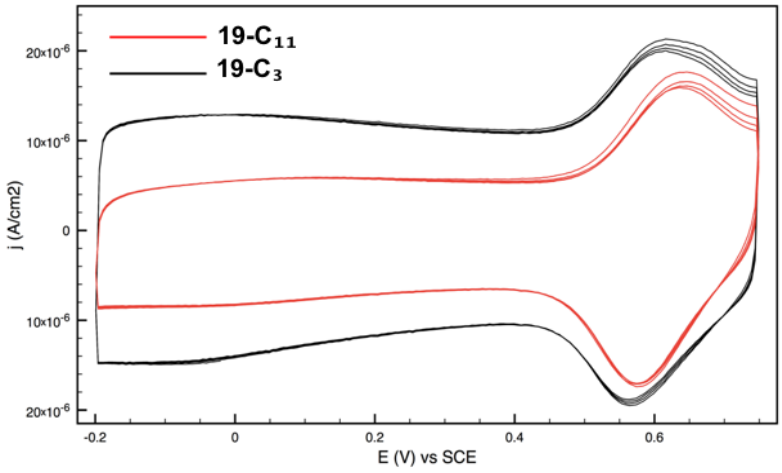

Figure 3. CV curves recorded at VMPP electrodes coated with 19-C_x/PEDOT in 0.1M$LiClO_4$ aqueous solution. Scan rate: 0.05 V s^{-1}.

The signal of both **19-C$_x$**/PEDOT coated electrodes is characterized by the faradaic signal of the NHC-iron complexes. The two redox peaks are located at potentials of 0.64 V and 0.57 V for **19-C$_{11}$** and at potentials of 0.61 V and 0.57 V for **19-C$_3$**, values typical of NHC-iron of type **10** redox couple (see chapter 4, paragraph 4.3.2). Moreover, we can note that when **19-C$_3$** is bonded to the PEDOT chain, a overall higher capacitive current

is recorded, even though the iron peak current is almost the same value, showing a much higher content of PEDOT over the **19-C$_3$** compared to the corresponding **19-C$_{11}$** deposition. This behaviour might be caused by a larger steric influence on electropolymerisation of the shorter chain linker **19-C$_3$**.

The polymeric films were also characterized by SEM-EDS. **19-Cx**/PEDOTs were coated on a platinum layer of 2 cm^2, previously treated with acid as described in the Experimental Section. Figure 4 shows SEM images of **19-C$_{11}$** and **19-C$_3$**: it is visible an heterogenous surface with random groups of material.

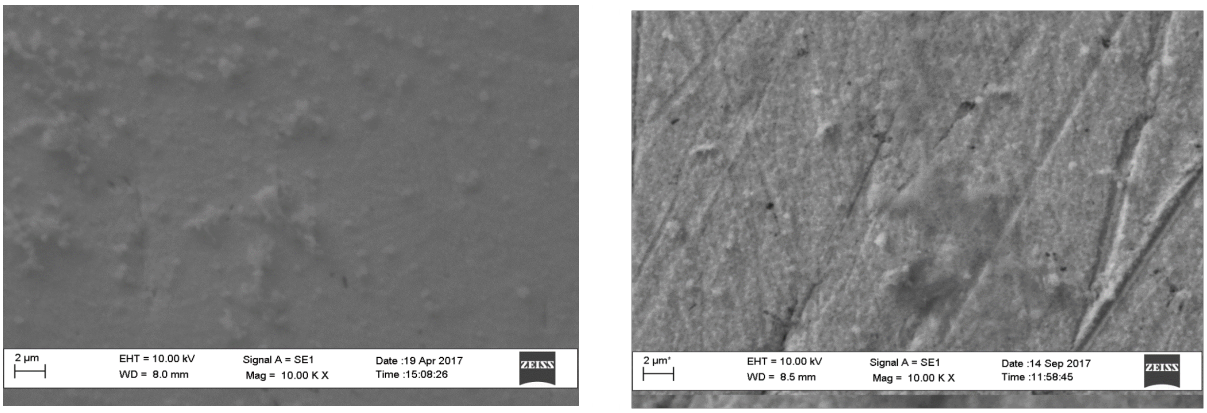

Figure 4. SEM maps of **19-C$_{11}$**(left) and **19-C$_3$**(right) at 10.00K X magnitude.

Furthermore, the EDS analysis measured atomic percentages of elements in a specific region of the surface, in our specific case iron and sulfur were exploited in order to evaluate an average ratio between **19-Cx/**PEDOT. Sulphur value represents the sum of all EDOT monomers present in polymer, whilts iron value can be correlated to the number of EDOT monomers bearing iron-NHC complexes. The values are reported in Table 1 and confirmed the CVs observations. Indeed, a lower **19-C$_3$**/PEDOT ratio compared to **19-C$_{11}$**/PEDOT was found, likely due to the shorter chain linker of **19-C$_3$**, hence a greater steric influence on the electropolymerisation mechanism.

Table 1.SEM-EDS analysis. S and Fe values of two copolymers coated on a platinum layer.

	S value (%)	Fe value (%)	**19-C$_x$**/PEDOT (%)	**19-C$_x$**/EDOT ratio
17-C$_{11}$	1.60±0.17	0.25±0.10	16	1/6
17-C$_3$	2.79±0.50	0.35±0.10	13	1/7

Finally, polymeric films were coated over a graphite layer of 2 cm^2 and characterised by ATR-IR spectroscopy (Figure 6). The CO stretching frequencies were in accordance with a NHC-iron species covalently bonded to the polymer (υ(CO)Fe-C_{11}: 2010, 1960 cm^{-1}; (υ(CO)Fe-C_3: 2017, 1974 cm^{-1}). Stretching frequencies experience a shift to higher value compared to the same neutral complexes as monomer (υ(CO)Fe-C_{11}: 1982, 1921 cm^{-1}; (υ(CO)Fe-C_3: 1981, 1921 cm^{-1}), that could be probably ascribed to interaction between the PSS of the polymer PEDOT chain. Indeed, sulfonic group (Figure 5) might engage either a hydrogen bond with cyclopentadienone or directly protonate the Cp=O moiety, resulting in the observed shift.

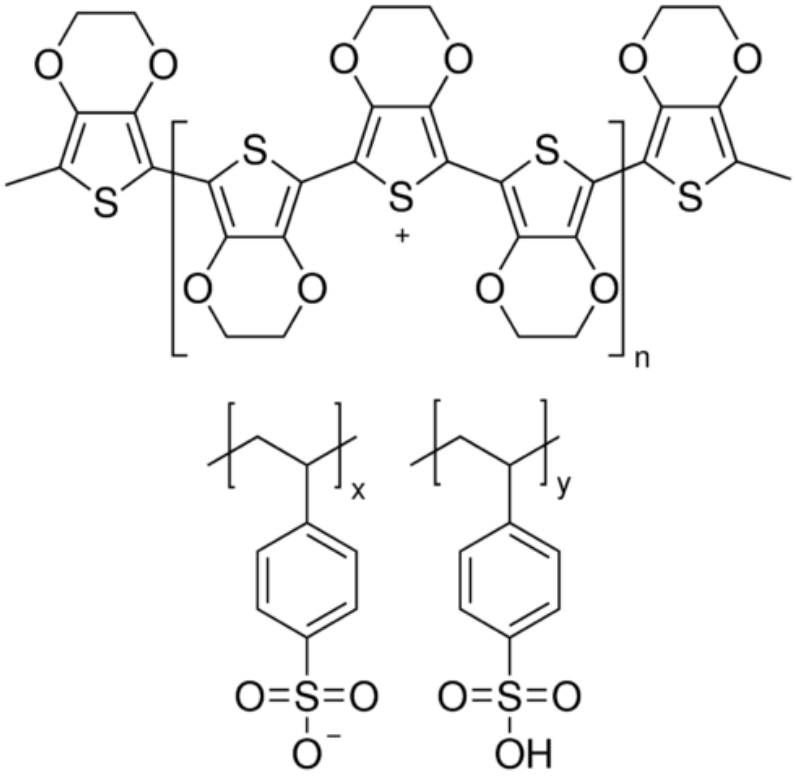

Figure 5. PEDOT:PSS chain.

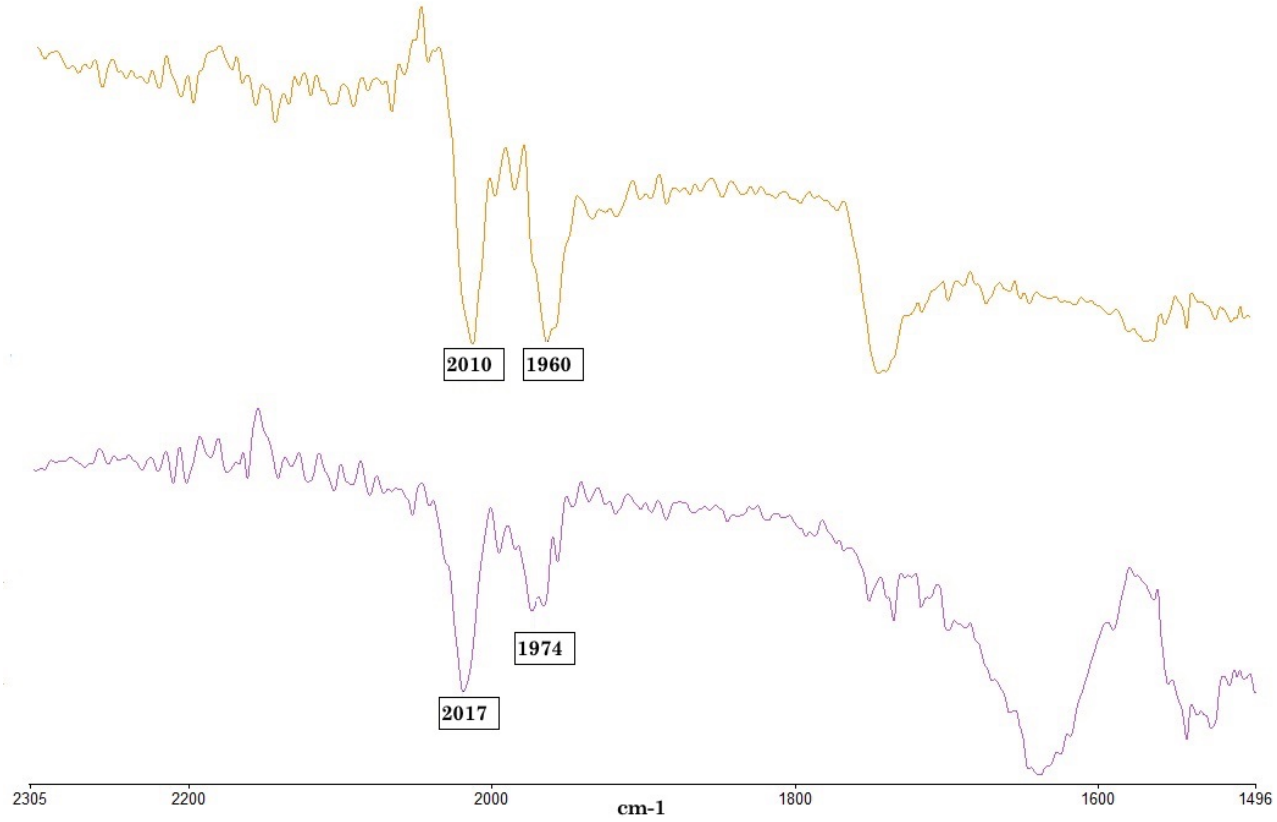

Figure 6. ATR-IR spectrum of **19-C11** (top) and **19-C3** (bottom). Zoom in the carbonyl region.

6.3.5 Dopamine amperometric detection

To assess the electrocatalytic properties of the covalently bonded **19-C11**, cyclic voltammograms scans were recorded in 0.1 M $LiClO_4$ solution containing different amounts of DA (Figure 7).

The **19-C11** anodic peak current disappeared as PEDOT peak current increased with increment of DA concentration, demonstrating that **19-C11** cannot mediate the electroxidation of dopamine, furthermore PEDOT itself gives a non-linear answer to DA addition.

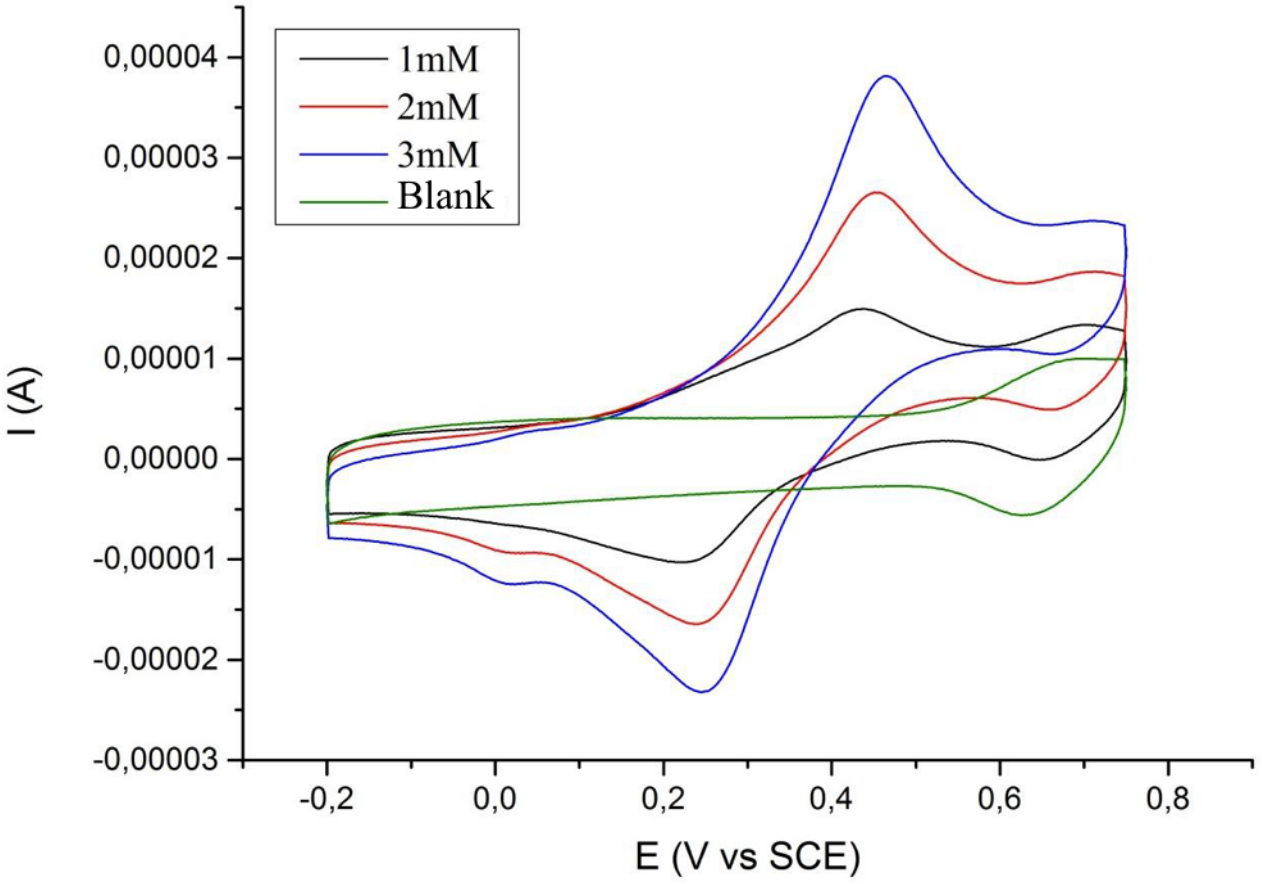

Figure 7. Cyclic voltammograms recorded in 0.1 M $LiClO_4$ solution containing different amount of DA. Potential scan rate: 0.02 Vs^{-1}.

6.3.6 Glucose amperometric detection

Since the disappointing results in DA detection, **19-C$_x$**/PEDOT copolymers were assessed in glucose amperometric detection. A layer of glucose oxidase (GOx) was deposited over the **19-C$_x$**/PEDOT film: 30µL of phosphate buffer 0.1 M at pH7 containing 10 mg GOx/ml has been spread over the copolymer films and was left to dry in the air. A layer of chitosan was then applied in order to avoid dissolution of the enzyme during analysis (See experimental for detailed procedure).

Glucose determination was therefore realized under hydrodynamic conditions, by chronoamperometry under magnetic stirring, at E_{app}=0.65 V with successive additions of glucose to a phosphate buffer solution at pH=7. As an example, Figure 7 shows the response of the **19-C$_3$**/PEDOT device under seven successive 3mM additions of glucose, demonstrating that **19-Cx**/PEDOT can act as redox mediator in glucose oxidation according to the reaction reported in scheme 3.

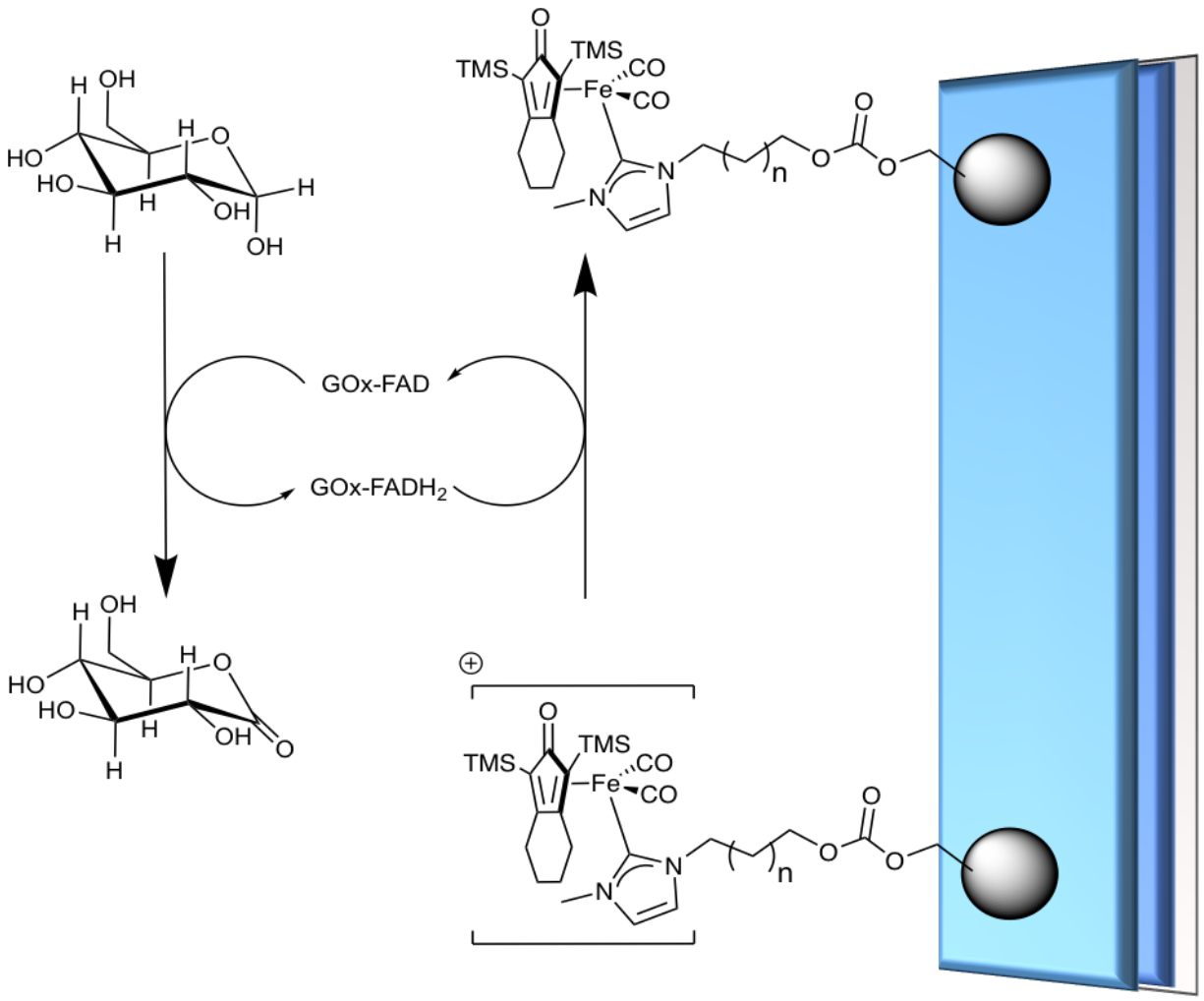

Scheme 3. Proposed mechanism of 1**9-C$_x$** as redox mediators in glucose oxidation. The active site of enzyme GOx-FAD is reduced to GOx-FADH$_2$, which is re-oxidised to starting point by [19-C$_x$]$^+$. Species [19-C$_x$]$^+$ is the mono-oxidised form of 17-C$_x$, generated by the electrode.

Calibration curves were obtained by plotting the steady state current, measured after subtraction of the base line current, vs. substrate concentration (see the inset in Figure 8). Two different **19-C$_x$**/PEDOT electrodes were prepared and the reproducibility and repeatability of the sensors were examined. For a given **19-C$_3$**/PEDOT electrode, the relative standard deviation (RSD) was 3% for seventeen additions of 3 mM glucose. These sensors presented a linear range between 3 mM and 51 mM and a mean sensitivity of 7.5 μA M^{-1} cm^{-2}. For a given **19-C$_{11}$**/PEDOT electrode, the relative standard deviation (RSD) was 8% for seventeen additions of 3 mM glucose. These sensors presented a linear range between 5.8 mM and 47 mM and a mean sensitivity of 6 μA M^{-1} cm^{-2}.

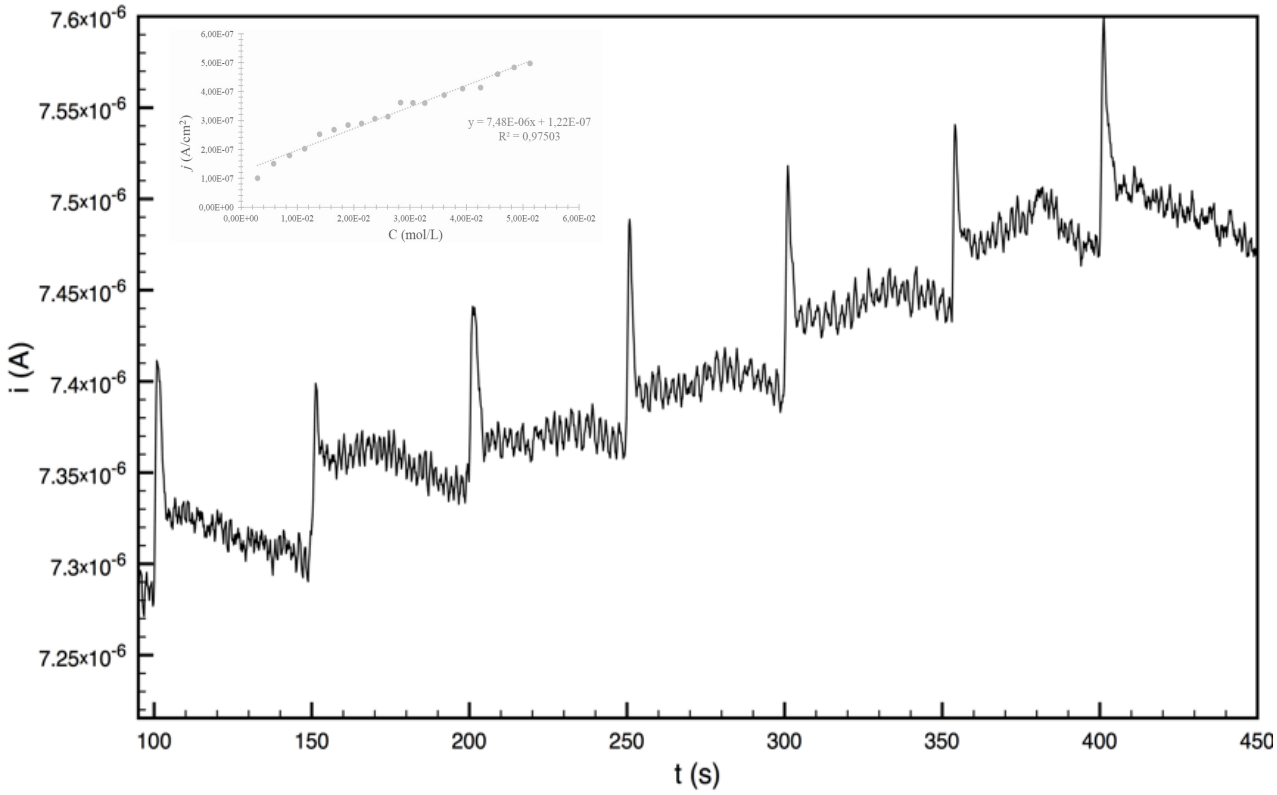

Figure 8. Chronoamperometric response at 0.65 V vs. SCE of an VMMP electrode coated with a **19-C3**/PEDOT film, in 0.1 M $LiClO_4$ solution, and a layer of GOx/chitosan to 3 mM successive glucose additions. The inset shows the relevant calibration curve.

6.4 Conclusions

We have coated VMPP slides with 19-Cx/PEDOT, by electrodeposition of co-monomer **19-Cx** and EDOT. Monomers **19-C$_{11}$** and **19-C$_3$** have been synthesised following transmetallation reaction described in Chapter I, employing the appropriate imidazolium salt as carbene precursor. The NHC-iron complexes have been coupled to an EDOT monomer exploiting the 1,1'-dicarbonylimidazolium (CDI) as coupling reagent. The VMPP coated electrodes have been characterized by CV: the signal of 17-Cx/PEDOT is dominated by the reversible faradaic signal of the corresponding NHC-iron complex with the presence of two redox peaks located at 0.64 V and 0.57 V for **19-C$_{11}$** and at 0.61 V and 0.57 V for **19-C$_3$**, values typical of the NHC-iron **10**-family redox couple. The coatings are stable in aqueous solution.

To demonstrate the successful immobilization, and to make sure that iron complexes are covalently bonded to the polymer chain, the coated electrodes have been characterized by ATR-IR and SEM-EDS, the average copolymerisation ratio between 17-Cx/PEDOT found are: 1/6 for **19-C$_{11}$** and 1/7 for **19-C$_3$**.

The electrocatalytical performance of the device has been assessed by analysing 3,4-dihydroxyphenyl ethylamine, also commonly known as dopamine (DA), without any activity. After deposition of Glucose Oxidase enzyme (GOx) over the 17-Cx/PEDOT film, the device has been assessed by analysing glucose in solution. Both sensors present comparable activity, among which **19-C$_3$** is the best with a linear range between 3 and 51 mM and a mean sensitivity of 7.5 $\mu A\ M^{-1}\ cm^{-2}$.

Although the sensor needs to be further developed for practical application, the possibility of immobilisation with various linkers and of fine-tuning of NHC-iron complexes both on cyclopentadienone substituents and on N atoms of carbene, paves the way for new developments on chemically modified electrodes.

6.5 Experimental Section

General data. All reactions were routinely carried out under a nitrogen atmosphere, using standard Schlenk techniques. Glassware was ovendried before use. Solvents: dichloromethane (CH_2Cl_2), tetrahydrofuran (THF), diethyl ether (Et_2O), petroleum ether referring to a fraction of bp 60-80 °C, acetonitrile (CH_3CN) were dried and distilled prior to use. Acetone has been degassed and stored under inert atmosphere on molecular sieves. Other solvents such as ethylacetate (EtOAc), ethanol (EtOH), methanol (MeOH), heptane, toluene, $CDCl_3$, C_7D_8, (Eurisotop) have been employed without further purification. Reagents: $Fe_2(CO)_9$ (Strem), silver oxide, trimethylamine-N-oxide, 1-N-methylimidazole, potassium tert-butoxide, 1,1'-carbonyldimidazole, 3-bromo-1-propanol and 11-bromo-1-undecanol have been employed as purchased.
1-(4-idroxypropyl)-3-methyl-1H-imidazolium bromide [15] and 1,8-bis(trimethylsilyl)octa-1,7-diyne[16] have been prepared following procedures reported in the literature.
The prepared derivatives were characterized by spectroscopic methods. The NMR spectra were recorded using Varian Inova 300 (^1H, 300.1; ^{13}C, 75.5 MHz), Varian Mercury Plus VX 400 (^1H, 399.9; ^{13}C, 100.6 MHz), Varian Inova 600 (^1H, 599.7; ^{13}C, 150.8 MHz) spectrometers at 298 K; chemical shifts were referenced internally to residual solvent peaks. Full ^1H- and ^{13}C-NMR assignments were done, when necessary, by gHSQC and gHMBC NMR experiments using standard Varian pulse sequences. Infrared spectra were recorded at 298 K on a Perkin-Elmer Spectrum 2000 FT-IR spectrophotometer. ESI-MS spectra were recorded on Waters Micromass ZQ 4000 with samples dissolved in MeOH or CH_3CN. Elemental analyses were performed on a Thermo-Quest Flash 1112 Series EA instrument. UV irradiation was performed by using a commercial Hg lamp.

1-(11-idrossiundecil)-3-metil-1H-imidazolio bromuro (1g). In a round-bottom flask 1-N-methylimidazole 0.3mL (3.76mmol) and 11-bromo-1-undecanol 0.3mL (3.76 mmol) were dissolved in 15 mL of ethyl acetate and left under stirring at 65°C for 24h. The mixture was filtered and the solid washed several time with ethyl acetate. Quantitative yield.
Suitable crystals of **1g** for X-ray diffraction were obtained by double layer (Dichloromethane/Hexane). **1g** has been analysed by ^1H-NMR, ^{13}C-NMR, ESI-MS and

X-ray Crystallography. ^{1}H-NMR (399.9 MHz, $CDCl_3$): δ(ppm): 10.65 (s, 1H, NCHN), 7.32 (s, 1H, CHim), 7.25 (s, 1H, CHim), 4.32 (t, 2H, CH_2N), 4.13 (s, 3H, CH_3N), 3.63 (t, 2H, CH_2O), 1.92 (m, 2H, CH_2CH_2N), 1.57 (m, 2H, CH_2CH_2O), 1.4-1.2 (m, 14H, -CH_2-). ^{13}C-NMR (150.8 MHz, $CDCl_3$): δ(ppm): 138.05 (N*C*HN), 123.12 (*C*H_{im}), 121.53 (*C*H_{im}), 62.81 (*C*H_2O), 50.21 (N*C*H_2), 36.75 (*C*H_3N), 32.76-25.61 (-*C*H_2-). ESI-MS (m/z): (+) 253 [M^+]; (-) 79/81 [Br^-]

1-(11-((1*H*-imidazol-1-carbonyl)oxy)undecil)-3-methyl-1*H*-imidazolium bromide (**1g$_{im}$**). In a 50mL Schlenk 1,1'-carbonyldimidazole 0.438 g (2.70 mmol) and 1g 0.299 g (0.90 mmol) were dissolved in 10 mL of CH_2Cl_2 and left under stirring for 4h. The reaction mixture was washed with water (2x20 mL) and organic layer dried over $MgSO_4$, filtered and concentrated. The white oil was washed several times with Et_2O to leave a white solid. Quantitative yield.

1g$_{im}$ has been analyzed by IR, ^{1}H-NMR and ^{13}C-NMR. ^{1}H-NMR (399.9 MHz, $CDCl_3$): δ(ppm): 10.61(s, 1H, NC*H*N), 8.13 (s, 1H, C*H*$_{im}$), 7.42 (s, 1H, C*H*$_{im}$), 7.29 (s, 1H, C*H*$_{im}$), 7.25 (s, 1H, C*H*$_{im}$), 7.06 (s, 1H, C*H*$_{im}$) 4.41 (t, 2H, C*H*$_2$O), 4.31 (t, 2H, C*H*$_2$N), 4.12 (s, 3H, C*H*$_3$N), 1.92 (m, 4H, C*H*$_2$CH$_2$N), 1.79 (m, 4H, C*H*$_2$CH$_2$O), 1.5-1.2 (m, 14H, -C*H*$_2$-). ^{13}C-NMR (150.8 MHz, $CDCl_3$): δ(ppm): 148.70 (O*C*N), 137.75 (*C*H_{im}), 137.00 (*C*H $_{im}$), 130.50 (CH$_{im}$), 123.28 (*C*H$_{im}$), 121.64 (*C*H$_{im}$), 117.10 (*C*H$_{im}$), 68.48 (*C*H_2O), 50.16 (N*C*H_2), 36.72 (*C*H_3N), 30.23-25.62 (-*C*H_2-). IR (CH_2Cl_2, cm^{-1}): ν 1760, 1732 cm^{-1}

1-(11-((((2,3-dihydrothyeno[3,4-b][1,4]dioxyn-2-il)methoxy)carbonyl)oxy)-undecil)-3-methyl-1H-imidazolium bromide (EDOT$_{im}$). In a 50 mL Schlenk potassium tert-butoxide 0.099 g (0.88 mmol) was suspended in 10 mL CH_3CN. EDOT-OH 0.152 g (0.88 mmol) was added to the solution and left under reflux for 2h. Solution was cool down to room temperature and 5 mL of CH_3CN solution containing **1g$_{im}$** 0.377 g (0.88 mmol) was added dropwise. The reaction mixture was left under stirring at room temperature overnight. Solvent was removed under vacuum. The residue was dissolved in CH_2Cl_2 and washed with water (2x). Organic layers were dried over $MgSO_4$, filtered and concentrated. The oil was washed with Et2O to leave a white solid. Yield = 42%.

EDOT$_{im}$ has been analyzed by IR, ^{1}H-NMR and ^{13}C-NMR. ^{1}H-NMR (399.9 MHz, $CDCl_3$):^{1}H-NMR (599.7 MHz, $CDCl_3$): δ(ppm): 10.74 (s, 1H, C*H*$_{im}$), 7.28 (s, 1H, C*H*$_{im}$),

7.21 (s, 1H, C*H*$_{im}$), 6.35 (q, 2H, *H*CS), 4.40 (m, 1H, C*H*O$_{EDOT}$), 4.34 (m, 2H, OC(O)OC*H*$_{2,EDOT}$), 4.31 (t, 2H, C*H*$_2$N) 4.25 (m, 1H, C*H*$_2$O$_{EDOT}$), , 4.15 (t, 2H, C*H*$_2$O), 4.13 (s, 3H, C*H*$_3$N) 4.07 (m, 1H, C*H*$_{2,EDOT}$), 1.92 (m, 2H, C*H*$_2$CH$_2$N), 1.67 (m, 2H, C*H*$_2$CH$_2$O), 15-1.2 (m, 14H, -C*H*$_2$-). ^{13}C-NMR (150.8 MHz, $CDCl_3$): δ(ppm): 154.90 (O*C*(O)O), 141.14 (C$_{q,EDOT}$), 140.87 (C$_{q,EDOT}$), 138.75 (N*C*N), 122.77 (*C*H$_{im}$), 121.29 (*C*H$_{im}$), 100.17 (S*C*$_{EDOT}$), 100.00 (S*C*$_{EDOT}$), 71.23 (*C*HO$_{EDOT}$), 68.74 (*C*H$_2$OC(O)O), 65.41 (OC(O)O*C*H$_{2,EDOT}$), 65.31 (*C*H$_2$O$_{EDOT}$), 50.36 (*C*H$_2$N), 36.87 (N*C*H$_3$), 30.28-25.60 (-CH$_2$-). IR (CH_2Cl_2): ν 1749cm^{-1}

Triscarbonyl-(2,4-bis(trimethylsilyl)bicyclo[3.3.0]nona-1,4-dien-3-one)iron (8). In a 75 mL Teflon tube equipped with magnetic stirrer, 1,7-octadiyne 0.027 g (0.11 mmol) and $Fe_2(CO)_9$ 0.039 g (0.11 mmol) were dissolved in 40 mL of toluene. The container is closed with a cap, equipped with a temperature sensor, and placed into microwave reactor. The reaction is heated to 140 °C for 140 min. Upon removal of the solvent, the crude was purified to afford the yellow triscarbonyl-(2,4-bis(trimethylsilyl)bicyclo[3.3.0]nona-1,4-dien-3-one)iron (**8**) by neutral alumina column chromatography using dichloromethane/ethyl acetate (100/0 to 0/100). Yield = 83%
8 has been analyzed by IR, ^{1}H-NMR. ^{1}H-NMR (399.9 MHz, $CDCl_3$): δ (ppm) 2.56 (m, 4H, CH_2), 1.82 (m, 4H, CH_2), 0.27 (s, 18H, CH_3, TMS). IR (CH_2Cl_2, cm^{-1}): (ν$_{CO}$) 2063, 2004, 1987; (ν$_{C=O}$). Anal. Calcd (%) for $C_{18}H_{26}O_6Fe$: C, 51.67; H, 6.26. Found: C, 49.08; H, 5.93.

Dicarbonyl-(2,4-bis(trimethylsilyl)bicyclo[3.3.0]nona-1,4-dien-3-one)[(1-(11-((((2,3-dihydrothyeno[3,4-b][1,4]dioxin-2-il)methoxy)carbonyl)oxy)undecil)-3-methyl-ilidene)]iron (19-C$_{11}$). Imidazolium salt **EDOTim** 0.380 g (0.71 mmol), silver oxide 0.207 g (0.89 mmol), triscarbonyl-(2,4-bis(trimethylsilyl)bicyclo[3.3.0]nona-1,4-dien-3-one)iron 0.299g (0.71 mmol) and trimethylammine-N-oxide 0.080 g (1.07 mmol) were reacted in CH_3CN under inert atmosphere and with protection from light. After stirring the reaction for 1h at room temperature, the solvent was removed under vacuo, then the solid dissolved in toluene. The reaction mixture was stirred under reflux for 1 hour. Upon removal of the solvent, the crude was purified by neutral alumina column chromatography using ethyl acetate/methanol (40/1). Yield: 50 %.
17-C$_{11}$ has been analyzed by IR, ^{1}H-NMR, ^{13}C-NMR, ESI-MS. ^{1}H-NMR (399.9 $CDCl_3$) δ (ppm): 7.01 (s, 2H, C*H*$_{im}$), 6.35 (q, 2H, SC*H*), 4.40 (m, 1H, C*H*O$_{EDOT}$), 4.34 (m, 2H,

OC(O)OC$H_{2,EDOT}$), 4.24 (m, 1H, CH_2O_{EDOT}), 4.18 (t, 2H, CH_2N), 4.15 (t, 2H, CH_2O), 4.07 (m, 1H, CH_2O_{EDOT}), 3.95 (s, 3H, CH_3N), 2.42 (m, 4H, CH_2ex), 1.83 (m, 2H, CH_2ex), 1.77 (m, 2H, CH_2CH_2N), 1.76 (m, 2H, CH_2ex), 1.67 (m, 2H CH_2CH_2O), 1.43 (m, 2H, C$H_2(CH_2)_2$N), 1.4-1.2 (m, 12H, -CH_2-), 0.164 (s, 18H, CH_{3TMS}). ^{13}C-NMR (150.8 MHz, $CDCl_3$, g-HSQC, g-HMBC) δ (ppm): 216.99 (*C*O), 183.79 ($C_{carbene}$), 154.89 (O*C*OO), 141.12 ($C_{q,EDOT}$), 140.85 ($C_{q,EDOT}$), 124.19 (*C*H_{im}), 121.72 (*C*H_{im}), 103.99 ($C_{3,4q}$), 100.15 (SC_{EDOT}), 99.98 (SC_{EDOT}), 71.20 (CHO_{EDOT}), 71.10 ($C_{2,5q}$), 68.72 (*C*H_2OC(O)O), 65.38 (OC(O)O*C*$H_{2,EDOT}$), 65.29 (CH_2O_{EDOT}), 51.97 (*C*H_2N), 40.26 (N*C*H_3), 31.80 (*C*H_2CH_2N) 29.66-25.60 (-*C*H_2-), 24.41 (*C*H_2ex), 22.53 (*C*H_2ex), 0.22 (*C*H_{3TMS}). IR (CH_2Cl_2, cm^{-1}): (ν_{CO}) 1982, 1921, 1747. ESI-MS (m/z): 841 $[M+H]^+$, 863 $[M+Na]^+$, 525 $[M+K]^+$.

Dicarbonyl-(2,4-bis(trimethylsilyl)bicyclo[3.3.0]nona-1,4-dien-3-one)[1-(3-idroxypropyl)-3-methyl-ilidene)]iron (10i). Imidazolium salt 1-(4-idroxypropyl)-3-methyl-1H-imidazolium bromide 0.080 g (0.36 mmol), silver oxide 0.092 g (0.39 mmol), triscarbonyl-(2,4-bis(trimethylsilyl)bicyclo[3.3.0]nona-1,4-dien-3-one)iron 0.154g (0.36 mmol) and trimethylammine-N-oxide 0.044 g (0.59 mmol) were reacted in CH_3CN under inert atmosphere and with protection from light. After stirring the reaction for 1h at room temperature, the solvent was removed under vacuo, then the solid dissolved in toluene. The reaction mixture was stirred under reflux for 1 hour. Upon removal of the solvent, the crude was purified by neutral alumina column chromatography using ethyl acetate/methanol (40/1). Yield: 30 %.

10i has been analyzed by IR, ^{1}H-NMR, ^{13}C-NMR, ESI-MS. ^{1}H-NMR (399.9 $CDCl_3$) δ (ppm): 7.17, 7.02 (s, 2H, CH_{im}), 4.35 (t, 2H, CH_2O), 3.89 (s, 3H, CH_3N), 3.70 (t, 2H, CH_2N), 2.42 (m, 4H, CH_2ex), 2.08 (t, 2H, CH_2), 1.86 (m, 2H, CH_2ex), 1.76 (m, 2H, CH_2ex), 0.16 (s, 18H, CH_{3TMS}). ^{13}C-NMR (150.8 MHz, $CDCl_3$, g-HSQC, g-HMBC) δ (ppm): 217.13 (*C*O), 182.58 ($C_{carbene}$), 124.18 (*C*H_{im}), 122.12 (*C*H_{im}), 104.11 ($C_{3,4q}$), 75.33 ($C_{2,5q}$), 58.57 (CH_2OH), 48.31 (*C*H_2N), 40.19 (N*C*H_3), 33.19 (*C*H_2) 24.54 (*C*H_2ex), 22.60 (*C*H_2ex), 0.20 (*C*H_{3TMS}). IR (CH_2Cl_2, cm^{-1}): (ν_{CO}) 1981, 1921. ESI-MS (m/z): 531 $[M+H]^+$.

Dicarbonyl-(2,4-bis(trimethylsilyl)bicyclo[3.3.0]nona-1,4-dien-3-one)[1-(3-((1H-imidazol-1-carbonyl)oxy)propryl)-3-methyl-ilidene]iron (10l). In a 50mL Schlenk 1,1'-carbonyldimidazole 0.039 g (0.24 mmol) and **10i** 0.040 g (0.08 mmol) were

dissolved in 10 mL of CH_2Cl_2 and left under stirring for 4h. The reaction mixture was washed with water (2x20 mL) and organic layer dried over $MgSO_4$, filtered and concentrated. The yellow oil was washed several time with hexane to leave a yellow solid. Quantitative yield.

10l has been analyzed by IR, ^{1}H-NMR, ^{13}C-NMR, ESI-MS. ^{1}H-NMR (399.9 C_7D_8) δ (ppm): 8.01 (s, 1H, CH_{im}), 7.56 (s, 1H, CH_{im}), 7.23 (s, 1H, C*H*$_{im}$), 6.45 (s, 1H, CH_{im}) 6.30 (s, 1H, CH_{im}), 4.23 (t, 2H, C*H*$_2$), 4.10 (t, 2H, C*H*$_2$), 3.49 (s, 3H, C*H*$_3$N), 2.36 (m, 4H, C*H*$_2$ex), 1.78-1.56 (m, 4H+2H, C*H*$_2$ex + CH_2), 0.20 (s, 18H, C*H*$_{3TMS}$). ^{13}C-NMR (150.8 MHz, C_7D_8) δ (ppm): 217.13 (*C*O), 186.18 (*C*$_{carb}$), 177.70 (C=O$_{Cp}$), 167.32 (OCN), 133.38 (*C*H$_{im}$), 130.72 (*C*H$_{im}$), 104.31 (*C*$_{3,4q}$), 67.93 (*C*$_{2,5q}$), 39.37 (CH_2O), 30.81 (*C*H$_2$N), 30.20 (N*C*H$_3$), 29.41 (*C*H$_2$) 25.24 (*C*H$_2$ex), 22.96 (*C*H$_2$ex), 0.49 (*C*H$_{3TMS}$). IR (CH_2Cl_2, cm^{-1}): (ν_{CO}) 1981, 1921, 1765.

Dicarbonyl-(2,4-bis(trimethylsilyl)bicyclo[3.3.0]nona-1,4-dien-3-one[1-(3-((((2,3-dihydrothyeno[3,4-b][1,4]dioxin-2-il)methoxy)carbonyl)oxy)propyl)-3-metyl-ilidene]iron (19-C$_3$). In a 50 mL Schlenk potassium tert-butoxide 0.011 g (0.10 mmol) was suspended in 10 mL CH_3CN. EDOT-OH 0.017 g (0.10 mmol) was added to the solution and left under reflux for 2h. Solution was cool down to room temperature and 5 mL of CH_3CN solution containing **10l** 0.053 g (0.08 mmol) was added dropwise. The reaction mixture was left under stirring at room temperature overnight Upon removal of the solvent, the product was purified by neutral alumina column chromatography using ethyl acetate/methanol (50/1). Yield = 53%.

17-C$_3$ has been analyzed by IR, ^{1}H-NMR, ^{13}C-NMR, ESI-MS. ^{1}H-NMR (399.9 C_7D_8) δ (ppm): 6.48 (s, 1H, CH_{im}) 6.13 (s, 1H, CH_{im}), 6.07 (s, 2H, CHS), 4.24 (t, 2H, C*H*$_2$), 3.64 (m, 4H, CH_{2EDOT}), 3.48 (t, 2H, CH_2OCO), 3.39 (t, 2H, C*H*$_2$), 3.49 (s, 3H, C*H*$_3$N), 3.27 (s, 1H, CH_{EDOT}), 2.36 (m, 4H, C*H*$_2$ex), 1.99 (m, 2H, CH_2), 1.77-1.68 (m, 4H, C*H*$_2$ex), 0.26 (s, 18H, C*H*$_{3TMS}$). ^{13}C-NMR (150.8 MHz, C_7D_8) δ (ppm): 217.83 (*C*O), 183.18 (*C*$_{carb}$), 175.10 (C=O$_{Cp}$), 142.42 (Cq$_{EDOT}$), 123.98 (*C*H$_{im}$), 122.22 (*C*H$_{im}$), 103.71 (*C*$_{3,4q}$), 99.73 (CHS), 74.45 (CH_{EDOT}), 72.93 (*C*$_{2,5q}$), 66.22 (CH_{2EDOT}-OCO_2), 58.67 (CH_2-OCO_2), 49.11 (*C*H$_2$N), 39.62 (N*C*H$_3$), 33.81 (*C*H$_2$) 25.14 (*C*H$_2$ex), 22.86 (*C*H$_2$ex), 0.51 (*C*H$_{3TMS}$). IR (CH_2Cl_2, cm^{-1}): (ν_{CO}) 1981, 1921, 1748. Anal. Calcd (%) for $C_{22}H_{34}N_2O_3Si_2Fe$: C, 54.31; H, 7.04. Found: C, 51.82; H, 6.72.

Electrochemical Studies. Cyclic voltammograms and chronoamperometric measurements were performed on a CH1660C (CH Instruments) electrochemical analyser using a three-electrode cell: depending on the working conditions a VMPP (1 cm^2) or a glassy-carbon disk (0.071 cm^2) or a graphite sheet (2 cm^2) as the working electrode, a $Ag/AgNO_3$ (0.1 M) reference electrode, and a platinum-wire counter electrode. All experiments were performed under a nitrogen atmosphere and solutions were degassed for 10 minutes. All potentials have been quoted relative to SCE electrode.

Electrochemical polymerisation of 19-C_x. The electrochemical polymerization was carried out on an VMPP, that is a PEDOT:PSS film spin-coated over a glass slide of 1 cm^2. The electrosynthesis of **19-C_x** was carried out, under a N_2 atmosphere, potentiodynamically, by cyclic voltammetry, cycling one time in the potential range between 0.0 V and 1.5 V at a scan rate of 0.05 V s^{-1}, in a 0.1 mM $LiClO_4$ CH_3CN solution containing 10 mM 17-C_x/EDOT (1:1) monomers. Prior to the application of the potential pulse, the CH_3CN suspension was vigorously stirred for 20 min, and the electrochemical polymerization was carried out under moderate stirring. After the electrodeposition, the film was repeatedly washed with deionized water to remove both the supporting electrolyte and the excess monomer and finally allowed to dry in air.

SEM-EDS analysis preparation. The electrochemical polymerisation was carried out on a platinum slide of 2cm^2 by cyclic voltammetry, as for VMPP electrode. The platinum slide was previously cleaned by cyclic voltammetry in a 0.1 M H_2SO_4 aqueous solution and then rinsed with ethanol in order to remove any acidic residue. A blank measurement (i.e. platinum slide without polymer) showed no traces of sulphur derived from the treatment with H_2SO_4.

Glucose Oxidase device preparation. On a VMPP of 1cm^2 coated with 17-Cx/PEDOT as previously described, a layer of glucose oxidase (GOx) was deposited over the 17-C_x/PEDOT film: 30μL of phosphate buffer 0.1 M at pH7 containing 10 mg GOx/ml has been spread over the copolymer films and was left to dry in the air. A layer of chitosan was then applied in order to avoid dissolution of the enzyme during analysis:

40µL of 1% v/v acetic acid solution containing 4 mg chitosan/mL was deposited and left to dry in the air. The following scheme is a representation of the GOx device.

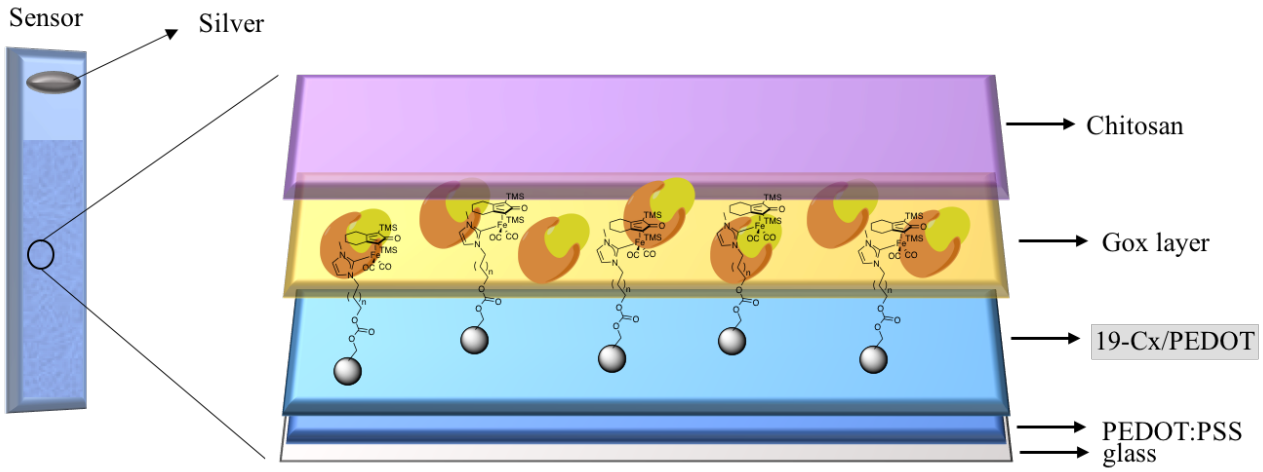

X-ray Crystallography. Crystal data and collection details for **1g** are reported in Table X. The diffraction experiments were carried out on a Bruker APEX II diffractometer equipped with a CCD detector using Mo–Kα radiation. Data were corrected for Lorentz polarization and absorption effects (empirical absorption correction SADABS).[17] Structures were solved by direct methods and refined by full-matrix least-squares based on all data using F^2.[18] All hydrogen atoms were fixed at calculated positions and refined by a riding model. All non-hydrogen atoms were refined with anisotropic displacement parameters.

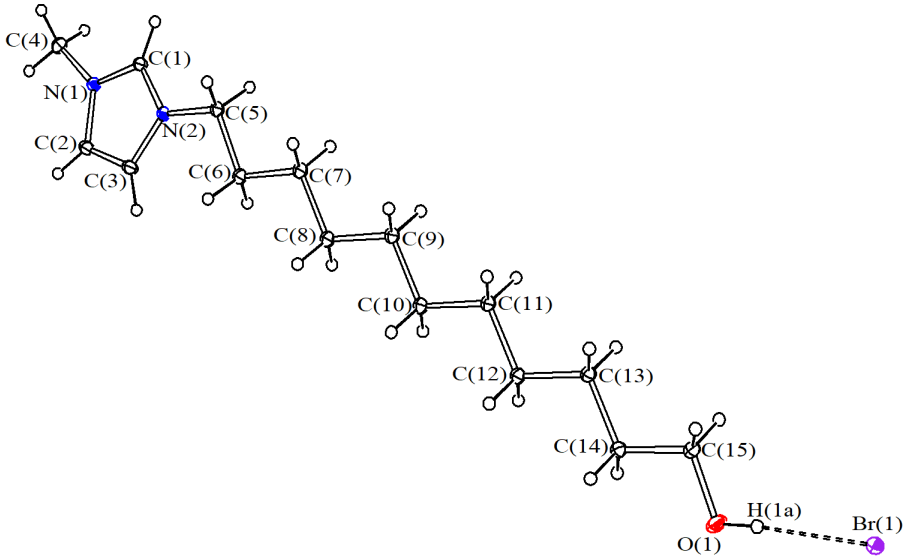

Figure 9. ORTEP drawing of **1g**. Displacement ellipsoids are at the 30% probability level. H-bond between anion and cation in dotted line. Selected bondlength (Å): H(1)-Br(1) 2.3926(2).

Table 2. Crystal data and experimental details for **1g**.

	1g
Formula	$C_{15}H_{29}BrN_2O$
Fw	414.23
T, K	100(2)
λ, Å	0.71073
Crystal system	Triclinic
Space group	*P*-1
a, Å	5.58410(10)
b, Å	7.6477(2)
c, Å	19.5696(35
α, °	86.1130(10)
β, °	86.7370(10)
γ, °	886660(5)
Cell Volume, $Å^3$	889.74(8)
Z	2
D_c, g cm^{-3}	1.546
μ, mm^{-1}	4.555
F(000)	424
Crystal size, mm	0.15·0.12·0.09

6.6 Notes and References

[1] (a) P. Marianne, *Anal. Chim. Acta*, **1986**, *187*, 333. (b) J. Kulys and E. J. D'Costa, *Anal. Chim. Acta*, **1991**, *243*, 173. (c) A. Escorcia and A.-A. Dhirani, *J. Electroanal. Chem.*, **2007**, *601*, 260. (d) J. Qiu, H. Peng and R. Liang, *Electrochem. Commun.*, ***2007, 9***, 2734. (e) J. D. Qiu, J. Guo, R. P. Liang and M. Xiong, *Electroanalysis*, **2007**, *19*, 2335. (f) T. T. Hien Pham, C. Cao and S. J. Sim, *J. Magn. Magn. Mater.*, **2008**, *320*, 2049. (g) L. Fernandez and H. Carrero, *Electrochim. Acta*, **2005**, *50*, 1233.

[2] M. A. Rampi, O. J. A. Schueller and G. M. Whitesides, *Appl. Phys. Lett.*, **1998**, *72*, 1781.

[3] D. J. Wold, R. Haag, M. A. Rampi and C. D. Frisbie, *J. Phys. Chem. B*, **2002**, *106*, 2813.

[4] A. Callegari, M. Marcaccio, D. Paolucci, F. Paolucci, N. Tagmatarchis, D. Tasis, E. Vazquez and M. Prato, *Chem. Commun.*, **2003**, 2576.

[5] S. L. Brooks, R. E. Ashby and A. P. E. Turner, *Biosensors*, **1987**, *3*, 45.

[6] (a) L. Su, X. P. Qiu, L. H. Guo, F. S. Zhang and C. H. Tung, *Sens. Actuators, B*, **2004**, *99*, 499. (b) S. Koide and K. Yokoyama, *J. Electroanal. Chem.*, **1999**, *468*, 193.

[7] M. Dletrlch, J. Hemze, G. Heywang and F. Jonas, *J. Electroanal. Chem.*, **1994**, *369*, 87.

[8] L. B. Groenendaal, F. Jonas, D. Freitag, H. Pielartzik and J. R. Reynolds, *Adv. Mater.*, **2000**, *12*, 481.

[9] See for example: (a) G. Li and P. G. Pickup, Phys. *Chem. Chem. Phys.*, **2000**, *2*, 1255. (b) J. Bobacka, A. Lewenstam and A. Ivaska, *J. Electroanal. Chem.*, **2000**, *489*, 17. (c) X. Cui and D. Martin, *Sens. Actuators, B*, **2003**, *89*, 92. (d) A. Lisowska-Oleksiak and A. Kupniewska, *Solid State Ionics*, **2003**, *157*, 241. (e) D. Han, G. Yang, J. Song, L. Niu and A. Ivaska, *J. Electroanal. Chem.*, **2007**, *602*, 24.

[10] See for example: (a) L. Basiricò, P. Cosseddu, B. Fraboni and A. Bonfiglio, *Thin Solid Films*, **2011**, *520*, 1291. (b) L. Basiricò, P. Cosseddu, A. Scidà, B. Fraboni, G. G. Malliaras and A. Bonfiglio, *Org. Electron.*, **2011**, *13*, 244. (c) M. Demelas, E. Scavetta, L. Basiric`o, R. Rogani and A. Bonfiglio, *Appl. Phys. Lett.*, **2013**, *102*, 193301.

[11] E. Scavetta; R. Mazzoni; F. Mariani; R. G. Margutta; A. Bonfiglio; M. Demelas; S. Fiorilli; M. Marzocchi; B. Fraboni; *J. Mater. Chem. B*, **2014**, *2*, 2861.

[12] S. T. Liddle; Ian S. Edworthya; Polly L. Arnold; *Chem. Soc. Rev.*, **2007**, *36*, 1732.

[13] F. E. Hahn; M. C. Jahnke; *Angew. Chem. Int. Ed.*, **2008**, *47*, 3122.

[14] W. A. Herrmann; *Angew. Chem. Int. Ed.*, **2002**, *41*, 1290.

[15] J. Fraga-Dubreuil; M.-H. Famelart; J. P. Bazureau; *Organic Process Research & Development*, **2002**, *6*, 373.

[16] L. M. Bushnell, E. R. Evitt, and R. G. Bergman, *J. Organomet. Chem.*, **1978**, *157*, 445.

[17] Sheldrick, G. M. *SADABS*, Program for empirical absorption correction, University of Göttingen, Germany, **1996**.

[18] Sheldrick, G. M. *SHELX97*, Program for crystal structure determination, University of Göttingen, Germany, **1997**.

Cyclopentadienone-NHC iron(0) complexes as anticancer drugs

7.1 Abstract

In this chapter, cyclopentadienone N-heterocyclic carbene iron complexes bearing amino group on lateral chain have been investigated as possible anti-cancer drugs. All but one, bearing a positive charge, display good activity against AsPC1 pancreatic cancer cells comparable to Carboplatin. The activity is remarkable and CO releasing seems to be not involved.

7.2 Introduction

Inorganic medicinal chemistry, also called elemental medicine, is a branch of bioinorganic chemistry, that is rapidly expanding. Since the discovery that inorganic elements play a crucial role in several bio-relevant reactions, coordination compounds, including organometallic complexes, are used in medicine both as diagnostic and therapeutic agents.[1] One of the most growing field concerns the study of metal complexes as drugs in the treatment of cancers. Cancer is indeed a major public health issue and it is the second cause of mortality after cardiovascular disease.[2]

The most famous example of anticancer metal drug is certainly cisplatin. The accidental discovery of cisplatin (Figure 1) by Rosenberg et al. in 1965[3] paved the way to the use of Pt salts and complexes as anticancer drugs. Even though several platinum complexes are now employed as chemotherapeutic agents, not all tumours can be treated with platinum-based drugs. Furthermore, several serious side-effects are experienced by patients (such as gastrointestinal and haematic toxicity) and drug-resistance phenomena reduce the possibility of further treatment in case of relapses.[4]

For these reasons, the research of new non-platinum-based compounds as anti-cancer drugs is nowadays under study. Although no non-platinum drugs have been approved as chemotherapeutic agents, metals such as Ti, Ru and Ga displayed promising results in in clinical phase and Fe, Co and Au at preclinical stage.[1,3] Regarding Ti(IV) species, titanocene dichloride (Figure 1) has been investigated in clinical trials and showed interesting results in phase I, but did not pass the phase II. The poor results on phase II trial were due to poor solubility in water and low stability due to hydrolysis.[5] Concerning Ru(III) compounds, some promising non-platinum based drugs such as

NAMI-A[6] (Figure 1) have been obtained. Ruthenium takes advantage of the iron pathways to be delivered inside cells (eg. transferrin) and they are activated by reduction to Ru(II) *in vivo* (good candidates as reductants are ascorbic acid and glutathione). NAMI-A, a Ru(III) imidazolium salt, displays anti-tumour activity *in vivo* due to its anti-metastatic properties and it was successfully applied in phase I trials, but clinical trials were terminated in phase II.[7]

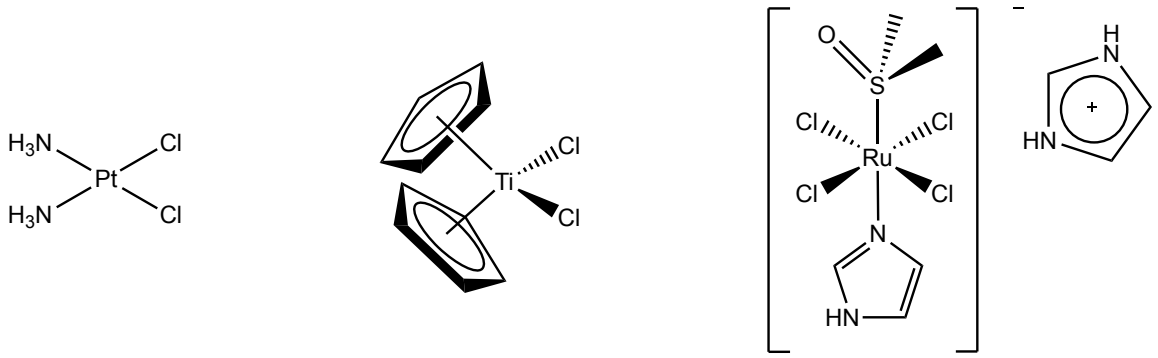

Figure 1. Platinum, titanium and ruthenium-based anti-cancer compounds.

Other more available metals are currently taken into consideration for the development of new anticancer drugs. Iron is acknowledged as a good candidate in that it is non-toxic and a key component in many important biological processes.[8] The involvement of iron in a wide range of biochemical functions, makes it suitable for anticancer drug development, exploiting different biological pathways other than the direct linking to DNA.[9] Among the most studied iron complexes for their anticancer properties are the ferrocene derivatives of anti-estrogen tamoxifen, also called ferrocifens (Figure 2).[10] Ferrocifens showed anti-citostatic effect on tumour treatment and death of cells by senescence other than apoptosis, typical of cisplatin type complexes. Mechanistic insights associate this behaviour to the unique redox properties of ferrocene, which exhibits a reversible redox wave at around +0.4 V, and might follow two separate mechanisms of action: production of reactive oxygen species (ROS) or formation of quinone methides (QM, Figure 2). Production of ROS such as •OH by iron compounds induces oxidative stress to the cell, which leads to DNA damage. Reaction involved in ROS production is the Fenton-type reaction,[11] catalysed by the Fe(II)/Fe(III) redox couple. The QM and radical precursors derived from the oxidation of ferrocifen complexes instead, are both very active intermediates, which can then interact with protein and DNA, inducing cell death. Interestingly, the presence of amine group on

side-chain is at the origin of major toxicity on ferrocene complexes,[12] and the same effect was observed with other metallocenes.[13] At the physiological pH, the amino group is protonated and it likely behaves as detergent.

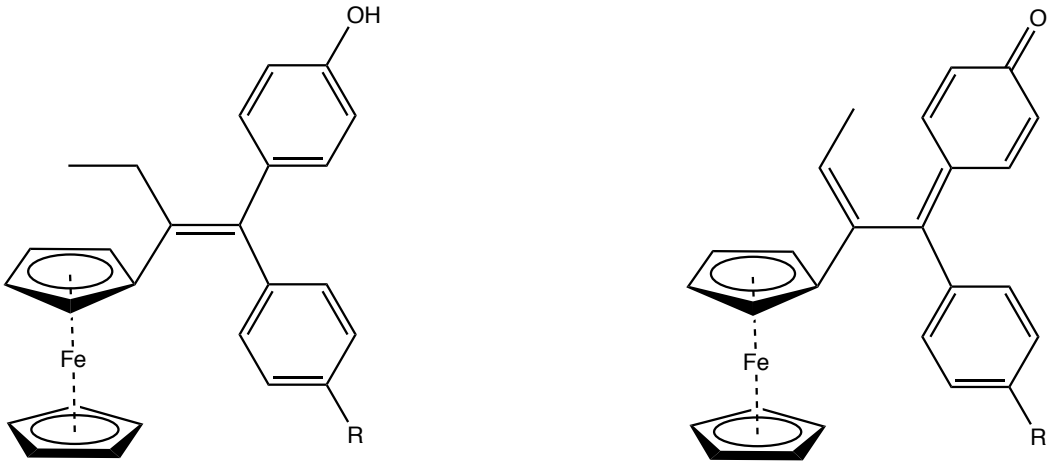

tamoxifen ferrocene derivative QM

Figure 2. A ferrocifen and the corresponding quinone methide (QM). R=alkyl or amine groups.

In these chapter, we described CpO-NHC iron complexes, bearing an amino group in lateral chains, as promising anti-cancer drugs. The typical reversible redox process of this type of iron compound (see Chapter 4 for CVs) resembles the one of ferrocene, even though a Fe(0)/Fe(I) redox couple is involved in the process. Furthermore, the presence of an amino group, acting as chelating agent on the iron centre as previously described in Chapter 1, might enhance the CO release, which can promote even a higher damage on cells.

7.3 Results and Discussion

7.3.1 Synthesis of iron complexes.

A straightforward synthesis that allows the addition of an N-heterocyclic carbene (NHC) ligand on iron(0) complexes already bearing non-innocent ligands such as carbonyl and cyclopentadienone(CpO) has been recently developed (see Chapter 1). Here, the synthetic approach is exploited in order to insert an amine group in a lateral chain of the NHC leading to the isolation of novel stable complexes **7g**-**12** (Scheme 1). Complexes **7g**, **10g** and **10m** have been prepared by simple deprotection of the NHBOC complexes *via* HBF_4 addition, followed by neutralization reaction with a 73% yield. They contain a lateral chain of different length, respectively 2(**7g, 10g**) and 3(**10m**) CH_2 as linker between NHC nitrogen and terminal NH_2, that could affect the reactivity in term of CO releasing trend. Moreover, lipophilicity can be tuned by changing substituents in cyclopentadienone ring with aromatics, as in complex **7g**. Further features of the reactivity of **10g** include the quantitative alkylation to form the ammonium group[14] leading to water soluble complex **10h**, as described in Chapter 1. Under photolytic conditions **10g** undergoes CO release with the formation of a stable chelated complex **12** (Scheme 1).

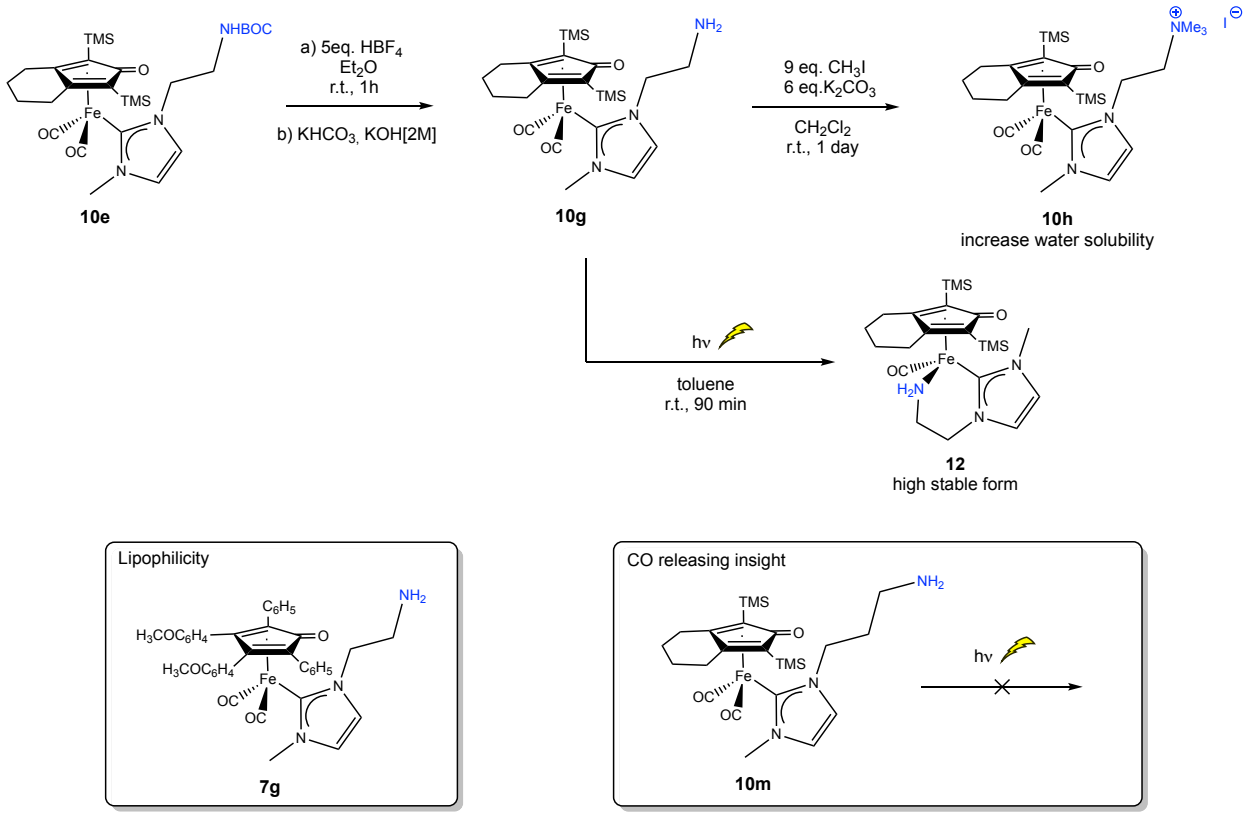

Scheme 1. Amino functionalized Fe(0) complexes employed in this study (TMS, trimethylsilyl, BOC, *tert*-butyloxycarbonyl).

All the complexes have been characterized by means of IR, NMR and ESI-MS (see experimental). All compounds but **10m** have been already described in Chapter 1. **10m** appears as yellow powder stable to air- and moisture both in solid state and in solution, as for its analogues. Likewise, spectroscopic data of **10m** are consistent with those of the analogous complexes previously reported. ^{13}C-NMR spectra showed the diagnostic signal for the Fe-$C_{carbene}$ at184 ppm, while CO stretching were easily followed in the terminal CO region, where a couple of bands arose around 1986 and 1930 cm^{-1} in CH_2Cl_2.

7.3.2 CO releasing.

As already reported in Chapter 1, upon irradiation, a yellow solution of **10g** in toluene, turned deep red in about 1 hour, affording the corresponding chelated complex **12** (Scheme 1). The reaction was followed by IR spectroscopy: the two carbonyl stretching frequencies typical of **10g** [ν(CO) = 1982, 1922 cm^{-1}] slowly disappeared, replaced by a new single stretching assigned to **12** [ν(CO) = 1879 cm^{-1}]. ^{13}C-NMR showed a shift to lower and higher fields of $C_{carbene}$ (δ**10g**: 185ppm vs **12**: 193 ppm) and C=O (δ10g**4**: 176ppm vs **12**: 168 ppm) respectively. As its precursor, **12** is air- and moisture-stable at room temperature, and it is red coloured. Compound **10g** shows high tendency to undergo CO displacement: even exposure to sun-light in the solid state promotes the reaction. This is clearly visible by a change from yellow to orange solid (a mixture of both species) confirmed by a concurrent change in the IR and UV-vis spectra. On the contrary, solution of **12** under CO atmosphere (1.5 atm) did not show any reverse reaction to form **10g**, demonstrating the high stability of the chelated form.

Analogous experiments have been performed with complex **10m,** bearing three CH_2 groups on the NH_2 lateral chain. Leaving the solution of **10m** in toluene under UV irradiation for several hours did not afford the corresponding chelated form. Only after 8 hours of irradiation, **10m** eventually decomposed, suggesting that the formation of a 6-membered ring in the case of **10g** stabilizes the chelate form **12**. On the other hand, 7-membered ring is not stable enough to promote CO releasing from **8**.

7.3.3 Lipophilicity measurements.

In order to evaluate the ability of iron complexes in passing across cell membranes, the lipophilicities of iron complexes, measured as their logD values, were determined by the shake-flask methods (see Experimental) and reported in Table 1.

Table 1. LogD values for 7g and 10g at different pH.

$logD_{pH}$	$logD_{4.6}$	$logD_{7.4}$
7g	1.79±0.02	2.05±0.05
10g	1.6±0.1	1.97±0.05
10h	0.99±0.05	1.01±0.09
10m	1.09±0.07	2.0±0.3
12	2.6±0.2	2.4±0.4

The influence of amino group is clearly visible in different logD values at different pH values: in acetate buffer (pH4.6) and phosphate buffer (pH7.4) solutions. Under acidic pH, iron complexes are more soluble in water media since the amino group is protonated. Furthermore, the phenyl rings on CpO ligands in **7g** showed an overall higher lipophilicity compared to TMS groups in **10g**. The amino salt **10h**, which is soluble both in acidic and basic water, showed no difference of logD values under different pH. Compound **12**, where the amino group chelates the iron centre, displayed an overall higher lipophilicity independent of pH value. Finally, **10m** bearing 3 CH_2 as linker to NH_2, showed a lower $logD_{4.6}$ value compared to **7g** and **10g**; this behaviour might be due to the longer linker chain which does not allow the amino group to engage a hydrogen bond with CpO, hence increasing the lipophilicity under acidic conditions.

7.3.4 Cytotoxicity tests.

Iron compounds were tested against AsPC1 pancreatic cancer cells at an initial concentration of 10 μM, to screen for anticancer properties. All of the iron compounds, with the exception of **10h**, led to a decrease in cell number by 50% or more (relative to controls), and so IC_{50} values of these four complexes were measured (Table 2). All complexes tested displayed an activity equal to or better than carboplatin against AsPC1 cells which, given the robustness of pancreatic cancer cells, is remarkable. Given that **7g**, **10g**, **10m** and **12** are neutral complexes and **10h** is positively charged, it appears that modification of the cyclopentadienyl ring has little effect on the anticancer

properties but quaternisation of the pendent amine leads to loss of activity. Whether this is due to altered cell uptake or localisation is unclear. It is also remarkable the similar activity profile of complexes **10g** and **10m** (the latter derived from photoinduced CO release from **10g**), which suggests that liberation of CO *in situ*, were it to occur, would have little to no effect on the biological activity of the iron species.

Table 2. IC_{50} (μM) values for compounds **7g**, **10g**, **10m** and **12** against AsPC1 pancreatic cancer cells.

Compound	**IC_{50} (μM) against AsPC1**
10g	5.4 ± 1.5
7g	4.5 ± 0.2
12	8.9 ± 1.0
10m	6.9 ± 1.5
Carboplatin	6.8 ± 2.0 [a]

[a] Literature data.

7.4 Conclusions

Organometallic CpO-NHC iron(0) compounds were evaluated as possible anticancer drugs. The affinity to water phase of this class of iron complexes is highly influenced by the amino group, which is susceptible to protonation. Alkylation of the amino group to the corresponding ammonium salt **10h** resulted in increased affinity to water phase both under acidic and basic conditions. Furthermore, complexes **7g** and **10g** are both prone to CO release under UV or light irradiation.

Iron compounds were tested against AsPC1 pancreatic cancer cells and showed an IC_{50} value comparable to carboplatin. Only ammonium salt **10h** was not active, which might be correlated to the lower $logD_{7.4}$ value compared to the other complexes. Given the robustness of the pancreatic cancer cells, the result is remarkable and further studies are now underway to address the mechanism involved. CO releasing under physiological condition does not seem to have an effect, since also **12** displayed a good activity. The redox of the complexes investigate here, similar to those of ferrocene, as observed in previous chapters, might have a role in mechanisms involving ROS production.

7.5 Experimental Section

General data. All reactions were routinely carried out under a nitrogen atmosphere, using standard Schlenk techniques. Glassware was ovendried before use. Solvents: dichloromethane (CH_2Cl_2), tetrahydrofuran (THF), diethyl ether (Et_2O), petroleum ether referring to a fraction of bp 60-80 °C, acetonitrile (CH_3CN) were dried and distilled prior to use. Acetone has been degassed and stored under inert atmosphere on molecular sieves. Other solvents such as ethylacetate (EtOAc), chloroform, ethanol (EtOH), methanol (MeOH), toluene, $CDCl_3$ (Sigma Aldrich) have been employed without further purification. Reagents: $Fe_2(CO)_9$ (Strem), methyl iodide, silver oxide, 1-methylimidazole, Bu_4NPF_6, potassium hydroxide, trifluoroboric acid have been employed as purchased.

1,3-dimethylimidazolium iodide,[15] NHBoc (JOMC 2008), 1-methyl-3-(2-hydroxyethyl)imidazolium chloride, 1,8-bis(trimethylsilyl)octa-1,7-diyne[16] have been prepared following procedures reported in the literature.

The prepared derivatives were characterized by spectroscopic methods. The NMR spectra were recorded using Varian Inova 300 (^{1}H, 300.1; ^{13}C, 75.5 MHz), Varian Mercury Plus VX 400 (^{1}H, 399.9; ^{13}C, 100.6 MHz), Varian Inova 600 (^{1}H, 599.7; ^{13}C, 150.8 MHz) spectrometers at 298 K; chemical shifts were referenced internally to residual solvent peaks. Infrared spectra were recorded at 298 K on a Perkin-Elmer Spectrum 2000 FT-IR spectrophotometer. ESI-MS spectra were recorded on Waters Micromass ZQ 4000 with samples dissolved in MeOH or CH_3CN. Elemental analyses were performed on a Thermo-Quest Flash 1112 Series EA instrument.

Synthesis of dicarbonyl-(2,4-bis(trimethylsilyl)bicyclo[3.3.0]nona-1,4-dien-3-one)[1-(3-aminopropyl)-3-methylilidene]iron (10m). In a dried 25 mL Schlenk flask, dicarbonyl-(2,4-bis(trimethylsilyl)bicyclo[3.3.0]nona-1,4-dien-3-one)[1-(2-BocNH-ethyl)-3-methylilidene]iron (0.094 g, 0.150 mmol) was dissolved in Et_2O (2 mL) and HBF_4 (0.103 mL, 0.750 mmol) was added dropwise. Reaction mixture was stirred at room temperature for 1 hour. The precipitate was dissolved in CH_2Cl_2 and the excess of HBF_4 neutralized with a saturated solution of sodium carbonate (pH=7-8). Aqueous phase was extracted with dichloromethane and washed with potassium idroxide solution (1.5 M, 3x10mL). Organic phase was dried with sodium sulfate and filtrated. Solvent was removed to leave a yellow solid. Yield = 75 %. ^{1}H-NMR (399.9 MHz, CD_3Cl)

δ (ppm): 7.06 (s, 2H, -CH_{im}), 4.39 (t, CH_{2im}), 3.94 (s, 3H, -NCH_3), 3.53 (t. 2H, -CH_{2im}), 2.43 (t, 4H, CH_2), 1.83-1.79 (m, 4H, CH_2), 1.71 (m, 2H, CH_2), 0.16 (s, 18H, CH_{3TMS}); ^{13}C-NMR (150.8 MHz, CD_3Cl) δ (ppm): 217.22 (CO), 184.45 (C_{im}), 176.85 (C_1=O, Cp), 124.21 (CH_{im}), 121.85 (CH_{im}), 104.02 ($C_{3,4}$, Cp), 70.87 ($C_{2,5}$, Cp), 49.29 (-NCH_2-), 40.20 (-NCH_2-), 39.50 (-NCH_3), 28.37 (CH_2), 24.47 (-CH_2), 22.52 (-CH_2), 0.20 (CH_{3TMS}). IR (CH_2Cl_2, cm^{-1}) ν 1986, 1930. ESI-MS (m/z) (+): 530$[M+H]^+$, 552 $[M+Na]^+$. Anal. Calcd (%) for $C_{24}H_{39}FeN_3O_3Si_2$: C, 54.43; H, 7.42; N, 7.93. Found: C, 54.22; H, 7.43; N 7.94.

Partition Coefficient (log$D_{7.4}$). Log$D_{7.4}$ values, partition coefficient n-octanol/water, were determined using the shake-flask method. Phosphate buffer solution (PBS, 10mM, pH adjusted to 7.4 with HCl) and n-octanol were shaken together for 3 days to allow saturation of both phases. Then, 750µl of both phases and 50µl of a complex stock solution (1 mg in 200µl DMSO) were combined in an Eppendorf tube (2mL) and shaken in a lab vortex for 10 min (VWR Analogue Vortexer). The emulsion was centrifuged (10min, 15000rpm) to separate the two phases. UV/Vis absorption were determined for both phases at 280nm or 325nm. The aqueous phase was diluted 3-fold and the n-octanol phase 20-fold. The values of log$D_{7.4}$ were calculated according to eq.1, f_{dil} is the dilution factor. The given values are the mean of three separate determinations.

$$\boldsymbol{logD_{7.4} = log\left(\frac{A_{octanol}\cdot f_{dil}}{A_{buffer}\cdot f_{dil}}\right)} \qquad (\mathbf{1})$$

Partition Coefficient (log$D_{4.6}$). Log$D_{4.6}$ values were determined following the same procedure of log$D_{7.4}$, but the water phase was an acetate buffer solution (10 mM, pH adjusted to 4.6 with NaOH).

Cell growth assays. For cell counting, AsPC1 cells were seeded in 12 well plates (50,000 cells per well) and grown in cell culture medium supplemented with 10% FBS. After an overnight incubation, the complete media was replaced with fresh one containing DMSO 0.1%, and 10 µM of iron compounds. After 72 Hours of incubation at 37 °C and 5% CO_2, the cells were washed once in warm PBS, and detached with tripsyn-EDTA 0.25% at 37 °C and 5% CO_2. When a complete cells detachment was achieved, the proteasic activity was stopped with one volume of complete media. The total number

of cells per well was quantified by manual cell counting under bright field microscopy using Neubauer or Burker chambers.

Alamar blue IC_{50} determination. The cell viability in response to iron compounds was evaluated with the alamar blue assay. AsPC1 cells were cultured in a 96 wells plate at a seeding density of 2,000 cells per well. After an overnight incubation at 37 °C and 5% CO_2 in complete media, cells were exposed in triplicate to increasing amount of iron complexes resuspended in fresh media (DMSO 0.1%). After 72 hours, cells were incubated with fresh complete media added with 25 µg/ml of Resazurin [Sigma], and incubated for 1 to 4 hours at 37 °C and 5% CO_2. 100 µl of media per well were transferred to a 96 well-black-walled plate. Upon excitation at 530 nm the, fluorescence emitted by the reduced product Resorufin was quantified at 590 nm.

7.6 Notes and References

[1] Z. Guo; P. J. Sadler; *Angew. Chem. Int. Ed.*, **1999**, *38*, 1512.

[2] R. L. Siegel; K. D. Miller; A. Jemal; *CA Cancer J Clin.*, **2017**, *67*, 7.

[3] B. Rosenberg; L. Van Camp; T. Krigas; *Nature*, **1965**, *205*, 698.

[4] I. Ott; R. Gust; *Arch. Pharm. Chem. Life Sci.*, **2007**, *340*, 117.

[5] M. H. Harding; G. Mokdsi; *Curr. Med. Chem.*, **2000**, *7*, 1289.

[6] E. Alessio; G. Mestroni; A. Bergamo; G. Sava; *Current Topics in Medicinal Chemistry*, **2004**, *4*, 1525.

[7] S. Leijen; S. A. Burgers; P. Baas; D. Pluim; M. Tibben; E. van Werkhoven; E. Alessio; G. Sava; J. H. Beijnen; J. H. M. Schellens; *Invest New Drugs*; **2015**, *33*, 201.

[8] M. Arredondo; M. T. Núñez; *Mol. Aspects Med.*; **2005**, *26*, 313.

[9] W. A. Wani; U. Baig; S. Shreaz; R. A. Shiekh; P. F. Iqbal; E. Jameel; A. Ahmad; S. H. Mohd-Setapar; Md. Mushtaqueh; L. T. Hun; *New. J Chem.*, **2016**, *40*, 1063.

[10] G. Jaouen; A. Vessières; S. Top; *Chem. Soc. Rev.*, **2015**, *44*, 8802.

[11] D. Osella; M. Ferrali; P. Zanello; F. Laschi; M. Fontani; C. Nervi; G. Cavigiolio; *Inorg. Chim. Acta*, **2000**, *306*, 42.

[12] C. Lu; J.-M. Heldt; M. Guille-Collignon; F. Lemaitre; G. Jaouen; A. Vessieres; C. Amatore; *ChemMedChem*, **2014**, *9*, 1286.

[13] H. Z. S. Lee; O. Buriez; F. Chau; E. Labbé; R. Ganguly; C. Amatore; G. Jaouen; A. Vessières; W. K. Leong; S. Top; *Eur. J. Inorg. Chem*., **2015**, 4217.

[14] D. S. Mérel, M. Elie, J-F. Lohier, S. Gaillard, and J.-L. Renaud, *ChemCatChem*, **2013**, *5*, 2939.

[15] a) A. M.Oertel, V.Ritleng, L.Burr, C.Harwig and M. J.Chetcuti, *Organometallics,* **2011**, *30*, 6685; b) L. B.Benac, E. M.Burgess, L.Burr and A. J.Arduengo, *Organic Syntheses, Coll.*, **1990**, **7**, 195; **1986**, *64*, 92.

[16] L. M. Bushnell, E. R. Evitt, and R. G. Bergman, *J. Organomet. Chem.*, **1978**, *157*, 445.